Non-aqueous Protonation, Protonolysis and Related Reactions of Polyoxometalates.

Daniel Lebbie

A thesis submitted in partial fulfilment of the requirements for the award of

Doctor of Philosophy

School of Natural and Environmental Sciences

(Chemistry)

May 2020

Abstract

A sound knowledge of the complex solution processes underlying molecular metal oxide aggregation and structural inter-conversion is crucial to developing efficient synthetic routes to accessing unprecedented structures and understanding their properties. The nonaqueous aggregation of $(TBA)_2[W_6O_{19}]$ from $WO(OMe)_4$ and $(TBA)_2[WO_4]$ was studied systematically using ^{17}O NMR spectroscopy. The study resulted in the development of a novel and efficient synthetic route to a series of heterometallic Lindqvist POMs, {M′M$_5$} from $[M_6O_{19}]^{2-}$ anion. Using a combination of NMR techniques (^1H, ^{17}O and 2D ^1H EXSY) and DFT calculations, the hydrolysis and condensation of $(TBA)_3[(MeO)TiW_5O_{18}]$ and $(TBA)_3[(MeO)SnW_5O_{18}]$ were investigated to understand factors influencing subtle differences in the POMs. The study led to the isolation and characterization of $(TBA)_3[(HO)TiW_5O_{18}]$ - a new member of the [M′M$_5$] family. The study further revealed that the tin hydroxido POM, $(TBA)_3[(HO)SnW_5O_{18}]$ was more readily accessible than the titanium anologue, $(TBA)_3[(HO)TiW_5O_{18}]$ under similar conditions whereas the tin oxo-bridge dimer, $(TBA)_6[(\mu\text{-}O)(SnW_5O_{18})_2]$ was less stable and hence more difficult to isolate compared to the titanium oxo-bridged POM, $(TBA)_6[(\mu\text{-}O)(TiW_5O_{18})_2]$. These behaviours were ascribed to differences in relative free energies. Furthermore, the surface oxygen basicity of the POMs, $(TBA)_3[(MeO)TiW_5O_{18}]$ and $(TBA)_6[(\mu\text{-}O)(TiW_5O_{18})_2]$ and the behaviour of $(TBA)_6[(\mu\text{-}O)(TiW_5O_{18})_2]$ towards a range of electrophiles were explored using ^{17}O NMR spectroscopy. Generally, it was demonstrated that the TiOW oxygens are the most basic sites in $(TBA)_6[(\mu\text{-}O)(TiW_5O_{18})_2]$. The reactions resulted in the isolation and characterization of the dmso adduct $(TBA)_4[(\mu\text{-}O)(TiW_5O_{18}H)_2(dmso)]$ and $(TBA)_4[(\mu\text{-}O)(TiW_5O_{18})_2(SnMe_2)]$ wherein Sn(IV) is bonded to the Ti-O-W oxygens suggesting the possibility of “POM-pincer” complexes. Additionally, $[O{=}TiW_5O_{18}]^{4-}$, which is possibly the first member of the oxo-titanium Lindqvist family was isolated and characterized in an excellent yield by treating $[(CH_3O)TiW_5O_{18}]^{3-}$ with an organic base. The new POM was subsequently reacted with alkyl and aromatic isocyanate providing insights into the reactivity of the titanyl bond. Generally, products were further characterised by FT-IR, Multinuclear NMR (^1H, ^{13}C, ^{31}P, ^{119}Sn, and ^{183}W) and/or single crystal XRD. While DFT calculations provided support for experimental observations.

Dedication

To the Lebbie family

Acknowledgments

I am deeply indebted to my supervisor, Dr. R.J. Errington of Newcastle University, UK for being such a great motivator, his interest in polyoxometalates and metal alkoxides chemistry fostered a conducive environment of creative research for me. He has been a constant support and guide for me during the many trials I experienced throughout my PhD. Without him this work would have not come so far. I would like to offer my sincere gratitude to him for his advice both at the personal and technical level. His effort and support will never be forgotten.

I sincerely thank Prof. Walter Klemperer of University of Illinois for academic guidance and financial contributions that enabled me to complete my studies.

I am also grateful to Newcastle University for the award of an Overseas Research Scholarship.

My special thanks are also due to Prof. William and Dr. Corinne of Newcastle University, UK for the training and support in NMR spectroscopy. Thanks to them I have developed a good capability in NMR spectroscopy. I also appreciate Dr. Paul for Single Crystal X-ray Crystallography, Dr. Magda and the group of Prof. Josep M. Poblet at the Universitat Rovira i Virgili, Tarragona, Spain for computational analysis.

I acknowledge the technical and research support staff of Chemistry including Geoffrey and Christopher (Electrical workshop), John and, Gary (Mechanical workshop), William and Robyn (Glassblowers), Dr. Mark (IT support), Joanne, Claire, Kate and Jane of the School Office and Robin retired stores officer.

I also acknowledge funding support from COST Action PoCheMoN for providing me with funding to participate in the 7th European School on Molecular Nanoscience (ESMolNa 2014) in Spain.

I would also like to thank my former colleague in the RJE group, Dr. Thompson for his friendship and support. Equally, I greatly appreciate my other colleagues in the group for the good time we shared together during this period and those memories will never be forgotten.

Finally, thanks to my family for the financial support and encouragement, and for that I would like to dedicate this entire work to the Lebbie family.

Table of contents

List of Figures

List of Tables

List of Schemes

Abbreviations

2D-INADEQUATE: Two-dimensional Incredible natural-abundance double-quantum transfer experiment

2D: Two-dimensional

ATR: Attenuated Total Reflectance

CHN: Carbon, Hydrogen and Nitrogen

COST: An intergovernmental framework for European Cooperation in Science and Technology

COSY: Correlation Spectroscopy

DCC: N, N'-dicyclohexylcarbodiimide

DCM: Dichloromethane

DFT: Density Functional Theory

DMF: Dimethylformamide

DMSO: Dimethyl sulfoxide

EXSY: Exchange Spectroscopy

FTIR: Fourier Transformed Infrared

MOF: Metal Organic Framework

NMR: Nuclear Magnetic Resonance

POM: Polyoxometalate

ppm: Parts per million

REDOX: Reduction and Oxidation

TBA: tetra–*n*–butylammonium

THF: Tetrahydrofuran

TM: Transition metal

UV-Vis: Ultraviolet and Visible

XRD: X-ray Diffraction

Chapter 1
Introduction

This chapter presents a background to the projects described in this thesis, outlining the thesis aims and objectives. It further highlights some fundamental aspects of non-aqueous solution studies of polyoxometalates (POMs). Additionally, some recent developments in POM functionalization and the applications of these POM-derived materials are reviewed.

1. Introduction

1.1 Background of the study

The early-transition metal oxygen cluster anions or polyoxometalates (POMs)[1, 2] and their transition-metal substituted derivatives are a large group of anionic clusters that have multiple applications, many of which are related to their redox properties.[3] Interest in this class of compounds is rapidly growing, part of this is as a consequence of the unique collective properties and their compatibility with environmentally friendly chemical processes (e.g. oxidation using O_2 and H_2O_2). The composition of the metal and the shape of the framework define the properties of the POM. For example, studies have shown that the improvement in the catalytic activity of polyanions is closely related to the substituted addenda atoms.[4, 5]

Over the years, activity in the area of non-aqueous polyoxometalate chemistry has rapidly increased due to the recognition that these molecular oxides display novel reactivity in organic media and that structures can be accessible that are otherwise unstable in aqueous solution.[6-8] Despite this, however, the vast majority of POMs are usually synthesised in aqueous solution.[1]

There have been several advances to understand the aggregative processes involved in the formation of these molecules, however, it is clear that there is still plenty of scope for further work in non-aqueous chemistry of polyoxoanions as many fundamental questions regarding the aggregative mechanisms and reactivity remain unanswered.

1.2 Aims and Objectives

The aim of the thesis focussed on developing a fundamental understanding of non-aqueous aggregative processes and reactivity of heterometallic POMs. Previous works in the Errington research group have devoted significant effort in this area but there still remain challenges in understanding these complex processes. Therefore, detailed knowledge of these fundamental chemistry is significantly important in order to provide a platform for more sophisticated studies of these class of compounds.

A fundamental aim of the thesis was to establish a detailed understanding of the electronic factors underlying the reactivity of heterometallic polyoxometalates (POMs) through rational synthesis and systematic reactivity studies coupled with theoretical

computational studies. An underlying theme was to design models for multifunctional catalysts at the molecular level.

The work was to extend the studies carried out by past members of the Errington group including my MPhil studies, which investigated non-aqueous proton-transfer reactions of $[(MeO)TiW_5O_{18}]^{3-}$ and $[(MeO)SnW_5O_{18}]^{3-}$. To build on this platform, several goals were identified (as outlined below), which target aspects of reactivity that are important in catalysis, including redox reactions that might be coupled with proton-transfer for small-molecule transformations such as oxygen reduction. The specific objectives are:

- Extended studies of fundamental non-aqueous aggregation of the Lindqvist-type $(TBA)_2[W_6O_{19}]$ POM and the possible isolation and characterisation of intermediate POMs in the aggregation process.
- Explore routes to reactive transition metal hydrocarbyl derivatives such as $[RTiW_5O_{18}]^{3-}$ and $[R_2C{=}TiW_5O_{18}]^{4-}$.
- Investigate the synthesis and reactivity of Ti-peroxo and hydroperoxo species. This involved collaboration with the Kholedeeva group from the Boreskov Institute of Catalysis in Novisibirsk, Russia, who are also interested in such species as alkene epoxidation catalysts.
- Use multinuclear NMR to monitor structural growth in non-aqueous solution (^{17}O, ^{183}W, ^{119}Sn etc.).

1.3 Structure of the thesis

The thesis is divided into five chapters. Chapter 1 gives a background to the study including historical developments in polyoxometalates chemistry, classification, synthetic methods, characterisation techniques and some application aspect of POMs. In Chapter 2 the investigation of non-aqueous self-assembly of $(TBA)_2[W_6O_{19}]$ and its conversion to $(TBA)_3[(MeO)M'M_5O_{18}]$ (M′ = Ti, Sn; M = W, Mo and $(TBA)_3[NbW_5O_{19}]$ is discussed. In Chapter 3, studies of protonolysis and condensation of $(TBA)_3[(MeO)M'W_5O_{18}]$ (M′ = Ti, Sn) are described revealing subtle differences resulting from the electronic effect of metal substitution in the two anions. In addition, studies on the hydrolysis of $(TBA)_3[(MeO)TiW_5O_{18}]$ with H_2O_2 is also described. In Chapter 4 protonation site on the mono-substituted and the oxo-bridged dimer of Ti-substituted Lindqvist-type POM is described and also the addition of electrophilic metal centres to $(TBA)_6[(\mu\text{-}O)(TiW_5O_{18})_2]$ is discussed. The last chapter of the thesis

describes the preparation of the first Lindqvist-type POM with a terminal Ti=O bond, $(TBA)_4[O=TiW_5O_{18}]$.

1.4 Polyoxometalates (POMs)

As mentioned above, polyoxometalates or polyoxoanions (POMs)[1,9] are discrete molecular metal-oxides of the early transition metals, mainly members of groups 5 and 6 (V, Nb, Ta, Mo, W) in their highest oxidation states. These molecular metal oxoanions can possess nuclearities up to 368 metal atoms per molecule, making them nanoscale in dimension.[10] The electronic versatility and structural variation are remarkable giving rise to a wide range of applications for example in catalysis,[11,12] medicine,[13,14] electronics,[15,16] and material science.[2,17-19] POMs have been in existence for almost 200 years[20,21] but novel structures with diverse reactivity continues to emerge mainly because the structural framework can be fine-tuned to certain degree under certain conditions such as pH, temperature etc.[3,10,15,22,23]

1.4.1 History of Polyoxometalates

Though some POMs exist in nature,[24] the history of POMs began in 1788 when Scheele observed the intense blue colour of the Mo-blue clusters[25] which he ascribed to be reduced molybdenum oxide. In 1826 Berzelius reported the yellow precipitate formed from ammonium molybdate and phosphoric acid which later became known to be the $(NH_4)_3[PW_{12}O_{40}]$ Keggin structure.[20] This was followed by Marignac who successfully synthesised and analysed the isomers (known to be α and β forms) of 12-tungstosilicic acid $[SiW_{12}O_{40}]^{4-}$ in 1862.

In the early 20th century, Rosenheim began characterisation of POMs and the systematic study of their properties. Rosenheim and Miolati applied the ionic coordination theory, attempting to explain the structure of POMs by suggesting that the central atom possesses an octahedral geometry and the metal forming a cage around it composed of MO_4^{2-} or $M_2O_7^{2-}$ units. This was eventually proved to be wrong by Pauling (1929) who suggested an alternative explanation that the metals forming the cage possess an octahedral MO_6 geometry while the central atom had a tetrahedral geometry.[26]

Pauling's proposal led to structural characterisation of POMs through X-ray analysis when Laue[27] and Bragg[28] were key contributors in X-ray development. Keggin determined the X-ray crystal structure of $H_3PW_{12}O_{40}.5H_2O$ that was named after him.[21, 29]

Keggin pioneering analysis led to the proposed structure of 6-heteropolyanions such as $[IMo_6O_{24}]^{5-}$ by Anderson (1937). In Anderson's report, the structure was based on edge-share MO_6 octahedra and it was confirmed by Evans in 1968 who later determined the structure of $K_6[TeMo_6O_{24}]$.[30] Dawson reported the structure for $K_6[P_2W_{18}O_{62}]$[31] in 1953 which was seen to be comprised of two Keggin fragments $\{PW_9\}$ linked together. These developments in POM history are summarised below.

Timeline of POM progression

1788: Scheele – Observed a Mo-blue compound while working on Mo oxides

1826: Berzelius – First synthesised Keggin compound

1862: Marignac – Determined the formula of Silicotungstic acid

1893: Werner – Presented his co-ordination theory

1908: Miolati – Applied Werner's theory to POMs

1921: Rosenheim – Presented the Miolati-Rosenheim theory of POMs

1929: Pauling – Proposed POM structure based on octahedra and tetrahedra units

1934: Keggin – Determined the X-ray structure of phosphotungstic acid.

1937: Anderson – Proposed the structure of the Anderson Cluster

1953: Dawson – Determined the X-ray structure of the Phosphate Dawson

1968: Evans – Determined the X-ray structure of the Anderson Cluster

1.4.2 Iso- and Hetero-polyoxoanions

In the early 1980's Pope classified POMs as either isopoly- or heteropoly-oxoanions with the general formulas $[M_mO_y]^{p-}$ and $[X_xM_mO_y]^{q-}$ respectively.[1]

Isopolyanions (IPAs) $[M_nO_y]^{p-}$

Heteropolyanions (HPAs) $[X_zM_nO_y]^{q-}$, with $z \leq n$

These iso- and heteropoly-anions form the different types of POMs including the Lindqvist-type, Keggin-type, Dawson, etc. (described in detail later). POM frameworks consist of addenda and heteroatoms. The addenda atoms are characterised by a metallic centre, **M**, which acts as the main structural components of POMs. In most

cases, the structures are derived from the aggregation of octahedra units MO_6. The addenda metals form M(dπ) – O(pπ) overlap due to the available non-bonding d-orbitals. Oxygen atoms consisting simple M-O-M bonds allow the condensation between two octahedra units, with the formation of μ-oxo bridges between two metal ions. In the structure one oxygen form M=O bond with the central metal atom which are not shared with other metal atoms. These terminal oxygens are essential for the aggregation process to take place into discrete units and not in an extended material. Polyoxometalates mostly contained the larger members of the group 6 elements i.e. Mo and W although Nb, or Ta are becoming increasingly of interest. The fewer numbers of polyniobates or polytantalates are mainly due to availability of synthesis methods and their solution properties.

The heteroatoms are non-addenda atoms and can be almost any element in the periodic table capable of coordinating to at least three other atoms. The p-block elements (Si, Ge, P, As or S) are therefore frequently found as heteroatoms in POM structures.

1.4.3 Self-assembly process of POMs in solution

POMs are typically synthesised from low nuclarity precursors such as MoO_4^{2-}, WO_4^{2-} or VO_4^{3-} units. In aqueous media, the protonation-condensation reactions involve acidification of these monomeric oxometalates. The basic structural arrangement of POM is based on the monomeric MO_x unit (where x range between 4 and 7) and usually exist as MO_6 octahedron as mentioned above. The MO_6 metal centre is bonded to six oxygen atoms such that the bridging M-O-M are linked together by coordinative bonding and the terminal M=O bonds exist in a strong *pπ-dπ* bonds by the empty d orbitals of the metal ions.[32] The octahedral metal centre in the POMs can thus condensed in three different ways commonly referred to as *corner-sharing* (one oxygen), *edge-sharing* (two oxygen) and *face-sharing* (three oxygen) although the most common ones are the corner- and edge-sharing as shown in Figure 1.1.

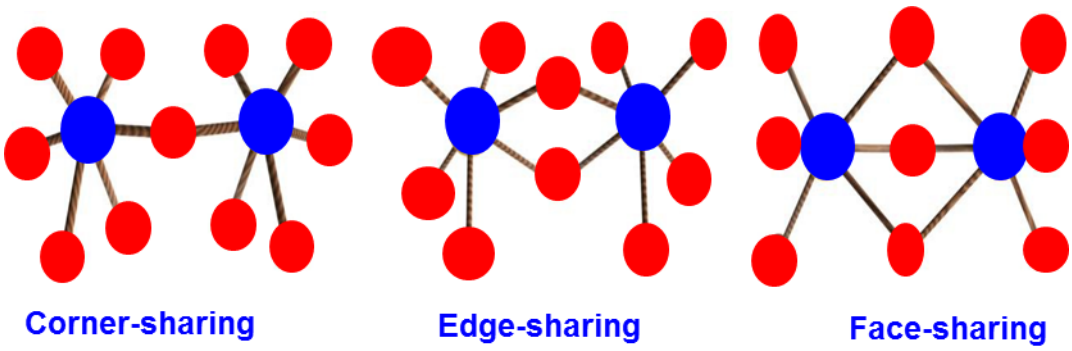

Figure 1.1: *The MO_6 structural arrangements in POMs*

The process of linking these small MO_x monomeric units into more complex polymeric units is often referred to as "*self-assembly*" which is often a complex process. Theoretical calculations have been carried out to investigate the mechanistic processes involved in these complex processes and as a means to identify the most likely building block or intermediates in these polymeric species. In 2009 Vilà-Nadal *et al.* carried out such an investigation by electrospray fragmentation experiment and analysed by Density Functional Theory (DFT) calculations. The results suggest that $[W_3O_{10}(OH)]^{3-}$ was most likely the building block in the self-assembly of POMs due to its inherent stability as an open isomer,[33] although the stability and aggregation mechanisms of the anion have not been unambiguously identified in solution.

The aqueous acidification process is still the main synthesis route to POMs but there are certain species (particularly air sensitive material) that are not accessible *via* the aqueous route therefore an alternative route was developed using organic solvents to access some of these species.

The extension of POMs synthesis to non-aqueous route using organic solvents and large organic cations such as Bu_4N^+ and $(PhCH_2)Me_3N^+$ resulted in the isolation of several new anions $[Mo_2O_7]^{2-}$, $[Mo_6O_{19}]^{2-}$ and $[W_6O_{19}]^{2-}$.[1,34] A non-aqueous approach which is the main synthesis route in the Errington group involves soluble oxoalkoxido-anions generated in reactions between mononuclear oxo-anions and metal alkoxides through hydrolysis in organic solvents. This synthesis route has been used to synthesise and fully characterise various Lindqvist-type $\{XM'M_5O_{18}\}^{n-}$ hexametalate POMs.[35] The use of ^{17}O enriched water in the hydrolysis reactions enables a convenient monitoring of the hydrolysis reactions by ^{17}O NMR spectroscopy in organic solvents.

1.5 Structures of Polyoxometalates

1.5.1 Lacunary structures

It is well-known that POMs are stable in a wide range of pH, from neutral to slightly basic or acidic media. Increasing the pH progressively, however, can result to degradation towards lacunary form by the formation of vacant site known as *lacuna*. These vacant sites can accept $[M^{n+} =O]^{(n-2+)}$ fragments or organic groups for functionalization,[36] reactivity,[37] or electrochemistry[38] purposes. Note that the addition of these groups into the metal-oxide framework can result to significant effects on the properties of the resulting POM.

1.5.2 Basicity of Oxygen sites

The two main accessible oxygen atoms in POM structure are the bridging M-O-M and the terminal M=O sites. In some cases, for example the Anderson and Preyssler anions, internal oxygens bonded to the heterometal (X-O-M) are accessible and studies have shown that they are the most basic ones. Theoretical calculations on the relative basicity of the oxo-site[39] in $[Mo_6O_{19}]^{2-}$ have been analysed and the studies showed that protonation at the Mo-O-Mo is the favoured one. In another report studies were conducted to investigate the most basic oxo-sites in $[V_{10}O_{28}]^{6-}$ and it was showed by ^{17}O NMR spectroscopy that the protonation site is at M-O-M which was considered to be the most basic sites.[40] Some aspect in this present studies were based on the investigation of the basicity of oxygen sites in POM which will be discussed in detailed in a separate chapter.

1.5.3 The Lindqvist structure

The Lindqvist-type POMs $[M_6O_{19}]^{n-}$ are the smallest and most symmetrical (O_h symmetry) structural types. The $[M_6O_{19}]^{n-}$ type of POMs and their derivatives are attractive because of solution reactivity studies. They consist of six edge-sharing octahedra with six terminal oxo ligands (O_T) as labelled in Figure 1.2, twelve μ_2 bridging oxygens (OM_{2B}) (O_B) and a unique central μ_6 oxygen atom (OM_6) (O_C) shared between all six metal centres. The synthesis of the highly charged anions $[M_6O_{19}]^{8-}$ derived from M_2O_5 (M = Nb, Ta) requires strongly alkaline solutions. The $[Nb_6O_{19}]^{8-}$ was the first member of this family and was structurally characterized by Lindqvist in 1953.[41]These niobates and tantalates are usually studied in aqueous

solution as alkali metal salts, but the tetra-alkylammonium salts will dissolve in organic solvents.[42]

Significant effort has been made in recent years to carry out detailed studies of niobates and tantalates, aided by milder and more convenient synthetic routes.[43] Although the hexavanadate $[V_6O_{19}]^{8-}$ has not been isolated, alkoxido derivatives $[V_6O_{19-x}(OR)_x]^{n-}$, including partially reduced species, have been characterized.[44]

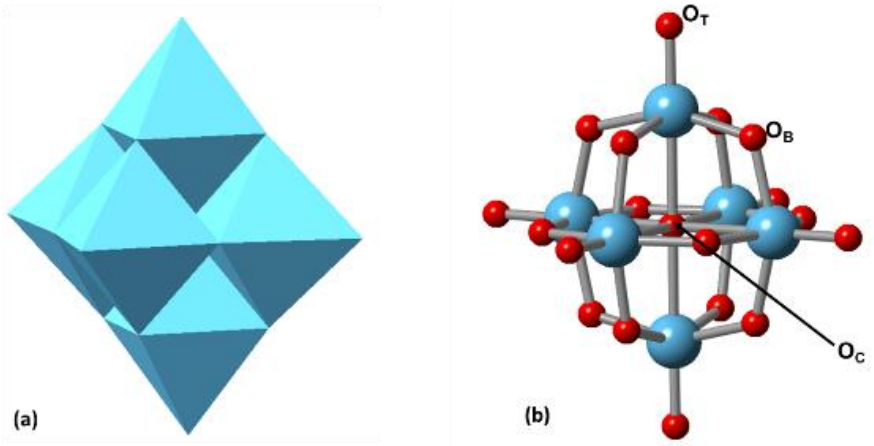

Figure 1.2: *Representation of the Lindqvist-type hexametalate structure (a) Polyhedral representation and (b) Ball and stick representation; oxygen (red), metal (royal blue); O_T, terminal oxygens; O_B, bridging OM_2 oxygens and O_C, central OM_6 oxygens*

Amongst the Lindqvist-type structures the most commonly studied members have been the group 6 metals mostly Mo and W, which may be obtained by acidification of $[MO_4]^{2-}$ in organic solvents,[45] and by alkaline hydrolysis of $MO(OR)_4$ in organic solvents.[46] The hexamolybdate and hexatungstate isopolyanions have been isolated and structurally characterized.[6,47] in addition other structurally characterized Lindqvist-type POMs containing other metals have also been reported.[35,48,49]

In terms of reactivity, the hexatungstate is comparatively rather inert, whereas the hexamolybdate is more labile thus allowing framework derivatisation by replacement of one or more of the oxido ligands by Mo–N multiply-bonded nitrogenous ligands such as organoimido NAr ligands.[2,50-52] The introduction of heterometal and associated ligands $\{M'L\}^{z+}$ to give substituted anions $[(LM')_xM_{6-x}O_{19-x}]^{n-}$ provides an alternative means of introducing reactive sites into these Lindqvist hexametalates. This approach to fine-tune these anions has enabled the design of mixed-addenda Lindqvist-type POMs $[H_2V_2W_4O_{19}]^{2-}.4H_2O$,[53] the sodium salt of $[ErW_{10}O_{36}]^{9-}$.[54]

1.5.4 The Keggin Structure

The Keggin heteropolyanions are among the most important classes of POMs with the general formula; $[XM_{12}O_{40}]^{n-}$ [M = Mo (VI) or W (VI)]. The Keggin structure as

mentioned above was first proposed in 1922 by Pauling[26] and confirmed by Keggin in 1933 as $[PW_{12}O_{40}]^{3-}$,[55] by X-ray diffraction. The 12 metal atoms (M = V, Nb, Ta, Mo or W) are arranged around one single heteroatom (X = P, As, Si Ge etc.) which constitute a Keggin based POM. The arrangement of different M-O-M (μ_2-O) bridging angles associated with edge- and corner-sharing in which 4 of $[W_3O_{13}]$ units linked by edge-shared and joined by $[W_3O_{10}]_4$ through corner-shared form the polyhedral structural representation (Figure 1.3).

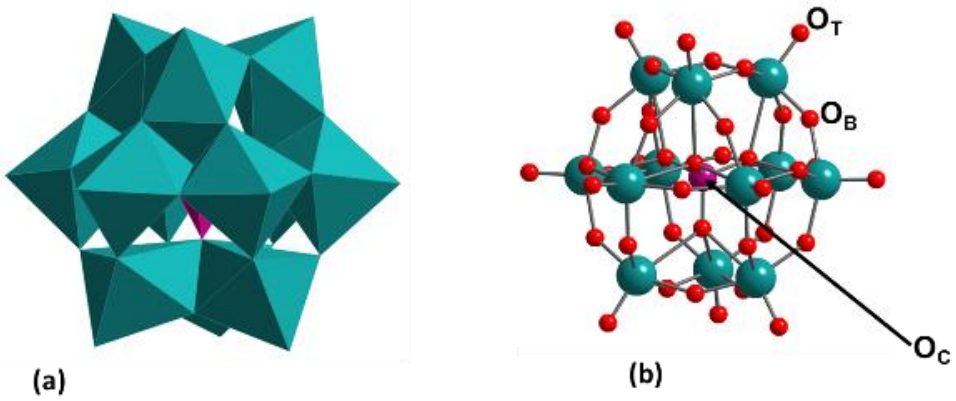

Figure 1.3: *Representation of the Keggin structure (a) Polyhedral and (b) ball and stick model; oxygen (red), metal (royal blue), central heteroatom (purple).*

The Keggin structure can exist in five different isomeric forms (Figure 1.4) and the isomers are obtained by rotation of one or more of the M_3O_{13} unit through 60° about the C_3 axes. The first isomer (α-isomer) [56,57] which is the most stable isomer has a T_d symmetry while the second isomer (β-isomer)[56] with C_{3v} symmetry is observed when there is a 60° rotation of one of the four M_3O_{13} groups about the C_3 axes of the T_d symmetry. The third isomer (γ-isomer)[58] has C_{2v} symmetry observed when two of the four M_3O_{13} groups are rotated by 60° and the fourth isomer is obtained by rotating three of the four M_3O_{13} groups by 60°, resulting in the δ isomer with C_{3v} symmetry. The fifth isomer (ε-isomer)[59] is observed when all of the M_3O_{13} groups are rotated by 60° and it has T_d symmetry.

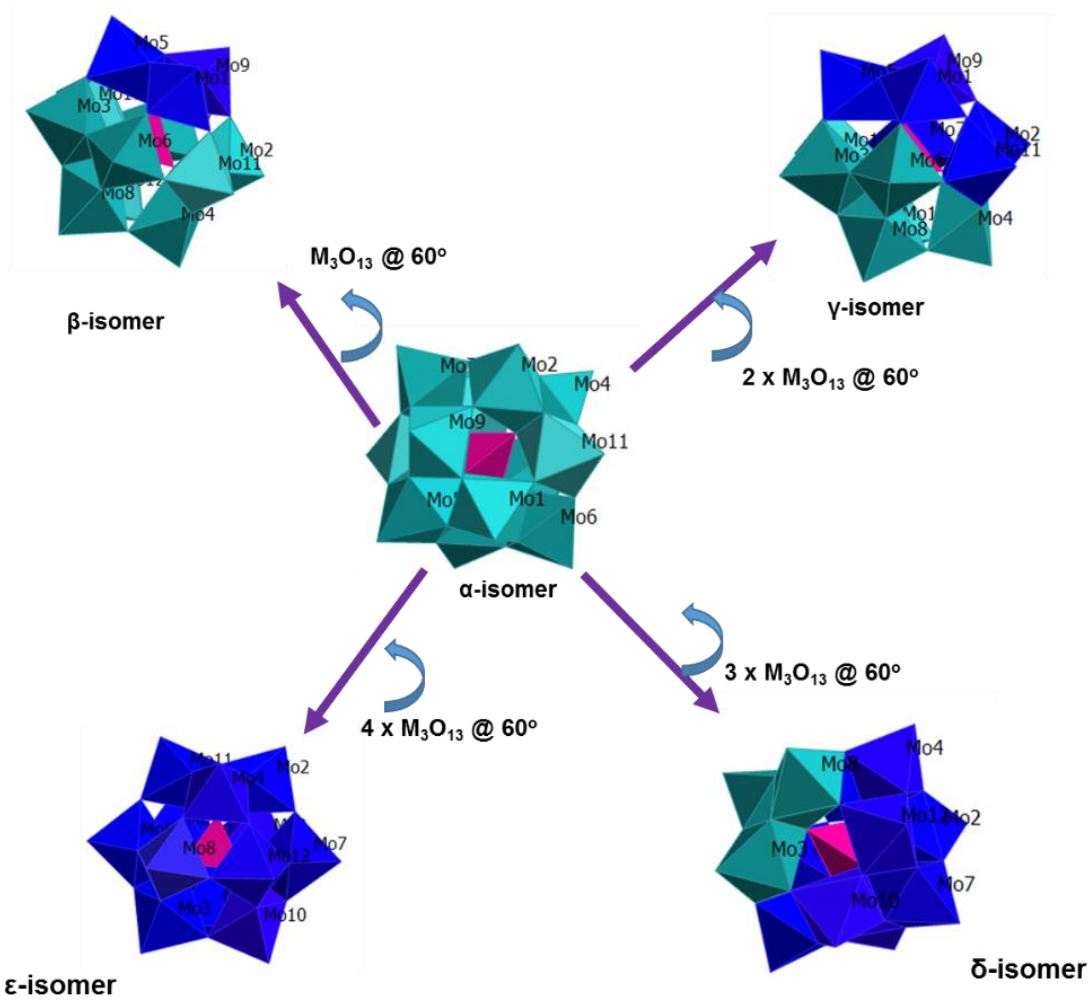

Figure 1.4: *Polyhedral Representation of the five isomers of the Keggin anion*

1.5.5 The Wells-Dawson structure

The Dawson POM represented as $[X_2M_{18}O_{64}]^{p-}$ was reported over a century ago, the structure is obtain from two lacunary $\{XM_9\}^5$ Keggin monomers $[XM_9O_{34}]^{p-}$ and are bound together by six equatorial oxo ligands. Souchay in 1947 reported the dimeric structure of Dawson by demonstrating that the X/M = 1/9 in each half of the dimer. In the Dawson structure there are two structural arrangements (i) the dimetallic (M_2O_{10}) groups arrangement resulting from condensation of two MO_6 octahedra units of which the centres occupied by metal atoms and the vertices by oxygen atoms and (ii) by trimetallic groups (M_3O_{13}) which result from linking three octahedra MO_6 as in the Keggin structure. Each of the trimetallic group is connected to the heteroatom, X and the two $[XW_9O_{34}]^{p-}$ fragments are connected together through M-(μ-O)-M bridges as shown in Figure 1.5.

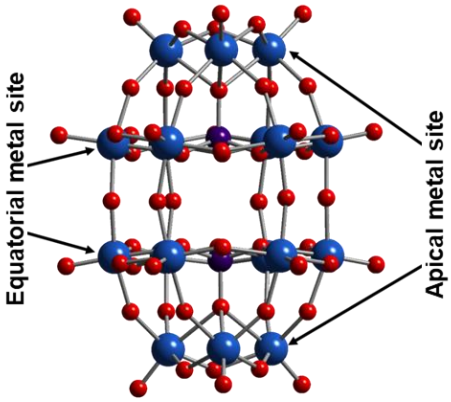

Figure 1.5: *Representation of ball and stick Wells-Dawson POM; oxygen (red), metal (royal blue), central heteroatom (purple).*

The Wells-Dawson POMs can be represented in six isomeric forms i.e. as α, β, γ, α*, β* and γ* first reported by Constant and Thouvenot.[60] The α isomer has D_{3h} symmetry while the β isomer results from rotation of one M_3 cap by 60° to give overall C_{3v} symmetry due to the loss of the symmetry plane. The third isomer, γ is observed when D_{3h} symmetry is restored, by rotation of the second M_3 cap around the C_3 symmetry axis by 60°. The isomers α*(D_{3d}), β*(C_{3v}) and γ*(D_{3d}) are formed by rotating one XM_9 unit by 180° with an inversion centre between the two $XW_9O_{34}^{z-}$ units.[60]

1.5.6 Other types of POMs

Besides the Lindqvist, Keggin or Dawson POMs mentioned above, other types of POMs (Figure 1.6) including the Anderson-Evans $[TeW_6O_{24}]^{6-}$, Strandberg $[P_2Mo_5O_{23}]^{6-}$ and the Preyssler structure $[P_5W_{30}O_{110}]^{15-}$ can be obtained by systematic manipulation of some specific parameters e.g. concentration, temperature or pH of the reaction.

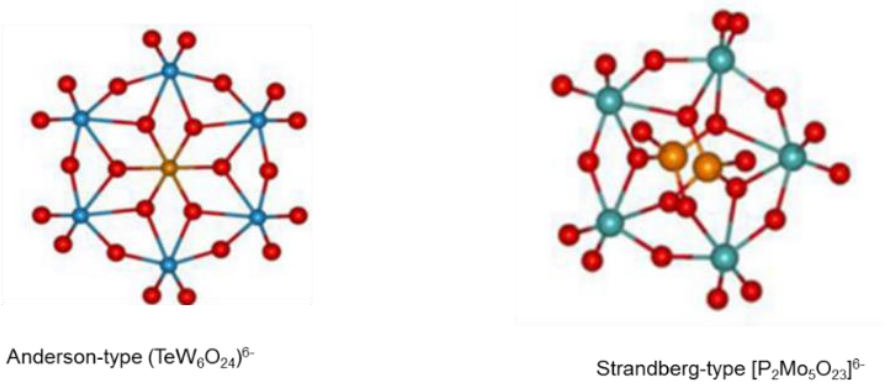

Figure 1.6: *Ball and stick representation of Anderson-type $(TeW_6O_{24})^{6-}$ Strandberg-type $[P_2Mo_5O_{23}]^{6-}$ structure.*[61]

1.6 Convergence of Polyoxometalate and metal oxide chemistry

Interest in POM chemistry has been expanding in recent years mainly because of the structural features of POMs. POM framework provides the basis for systematic manipulation of the composition within the metal oxide structure. Metal alkoxides (Mx(OR)y can be related to molecular compounds referred to as alkylated metal oxides.[62,63] their solubility in organic solvent and sensitivity towards hydrolysis provides the basis for the extensive use of metal alkoxides as precursors in the "sol-gel" processes.[64-66] In the non-aqueous synthesis of POMs, tungsten oxoalkoxides $WO(OR)_4$ are often used as precursors they are soluble in organic solvents and provide a non-aqueous source of WO_3 in solution . The W(VI) in these compounds is considered to be Lewis acidic and, with less bulky R groups, reactions may result in dimerization through the formation of OR bridges. Alkylated POMs (i.e. alkoxido substituted species), have been greatly expanded since Knoth's initial work on the O-alkylation of $[Mo_{12}PO_{40}]^{3-}$ and $[W_{12}PO_{40}]^{3-}$[67] and those with multidentate alkoxido ligands have received greater attention in recent years as versatile POM-organic hybrids.[68-70]

1.7 Characterisation Techniques

1.7.1 Nuclear Magnetic Resonance (NMR)

The formation and reactivity studies of POMs in solution is often complex and to obtain accurate information about solution reactivity, structural analysis, motions, and interactions between intermediates required techniques that can relay precise information without perturbing the system. One such technique is Nuclear Magnetic Resonance (NMR) spectroscopy. The development of ^{17}O NMR spectroscopy began in 1965 by two independent investigations on the $Cr_2O_7^{2-}$ anion.[71,72] Poor sensitivity of the technique resulting from the low natural abundance of ^{17}O nucleus (0.0373 %) the active I = 5/2 hindered the application of this technique. With the development of Fourier Transform NMR (FT-NMR) spectroscopy in the mid 1970's application of the technique in POM chemistry became prominent and spectral assignments were reported for a range of polyoxomelates such as polyvanadates, polyniobates, polytantalates, polymolybdates and polytungstates.[73-76]

A new era for POM chemistry began with the use of organic solvents for their synthesis and subsequent reactivity studies.[77-79] Despite the low natural abundance

of oxygen nucleus, detailed studies of solution reactivity is within reach for ^{17}O-enriched compounds.[73,75,80] Although oxygen is among the most important elements chemically and biologically, other nuclei such as ^{1}H, ^{13}C, ^{31}P or even ^{183}W have been prevalent in NMR studies of polyoxometalates.

The chemical shift (δ) of ^{17}O NMR signals are often difficult to determine accurately compared with ^{1}H or ^{13}C due to the relaxation time and the nuclear quadrupolar interaction which is often much larger than the magnetic shielding interaction, causing significant line broadening in ^{17}O NMR spectra.[81,82] Klemperer and co-workers carried out systematic study on ^{17}O NMR parameters of POMs structures, wherein they determined the relationship between chemical shift and the nature of metal–oxygen bond,[74] therefore ^{17}O NMR spectroscopy has been used to identify the oxygens in the different oxygen environment in POMs or POM-based compounds.

1.7.2 FT-IR Spectroscopy

Fourier Transform infrared (FTIR) spectroscopy is a form of vibrational spectroscopy that is useful to determine the structures of molecules based on the molecules' characteristic absorption of infrared radiation. In this technique, the sample is exposed to infrared radiation, and the sample molecules selectively absorb radiation of specific wavelengths causing a change of dipole moment of sample molecules. Consequently, the vibrational energy levels of sample molecules changes from ground state to excited state and the frequency of the absorption is determined by the vibrational energy gap. As molecular vibrations are related to the symmetry of molecules it is therefore possible to determine the existing bonding within the molecule or how a molecule is bonded on surfaces or as a component in a solid phase from its infrared spectrum.[83,84] The framework of POMs consist of metal oxygen bonds and therefore the difference in dipole moment provide specific metal-oxygen stretching frequencies and the most characteristic region of POM spectrum range between ca. 1000 – 400 cm^{-1} where these absorptions due to metal-oxygen stretching vibrations are observed.[63] The methods normally used in FT-IR spectroscopy are transmission and reflectance. The attenuated total reflectance (ATR) which is based on the principle of total internal reflection was used in sample analysis for this thesis.

1.8 Derivatised Lindqvist-type POMs based on W or Mo

The replacement of metal atom (addenda atom) with another atom in POM framework without distorting the framework is one of the unique properties of POMs and has led

to new redox and acid/base properties. For example when one or few $M^{6+}O$ (M =W, Mo) units are remove by replacing it with different metal atom can in some cases have a profound electronic effect on the resulting structure,[85] report shows that replacement of atom can affect the redox properties of the resulting molecule.[86-89] Bridgeman and co-workers conducted some theoretical studies on the bonding and atomic properties in $[M'M_5O_{19}]^{n-}$ (n = 3, M′ = V, Nb, Ta; M = Mo, n = 2 and M′ = M = W, Mo) which has been reported.[90]

1.8.1 Substituted polytungstates

As mentioned above the replacement of one or more addenda metal in POM framework can introduce interesting chemical properties for example different redox properties, different surface nucleophilicity etc. DFT modelling shows that the Keggin trisubstituted $[SiW_9M_3O_{40}]^{n-}$ anions [M = V, Nb, Mo] shows a remarkable chemical effect of substitution.[91] In some cases organic functionalization of POM framework with metal elements such as (V^{5+}, Nb^{5+}, Ti^{4+}) have shown to lead to new electronic properties of the resulting POM.[92] H. N. Miras, and co-workers have also shown by DFT calculation that metal replacement in the Well-Dawson and Preyssler compounds has a significant effect on the charge, basicity and the HOMO-LUMO gap in particular if a more negative V^{5+} is incorporated in the polar region.[93] In the Lindqvist type POMs Errington and co-workers have been able to in cooperate metal alkoxides by the removal of W atom in the presence of an organic-soluble oxoanion providing access to heterometallic {M′M_5} Lindqvist species containing reactive M′–OR bonds.[35,94,95] The introduction of these M′–OR bond have shown to have significant effect on the resulting POMs.

1.8.2 M(IV)-substituted tungstates $(TBA)_3[(RO)MW_5O_{18}]$

In the non-aqueous synthetic route to POMs, the nature of the alkoxido groups is significantly important, as they affect the degree of association of the alkoxide precursors and hence the dynamics and kinetics of the reaction. Typical heterometal alkoxide precursors previously used include $[\{Ti(OMe)_4\}_4]$, $[\{Zr(O^iPr)_3(\mu\text{-}O^nPr)(HO^iPr)\}_2]$[96] and $[Sn(O^tBu)_4]$.[97] In the process of dissociating the oligomeric structures, MOW bonds are generated which initiate ligand redistribution.[98] Heating the solution with $(TBA)_2[WO_4]$ and $[\{WO(OMe)_4\}_2]$ and subsequent hydrolysis can result in the aggregation of $[(RO)MW_5O_{18}]^{3-}$ anions and the structurally characterized

monomeric anions $[(MeO)TiW_5O_{18}]^{3-}$,[35] $[(MeO)SnW_5O_{18}]^{3-}$ [85] and $[(\mu\text{-}MeO)(ZrW_5O_{18})_2]^{6-}$ have been reported.[94]

1.8.3 Molybdate derivatives POMs

Polyoxomolybdates are more labile than the polyoxotungestate but the mixed addenda polyoxomolybdates are less common probably due to their inherent low stability. A few studies on the replacements of one or more of the Mo atoms show diversity of structures and electronic properties. Kortz and co-workers prepared hexamolybopyrophosphate $[(O_3POPO_3)Mo_6O_{18}(H_2O)_4]^{4-}$,[99] and they showed that the dimeric $[\{(P_2O_7)Mo_{15}O_{45}]^{8-}$ has a remarkable structural properties.[100] Those functionalized with organic groups for example have shown to present interesting properties. Derivatives of $[Mo_6O_{19}]^{2-}$ for example substituted titanomolybdates $(TBA)_3[(RO)TiMo_5O_{18}]$ have been reported,[101] although preparation of the molybdenum oxoalkoxide $MoO(OMe)_4$ is not as straightforward as its tungsten analogue.[102] Theoretical analysis of some of the organic functionalized structures suggest that the organic moieties have an effect on the spectroscopic properties of the parent POM typically some participation in the frontier orbitals of the POM.[103,104]

1.8.4 Vanadate and Niobate

Although they are quite limited in numbers compared to the tungstate and molydbates counterparts a number of families based upon NbOx and VOx blocks have been reported for example the vanadotellurate $[HxTeV_9O_{28}]^{(5-x)-}$[105] (x = 1, 2). The mixed addenda polyoxoniobotitanate $[Nb_8Ti_2O_{28}]^{8-}$ have been reported.[106] Interest in this mixed addenda compound arises from the uncommon combination of Nb and Ti addenda metals.

1.9 Halide-substituted Polyoxometalates

Polyoxometalates containing halide ligands are important in that they potentially provide access to a range of organometallic compounds. The Keggin-type anions $(TBA)_4[ClTiPW_{11}O_{39}]$, $(TBA)_4[ClSnPW_{11}O_{39}]$ and $(TBA)_4[ClAlPW_{11}O_{39}H]$ have been described,[107] but similar Lindqvist-type derivatives have not been previously successfully isolated. A previous report by the Errington group indicate that a 'virtual' $[W_5O_{18}]^{6-}$ precursor provided a suitable route to access the chlorido species $(TBA)_3[ClTiW_5O_{18}]$.[52,108,109] The same group have used Me_3SiCl as a chlorinating agent

for conversion of $(TBA)_3[(MeO)TiW_5O_{18}]$ to $(TBA)_3[ClTiW_5O_{18}]$ anion. The tin analogue $(TBA)_3[(MeO)SnW_5O_{18}]$ is much more sensitive to chloride and reaction with Me_3SiCl readily forms $(TBA)_3[ClSnW_5O_{18}]$.

1.10 Ligand metathesis in Polyoxometalates

It is well established that the ease with which alkoxido ligands are exchanged in alcoholysis reactions are related to the steric bulk of the alkoxido group bonded to the metal, which disfavours methoxido ligand exchange. The Errington group has explored reactions involving the treatment of the $\{(MeO)M'M_5\}$ POMs with an excess of primary, secondary or tertiary alcohols and were able to afford the desired ligand-exchanged products.[101]

Errington and co-workers have also explored reactions with protic reagents HX where the anion X^- acts as a ligand towards the heterometal M′, to provide straightforward access to derivatives $[XM'M_5O_{18}]^{n-}$.The resulting families of POMs provide insight into bonding variations.[94,95,101] Table 1.1 shows some $\{LM'M_5\}$ Lindqvist anions obtained by protonolysis of $\{(RO)M'M_5\}$ species.

Table 1.1: *{LM'M5} Lindqvist anions obtained by protonolysis of {(RO)M'M$_5$} species.* [94, 95, 101]

Structure type	{M'M$_5$}	L
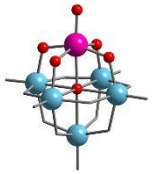	{TiW$_5$}[35]	OH, OMe, OEt, O^{i}Pr, O^{t}Bu OPh, OC$_6$H$_4$Me-4, OC$_6$H$_4$^{t}Bu-4, OC$_6$H$_4$OH-4 OC$_6$H$_4$OH-3, OC$_6$H$_3$(OH)$_2$-3,5, OC$_6$H$_4$CHO-2
	(ZrW$_5$)[94]	OPh, OC$_6$H$_4$Me-4, OC$_6$H$_4$CHO-2
	(SnW$_5$)[85]	OH, OMe, OEt, O^{i}Pr, O^{t}Bu OPh, OC$_6$H$_4$Me-4, OC$_6$H$_4$^{t}Bu-4, OC$_6$H$_4$OH-4 OC$_6$H$_4$OH-3, OC$_6$H$_4$CHO-2
	(TiMo$_5$)[101]	OMe, O^{i}Pr, O^{i}Bu, O^{t}Bu OC$_6$H$_4$Me-4, OC$_6$H$_4$CHO-2
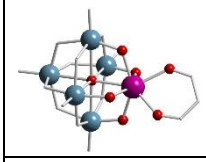	(ZrW$_5$)[94]	OAc, acac, OC$_6$H$_4$CHO-2
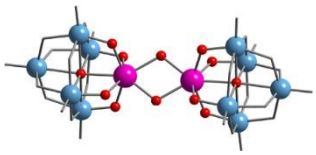	(ZrW$_5$)[94]	OH, OMe,
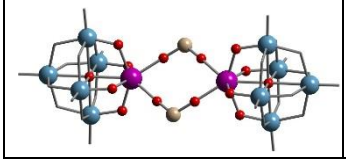	(ZrW$_5$)[94]	O$_2$PPh$_2$

1.11 Applications of POMs

1.11.1 Polyoxometalates in Catalysis

The Lewis acidic nature of POMs and their ability to form peroxo and hydroperoxo species have provided the opportunities to use POMs in oxidation catalysis including selective oxidation with molecular oxygen and H_2O_2. POMs have shown higher activities in acid catalysis and also serve as well-defined molecular models for mechanistic properties of POM-based catalysis reaction.

Polyoxotungstates are known to be efficient oxidation catalysts because of the ability to transfer oxygen atom. Series of polyoxotungstates have been investigated in terms of their homogenous and heterogeneous catalytic properties. The Keggin-type POMs are amongst the most widely investigated POMs as catalyst in a range of catalytic processes.[110-112] recent report suggest that the Keggin-type Ti-monosubstituted POM

$[PTi(OH)W_{11}O_{39}]^{4-}$ and the Ti-disubstituted sandwich-type POM $[Ti_2(OH)_2As_2W_{19}O_{67}(H_2O)]^{8-}$ were efficient in the epoxidation of alkenes using H_2O_2. In addition the Ti-disubstituted sandwich-type POM $[Ti_2(OH)_2As_2W_{19}O_{67}(H_2O)]^{8-}$, with a five-coordinated Ti environment, displayed better activity and selectivity for epoxide than the Ti-monosubstituted $[PTi(OH)W_{11}O_{39}]^{4-}$, with a six-coordinated Ti-atom environment.[110-112]

In another investigation it was revealed that protonated $[PTi(OH)W_{11}O_{39}]^{4-}$ greatly improved the activity and selectivity of alkene oxidation.[113,114] Recently, silanol-decorated modified Keggin-type POMs $[PW_{10}O_{36}(^tBuSiO)_2VO(^iPrO)]^{3-}$,[36] with site isolated V^{5+}, demonstrated a catalytic behaviour in the epoxidation of allylic alcohol. Furthermore In recent studies a series of Keggin-type POMs ($H_5[PMo_{10}V_2O_{40}]$, ($H_4[PMo_{11}VO_{40}]$, $H_4[SiMo_{12}O_{40}]$, ($H_3[PMo_{12}O_{40}]$ and ($HNa_2[PW_{12}O_{40}]$ was shown to provide efficient catalysts for various organic reactions, particularly in acetylation of alcohols and phenols with acetic anhydride.[115] Also Mizuno and co-workers reported the Keggin-type POM $(TBA)_4[\gamma\text{-}HPV_2W_{10}O_{40}]$ (TBA= tetra-n- butylammonium) which has been used for H_2O_2 based oxidative bromination of alkanes, alkenes and aromatic compounds.[116]

1.11.2 Biological and Medicinal applications of Polyoxometalates

The biological and pharmacological importance of POMs was established in the 1970's by early contributors when it was noted that polytungstosilicate heteropoly compounds inhibited murine leukemia sarcoma (MLSV). Raynaud and others suggest that biological activities of POM are likely to depend upon interactions between POMs and bio macromolecules like proteins. In 1998, a review published on polyoxometalates in medicine showed series of polytungstosilicate compounds to show efficiency in inhibitory or antiviral activity example $[A\text{-}\alpha\text{-}SiNb_3W_9O_{40}]^{7-}$, $[SiTaW_{11}O_{40}]^{5-}$ $[SiNbW_{11}O_{40}]^{5-}$.[117,118]

1.11.3 Polyoxometalates in Sensors

The technological importance of sensors is attracting growing interest in recent research and in particular in POM chemistry. One of the fundamental properties of POMs is their ability to undergo redox processes providing the capability to release or accept multiple electrons without perturbing the POM framework. Recent reports suggest that POM based materials can been used for building membrane based

devices and sensors,[119] gas detection devices, solid state electro chromic devices,[15] and also in selective electrode.[10] Xu *et al*. reported the fabricated multiple coloured "reversible" photochromic composite film using the Dawson type POM [P_2W_{18}].[120] Furthermore, recent investigations suggested that Pt- based functionalized POM show a good selectivity and stability when applied as sensor in the detection of herbicides in wastewater samples.[121]

1.12 Conclusion

In this chapter a detailed outline of the thesis content has been described and also highlighted the interest in non-aqueous studies of POMs. An extensive review on literature have also been presented and gave some fundamental historical background of this branch of chemistry. In addition, some important applications of these class of compounds in today's technological advances are also highlighted which is the crucial area of investigation in this project. Additionally, some recent developments in POM functionalization and the applications of these POM-derived materials are reviewed.

References

1. M. T. Pope, *Heteropoly and Isopoly Oxometalates*, Springer-Verlag, 1983.
2. M. Pope and A. Müller, *Polyoxometalates: From Platonic Solids to Anti-Retroviral Activity*, Springer Netherlands, 1994.
3. D. E. Katsoulis, *Chem. Rev.*, 1998, **98**, 359-388.
4. R. Neumann and A. M. Khenkin, *Inorg. Chem.*, 1995, **34**, 5753-5760.
5. Y. F. Song, *Polyoxometalate-Based Assemblies and Functional Materials*, Springer International Publishing, 2018.
6. J. Fuchs, W. Freiwald and H. Hartl. (1978). *Acta Cryst. B* **34**, 1764-1770.
7. V. W. Day and W. G. Klemperer, *Science*, **228**, 533 (1985).
8. M. T. Pope and A. Müller, *Polyoxometalates: From Platonic Solids to Anti-Retroviral Activity*, Springer Netherlands, 2012.
9. P. Souchay., *Polyanions and polycations*, Paris, Gauthier-Villars, 1963.
10. M. Ammam, *J. Mater. Chem. A*, 2013, **1**, 6291-6312.
11. I. V. Kozhevnikov, *Chem. Rev.*, 1998, **98**, 171-198.
12. Y. V. Geletii, Q. Yin, Y. Hou, Z. Huang, H. Ma, J. Song, C. Besson, Z. Luo, R. Cao, K. P. O'Halloran, G. Zhu, C. Zhao, J. W. Vickers, Y. Ding, S. Mohebbi, A. E. Kuznetsov, D. G. Musaev, T. Lian and C. L. Hill, *Israel J. Chem.*, 2011, **51**, 238-246.
13. B. Hasenknopf, *Front.biosci:*, 2005, **10**, 275-287.
14. C. E. Müller, J. Iqbal, Y. Baqi, H. Zimmermann, A. Röllich and H. Stephan, *Bioorg. Med. Chem. Lett*, 2006, **16**, 5943-5947.
15. M. Sadakane and E. Steckhan, *Chem. Rev.*, 1998, **98**, 219-238.
16. H. Wang, S. Hamanaka, Y. Nishimoto, S. Irle, T. Yokoyama, H. Yoshikawa and K. Awaga, *J. Am. Chem. Soc.*, 2012, **134**, 4918-4924.
17. M. T. Pope and A. Müller, *Angew. Chemie Int. Ed. Eng.*, 1991, **30**, 34-48.
18. E. Coronado and C. J. Gómez-García, *Chem. Rev.*, 1998, **98**, 273-296.
19. D.-Y. Du, J.-S. Qin, S.-L. Li, Z.-M. Su and Y.-Q. Lan, *Chem. Soc. Rev.*, 2014, **43**, 4615-4632.
20. J. J. Berzelius, *Annalen Physik*, 1826, **82**, 369-392.
21. J. F. Keggin, *Nature*, 1933, **132**, 351.
22. N. Anwar, M. Vagin, F. Laffir, G. Armstrong, C. Dickinson and T. McCormac, *Analyst*, 2012, **137**, 624-630.

23. P. Judeinstein, P. W. Oliveira, H. Krug and H. Schmidt, *Chem. Phys.Lett.*, 1994, **220**, 35-39.
24. A. Müller and C. Serain, *Chem. Research*, 2000, **33**, 2-10.
25. C. W. Scheele and S. F. Hembstadt, Niederwalluf bei Wiesbaden, 1971.
26. L. Pauling, *J. Am.Chem. Soc.*, 1929, **51**, 2868-2880.
27. M. Eckert, Acta Cryst. (2012). **227**, 27.
28. W. L. Bragg, *Nature*, 1912, **90**, 410-410.
29. J. F. Keggin and B. William Lawrence, *Pro. Royal Soc. A London. (*1934). **144**, 75-100.
30. H. T. Evans, *J. Am. Chem. Soc.*, 1948, **70**, 1291-1292.
31. B. Dawson, *Acta Cryst.* (1953). **6**, 113-126.
32. M. Kunz and I. D. Brown, *J.Solid State Chem.*,**115**, (1995). 395-406.
33. L. Vilà-Nadal, A. Rodríguez-Fortea and J. M. Poblet, *Eur. J. Inorg.Chem.*, 2009, **2009**, 5125-5133.
34. *Inorg. Synthes.*, pp. 74-85.
35. W. Clegg, M. R. J. Elsegood, R. J. Errington and J. Havelock, *J.Chem.Soc., Dalton Trans.*, 1996, 681-690.
36. G. Guillemot, E. Matricardi, L.-M. Chamoreau, R. Thouvenot and A. Proust, *ACS Catalysis*, 2015, **5**, 7415-7423.
37. S. Bordiga, E. Groppo, G. Agostini, J. A. van Bokhoven and C. Lamberti, *Chem. Rev.*, 2013, **113**, 1736-1850.
38. S. Gatard, S. Blanchard, B. Schollhorn, P. Gouzerh, A. Proust and K. Boubekeur, *Eur. J.*, 2010, **16**, 8390-8399.
39. A. Dolbecq, A. Guirauden, M. Fourmigué, K. Boubekeur, P. Batail, M.-M. Rohmer, M. Bénard, C. Coulon, M. Sallé and P. Blanchard, *J. Chem. Soc., Dalton Trans.*, 1999, 1241-1248.
40. J. Y. Kempf, M. M. Rohmer, J. M. Poblet, C. Bo and M. Benard, *J.Am. Chem. Soc.*, 1992, **114**, 1136-1146.
41. I. Lindqvist, *Acta Cryst*, **3**, (1950). 159-160.
42. W. G. Klemperer and K. A. Marek, *Eur J Inorg Chem*, 2013, **2013**, 1762-1771.
43. M. Nyman, *Dalton Trans.*, 2011, **40**, 8049-8058.
44. C. Daniel and H. Hartl, *J. Am. Chem. Soc.*, 2009, **131**, 5101-5114.
45. C. Sanchez, J. Livage, J. P. Launay and M. Fournier, *J. Am. Chem. Soc.*, 1983, **105**, 6817-6823.

46. K. F. Jahr, J. Fuchs and R. Oberhauser, *Chemische Berichte*, 1968, **101**, 477-481.
47. W. Clegg, G. M. Sheldrick, C. D. Garner and I. B. Walton, *Acta Cryst.*(1982). **38** *B*, 2906-2909.
48. G. A. Seisenbaeva, T. Mallah and V. G. Kessler, *Dalton Trans.*, 2010, **39**, 7774-7779.
49. M. Maekawa, Y. Ozawa and A. Yagasaki, *Inorg. Chem.*, 2006, **45**, 9608-9609.
50. T.-C. Hsieh and J. A. Zubieta, *Polyhedron*, 1986, **5**, 1655-1657.
51. H. Kang and J. Zubieta, *J. Chem. Soc., Chem. Commun.*, 1988, 1192-1193.
52. J. J. Borrás-Almenar, E. Coronado, A. Müller and M. T. Pope, *Polyoxometalate Molecular Science*, Springer Netherlands, 2012.
53. S. Yerra, S. R. Amanchi and S. K. Das, *J. Mole. Structure*, 2014, **1062**, 53-60.
54. M. A. AlDamen, J. M. Clemente-Juan, E. Coronado, C. Martí-Gastaldo and A. Gaita-Ariño, *J. Am. Chem. Soc.*, 2008, **130**, 8874-8875.
55. J. F. Keggin, *Nature*, 1933, **131**, 908-909.
56. W. A. Neiwert, J. J. Cowan, K. I. Hardcastle, C. L. Hill and I. A. Weinstock, *Inorg. Chem.*, 2002, **41**, 6950-6952.
57. G. Herve and A. Teze, *Inorg. Chem.*, 1977, **16**, 2115-2117.
58. A. Tézé, E. Cadot, V. Béreau and G. Hervé, *Inorg. Chem.*, 2001, **40**, 2000-2004.
59. P. Mialane, A. Dolbecq, L. Lisnard, A. Mallard, J. Marrot and F. Sécheresse, *Angew. Chemie Int. Ed.*, 2002, **41**, 2398-2401.
60. M. Ammam, *J. Mater. Chem.*, **1***A*, (2013). 6291-6312.
61. M. Carraro and S. Gross, *Mater.*, 2014, **7**, 3956-3989.
62. E. Weiß, *Angew. Chemie*, 1980, **92**, 975-975.
63. D. Bradley, R. C. Mehrotra, I. Rothwell and A. Singh, *Alkoxo and Aryloxo Derivatives of Metals*, Elsevier Science, 2001.
64. L. L. Hench and J. K. West, *Chem. Rev.*, 1990, **90**, 33-72.
65. J. Livage, M. Henry and C. Sanchez, *Pro. Solid State Chem.*, 1988, **18**, 259-341.
66. C. J. Brinker and G. W. Scherer, *Sol-Gel Science: The Physics and Chemistry of Sol-Gel Processing*, Elsevier Science, 2013.
67. W. H. Knoth and R. L. Harlow, *J. Am. Chem. Soc.*, 1981, **103**, 4265-4266.
68. Q. Chen and J. Zubieta, *Coord. Chem. Rev.*, 1992, **114**, 107-167.
69. M. I. Khan, Q. Chen, D. P. Goshorn and J. Zubieta, *Inorg. Chem.*, 1993, **32**, 672-680.

70. X. Hu, Z. Xiao, B. Huang, X. Hu, M. Cheng, X. Lin, P. Wu and Y. Wei, *Dalton Trans.*, 2017, **46**, 8505-8513.
71. J. A. Jackson and H. Taube, *J. Phy. Chem.*, 1965, **69**, 1844-1849.
72. B. N. Figgis, R. G. Kidd and R. S. Nyholm, *Canadian J. Chem.*, 1965, **43**, 145-153.
73. A. D. English, J. P. Jesson, W. G. Klemperer, T. Mamouneas, L. Messerle, W. Shum and A. Tramontano, *J. Am. Chem. Soc.*, 1975, **97**, 4785-4786.
74. M. Filowitz, R. K. C. Ho, W. G. Klemperer and W. Shum, *Inorg. Chem.*, 1979, **18**, 93-103.
75. M. Filowitz, W. G. Klemperer, L. Messerle and W. Shum, *J.Am. Chem.Soc.*, 1976, **98**, 2345-2346.
76. V. W. Day, M. F. Fredrich, W. G. Klemperer and W. Shum, *J. Am. Chem.Soc.*, 1977, **99**, 952-953.
77. P. T. Meiklejohn, M. T. Pope and R. A. Prados, *J. Am. Chem. Soc.*, 1974, **96**, 6779-6781.
78. R. K. C. Ho and W. G. Klemperer, *J. Am. Chem. Soc.*, 1978, **100**, 6772-6774.
79. D. E. Katsoulis and M. T. Pope, *J. Am. Chem. Soc.*, 1984, **106**, 2737-2738.
80. M. Filowitz and W. G. Klemperer, *J. Chem. Soc., Chem.Commun.*, 1976, 233-234.
81. J. H. Gardner and E. M. Purcell, *Physical Review*, 1949, **76**, 1262-1263.
82. E. M. Purcell, H. C. Torrey and R. V. Pound, *Physical Review*, 1946, **69**, 37-38.
83. R. White, *Chromatography/Fourier Transform Infrared Spectroscopy and its Applications*, Taylor & Francis, 1989.
84. W. L. Wolfe, G. J. Zissis and R. *Infrared Handbook*, 1978.
85. B. Kandasamy, C. Wills, W. McFarlane, W. Clegg, R. W. Harrington, A. Rodríguez-Fortea, J. M. Poblet, P. G. Bruce and R. J. Errington, *Eur. J.*, 2012, **18**, 59-62.
86. X. López, J. M. Maestre, C. Bo and J.-M. Poblet, *J. Am. Chem. Soc.*, 2001, **123**, 9571-9576.
87. J. M. Maestre, X. Lopez, C. Bo, J.-M. Poblet and N. Casañ-Pastor, *J. Am. Chem. Soc.*, 2001, **123**, 3749-3758.
88. M. Grabau, J. Forster, K. Heussner and C. Streb, *Eur. J. Inorg.Chem.*, 2011, **2011**, 1719-1724.
89. A. J. Bridgeman and G. Cavigliasso, *J. Phy. Chem. (*2003), **107***A*, 6613-6621.
90. A. J. Bridgeman and G. Cavigliasso, *Faraday Discussions*, 2003, **124**, 239-258.

91. X. López, J. J. Carbó, C. Bo and J. M. Poblet, *Chem. Soc. Rev.*, 2012, **41**, 7537-7571.
92. S. I. Yanling, C. Weilin, Z. Zhiming and W. Enbo, *J. Theoretical and Computational Chem.*, 2009, **08**, 773-781.
93. H. N. Miras, D. Stone, D.-L. Long, E. J. L. McInnes, P. Kögerler and L. Cronin, *Inorg. Chem.*, 2011, **50**, 8384-8391.
94. R. J. Errington, S. S. Petkar, P. S. Middleton, W. McFarlane, W. Clegg, R. A. Coxall and R. W. Harrington, *J. Am. Chem. Soc.*, 2007, **129**, 12181-12196.
95. R. J. Errington, S. S. Petkar, P. S. Middleton, W. McFarlane, W. Clegg, R. A. Coxall and R. W. Harrington, *Dalton Trans.s*, 2007, 5211-5222.
96. G. A. Seisenbaeva, S. Gohil and V. G. Kessler, *J. Mater. Chem.*, 2004, **14**, 3177-3190.
97. J. Caruso, T. M. Alam, M. J. Hampden-Smith, A. L. Rheingold and G. A. P. Yap, *J. Chem.Soc. Dalton Trans.*, 1996, 2659-2664.
98. R. J. Errington, M. D. Kerlogue and D. G. Richards, *J.Chem.Soc., Chem.Commun.*, 1993, 649-651.
99. U. Kortz, *Inorg. Chem.*, 2000, **39**, 625-626.
100. U. Kortz, *Inorg. Chem.*, 2000, **39**, 623-624.
101. L. Coyle, P. S. Middleton, C. J. Murphy, W. Clegg, R. W. Harrington and R. J. Errington, *Dalton Trans.*, 2012, **41**, 971-981.
102. V. G. Kessler, A. V. Mironov, N. Y. Turova, A. I. Yanovsky and Y. T. Struchkov, *Polyhedron*, 1993, **12**, 1573-1576.
103. L.-K. Yan, Z.-M. Su, W. Guan, M. Zhang, G.-H. Chen, L. Xu and E.-B. Wang, *J. Phy. Chem.* 2004, **108***B*, 17337-17343.
104. Q. Li, Y. Wei, H. Guo and C.-G. Zhan, *Inorganica Chimica Acta*, 2008, **361**, 2305-2313.
105. S. Konaka, Y. Ozawa, T. Shonaka, S. Watanabe and A. Yagasaki, *Inorg.Chem.*, 2011, **50**, 6183-6188.
106. M. Nyman, L. J. Criscenti, F. Bonhomme, M. A. Rodriguez and R. T. Cygan, *J. Solid State Chem.*, 2003, **176**, 111-119.
107. W. H. Knoth, P. J. Domaille and D. C. Roe, *Inorg. Chem.*, 1983, **22**, 198-201.
108. E. Constable, J. A. McCleverty and T. J. Meyer, *Comprehensive Coordination Chemistry II: From Biology to Nanotechnology*, Elsevier Science, 2003.
109. M. T. Pope, A. Mueller and Editors, *Polyoxometalate Chemistry From Topology via Self-Assembly to Applications*, Kluwer Academic Publishers, 2001.

110. O. A. Kholdeeva, B. G. Donoeva, T. A. Trubitsina, G. Al-Kadamany and U. Kortz, *Eur. J. Inorg.Chem.*, 2009, **2009**, 5134-5141.
111. O. A. Kholdeeva, T. A. Trubitsina, R. I. Maksimovskaya, A. V. Golovin, W. A. Neiwert, B. A. Kolesov, X. López and J. M. Poblet, *Inorg. Chem.*, 2004, **43**, 2284-2292.
112. O. A. Kholdeeva and O. V. Zalomaeva, *Coord. Chem. Rev.*, 2016, **306**, 302-330.
113. N. S. Antonova, J. J. Carbó, U. Kortz, O. A. Kholdeeva and J. M. Poblet, *J. Am.Chem. Soc.*, 2010, **132**, 7488-7497.
114. Q. Chen, C. Shen and L. He, *Acta Cryst.* (2018). **74***C*, 1182-1201.
115. M. Heravi, F. Behbahani and F. F. Bamoharram, *Acetylation of alcohols, phenols and salicylic acid by heteropoly acids in acetic anhydride: A green and eco-friendly protocol for synthesis of acetyl salicylic acid (Aspirin)*, 2007.
116. K. Yonehara, K. Kamata, K. Yamaguchi and N. Mizuno, *Chem.Commun.*, 2011, **47**, 1692-1694.
117. J. T. Rhule, C. L. Hill, D. A. Judd and R. F. Schinazi, *Chem. Rev.*, 1998, **98**, 327-358.
118. D. L. Barnard, C. L. Hill, T. Gage, J. E. Matheson, J. H. Huffman, R. W. Sidwell, M. I. Otto and R. F. Schinazi, *Antiviral research*, 1997, **34**, 27-37.
119. Y. Ji, L. Huang, J. Hu, C. Streb and Y.-F. Song, *Energy & Environmental Science*, 2015, **8**, 776-789.
120. L. Li, J.-R. Wang, Y. Hua, Y. Guo, C. Fu, Y.-N. Sun and H. Zhang, *J. Mater. Chem. (*2019). **7***C*, 38-42.
121. B. Ertan, T. Eren, İ. Ermiş, H. Saral, N. Atar and M. L. Yola, *J.Colloid and Interface Science*, 2016, **470**, 14-21.

Chapter 2

Hydrolytic Aggregation and Non-aqueous Degradation of $(TBA)_2[W_6O_{19}]$ – A Novel and Efficient Approach to a Series of heterometallic $\{M'M_5\}$ POMs

This chapter describes investigations into the non-aqueous stepwise aggregation of $(TBA)_2[W_6O_{19}]$ from $WO(OMe)_4$ and $(TBA)_2[WO_4]$ using ^{17}O NMR spectroscopy. The study has provided an in-depth understanding of the complex solution processes underlying molecular metal oxide aggregation and structural inter-conversion. Additionally, a new and efficient degradative synthetic route has been established which provides access to a series of heterometallic $\{M'M_5\}$ POMs from $[M_6O_{19}]^{2-}$ anions. The knowledge underpins the rational design and synthesis of families of related POMs.

2.1 Introduction

The group 5 and 6 metals are the most suitable metals in POMs formation. As mentioned earlier, these metals tends to future the octahedra metal centre and for the larger metals (**W and Mo**) prefer to expand their coordination through M(dπ) – O(pπ) interaction with neighbouring oxygens and that give more thermodynamic stability. These M-O bonds interactions often lead to linkage and form polynuclear species in solution, (Scheme 2.1) although these processes are often complex.

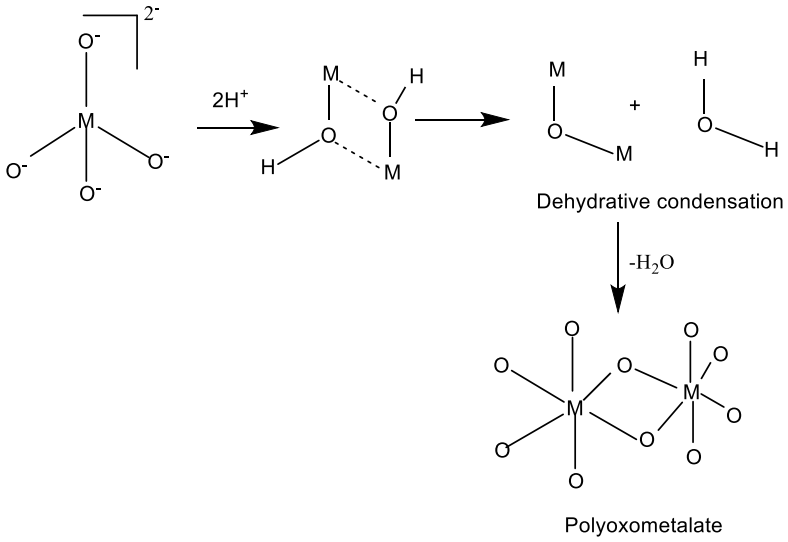

Scheme 2.1: *Formation of Polyoxometalates in solution (M = W, Mo).*

The mechanism of these aggregation processes in solution have not been fully understood although recent report shows two aggregation mechanisms based on fragments observed in CID-ESIMS spectra of acetonitrile solutions of $(TBA)_2[W_6O_{19}]$, and minimum energy structures were calculated for intermediates for W = 2 – 5 [1 2] In a follow-up paper, these intermediates were further investigated in aqueous solution under different pH conditions and the importance of interactions between solvent water and electrophilic tungsten centres was highlighted, whereby increased coordination number of the metal becomes more favourable at lower pH.

An independent investigation proposed similar mechanisms and intermediates and reached similar conclusions.[3] While these theoretical analyses provide valuable insights into the energetics of possible interconversion processes, they do not reflect the experimental observation that aqueous acidification of WO_4^{2-} produces $[H_2W_{12}O_{42}]^{10-}$ and $[W_7O_{24}]^{6-}$ as the dominant species rather than $[W_6O_{19}]^{2-}$.[4,5] This discrepancy is most likely because calculations were based on the fragment ions in

the ESI mass spectra from acetonitrile solutions of $(TBA)_2[W_6O_{19}]$, and probably the effects of counter-cation and solvent variation on speciation were neglected.

Interest in non-aqueous POMs formation is significantly important based on the greater control over the interconversion of intermediate species during the aggregation process. The intermediate polyoxoanions formed during the aggregation are expected to be more stable in organic solvent compared to reactions involving larger volume of H_2O whereby interactions between solvent water and electrophilic tungsten centres is a possibility and can results to different equilibria. Therefore, $[W_6O_{19}]^{2-}$ formation in reactions involving WO_4^{2-} and $WO(OMe)_4$ can be fully understood in non-aqueous route providing greater opportunity to access new POMs. Note that there are also some challenges associated with the non-aqueous media i.e. solvent viscosity and the low natural abundance of oxygen atom, however these challenges are overcome by using MeCN and ^{17}O-enriched H_2O the later provide a convenient way of monitoring the aggregation process in solution. These studies are significant because progress towards understanding these polymeric aggregations and their interconversion process is of great importance if the full potential of these versatile species is to be realized.

The monomeric oxometallate WO_4^{2-} are highly basic with the electron density residing on the oxygen atoms. In the aqueous acidification of WO_4^{2-}, various intermediates can be identified as mentioned above by varying the amount of H^+ per metal i.e. ratio of proton per metal described as (z/x) in (Figure 2.1).

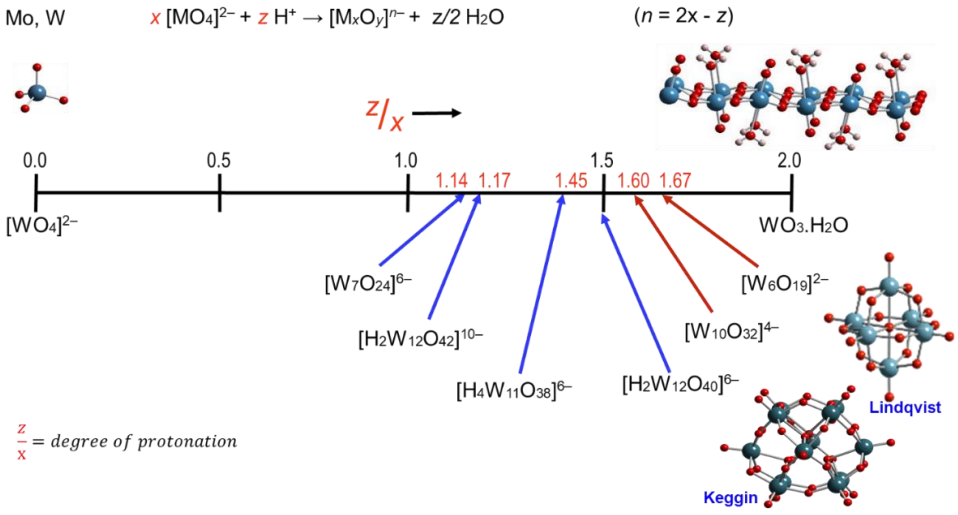

Figure 2.1: *Polytungstate formation upon increasing acidification of WO_4^{2-}*

The non-aqueous aggregation reactions in this early section of the chapter is essentially the reverse of the aqueous acidification reactions described above in Figure

2.1 but in this studies, the amount of the overall negative charge per metal is varied by adding more $WO(OMe)_4$ to WO_4^{2-} i.e. a decrease in overall negative charge per W metal and the ratio of charge per W metal is described as (n/x) shown in Figure 2.2.

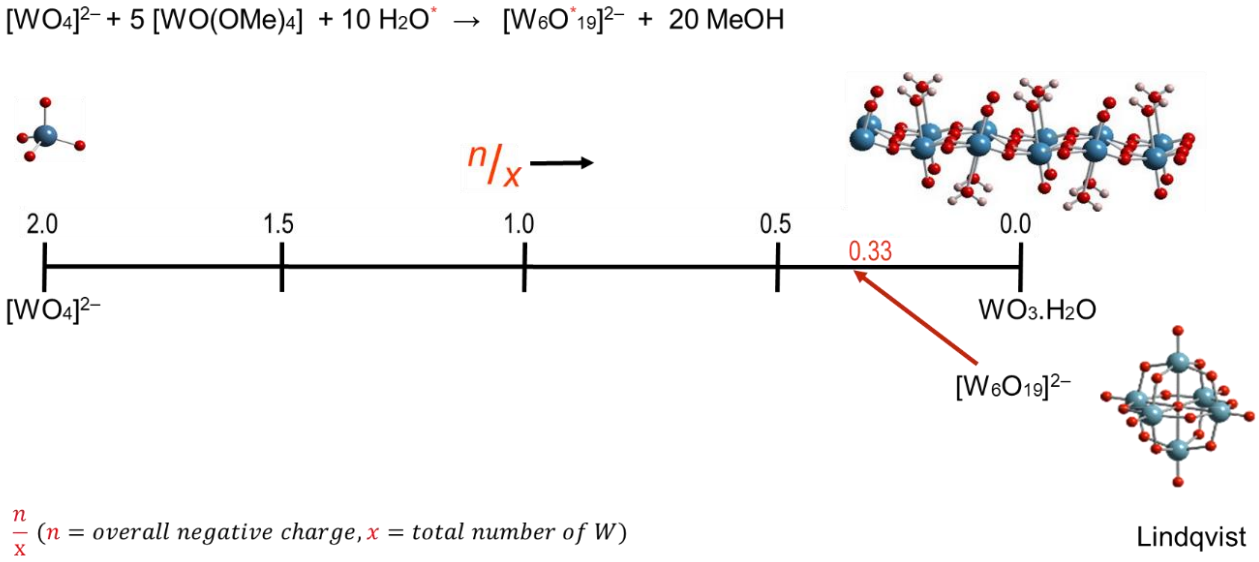

Figure 2.2: *Non-aqueous polytungstate formation*

In the second part of this chapter investigations are aimed to study the non-aqueous degradation of $(TBA)_2[W_6O_{19}]$ and incorporate an active site into the inert Lindqvist-type $(TBA)_2[W_6O_{19}]$ anion. Insights from these studies lead to the development of an efficient synthesis route and provided access to a series of heterometallic $\{M'M_5\}$ POMs from $(TBA)_2[M_6O_{19}]$ anion.

The synthesis of POMs in organic or mixed aqueous/organic solvents have been reported.[6,7] While the tungstate, $[W_6O_{19}]^{2-}$ has been shown to be inert, metathesis of oxido ligands in the molybdate, $[Mo_6O_{19}]^{2-}$ has been achieved in reactions involving for example $Ph_3P{=}NX$ (X = Ar, N=C(Me)Ar,[8-10] ArNCO,[11] RNCO,[12] or $ArNH_2$.[13] The NAr group in this case refers to a 2.6-(diisopropylphenyl)imido ligand which displaces a terminal oxygen atom forming an organoimido bond to the titanium. In the presence of an excess of the nitrogen containing reagent can result to the displacement of more than one terminal oxygen thereby forming organo-imido derivatives such as $[Mo_6O_{15}(NAr)_4]^{2-}$ and $[Mo_6O_{17}(NAr)_2]^{2-}$. The molecular structure of these two species seemed to favour a cis-arrangement of terminal NR ligands despite this being a more sterically strained structure. $ArNH_2$ reaction was adapted to provide access to arylimido and diazoalkane derivatives,[14-17] but the tungstate, $[W_6O_{19}]^{2-}$ remains inert under similar reaction conditions. The limited reactivity of the tungsten hexametalate has been ascribed to their low surface charge density and lower lability of W-O bonds

compare to Mo-O bonds. Therefore many of the reported organic derivatives of the tungstate have been prepared by indirect routes, that is, from $[WO_4]^{2-}$, $[W_2O_7]^{2-}$ rather than from $[W_6O_{19}]^{2-}$.[18] An established approach to the design of reactive Lindqvist-type hexametalates is the replacement of M^{VI} in the relatively inert hexametalates $[M_6O_{19}]^{2-}$ (M = Mo, W) by lower-valent metals, thereby increasing the charge density at the surface of the resulting heterometallic anions $[M'_xM_{(6-x)}O_{19}]^{n-}$.[19-22].

In the Errington research group, the establish approach to access these Lindqvist-type POMs involved reacting $[WO_4]^{2-}$, $WO(OMe)_4$ and heterometal alkoxides precursors, followed by hydrolysis with heating. However, the limitations of these reactions were moderate yields due to formation of $(TBA)_2[W_6O_{19}]$ as a side product. This work has been able to investigate non-aqueous degradation of $(TBA)_2[M_6O_{19}]$ with organic base TBAOH and subsequent reaction with stoichiometric amounts of H_2O under mild condition to form the desired Lindqvist-type POMs. The significant of this approach is that it maximizes the yield under mild conditions. These two approaches to the Lindqvist-type POMs is shown in Figure 2.3.

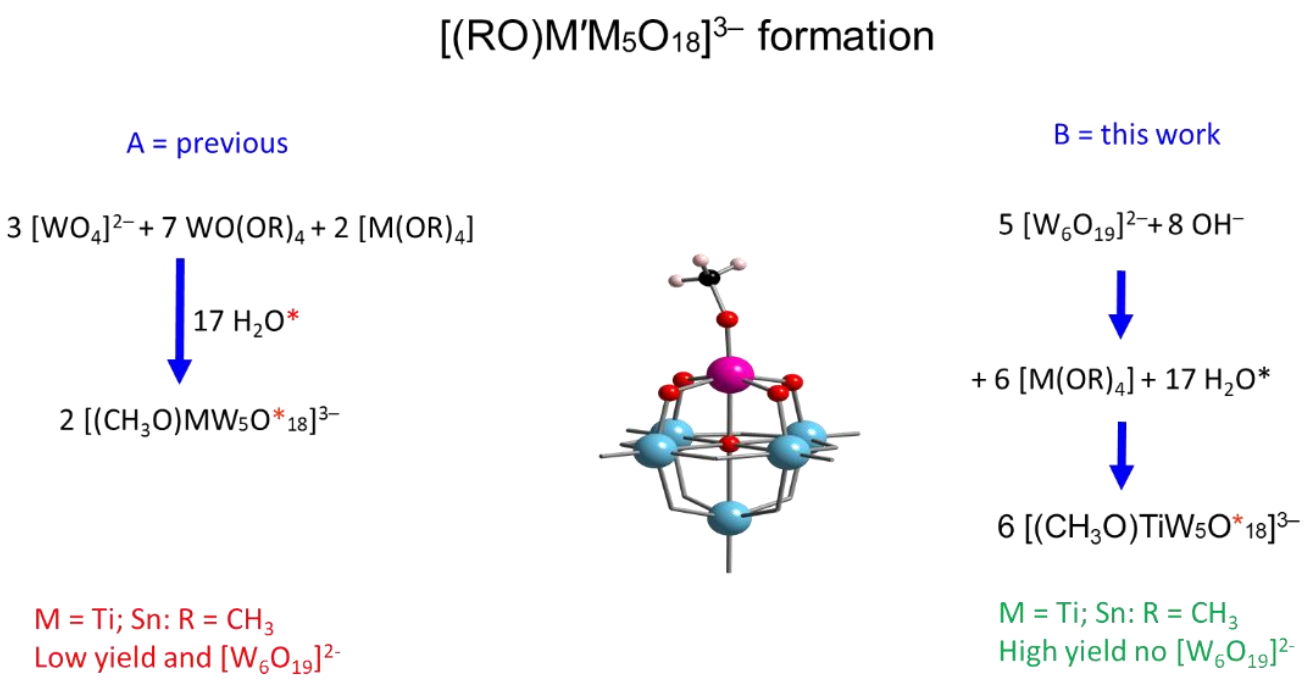

Figure 2.3: R*outes to $[M^{IV}(OR)]^{3+}$ substituted POMs in MeCN (A) previous rout and (B) this work*

2.2 Results and Discussion

2.2.1 Synthesis of ^{17}O-enriched $(TBA)_2[W^*O_4]$ and $WO(OCH_3)_4$

The reactions between a mixture of $[W^*O_4]^{2-}$ and $WO(OCH_3)_4$ was investigated by using ^{17}O-enriched $(TBA)_2[W^*O_4]$. ^{17}O-enriched $(TBA)_2[W^*O_4]$ was prepared by reacting 1.5 M dried aqueous TBAOH solution with $WO_3.H_2O$ (**see experimental section 2.4.3.2.).** The compound was isolated as a colourless solid, the ^{17}O NMR spectrum (Figure 2.4) contained a single peak at δ 442 ppm.

The enriched oxygens in $[W^*O_4]^{2-}$ are expected to exchange during ligand exchange reactions. The ^{183}W NMR spectrum (Figure 2.5) obtained in acetonitrile (referenced to 2 M Na_2WO_4 in H_2O) contained one single peak at δ 4.06 ppm. The downfield shift of this anion in MeCN can be related to the relative dielectric constant of the solvents (i.e. 80 and 36) for H_2O and MeCN respectively or due to the presence of different cations. The ^{1}H NMR spectrum obtained in MeCN contains cation peaks in their correct proportions. $WO(OCH_3)_4$ was prepared as described in the experimental **section 2.4.3.5.**

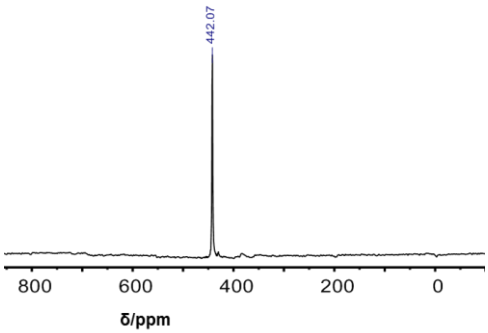

Figure 2.4: *^{17}O NMR spectrum of enriched $(TBA)_2[W^*O_4]$ in MeCN*

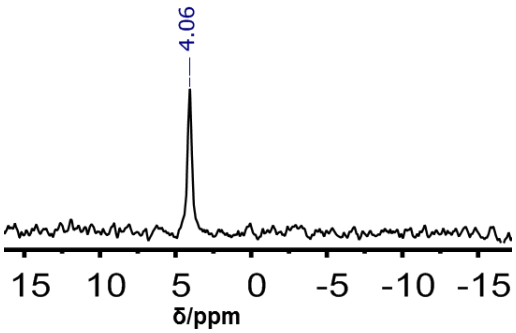

Figure 2.5: *^{183}W NMR spectrum of $(TBA)_2[W^*O_4]$ in MeCN*

2.3 Hydrolysis reaction of $[W_xO_y]^{n-}$ by stepwise addition of $WO(OCH_3)_4$ to $(TBA)_2W^*O_4$

2.3.1 Hydrolysis reaction of 1:1 mixture of $(TBA)_2[WO_4]$ and $WO(OCH_3)_4$ in MeCN

A mixture of ^{17}O-enriched $(TBA)_2[W^*O_4]$ and $WO(OCH_3)_4$ (1:1) was dissolved in MeCN and allowed to stir for 1 h before obtaining the first ^{17}O NMR spectrum 1. The NMR sample was transferred back into the reaction flask and ^{17}O-enriched H_2O was added and the mixture was stirred for an additional 1 h before recording ^{17}O NMR spectrum 2. The resulting mixture in the NMR sample tube was placed back in the reaction flask and stirred for further 1 h and subsequent removal of volatiles under reduced pressure before obtaining ^{17}O NMR spectrum 3 shown in Figure 2.6 (a) - (c). The first steps of this repeated cycle of the hydrolysis reaction is shown in (Scheme 2.2).

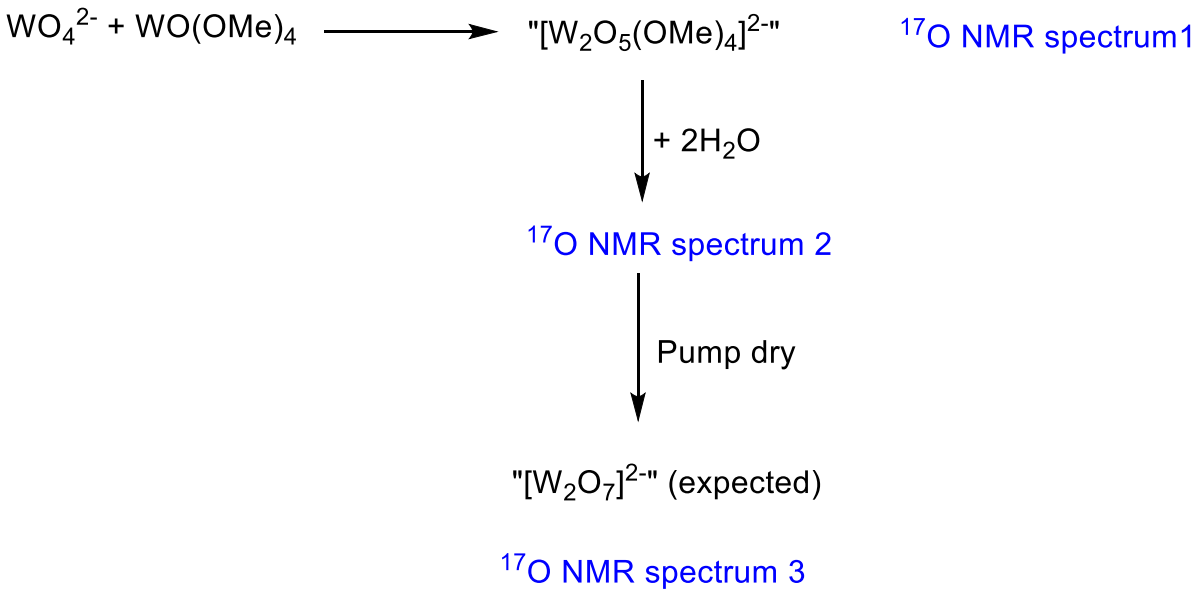

Scheme 2.2: *Hydrolysis of a mixture of $(TBA)_2[W^*O_4]$ and $WO(OCH_3)_4$ (1:1) in MeCN*

The ^{17}O NMR spectrum in (Figure 2.6c) indicate some insights into the complex ligand exchange and redistribution process in solution. The ^{17}O NMR spectrum 2.6c contained two characteristic peaks observed at δ 709 and 544 ppm these peaks are markedly different compared to the peak observed in the ^{17}O-enriched $[WO_4]^{2-}$ (δ 442 ppm) discussed above. The several smaller peaks in the spectra might arise from polymeric alkoxides species.

Figure 2.6 (a) indicate that even without the addition of H_2O the monomeric oxometallate $[WO_4]^{2-}$ is sufficiently basic to interact with the electrophilic tungsten centre in the alkoxide and the effect is evident in the ^{17}O NMR chemical shifts. The tungsten in these alkoxide environment are considered to be Lewis acidic and are expected to interact with the neighbouring oxygens from the highly basic oxygens in the oxometallate. The peaks observed at the terminal W=O region i.e. peaks with δ > 700 in the ^{17}O NMR spectrum are consistent with previous results reported by the Errington group in the 1:1 reaction mixture in the synthesis of $[W_2O_7]^{2-}$.[14]

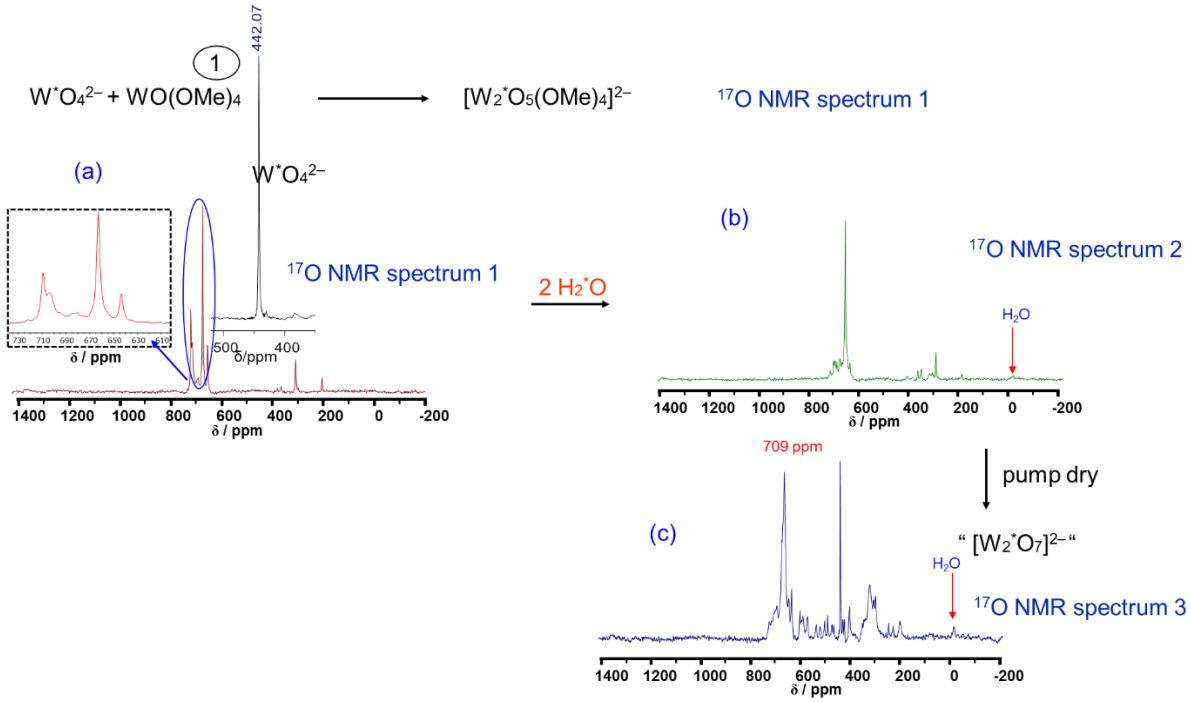

Figure 2.6: *^{17}O NMR spectrum of 1:1 mixture of $[WO_4]^{2-}$ and $WO(OCH_3)_4$ (a) prior to hydrolysis (b) after hydrolysis and (c) after removal of volatiles and dissolution in dry MeCN.*

2.3.2 Hydrolysis reaction of 1:2 mixture of $(TBA)_2[WO_4]$ and $WO(OCH_3)_4$ in MeCN

The product obtain from the repeated cycles above contained 2 W metals and expected to be "$[W_2O_7]^{2-}$"species. This product was dissolved in dried MeCN and added to one mole equivalent of $WO(OCH_3)_4$ the addition of the $WO(OCH_3)_4$ implies the overall charge per tungsten ratio $^n/_x$ is decreasing. The stepwise cycle described in step 1 above was repeated and the ^{17}O NMR in each cycle was recorded. The reaction scheme for the second step is shown in (Scheme 2.3)

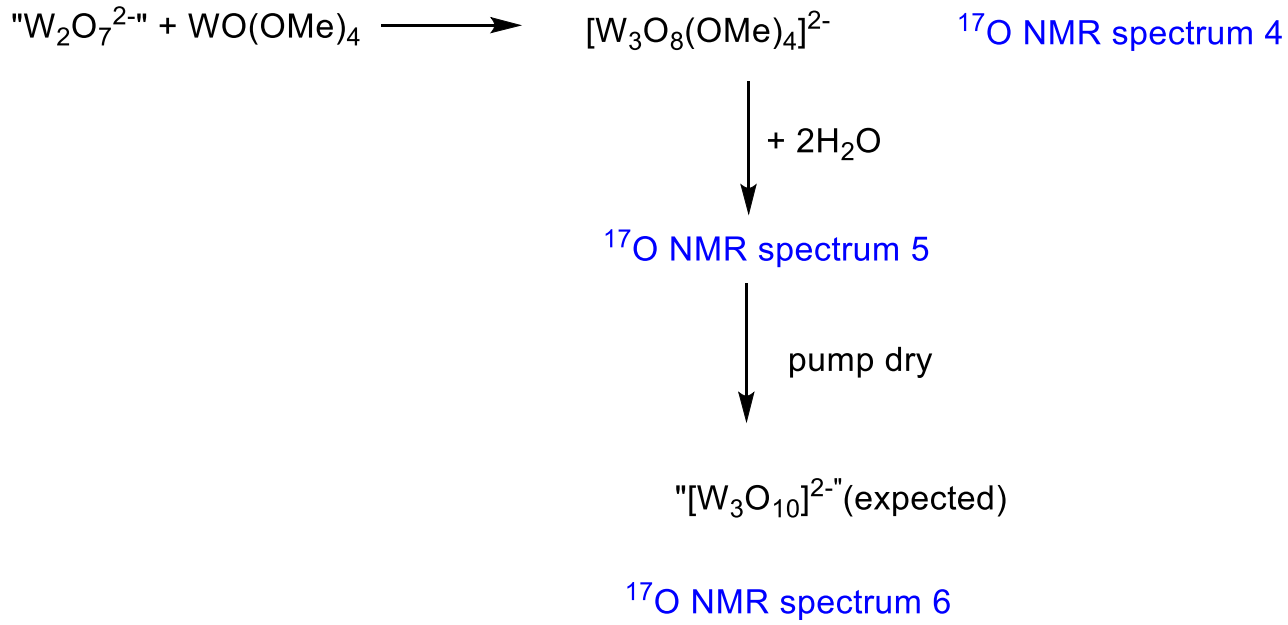

Scheme 2.3: *Hydrolysis of a mixture of $(TBA)_2[W^*O_4]$ and $WO(OCH_3)_4$ (1:2) in MeCN*

The ^{17}O NMR spectrum (Figure. 2.7a) before hydrolysis is remarkably simpler than spectrum 3 above and contain a peak at δ 777 ppm which is ascribed to terminal W=O peak for $(TBA)_2[W_6O_{19}]$ and has a corresponding bridging WOW at δ 416 ppm (mark with asterisks). It is important to note that the peak associated with the central μ_6-O is not sufficiently enriched to be observed in the ^{17}O NMR spectrum.

These remarkable observations from Figure 2.7a suggest that the WO_4^{2-} is sufficiently nucleophilic enough to lower the overall average negative charge per W even before the hydrolysis causing the peak to be shifted downfield. These chemical shifts are consistent with reported resonances for $[W_6O_{19}]^{2-}$ anion.[23,24,25]

The broad peaks observed at δ 708 and 721 ppm are also observed in spectrum 3 above and are in the region for terminal W=O peaks associated with $\{M_6\}^{3-}$ anion based on previous terminal W=O peaks reported.[25] The peak observed at δ 355 ppm might be associated with corresponding bridging WOW peak of this anion.

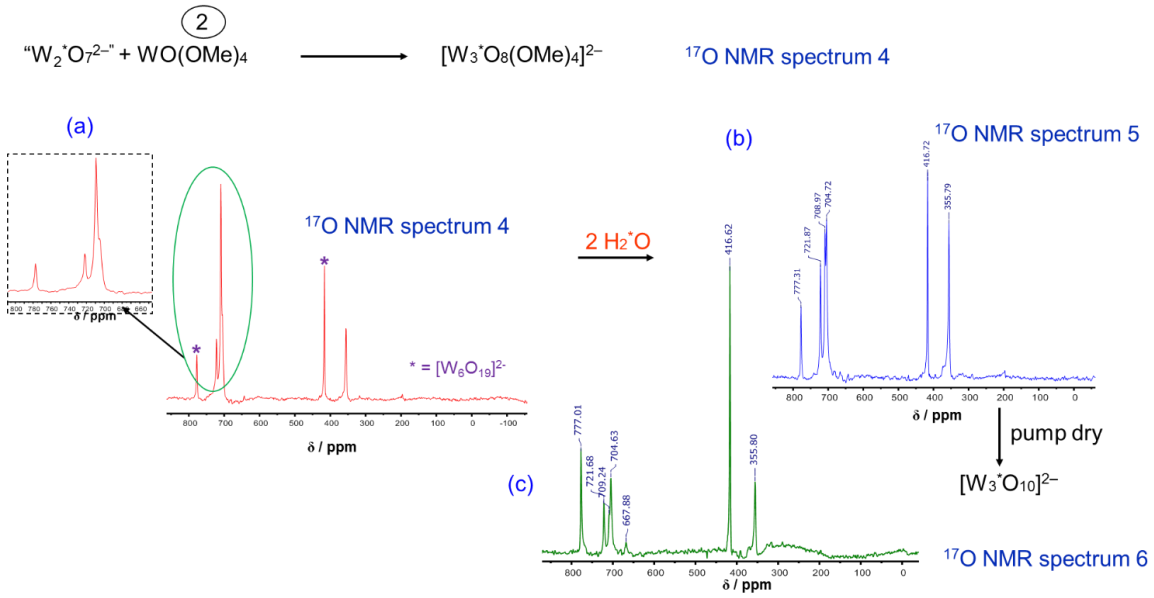

Figure 2.7: *^{17}O-NMR spectrum of $[WO_4]^{2-}$ and $WO(OCH_3)_4$ (1:2) (a) $[WO_4]^{2-}$ and $WO(OCH_3)_4$ prior to hydrolysis (b) after hydrolysis and (c) after removal of volatiles. Peaks mark with asterisks represent the terminal and bridging peaks for $[W_6O_{19}]^{2-}$ anion.*

2.3.3 Hydrolysis reaction of 1:3 mixture of $(TBA)_2[WO_4]$ and $WO(OCH_3)_4$ in MeCN

The product obtained in spectrum 6 expected to be "$[W_3O_{10}]^{2-}$"species with some $[W_6O_{19}]^{2-}$ anion, this was dissolved in dried MeCN and added to one mole of $WO(OCH_3)_4$. As previous described, addition of more $WO(OCH_3)_4$ essentially decreases the overall average negative charge per tungsten $^n/_x$. The various ^{17}O NMR spectra were recorded at each stage as shown in (Scheme 2.4) and these spectra become more simplified and less complex.

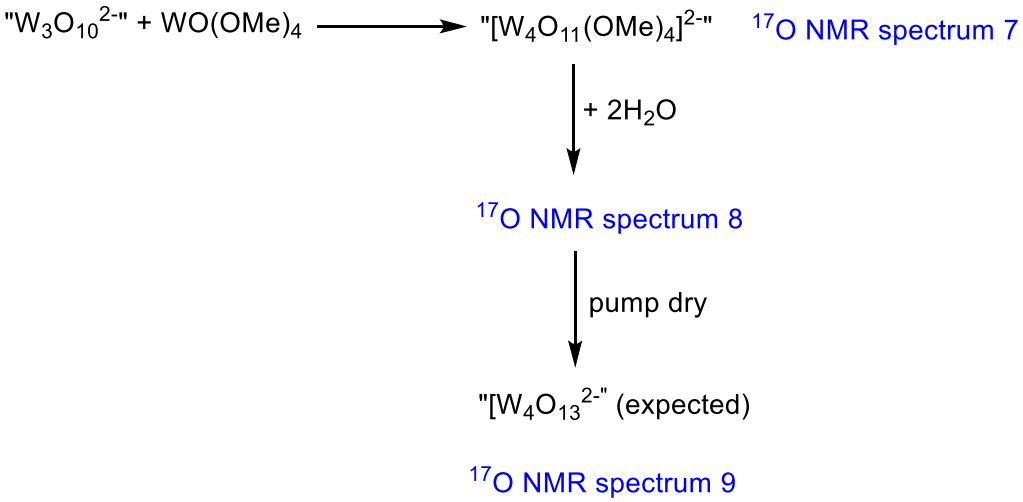

Scheme 2.4: *Hydrolysis of a mixture of $(TBA)_2[W^*O_4]$ and $WO(OCH_3)_4$ (1:3) in MeCN*

In the ^{17}O NMR spectrum Figure 2.8a the intensities of the peaks associated with $[W_6O_{19}]^{2-}$ at δ 777 and 416 ppm increases as the other peaks for intermediate species

slowly decreases suggesting that the intermediate polymeric species are slowly converted to $[W_6O_{19}]^{2-}$ anion. After hydrolysis and the removal of volatiles, the intensities of the peaks at δ 708 and 355 ppm significantly decreased while the intensities of the peaks for $[W_6O_{19}]^{2-}$ increased (Figure 2.8c).

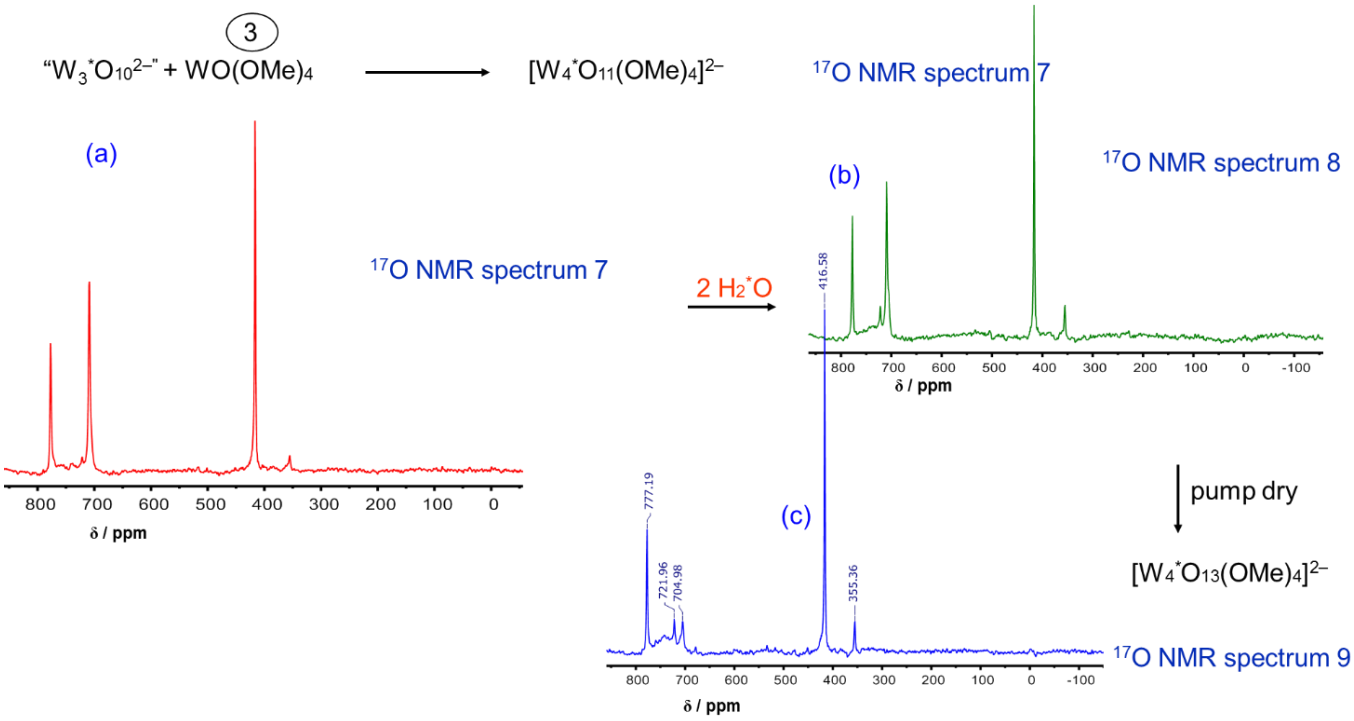

Figure 2.8: *^{17}O-NMR spectrum of the hydrolysis of 1:3 mixture of (a) $[WO_4]^{2-}$ and $WO(OCH_3)_4$ (b) after hydrolysis and (c) after removal of volatiles in dry acetonitrile.*

2.3.4 Hydrolysis reaction of 1:4 mixture of $(TBA)_2[WO_4]$ and $WO(OCH_3)_4$ in MeCN

The product "$[W_4O_{13}]^{2-}$" (expected) obtained in step 3 above was dissolved in dried MeCN and added to one mole of $WO(OCH_3)_4$. Again similar repeated cycles were adopted (Scheme 2.5) and the ^{17}O NMR spectrum after each cycle recorded (Figure 2.9).

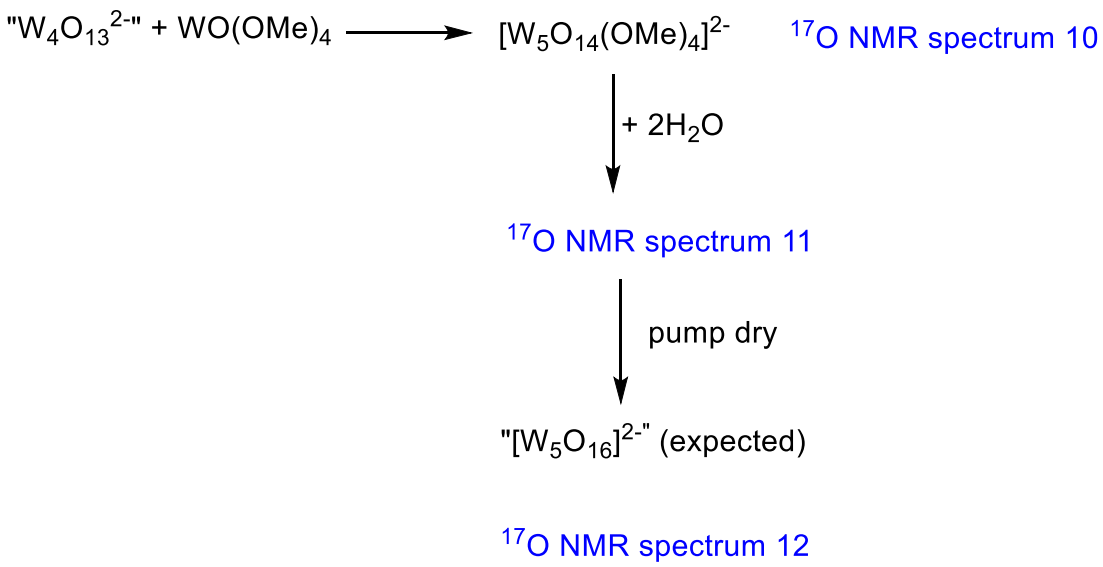

***Scheme 2.5**: Hydrolysis of a mixture of $(TBA)_2[W^*O_4]$ and $WO(OCH_3)_4$ (1:4) in MeCN*

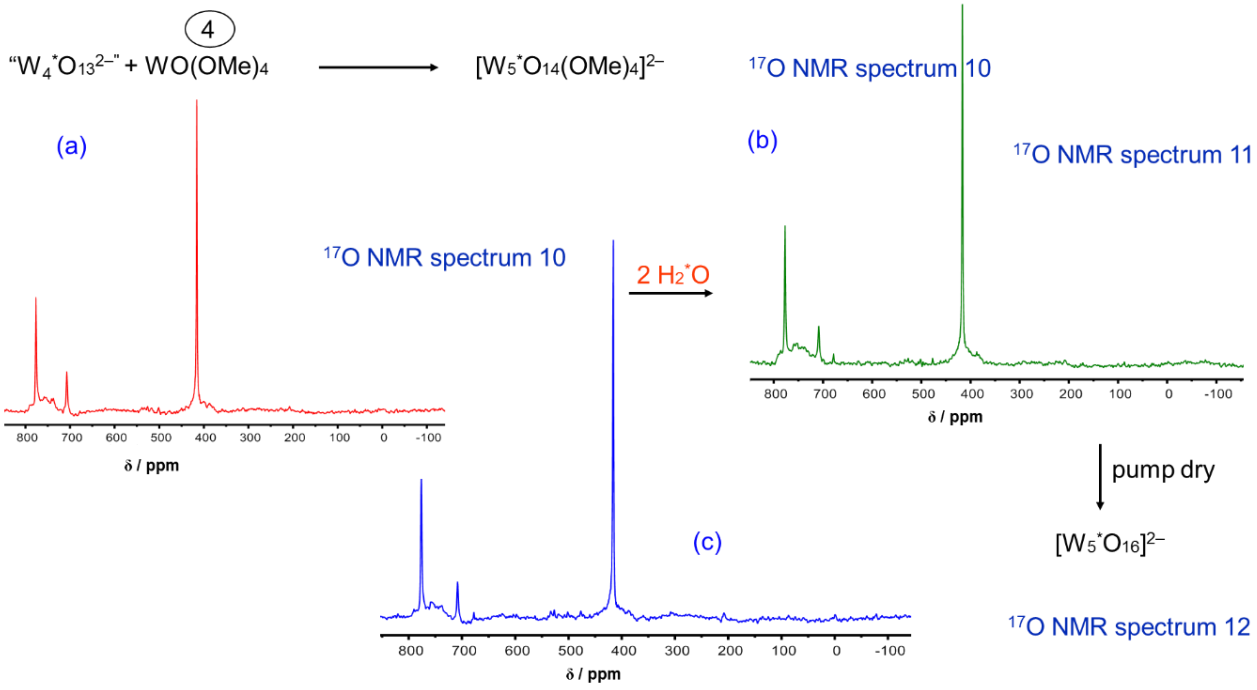

Figure 2.9: *^{17}O NMR spectrum of the hydrolysis of 1:4 mixture of (a) $[WO_4]^{2-}$ and $WO(OCH_3)_4$ (b) after hydrolysis and (c) after removal of volatiles in dry acetonitrile.*

The ^{17}O NMR spectrum in Figure 2.9a contain two major peaks for $[W_6O_{19}]^{2-}$ at δ 777 and 416 ppm other smaller peaks are also observed between δ 708 and 770 ppm. Note that after hydrolysis and the removal of volatiles, there is no significant changes in the intensities of these peaks between δ 708 and 770 ppm.

2.3.5 Hydrolysis reaction of 1:5 mixture of $(TBA)_2[WO_4]$ and $WO(OCH_3)_4$ in MeCN

In the final step of the reaction, the product from step 4 (expected "$[W_5O_{16}]^{2-}$") was dissolved in MeCN and added to one mole equivalent $WO(OCH_3)_4$ resulting to a further decrease in overall charge per tungsten (i.e. $^n/_x$ = 0.33) at this point $(TBA)_2[W_6O_{19}]$ anion was completely aggregated (Scheme 2.6).

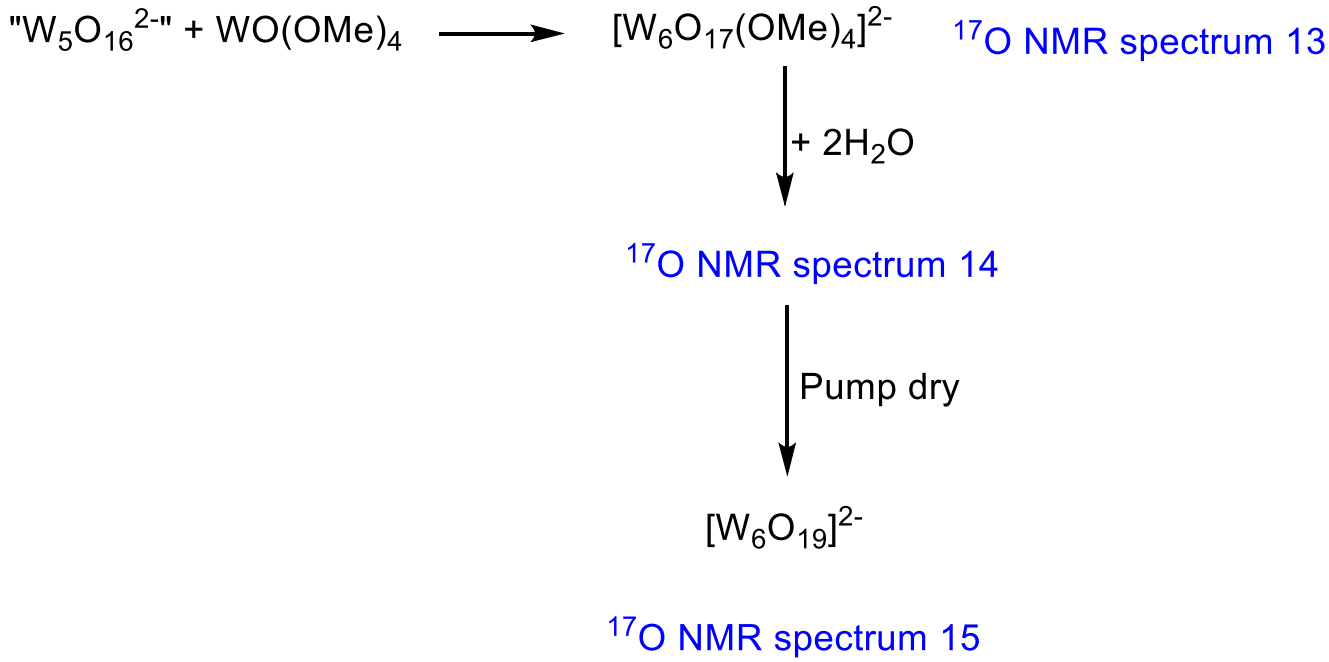

Scheme 2.6: *Hydrolysis of a mixture of $(TBA)_2[W^*O_4]$ and $WO(OCH_3)_4$ (1:5) in MeCN*

The ^{17}O NMR spectrum (Figure 2.10) after the addition of the $WO(OCH_3)_4$ at the final step contains only 2 peaks which suggest the formation of the desired product $(TBA)_2[W_6O_{19}]$. The results showed that $[W_6O_{19}]^{2-}$ anion is formed when the charge per tungsten decrease i.e. 0.33. The peaks observed at δ 777 and 416 ppm are for the 6 terminal W=O and 12 bridging W-O-W peaks respectively with no extra impurity peaks present. As expected, the peak integration reflects the 1:2 ratio of the terminal and bridging oxygens in $[W_6O_{19}]^{2-}$ anion.

The studies have showed that the reaction is quantitative, which is testament to the stability of the Lindqvist hexametalate structure.[25] Note that the central peak in this anion is apparently more difficult to enrich and therefore not easily observed in the spectrum probably due to lack of exchange depending on the formation mechanism and the intermediate structures formed.

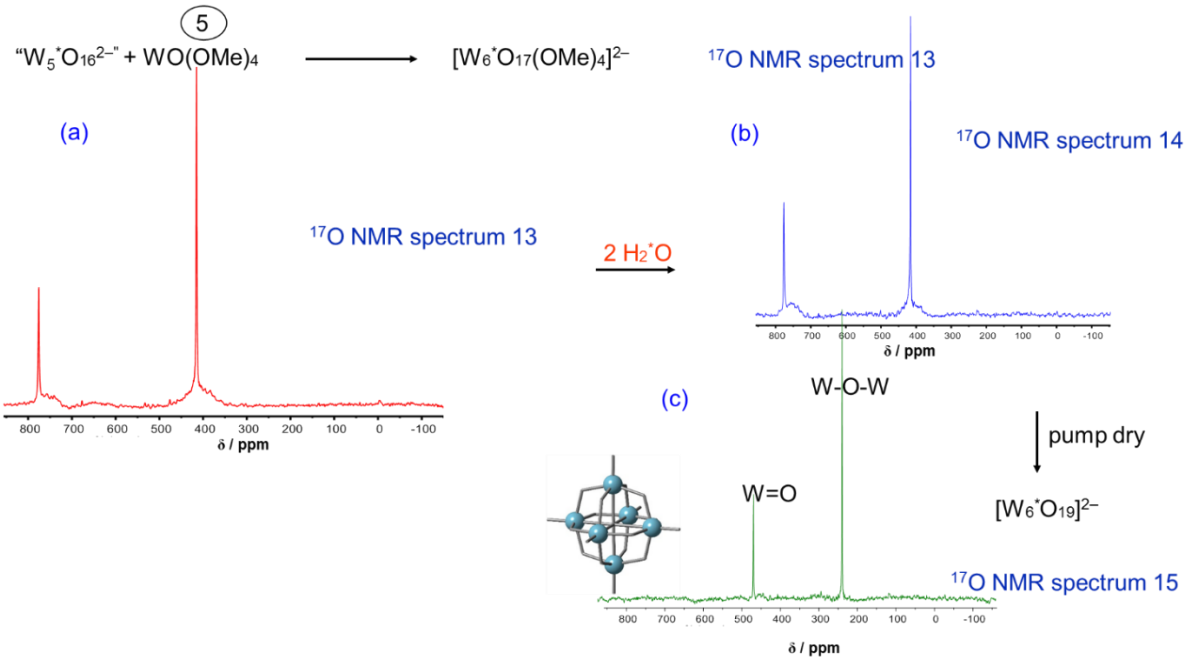

Figure 2.10: *^{17}O NMR spectrum of the hydrolysis of 1:5 mixture of (a) $[WO_4]^{2-}$ and $WO(OCH_3)_4$ (b) after hydrolysis and (c) after removal of volatiles in dry acetonitrile.*

The ^{17}O NMR data from the stepwise aggregation of $[W_6O_{19}]^{2-}$ anion suggest that during the formation of $[W_6O_{19}]^{2-}$ anion an intermediate species is formed but it slowly converts to $(TBA)_2[W_6O_{19}]$. These observations are important as it led to rational synthesis for the isolation and characterisation of the intermediate species.

2.3.6 Formation of $(TBA)_2[W_6O_{19}]$ and isolation of intermediate from the hydrolysis of 1:5 mixture of $(TBA)_2[WO_4]$ and $WO(OCH_3)_4$ in MeCN

In order to isolate the intermediate species observed in the stepwise aggregation process described above, a mixture of ^{17}O-enriched $(TBA)_2[W^*O_4]$ and $WO(OCH_3)_4$ in a 1:5 ratio was reacted, and the stoichiometric amount of H_2O added (Equation. 2.1) in MeCN. The ^{17}O NMR spectrum immediately after addition of enriched H_2O showed a complex mixture, although the two major peaks in the spectrum can be assigned to $[W_6O_{19}]^{2-}$.

$$(TBA)_2[W^*O_4] + 5WO(OCH_3)_4 + 10H_2O \rightarrow (TBA)_2[W_6O_{19}] + 20MeOH \qquad 2.1$$

After stirring for 2 h there were some undissolved solids present and the reaction was heated overnight at 60 ^oC in MeCN. The ^{17}O NMR spectrum simplified showing peaks at δ 777 and 416 ppm for terminal and bridging peaks of $(TBA)_2[W_6O_{19}]$ respectively. Other peaks are observed at 721, 708 and 704 ppm ascribed to the intermediate

species observed in the stepwise aggregation. These peaks are associated to terminal W=O peaks for a 3- charge.

When the solution was cooled to –20 ^oC, $(TBA)_2[W_6O_{19}]$ crystallised and was removed by cannula filtration. The mother liquor was heated overnight, and the solution cooled down to ambient temperature. The ^{17}O NMR spectrum (Figure 2.11(b)) showed peaks associated with $(TBA)_2[W_6O_{19}]$ which was removed after crystallisation at –20 ^oC by cannula filtration. The peaks marked with asterisk in the ^{17}O NMR spectrum (Figure 2.11 (d)) are $(TBA)_2[W_6O_{19}]$ anion which is the main product in the spectrum after repeated cycle of crystallisation.

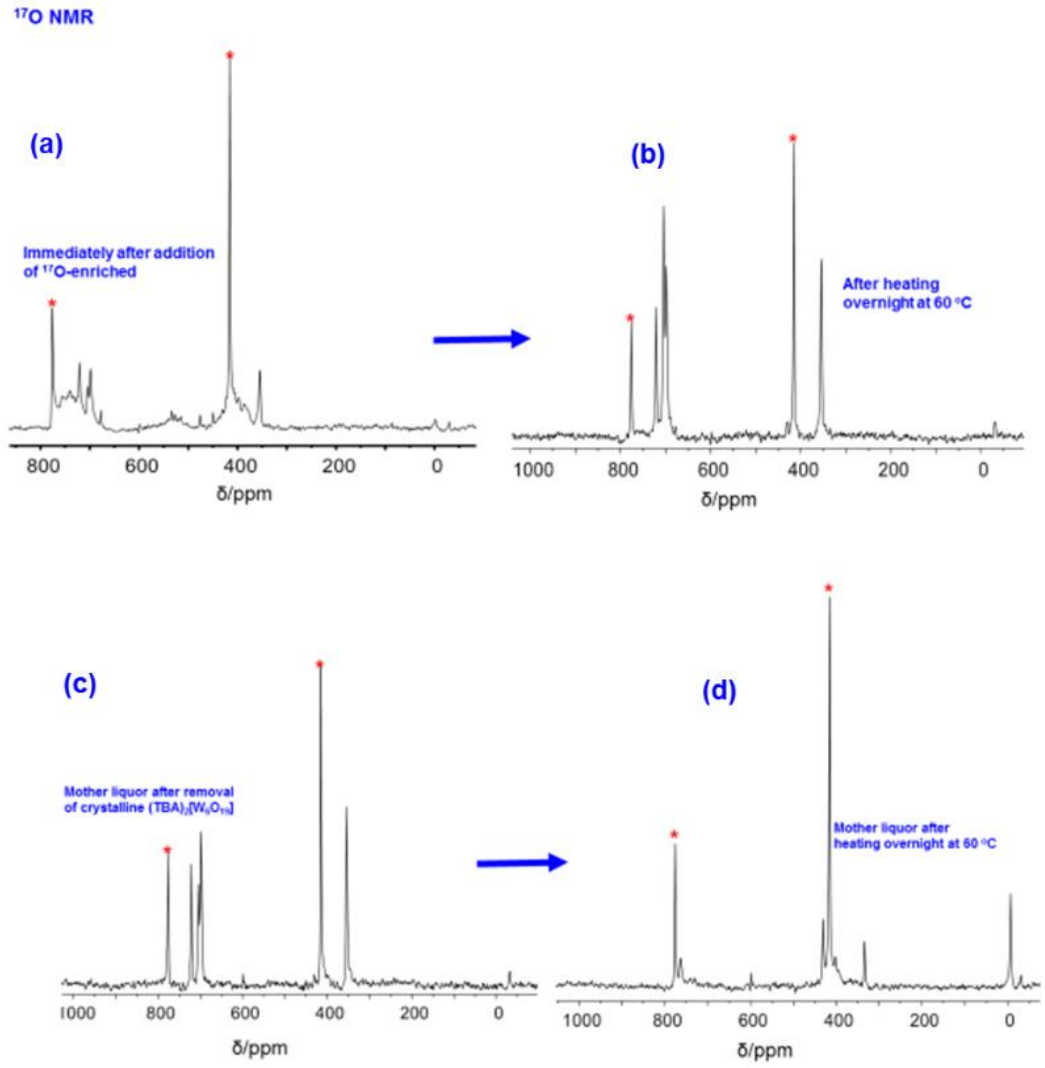

Figure 2.11: *^{17}O-NMR spectra of reaction of 1:5 mole ration of $[WO_4]^{2-}$ and $WO(OMe)_4$ in acetonitrile (a) immediately after hydrolysis (b) after solution being heated at 60 ^oC (c) mother liquor after removal of crystalline $(TBA)_2[W_6O_{19}]$ (d) mother liquor after heating overnight at 60 ^oC*

The intermediate species were removed and isolated by repeated recrystallisation of the mother liquor which was characterised by ^{17}O, ^1H and ^{183}W NMR spectroscopy and FT-IR.

2.3.7 Spectroscopic characterization of isolated intermediate

(a) ^{17}O-NMR spectroscopy

The ^{17}O NMR spectrum (Figure 2.12) of the intermediate product after recrystallization showed peaks at δ 721, 709 and 705 ppm, which were assigned to terminal W=O and a peak at δ 354 ppm assigned to the bridging WOW. These chemical shifts are relatively low compared to the peaks for $[W_6O_{19}]^{2-}$ but the shifts were close to the five peaks (δ 722, 689, 683, 678 and 657 ppm) observed in the ^{17}O NMR spectrum of the 1:1 mixture of WO_4^{2-} and $WO(OCH_3)_4$ in the attempted synthesis of $[W_2O_7]^{2-}$.[1,14]

The peaks were also consistent with the ^{17}O NMR spectrum of a 3^- charge anion for example $(TBA)_3[(MeO)TiW_5O_{18}]$,[25] $(TBA)_3[(MeO)SnW_5O_{18}]$,[26] or $(TBA)_3[(MeO)ZrW_5O_{18}]$,[25] though the peak observed for the bridging W-O-W was slightly lower than the peak observed for these species. Note that the peak marked with asterisk is due to small amount of $[W_6O_{19}]^{2-}$ anion.

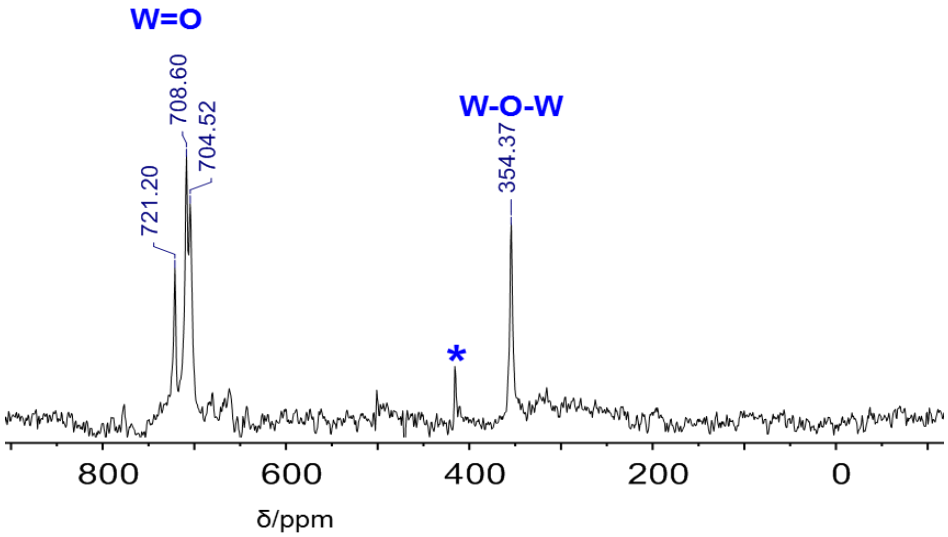

Figure 2.12: *^{17}O NMR spectrum of the isolated intermediate from the aggregation of $(TBA)_2[W_6O_{19}]$ in acetonitrile.*

(b) ^{1}H-NMR spectroscopy

In addition to tetrabutylammonium and solvent resonances, the ^{1}H NMR spectrum (Figure 2.13) contains unidentified peaks at δ 4.41, 4.27, 4.19, 4.17, 3.96 ppm in the region for W-OMe. These peaks are significantly different from peaks observed in the ^{1}H NMR spectrum of $WO(OMe)_4$ in MeCN which contains 3 peaks at 4.54, 4.4 and 4.38 ppm in a 2:1:1 ratio.[15, 26]

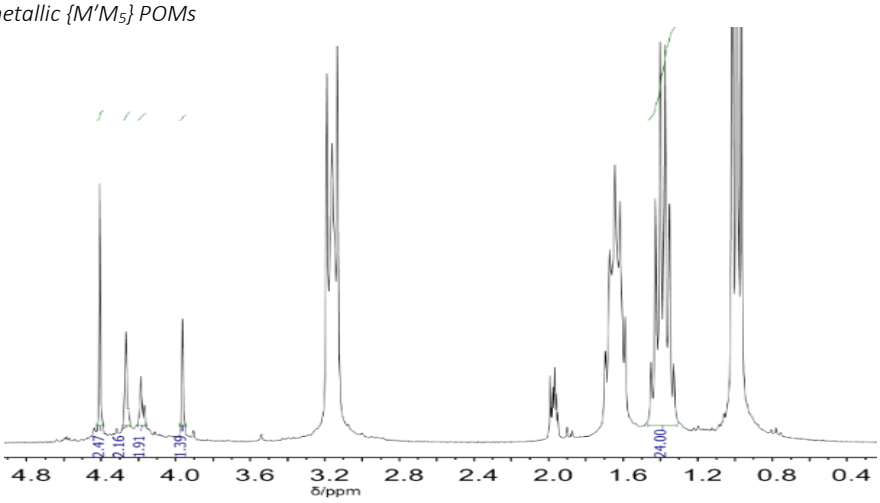

Figure 2.13: *^{1}H NMR spectrum of the isolated intermediate from the aggregation of $(TBA)_2[W_6O_{19}]$ in acetonitrile.*

(c) FT-IR spectroscopy

The FTIR spectrum of the isolated intermediate from the mother liquor shown in Figure 2.14 contains vibration at 2810 cm^{-1} which was assigned to ν(C-H) of O-CH_3, lower than ν(C-H) of $(TBA)_3[(CH_3O)TiW_5O_{18}]$ (2872 cm^{-1}). The band at 948 cm^{-1} can be assigned to terminal ν(W=O) stretching. The vibration is shifted to lower wavenumber compared to ν(W=O) of $[W_6O_{19}]^{2-}$ which occurs at 974 cm^{-1} due to higher overall negative charge. The vibrations at 725 cm^{-1} can be assigned to bridging ν(WOW) compare to 814 cm^{-1} for $[W_6O_{19}]^{2-}$. Comparing bands in the spectrum in Figure 2.14 with stretching vibrations of metal alkoxides in literature,[27] bands at 1154, 1104, 1077, and 1017 cm^{-1} can be assigned to ν(CO) and bands in the 500 – 550 cm^{-1} region may be due to ν(W-OC) vibrations.

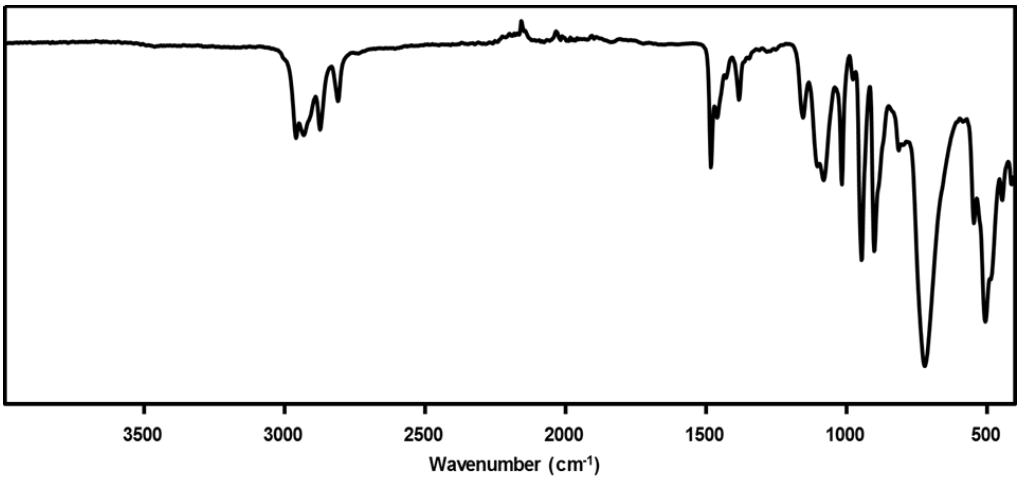

Figure 2.14: *FT-IR spectrum of the intermediate species*

(d) ^{183}W-NMR spectroscopy

The ^{183}W NMR spectrum (Figure 2.15) of the isolated intermediate in this work, clearly does not correspond to the ^{183}W NMR spectrum previously reported for the product from the attempted synthesis of $(TBA)_2[W_2O_7]$, which contains 5 lines in two distinct regions i.e. 3 low-field and 2 high-field peaks.[14] The two characteristic high-field peaks in the spectrum have typical negative values of δ – 66 and – 72 ppm. The integration of these peaks gives a ratio of about 1:1. Satellite peaks associated with the two peaks are not visible due to peak broadening and therefore the J_{ww} value could not be resolved. The peak at δ 51 ppm might be due to some amount of $[W_6O_{19}]^{2-}$ impurities (δ +47 ppm) previously reported. Table 2.1 shows typical ^{183}W NMR data for tungstate anions in previous reports.

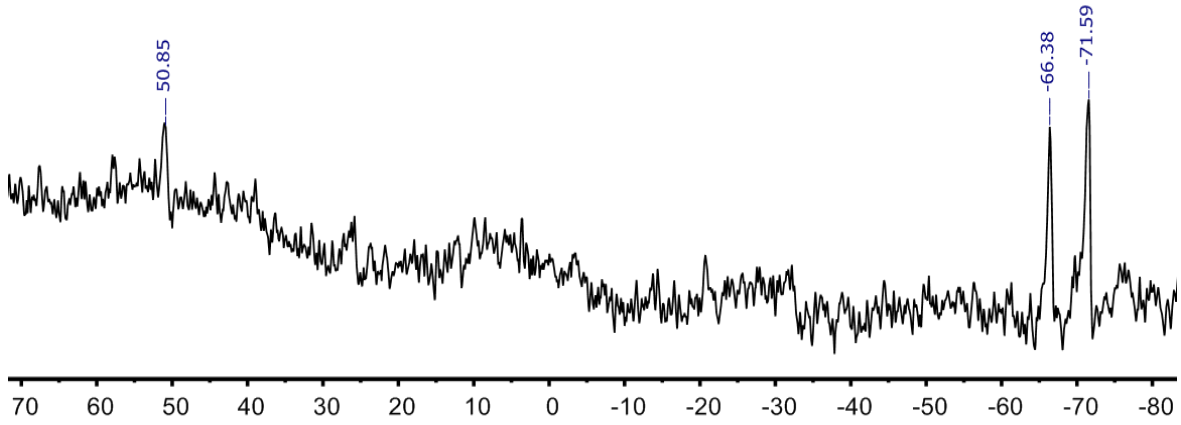

Figure 2.15: *^{183}W spectrum of the intermediate species*

Table 2.1: *^{183}W NMR data for tungstates[14]*

Anion	δ_w[a]	Cations	Solvent
$[WO_4]^{2-}$	442	$[Bu_4N]^+$	MeCN
$[W_7O_{24}]^{6-}$	+268, -106, -189	Li^+	H_2O
$[H_2W_{12}O_{42}]^{10-}$	-109, -114, -116, -147	Li^+	H_2O
$[H_2W_{12}O_{40}]^{6-}$	- 107	$[Bu_4N]^+$	MeCN
$[W_{10}O_{32}]^{4-}$	-30, -174	$[Bu_4N]^+$	MeCN
$[W_6O_{19}]^{2-}$	+ 47	$[Bu_4N]^+$	MeCN
[b]	+51, -66 -72	$[Bu_4N]^+$	MeCN

[a] Values referenced to 2 mol dm^{-3} aqueous $Na_2[WO_4]$ with peak integrations in parentheses. [b] is the intermediate isolated from this work.

X-ray crystal structural analysis was unsuccessful because we were not able to isolate a sufficiently pure sample for full characterisation, therefore there has been no overwhelming evidence in favour of any particular formula.

The above investigations suggested that $[W_6O_{19}]^{2-}$ anions can aggregate in solution through "self-assembly" process by gradually decreasing the overall average negative charge on WO_4^{2-} monomeric oxometallate. It also suggests that the metal in this oxometallate can easily expand it coordination to form more σ-bonds with neighbouring atoms thereby forming these polymeric species in solution. In addition, there is an apparent intermediate that can be isolated although more work needed to be to obtain pure single crystals for full X-ray analysis

2.4 A Novel and efficient route to $(TBA)_3[(MeO)M'M_5O_{18}]$ (M′ = Ti, Sn; M = W, Mo and $(TBA)_3[NbW_5O_{19}]$

2.4.1 Heterometallic Lindqvist POMs from $(TBA)_2[W_6O_{19}]$

As mentioned above, the non-aqueous hydrolytic aggregation was developed and established in the Errington group. This method is based on metal alkoxide hydrolysis and has provided access to a range of $[M^{IV}(OR)]^{3+}$ substituted POMs $(TBA)_3[(RO)MW_5O_{18}]$ (M = Ti, Zr, Hf, Sn) from alkoxides $M(OR)_4$ and their derivatives.[15,16,25,26,28,29]

The reactions are often affected by the degree of association of the alkoxide precursors. Some common examples of heterometal precursors include $[\{Zr(O^iPr)_3(\mu\text{-}O^nPr)(HO^iPr)\}_2]$,[30] $Ti(OMe)_4$,[25] and $[Sn(O^tBu)_4]$.[26] A milder and more efficient synthesis route to access these $[M^{IV}(OR)]^{3+}$ substituted POMs has now been developed in this project by using a modified approach providing access to $(TBA)_3[(RO)MW_5O_{18}]$ (M = Ti, Sn; M = W, Mo and $[NbW_5O_{19}]^{3-}$ *via* in situ degradation of $(TBA)_2[W_6O_{19}]$ with organic base TBAOH highlighted in Figure 2.3 above.

2.4.2 Preparation of $[(MeO)TiW_5O_{18}]^{3-}$ from degradation of $(TBA)_2[W_6O_{19}]$ in MeCN

The methoxido Lindqvist-type POM $(TBA)_3[(MeO)TiW_5O_{18}]$ was prepared by reacting $(TBA)_2[W_6O_{19}]$ with 1.5 M solution of methanolic TBAOH (**see experimental section 2.6.5.1**) in dried MeCN and addition of $Ti(OMe)_4$ with subsequent addition of ^{17}O-enriched H_2O (Eqn. 2.2).

$$(TBA)_2[[W_6O_{19}] + 8OH^- + 6Ti(OMe)_4 + 5H_2O \rightarrow 6[(MeO)TiW_5O_{18}]^{3-} + 18MeOH \quad 2.2$$

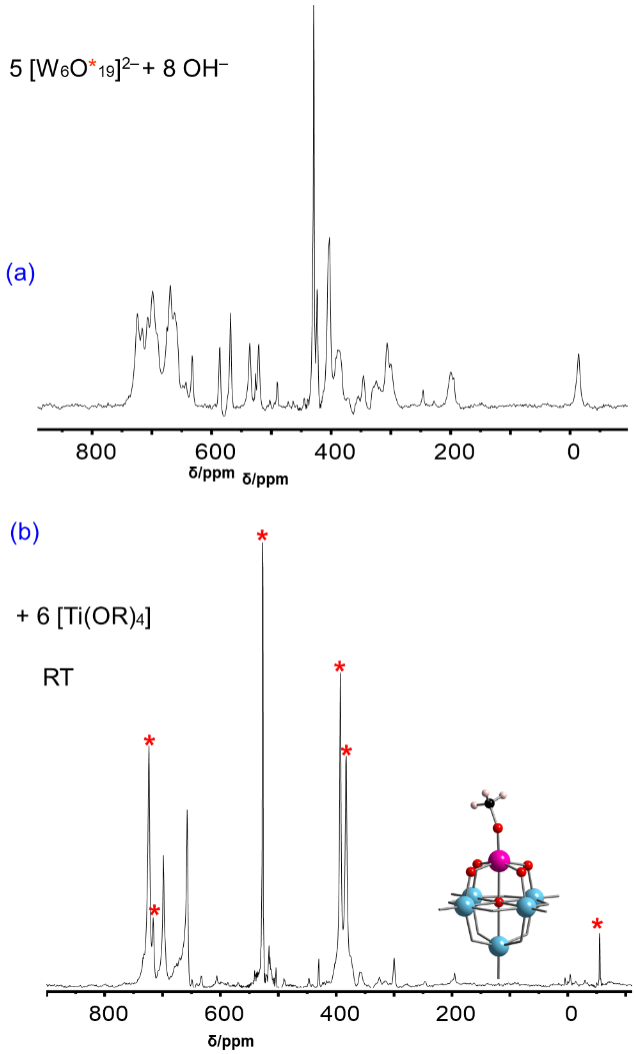

Figure 2.16: *^{17}O-NMR spectrum of the formation of $(TBA)_3[(MeO)TiW_5O_{18}]$ by degradation of $(TBA)_2[W_6O_{19}]$ (a) $[W_6O_{19}]^{2-}$ + TBAOH (b) addition of $Ti(OMe)_4$ and stirring for 2 h at room temperature in MeCN.*

The initial ^{17}O NMR spectrum (Figure 2.16a) was significantly complex showing several peaks. Interestingly, there is no peak that could be assigned to $[W_6O_{19}]^{2-}$ i.e. peaks are within δ 708 - 724 ppm region lower than the chemical shift for $[W_6O_{19}]^{2-}$ anions at δ 777 ppm.

In comparison, the chemical shifts for the terminal W=O peaks for $(TBA)_2[W_6O_{19}]$ at δ 777 ppm to the upfield shift of the terminal W=O peak within the δ 700 ppm region after the addition of $Ti(OMe)_4$ (Figure 2.16b) indicates an increase in overall negative charge of the anion. Upon addition of $Ti(OMe)_4$, as expected the six-coordinate titanium heterometal centre occupies the pocket of the pentadentate lacunary polyoxometalates 'ligand', $[W_5O_{18}]^{6-}$ which results in the formation of the Ti-substituted Lindqvist-type POM and hence simplify the ^{17}O NMR spectrum. The peaks marked with asterisks are the peaks associated with the enriched oxygen in the $(TBA)_3[(MeO)TiW_5O_{18}]$ anion.

Table 2.2: *^{17}O NMR chemical shifts for the formation of $(TBA)_3[(MeO)TiW_5O_{18}]$ from degradation of $(TBA)_2[W_6O_{19}]$ in acetonitrile at room temperature.*

Reaction Steps	W=O (δ_O)		Ti-O-W (δ_O)	W-O-W (δ_O)	W-O-W (δ_O)	W_6-O (δ_O)
$[W_6O_{19}]^{2-}$	776	-	-	416		-80
[a]	724,	699	586	490	393 389	-56
	716,	691	568	445	383 347	
	708	669	537	429	306	
		632	527	424		
			522	404		
[b]	723	698	527	430	393 383	-55
	716	657	516			
[c]	723		527		393 383	-55
	716					

[a] = mixture of $[W_6O_{19}]^{2-}$ and TBAOH, [b] = after addition of $Ti(OMe)_4$ *and H_2O and [c] = after removal of volatiles*

Upon addition of ^{17}O-enriched H_2O for complete hydrolysis and subsequent further stirring for 18 h at room temperature, most of the minor peaks in the ^{17}O NMR spectrum observed as impure polyoxoanions disappear after recrystallization leaving a clean spectrum with the expected chemical shifts of the desired compound as shown in Figure 2.17. Note that the yield from this reaction is much higher than the previous synthesis route and also reactions are purely conducted under milder conditions.

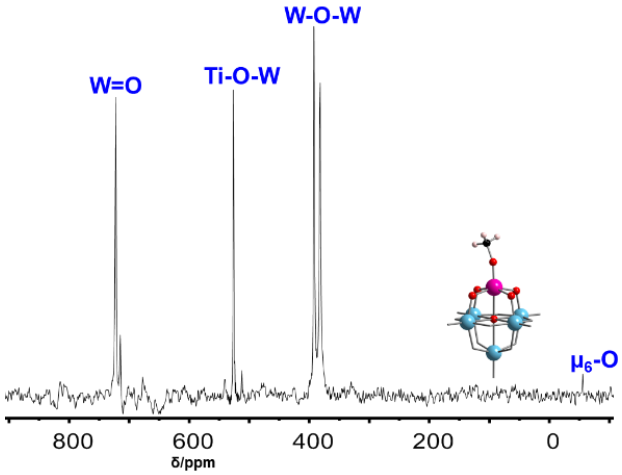

Figure 2.17: *^{17}O-NMR spectrum of $(TBA)_3[(MeO)TiW_5O_{18}]$ from tnon-aqueous degradation of $(TBA)_2[W_6O_{19}]$ in acetonitrile at room temperature.*

In the ^{17}O-NMR spectrum, peaks consistent with the Lindqvist-type TiW_5 core structure were observed. Using established correlations between M–O bond strengths and ^{17}O NMR chemical shifts in POMs,[31,32] peaks observed at δ 722 (4W) and 715 (1W) ppm were assigned to equatorial and axial terminal W_{eq}=O and W_{ax}=O respectively. These peaks have greater π-bond order and are shifted downfield on the ^{17}O-NMR scale. The peak observed at δ 526 was assigned to the bridging Ti-O-W while the two peaks at δ

392 and 382 were assigned to the two bridging W-O-W bonds. The unique central μ_6-O oxygen which is bonded to six tungsten atoms was observed at δ –55 ppm on ^{17}O NMR scale. The chemical shifts observed in the spectrum are consistent with that of mono-substituted $[(RO)MW_5O_{18}]^{n-}$.[25]

The ^1H NMR spectrum (Figure 2.18) contained a singlet at δ 4.11 ppm, in addition to tetrabutylammonium and solvent resonances appearing at lower chemical shift values below δ 4.11ppm, peak integration gave a ratio of OMe:$^nBu_4N^+$ of ~ 1:3.3 which is slightly above the expected ratio of 1:3. The lower than expected intensity may be hydrolysis due to moisture sensitivity of metal alkoxide species or due to the long relaxation time of Ti-OCH_3 which will reduce intensity if insufficient acquisition delay is used.

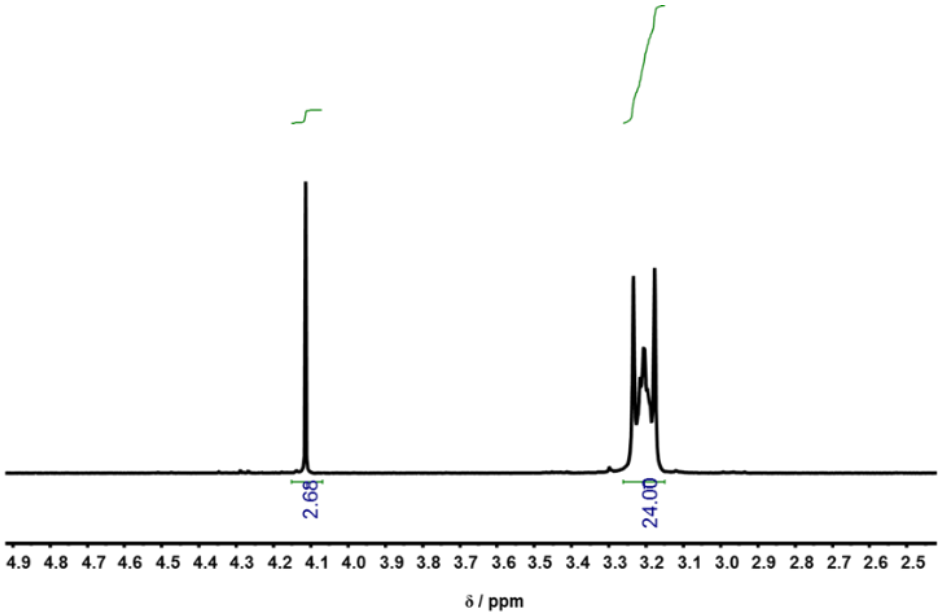

Figure 2.18: *^1H-NMR spectra of $(^nBu_4N)_3[(MeO)TiW_5O_{18}]$ from $(TBA)_2[W_6O_{19}]$ after crystallization in acetonitrile*

(a) FT-IR spectroscopy

The FTIR spectrum (Figure 2.19) contains bands at about 946 cm^{-1} assigned to ν(W=O). This band is shifted to lower wavenumber compare to ν(W=O) band for $[W_6O_{19}]^{2-}$ at 976 cm^{-1}. The ν(W-O-W) bands observed at 778 cm^{-1} is also at lower wavenumber compare to $[W_6O_{19}]^{2-}$ band observed at 814 cm^{-1}. By comparing the spectrum in Figure 2.19 with metal alkoxide stretching vibrations in literature,[27] the band observed at 1027 cm^{-1} can be assigned to ν(CO) of the TiOMe group, while the ν(TiO) vibration in the alkoxide group is associated with the peaks at 500 – 650 cm^{-1}.

Minor differences that exist in wavenumbers and intensities might be due to different sampling and IR technique used. In this case, solid samples were measured on ATR and in previous case by transmission on Nujol mull.[25]

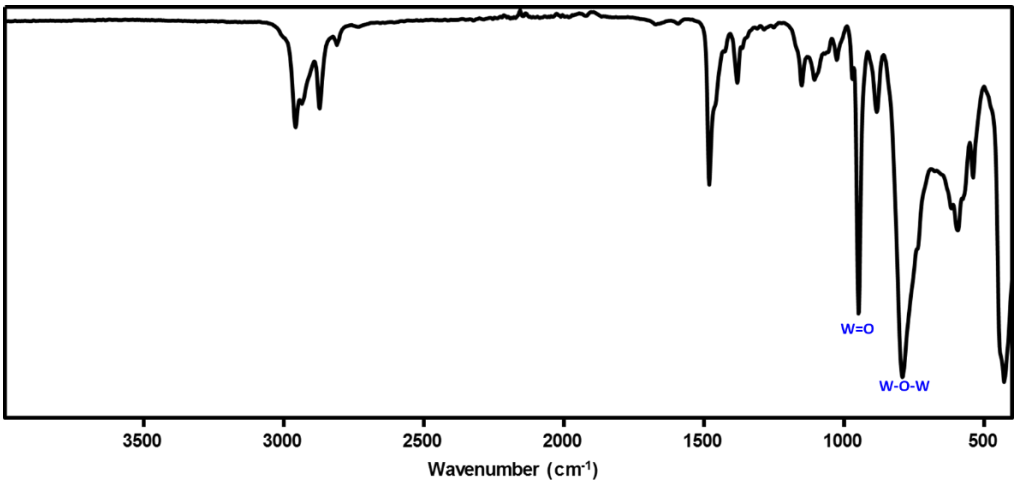

Figure 2.19: *FT-IR spectrum of $(TBA)_3[(MeO)TW_5O_{18}]$ from degradation of $[W_6O_{19}]^{2-}$ in acetonitrile*

2.4.3 Preparation of $(TBA)_3[(MeO)SnW_5O_{18}]$ from degradation of $(TBA)_2[W_6O_{19}]$ in MeCN

The tin analogue of the titanium methoxido Lindqvist-type POM $(TBA)_3[(MeO)SnW_5O_{18}]$ which was previously synthesised in the Errington group based on previous method i.e. metal alkoxide hydrolysis (**see route A Figure 2.3**) above was synthesised by the new method i.e. non-aqueous degradation of $(TBA)_2[W_6O_{19}]$.

In the preparation of the tin analogue, the same approach was adopted as described above for $[TiW_5]$ anion but with $Sn(^tOBu)_4$ as the heterometal precursor as shown in (Equation.2.3). in addition, stoichiometric amount of MeOH was added for the complete conversion of any residual SnOtBu groups been replaced by SnOMe and that any SnOH formed can be converted to SnOMe (**see experimental section 2.4.6.4 for full details**).

$$[W_6O_{19}]^{2-} + 8OH^- + 6Sn(^tOBu)_4 + 5H_2O \rightarrow 6[(MeO)SnW_5O_{18}]^{3-} + 18MeOH \qquad 2.3$$

(a) FT-IR spectroscopy

The FTIR spectrum of $(TBA)_3[(MeO)SnW_5O_{18}]$ (Figure 2.20) shows a band at 950 cm^{-1} assigned to the ν(WO) for terminal W=O. This is also shifted more to lower wavenumber compared to the corresponding band for $(TBA)_2[W_6O_{19}]$ at 976 cm^{-1} which is as a result of the more highly charged anion. The ν(W=O) band was

observed at higher wavenumber than the analogous band reported for $[MeSnW_5O_{18}]^{3-}$ at 940 cm^{-1},which is presumably a reflection of the difference in electronegativity between O and C.[7]

The band observed at 3648 cm^{-1} are due to ν(OH) which might be due to some hydrolysis from surrounding moistures. The bands observed at 798 and 756 cm^{-1} are due to ν(WO) associated with the WOW and SnOW bridges. Although, it is suggested that ν(SnO) from the SnOW bridges may also occur in this region.[26] The band observed at 1046 cm^{-1} was assigned to ν(CO) of the SnOMe group, while the ν(SnO) vibration in the alkoxide group is probably associated with one of the bands below 620 cm^{-1}

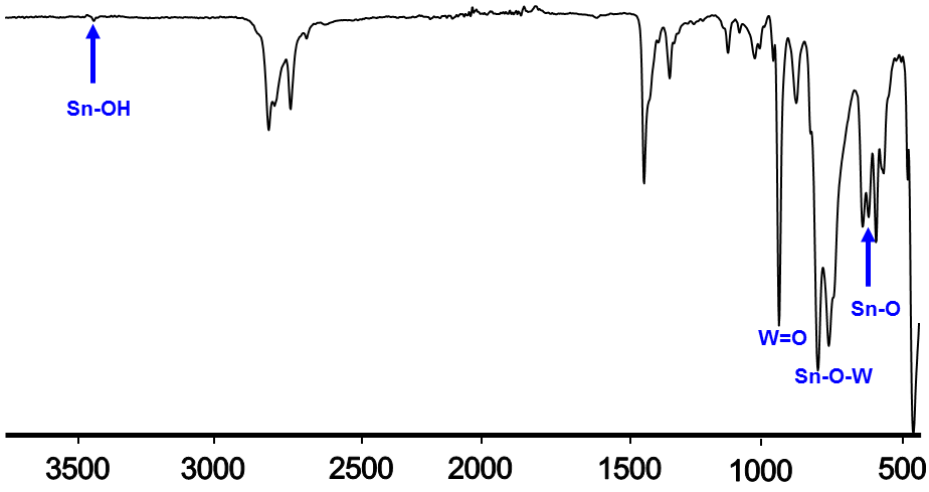

Figure 2.20: *FT-IR spectrum of $(TBA)_3[(MeO)SnW_5O_{18}]$ from $(TBA)_2[W_6O_{19}]$ in acetonitrile*

(b) Multinuclear NMR spectroscopy

NMR solution spectroscopy was consistent with the reported structure.[26] In the ^{1}H-NMR spectrum (Figure 2.21), the OMe:^{n}Bu$_4$N$^+$ ratio was ~1:3, and the OMe group is observed at δ 3.65 ppm. Satellite peaks associated with the OMe peak in the ^{1}H NMR spectrum, show ^3J couplings to ^{119}Sn and ^{117}Sn of 76.6 and 73.4 Hz respectively consistent with previous reported structure.[26] Line broadening and lower natural abundance of ^{115}Sn affected the satellite peaks associated with that isotope and therefore were not observed.

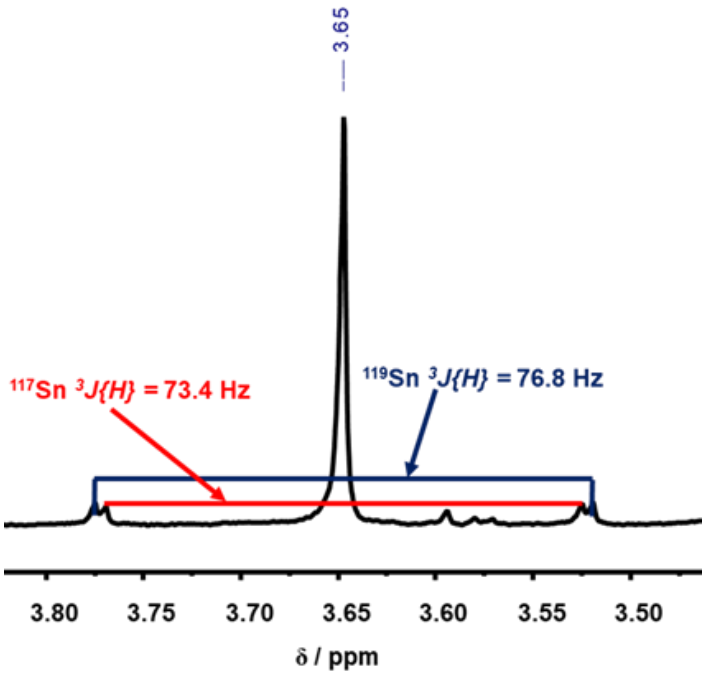

Figure 2.21: *^{1}H-NMR spectra of $(TBA)_3[(MeO)SnW_5O_{18}]$ from $(TBA)_2[W_6O_{19}]$ after crystallization in acetonitrile*

The ^{17}O-enriched $(TBA)_3[(MeO)SnW_5O_{18}]$ prepared by using ^{17}O enriched water in the controlled hydrolysis reaction gave an ^{17}O NMR spectrum (Figure 2.22) with peaks due to equatorial and axial terminal W=O at δ 721 and 684 ppm respectively, bridging SnOW at δ = 397 ppm while bridging WOW at δ = 384 and 369 ppm and central μ_6-O at δ 19 ppm.

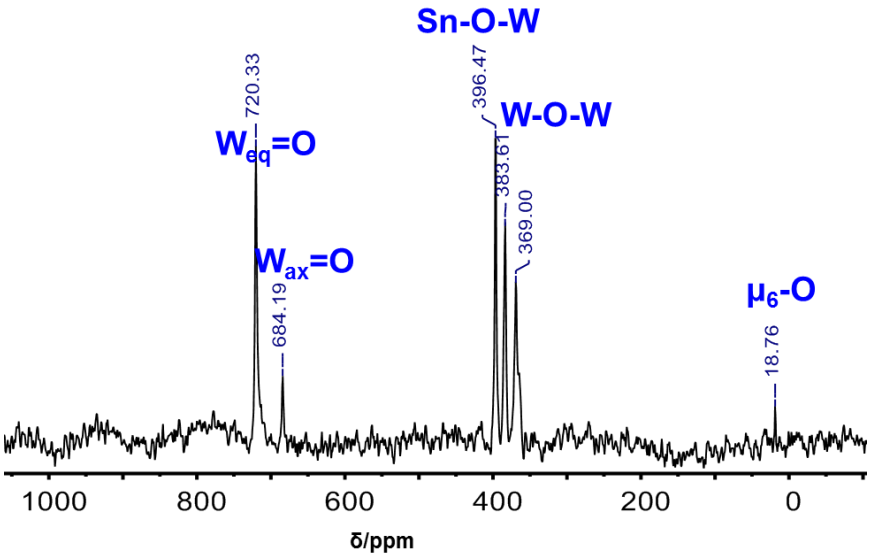

Figure 2.22: *^{17}O-NMR spectrum of $(TBA)_3[(MeO)SnW_5O_{18}]$ prepared by degradation of $[W_6O_{19}]^{2-}$ in acetonitrile at room temperature*

(c) ^{119}Sn NMR spectroscopy

The ^{119}Sn NMR spectrum of $(TBA)_3[(MeO)SnW_5O_{18}]$ after recrystallization, (Figure 2.23) shows a resonance at δ_{Sn} = –648 ppm with satellite peaks due to $^2J(^{119}Sn\ ^{183}W)$ of 39 Hz. The other peak mark with asterisk has a chemical shift at δ_{Sn}= –666 ppm in the ^{119}Sn NMR spectrum this was due to some amount of oxo-bridged $[(\mu\text{-}O)\{SnW_5O_{18}\}_2]^{6-}$ species although interestingly δ_{Sn} -633 ppm for $[OHSnW_5]^{3-}$ is not observed. This suggest that during the formation of the $(TBA)_3[(MeO)SnW_5O_{18}]$ the hydroxide $(TBA)_3[(HO)SnW_5O_{18}]$ would have formed in solution and subsequent condensation results to the formation of the oxo-bridged $[(\mu\text{-}O)\{SnW_5O_{18}\}_2]^{6-}$ and even after addition of MeOH there were still some amount of the oxo-bridged $[(\mu\text{-}O)\{SnW_5O_{18}\}_2]^{6-}$ present. These results are in good agreement with previous report.[26]

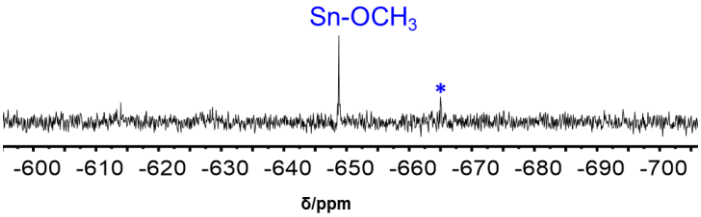

Figure 2.23: *^{119}Sn NMR spectrum of $(TBA)_3[(MeO)SnW_5O_{18}]$ in MeCN*

(d) ^{183}W NMR spectroscopy

The ^{183}W NMR spectrum of the recrystallized $(TBA)_3[(MeO)SnW_5O_{18}]$ (Figure 2.24) consists of two peaks at δ_w =72 and –123 ppm, which were assigned to W_{eq} and W_{ax}, respectively. These chemical shifts are markedly different from chemical shifts $\delta W_{(eq)}$ = –20 and $\delta W_{(ax)}$ = –16 ppm reported for $[MeSnW_5O_{18}]^{3-}$.[33] Peaks at δ_w = 71 and –131 ppm observed in the spectrum were due to $[(HO)SnW_5O_{18}]^{3-}$ impurities due to hydrolysis in solution**.** The difference in shifts between axial and equatorial W peaks for the two species present is consistent with the presence of $[(MeO)SnW_5O_{18}]^{3-}$ at 72 and –123 (giving a difference of 195 ppm cf 194 ppm previously observed) and $[(HO)SnW_5O_{18}]^{3-}$ at δ_w 71 and –131 ppm (giving a difference of 203 ppm cf 201 ppm previously observed).[25, 28, 34] The coupling constants values for $^2J(^{119}Sn^{183}W_{eq})$ and $^2J(^{119}Sn^{183}W_{ax})$) were 37 Hz and 12 Hz respectively. The peak marked with asterisks might be due to minor impurities due to small amount of $[W_6O_{19}]^{2-}$ which is observed in previous ^{183}W NMR spectrum.

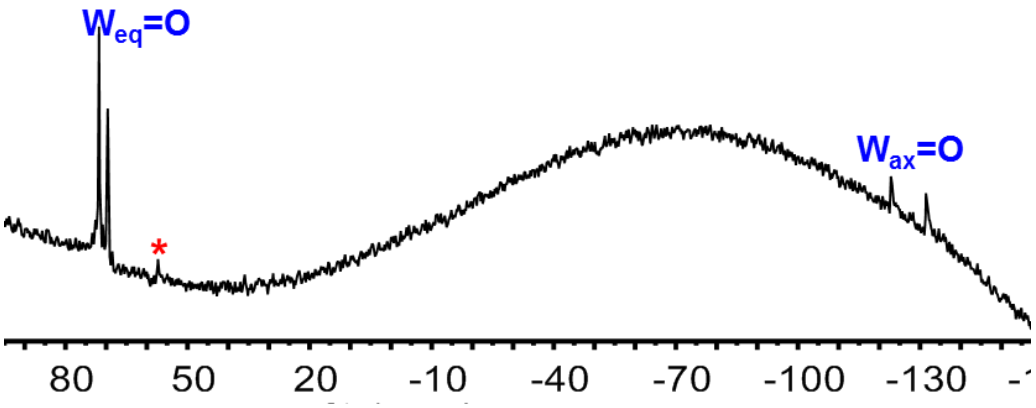

Figure 2.24: *^{183}W NMR spectrum of a mixture of $(TBA)_3[(MeO)SnW_5O_{18}]$ and $(TBA)_3[(HO)SnW_5O_{18}]$ in MeCN*

Table 2.3: *Comparative ^{17}O and ^{1}H NMR chemical shifts for $[TiW_5]$ and $[SnW_5]$ in MeCN*

Anion	^{17}O NMR / ppm				^{1}H NMR / ppm
	W=O	MOW	WOW	μ_6-O	OCH_3
$[(MeO)TiW_5O_{18}]^{3-}$	721(eq), 715 (ax)	525	390, 380	-55	4.10
$[(MeO)SnW_5O_{18}]^{3-}$	720(eq), 684 (ax)	395	383, 364	17	3.65

2.4.4 Preparation of $[(MeO)TiMo_5O_{18}]^{3-}$ from degradation of $(TBA)_2[Mo_6O_{19}]$ in MeCN

The non-aqueous degradation of $[W_6O_{19}]^{2-}$ has showed to be an efficient and reliable route to the tungstate Lindqvist-type POMs as described in the previous sections above, therefore extending similar approach to the molybdate $[Mo_6O_{19}]^{2-}$ anion can be significantly important to access new POMs designed from $[Mo_6O_{19}]^{2-}$ anion. To achieve this goal we adopted the same approach as in $[W_6O_{19}]^{2-}$ anion by degrading $[Mo_6O_{19}]^{2-}$ anion with 1.5 M solution of TBAOH (**see experimental section 2.4.4**) and reacted with the alkoxides precursor as shown in equation (Eqn. 2.4).

$$5[Mo_6O_{19}]^{2-} + 8OH^- + 6Ti(OPr^i)_4 + 5H_2O \rightarrow 6[(Pr^iO)TiMo_5O_{18}]^{3-} + 20MeOH \qquad 2.4$$

Upon addition of $Ti(OPr^i)_4$, as expected the six-coordinate titanium heterometal centre occupies the pocket of the pentadentate lacunary polyoxometalates 'ligand', $[Mo_5O_{18}]^{6-}$ which results in the formation of the $[TiMo_5]$ substituted Lindqvist-type POM. Note that some amount of MeOH was added during reaction to ensure that any residual $Ti(OPr^i)_4$ groups were replaced by Ti-CH_3O group. After recrystallisation the product was

characterised by FT-IR and multinuclear NMR spectroscopy and the results compared with previously reported [$TiMo_5$] species.[35]

(a) FT-IR spectroscopy

The FTIR spectrum (Figure 2.25) of the product contain a band at 957 cm^{-1} that could be assigned to ν(MoO) for terminal Mo=O. The band was shifted to lower wavenumber compared to the corresponding band for $(TBA)_2[Mo_6O_{19}]$ at 974 cm^{-1}. Bands observed at 1151 and 1105 cm^{-1} may be due to ν(CO) of the CH_3O group, while the ν(TiO) vibration in the alkoxide group is probably within 500 - 650 cm^{-1} region. The observed vibrations within the $[TiMo_5]^{3-}$ POM is at higher wavenumbers compared to the $[TiW_5]^{3-}$ species due to the different atomic mass of Mo to W.

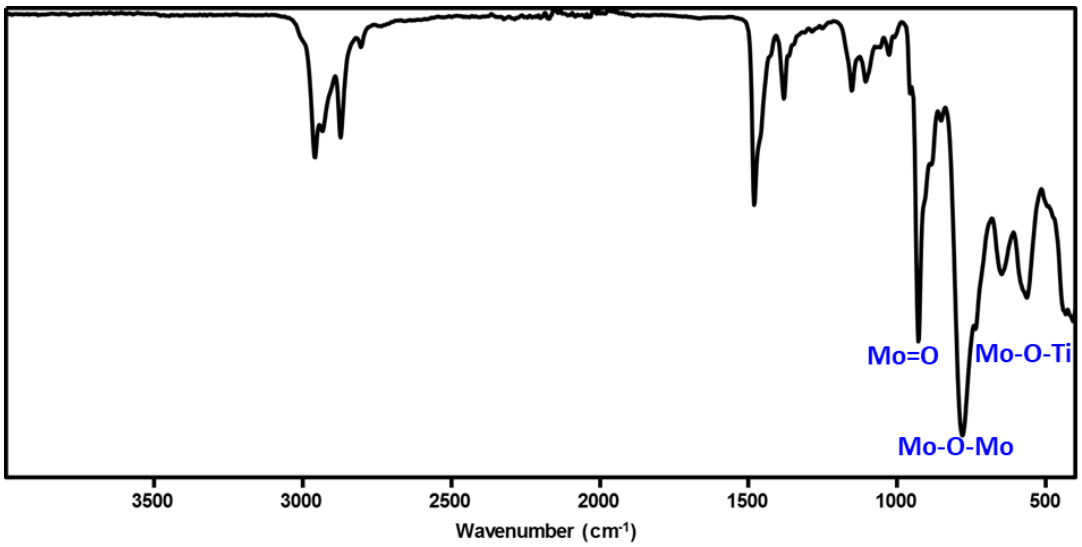

Figure 2.25: *FT-IR spectrum of $(TBA)_3[TiMo_5O_{18}]$*

(b) Multinuclear NMR spectroscopy

In the ^{1}H-NMR spectrum (Figure 2.26), the MeO:^{n}Bu_4N^+ ratio is ~1:3.6. This ratio is slightly higher by ~1 extra TBA. The low MeO:^{n}Bu_4N^+ ratio might be due to some hydrolysis of the highly moisture sensitive Mo_5TiOCH_3. Molybdenum oxides are quite moisture sensitive and therefore exposing the compound to moisture can cause some hydrolysis. The TiOMe peak in the molybdenum environment is observed at δ_H = 4.02 ppm slightly upfield of the $TiOCH_3$ peak in $[TiW_5]^{3-}$ system.

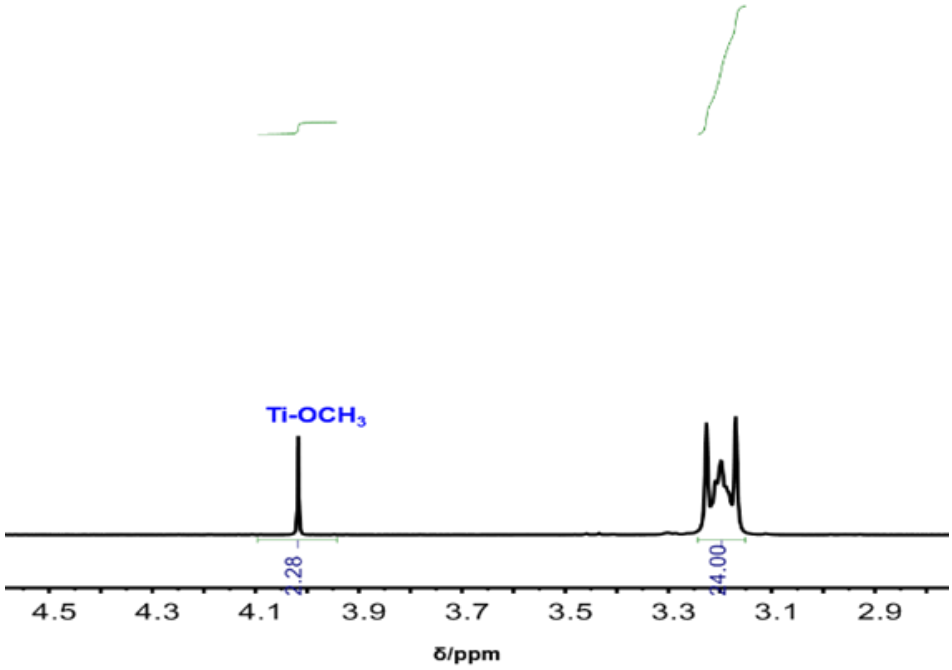

Figure 2.26**:** *^{1}H-NMR spectra of $(TBA)_3[(MeO)TiMo_5O_{18}]$ from degradation of $(TBA)_2[Mo_6O_{19}]$ after crystallization in acetonitrile.*

The ^{17}O NMR spectrum (Figure 2.27) which is characteristic of C_4v symmetry $[MM_5O_{18}]^{3-}$ Lindqvist structures[34] consisting of six unique non-equivalent oxygen sites. The equatorial and axial terminal W=O are observed at δ 877 and 858 ppm respectively. The peak at δ 620 ppm was assigned to be bridging Ti-O-Mo and the two peaks at δ 539 and 521 were assigned to Mo-O-Mo oxygens. The unique central peak μ_6-O was observed at 14 ppm. Although, this site is less enriched due to the position in the POM cage and therefore the peak is not very intense. The chemical shifts observed in the spectrum are consistent with the reported core $[TiMo_5O_{18}]^{3-}$.[34] In comparison with core $[TiW_5]^{3-}$, we observed that peaks were shifted to higher chemical shift in $[TiMo_5]^{3-}$ than in $[TiW_5]^{3-}$ due to electronic effect in Mo *vs* W. Peaks observed in this spectrum were all consistent with those observed in the reported $[TiMo_5]$ prepared in the previous route described above.[34]

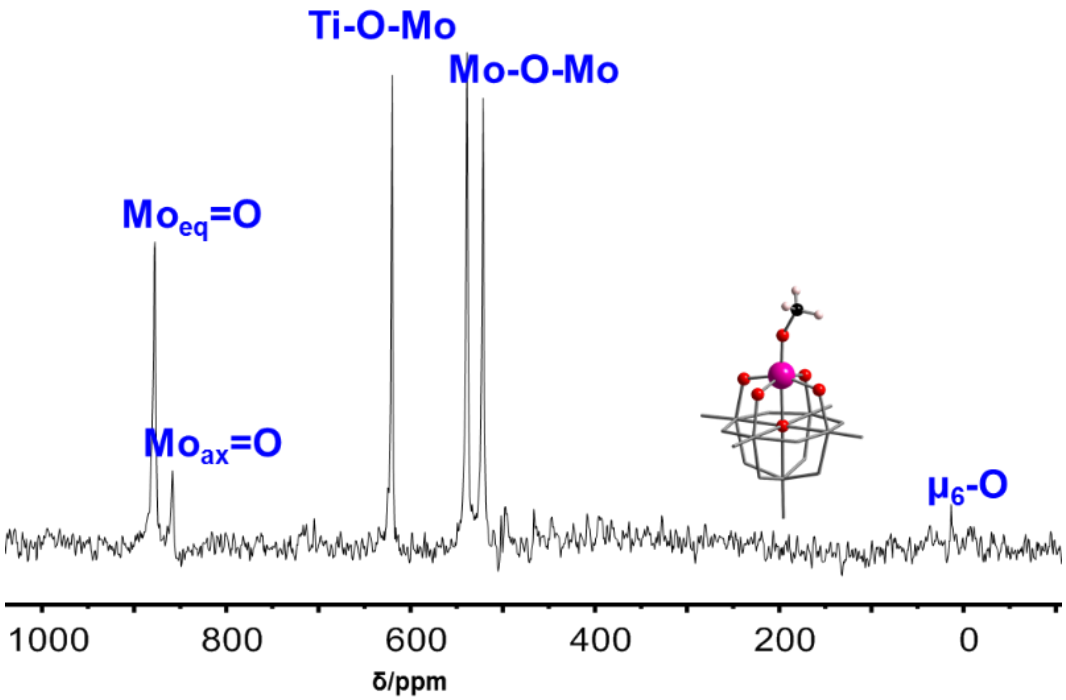

Figure 2.27: *^{17}O-NMR spectra of $(TBA)_3[(MeO)TiMo_5O_{18}]$ from $(TBA)_2[Mo_6O_{19}]$ after crystallization in acetonitrile*

2.4.5 Preparation of $[(MeO)SnMo_5O_{18}]^{3-}$ from degradation of $(TBA)_2[Mo_6O_{19}]$

The tin analogue $(TBA)_3[(MeO)SnMo_5O_{18}]$ was attempted according to (Equation 2.5). The preparation of the tin analogue from $(TBA)_2[Mo_6O_{19}]$ followed the same approach as above although $Sn(O^tBu)_4$ was added as the precursor similar to the $[SnW_5]$ synthesis. Upon addition of $Sn(O^tBu)_4$, initial ^{17}O NMR suggest some interaction. After 18 h of reactions and addition of some amount of MeOH resulted to any residual $Sn(O^tBu)_4$ groups been replaced by Sn-CH_3O group (**see experimental section 2.4.5 for details**).

$$5[Mo_6O_{19}]^{2-} + 8OH^- + 5Sn(O^tBu)_4 + 5H_2O \rightarrow 6[(MeO)SnMo_5O_{18}]^{3-} + 18MeOH \qquad 2.5$$

The ^{17}O NMR spectrum of the crude product (Figure 2.28) several peaks are observed, the terminal Mo=O peaks are located between δ 884 and 784 ppm and bridging Mo-O-Mo peaks between δ 553 to 392 ppm. Some peaks observed in the spectrum might be due to impurities. For example, the peak at δ 718 ppm could be due to terminal Mo=O oxygens, which might arise from impure due to hydrolysis product. Previously, peaks at δ 718 ppm in ^{17}O NMR spectra have been assigned to terminal Mo=O for $[Mo_2O_7]^{2-}$[35] suggesting that the dimolybdate anion is produced upon degradation of $[Mo_6O_{19}]^{2-}$.

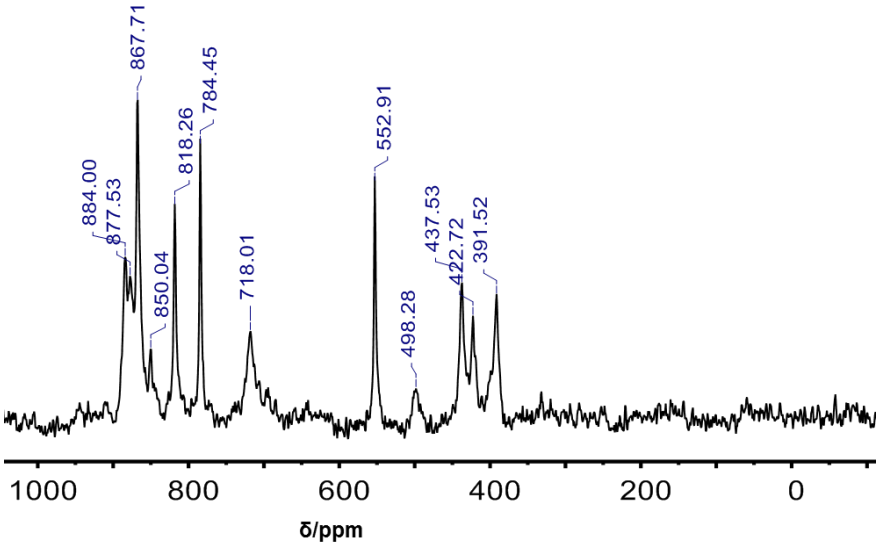

Figure 2.28: *^{17}O NMR spectrum of crude product of $(TBA)_3[(MeO)SnMo_5O_{18}]$ in MeCN*

After recrystallization, the ^{17}O NMR spectrum (Figure 2.29) became simplified with fewer peaks, although the axial and equatorial Mo=O peaks were not resolved and therefore a single peak was observed at δ 867 ppm and 717 ppm. These peaks appear to be a mixture of two species, which could not be identified. One with terminal Mo=O peaks at δ 867 ppm which might be associated with the bridging Sn-O-Mo or Mo-O-Mo at δ 499 and 400 ppm respectively. The other peaks at δ 717 for terminal Mo=O and bridging at 248 ppm MoOMo respectively could be assigned to the other species. The centra μ_6-O peaks were not fully enriched and therefore could not be observed in the spectrum.

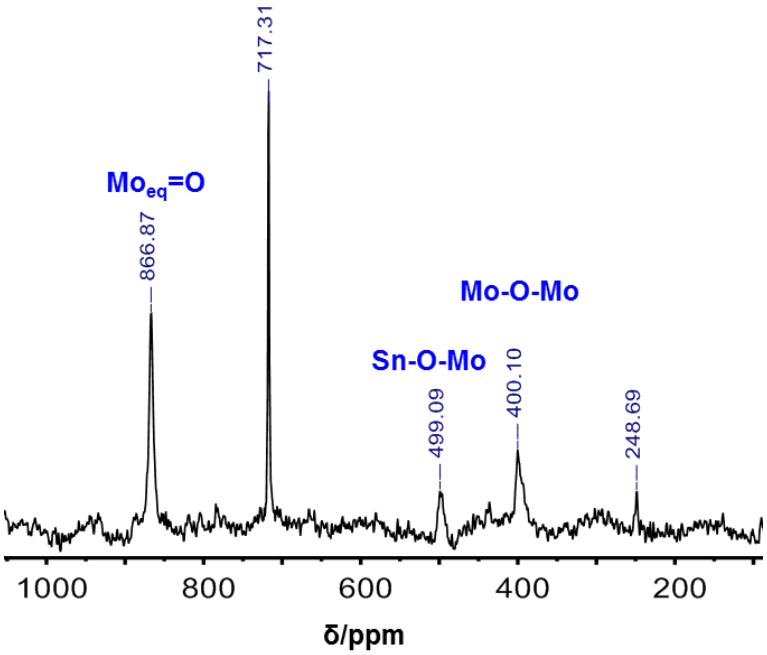

Figure 2.29: *^{17}O NMR spectrum of $(TBA)_3[(MeO)SnMo_5O_{18}]$ after recrystallized in MeCN*

In the ^{1}H NMR spectrum the OMe:$^{n}Bu_4N^+$ ratio was ~1:3, and the OMe group was observed at δ 3.73 ppm which is shifted slightly upfield compared to [MW_5] at δ 3.65 ppm. Satellite peaks associated with the O-CH_3 peak in the ^{1}H NMR spectrum showed ^{3}J couplings to ^{119}Sn and ^{117}Sn of 45.84 and 43.87 Hz respectively. Due to line broadening and lower natural abundance ^{115}Sn satellite peaks were not observed.

2.4.6 Attempted Preparation of $[(O)NbW_5O_{18}]^{3-}$ *via* degradation of $(TBA)_2[W_6O_{19}]$

This niobium substituted POM $[(O)NbW_5O_{18}]^{3-}$ was also prepared in a similar degradation route. In this method, $[W_6O_{19}]^{2-}$ was dissolved in 1.5 M solution of TBAOH and reacted with $Nb(OMe)_5$ with subsequent hydrolysis with ^{17}O-enriched H_2O shown in Equation 2.6.

$$5[W_6O_{19}]^{2-} + 8OH^- + 6Nb(OMe)_5 + 11H_2O \rightarrow 6[(MeO)NbW_5O_{18}]^{2-} + 30MeOH \qquad 2.6$$

(a) FT-IR spectroscopy

The FTIR spectrum (Figure 2.30) of the product showed a band at 931 cm^{-1} that was assigned to ν(WO) for terminal W=O. The band observed at 774 cm^{-1} was assigned to ν(WO) associated with the NbOW bridge, while the band at 569 cm^{-1} region was assigned to ν(NbO) or Nb–OC vibration.

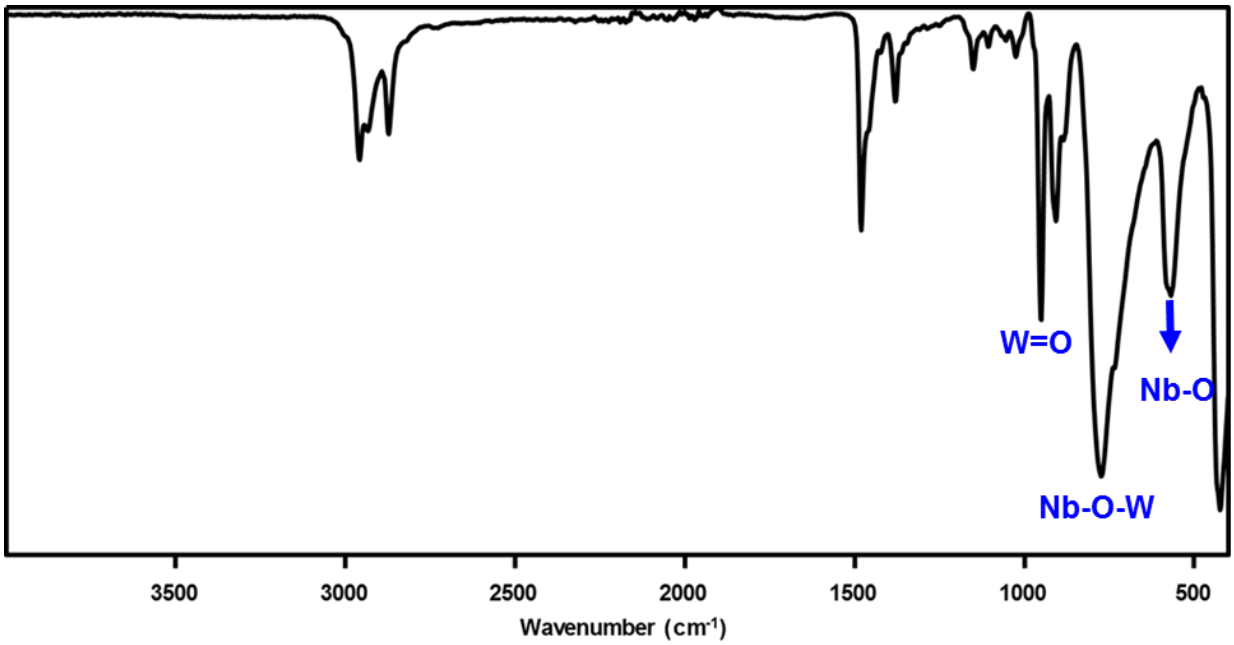

Figure 2.30: *FT-IR spectrum of $(TBA)_3[NbW_5O_{19}]$*

(b) Multinuclear NMR spectroscopy

The ^{17}O NMR spectrum (Figure 2.31) contains four non-equivalent types of oxygens, because of line broadening, the axial and the equatorial W=O peaks were not resolved. Hence a single peak was observed at δ 734 ppm for terminal W=O oxygen, a broad peak observed at δ 457 ppm was assigned to the doubly bridging ONbW oxygens. The broad line width has been ascribed to spin-spin coupling to quadrupolar niobium.[36] The peak at δ 394 ppm was assigned to bridging WOW and the unique central μ_6-O peak was observed at δ –65 ppm. The shifts are in agreement with ^{17}O NMR values reported for $[NbW_5O_{19}]^{3-}$ and the product of the reaction was identified as $[NbW_5O_{19}]^{3-}$.

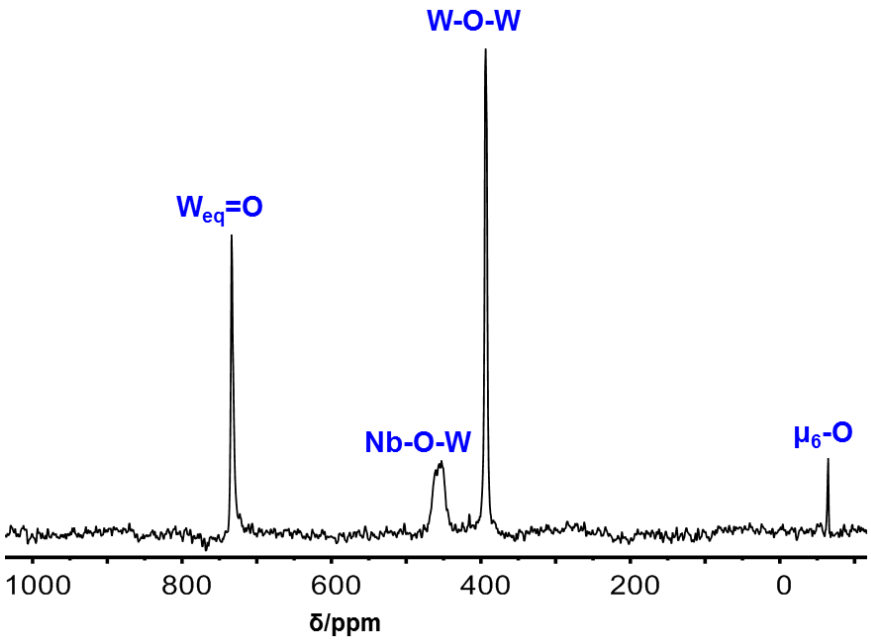

Figure 2.31: *^{17}O-NMR spectra of $(TBA)_3[(O)NbW_5O_{18}]$ from $(TBA)_2[W_6O_{19}]$ after crystallization in acetonitrile*

2.4.7 Attempted Preparation of $[(HO)PtW_5O_{18}]^{3-}$ *via* degradation of $(TBA)_2[W_6O_{19}]$

The Pt(IV) substituted POM $[(HO)PtW_5O_{18})]^{3-}$ was also attempted through the non-aqueous degradation route. As far as we know Pt(IV) substituted Lindqvist-type POM $[(HO)PtW_5O_{18})]^{3-}$ has not yet been reported. Structurally characterized Pt-substituted POMs are based on the Keggin-type and therefore it is interesting to explore the formation of this type of Lindqvist POM through the degradation route in order to access these important species.

Interest in platinum substituted POMs in recent years has been growing due to their catalytic activities which has been investigated and reported[37,38] and some Pt-POMs have showed to act as catalyst precursor.[39,40] Although, it has been reported that in the absence of terminal ligands the Pt centre in some cases is embedded in the metal oxide frame work and are apparently catalytically inactive until activated under certain conditions.[41, 42]

The attempted preparation involved degradation of $[W_6O_{19}]^{2-}$ anion with 1.0 M solution of TBAOH to form $[W_5O_{18}H_3]^{3-}$ species before the addition of $(TBA)_2Pt(OH)_6$ (Eqn. 2.7 and 2.8) (**see experimental section 2.4.7 for full details**). However, the initial ^{17}O NMR spectrum did not show the expected peaks for a $[XMW_5O_{18}]^{3-}$ species and therefore it was assumed the solution must have been too basic which prompted the addition of HBF_4 .Et_2O stepwise according to Equation 2.8.

$$5[W_6O_{19}]^{2-} + 8OH^- + 5H_2O \rightarrow 6[W_5O_{18}H_3]^{3-} \qquad 2.7$$

$$6[W_5O_{18}H_3]^{3-} + 6[Pt(OH)_6]^{2-} \rightarrow 6[(HO)PtW_5O_{18}]^{3-} + 12OH^- \ 18H_2O \qquad 2.8$$

Upon addition of the $HBF_4.Et_2O$ the ^{17}O NMR spectrum (Figure 2.32) became simplified. After recrystallization peaks were observed at δ 724 and 694 ppm which were due to terminal W=O peaks. These peaks are quite broad, but they however appeared in the expected region for terminal W=O peaks of a $[XMW_5O_{18}]^{3-}$ species. Peaks at δ 530 and 501 ppm are also present in the right region and these are assigned to bridging [M'OM] species while a peak at δ 383 ppm could be assigned to bridging M_2O. Note that these reactions were the first attempt therefore further investigations are required to obtain more information.

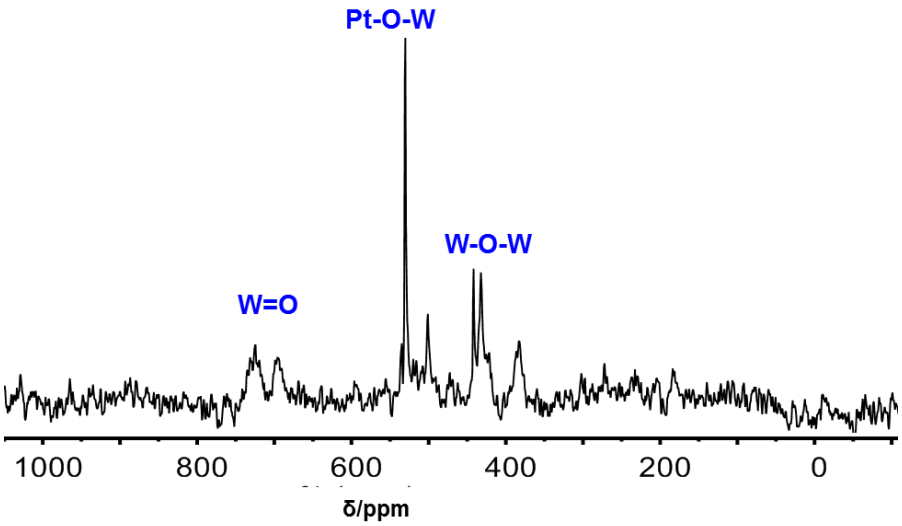

Figure 2.32: *^{17}O-NMR spectra of "$(TBA)_3[(HO)PtW_5O_{18}]$" from $(TBA)_2[W_6O_{19}]$ after crystallization in acetonitrile*

2.5 Conclusion

The first part of this chapter investigates a stepwise non-aqueous aggregation of $(TBA)_2[W_6O_{19}]$. The ^{17}O NMR spectroscopy data suggested that $[W_6O_{19}]^{2-}$ anions can aggregate in solution through "self-assembly" process by gradually decreasing the overall average negative charge per W. The aggregation process is significantly complex at the initial interaction of WO_4^{2-} and the metal alkoxides $WO(OMe)_4$. The results suggest that the W in these alkoxides can be Lewis acidic and with the lower alkyl group (R = CH_3) polymerisation occurs with the formation of alkoxide polymeric species which resulted to a complex ^{17}O NMR spectrum.

However, as the overall charge per tungsten ratio $^n/_x$ gradually decreases, $(TBA)_2[W_6O_{19}]$ can be obtained. In addition, there is an apparent intermediate which can be isolated although more work is needed to obtain pure single crystals for full X-ray analysis

The second part in the chapter show that access to a range of mono-substituted $[(L)M'M_5O_{18}]^{3-}$ can be achieved in high yield under mild conditions through the non-aqueous degradation of $(TBA)_2[W_6O_{19}]$. This investigation has laid the foundations to explore more new compounds in the Lindqvist-type POM family under these mild conditions.

2.6 Experimental

2.6.1 General procedures, solvents purifications and reagents

Manipulating air sensitive materials requires special techniques in order to avoid hydrolysis from atmospheric oxygen therefore all reactions and manipulations were conducted under an atmosphere of dry, oxygen-free nitrogen in screw-top flasks fitted with PTFE screw valves using standard Schlenk and dry-box. Sample filtration were always carried out *via* cannula filter sticks constructed using PTFE tape as described in literature.[43]

Glass syringes were used in all solvent and reagents measurements to avoid introduction of plasticizers into the sample. Hydrocarbon and ether solvents were dried over and distilled from sodium benzophenone ketyl. Acetonitrile was dried over and distilled from calcium hydride and methanol was pre-dried over 3Å molecular sieves and distilled from magnesium methoxide immediately prior to use. The 3Å sieves were activated by heating at 290 ^{o}C under vacuum for ~24 h.

All reagents were purchased commercially from Sigma Aldrich, Fisher Scientific, Alfa Aesar, Acros Organics, Fluka Chemika or Mersen and used without further purification. Most starting materials were prepared according to literature procedures for example. $(TBA)_2[WO_4]$,[44] $WOCl_4$,[45] $WO(OMe)_4$,[45] $Ti(OMe)_4$,[45] $Sn(^tOBu)_4$.[45]

2.6.2 Instrumentation

(a) ATR FT-IR spectroscopy

Fourier transform-Infrared spectra were recorded on a Bruker Alpha spectrometer (OPUS version 7.0 build) fitted with a Platinum ATR module or a Varian 600 FTIR spectrometer fitted with a Diamond ATR (4000 – 400 cm^{-1}). Spectra were recorded for solid samples after vacuum dried.

(b) Single Crystal X-ray diffraction analysis

All crystal structures were solved on analytical X-ray diffraction collected on Xcalibur Atlas Gemini ultra-diffractometer equipped with an Oxford Cryosystems CryostreamPlus open-flow N_2 cooling device. The single crystals were placed on a cryoloop using Fomlin YR-1800 oil under nitrogen. Enhance Ultra (Cu) X-ray Source ($\lambda_{CuK\alpha}$ = 1.54184 Å) and an Enhance (Mo) X-ray Source ($\lambda_{MoK\alpha}$ = 0.71073 Å)] were used to obtained data. CrysAlisPro software were used for cell refinement [46] intensities were corrected for absorption by a multifaceted crystal model based on the expressions derived by R.C. Clark & J.S. Reid.[47] The structures were solved by XT [48] and refined by XL[49] using the Olex2 graphical interface.[50]

Hydrogen atoms in all structures were positioned with idealised geometry whilst non-hydrogen atoms were refined anisotropically. For the hydrogen atoms the displacement parameters were constrained using a riding model SADI and EADP.

(c) Multinuclear NMR spectroscopy (^{1}H, ^{17}O, ^{13}C, ^{119}Sn, ^{183}W and ^{195}Pt)

The NMR spectra were recorded on either Bruker Avance 7.05 Tesla (300 MHz), 9.40 Tesla (400 MHz), 11.75 Tesla (500 MHz) or 16.44 Tesla (700 MHz) spectrometers. Chemical shifts were referenced relative to external standards for example 85% TMS (^{1}H and ^{13}C); D_2O (^{17}O); Me_4Sn 90 % in C_6D_6; (^{119}Sn); 85% H_3PO_4 (^{31}P), 1 M Na_2WO_4 in D_2O (^{183}W); 1.2 M Na_2PtCl_6 in D_2O (^{195}Pt). Relaxation delays were set at 30 s for ^{1}H, 0.0010 s for ^{17}O, 1 s for ^{13}C, 20 s for ^{31}P, 8 s for ^{119}Sn, 3 s for ^{183}W and 0.05 s for ^{195}Pt. NMR spectra were recorded at ambient probe temperature (~295K) in a 5-mm screw capped spinning tubes for all nuclei except for ^{183}W where 10-mm screw capped spinning tubes were used.

Samples were mostly locked with deuterated solvents NMR solvents (except water-d_2) were degassed on a Schlenk line and dried over activated 3Å molecular sieves for few days before use. All ^{183}W NMR analyses were recorded over 3 days (~72 h) Typical concentrations of NMR samples were 0.05 M (^{1}H); (^{17}O, ^{119}Sn) and 0.20 M (^{183}W). 2D ^{1}H EXSY experiments were recorded at 333 K with a relaxation delay of 60 s.

2.6.3 Preparation of Starting Materials

2.6.3.1 Preparation of $WO_3.H_2O$

A solution of $Na_2WO_4.2H_2O$ (132.16 g, 400.67 mmols) in deionized H_2O (250 mL) was prepared and the colourless solution was heated to about 90 ^{o}C. A 6.0 M HCl solution (467 mL, 2804 mmols) was slowly added from a burette over 30 min period. As the acid is added, the solution gradually formed yellow precipitate. After addition of HCl, the solution was stirred further for 30 mins at 90 ^{o}C to give a yellow suspension, which was cooled down to room temperature and allowed to settle for about 2 h before filtering under suction overnight. The yellow paste was washed with ethanol (20 mL x 5) and dither ether (20 mL x 5) and the yellow sticky solid transferred to vacuum desiccator over silica gel for 48 h. After drying, the yellow solid was crushed and dried in the same way as above (**86.2 % yield**).

2.6.3.2 Preparation of $(TBA)_2WO_4$

A solution of 1.5 M aqueous TBAOH (120 mL, 120 mmols) was placed in a 250 mL round bottom flask. $WO_3.H_2O$ (15 g, 60 mmols) was added in portion with stirring. After addition, stirring continue for 24 h. The pale-yellow solution gradually became clear as the reaction proceeded. The clear solution was filtered after stirring for 24 h on a

Buchner funnel and the filtrate was washed with dry acetonitrile. The solution was then evaporated to dryness under vacuum. The oily sticky material triturated with diethyl ether several times to obtain a crystalline solid material $(TBA)_2WO_4$ (**30.2 g, 68 % yield**). **^{17}O NMR** δ 442 ppm and **^{183}W NMR** δ 4.06 ppm.

2.6.3.3 6 M HCl solution

A concentrated solution of HCl (12.08 M, 250 mL) was diluted with deionized H_2O (200 mL) in a 500 mL volumetric flask and made up to 500 mL mark.

2.6.3.4 Preparation of $WOCl_4$ from literature procedure

$WO_3.H_2O$ (65.5g, 262.14 mmol) was added to excess $SOCl_2$ (300 mL) in a 1L round bottom flask to give bright yellow suspension. The solution gradually changed from orange to red after about an hour of reaction with the evolution of gas bubbles which was trapped with a KOH trap. The mixture was allowed to reflux overnight at ~85 ^oC and the resulting bright red solution was vacuum dried. The crude product (85 g) was transferred into a sublimation flask (20 – 25 g) x 3 and sublimed under vacuum for ~1 h by heating from an IR-Lamp. The sublimate was weighed and transferred into a sample bottle in a dry box. (**69.3 g, 78 % yield**).

2.6.3.5 Preparation of $WO(OMe)_4$ prepared from literature procedure

$WOCl_4$ (17.22g, 50.40 mmol) was dissolved in THF (180 mL) at ~ –30 ^oC in one side of a double round bottom filter flask to give a red solution. MeOH (8.2m, 202 mmol) was added and NH_3 gas bubbled through the resulting yellow solution for ~5 mins to give a white precipitate. N_2 was bubbled through the solution for 10 mins to remove any excess NH_3 and the solution was allowed to settle for overnight before filtering under vacuum. The pale-yellow filtrate was vacuum dried in a Schlenk flask giving crude material which was recrystallized to obtain a pure $WO(OMe)_4$ (**14.06g, 78 % yield**). **^{1}H NMR** (300.13 MHz, toluene-d_3): δ 4.48, 4.35, 4.33 ppm in a ratio 2:1:1.

2.6.4 Hydrolysis Reaction of $[W_xO_y]^{n-}$ by stepwise addition of $WO(OCH_3)_4$ to $(TBA)_2W^*O_4$

2.6.4.1 Hydrolysis reaction of 1:1 mixture of $(TBA)_2[WO_4]$ and $WO(OCH_3)_4$ in MeCN

A solution of $(TBA)_2WO_4$ (0.5 g, 0.68 mmols) and $WO(OMe)_4$ (0.22 g, 0.68 mmols) in MeCN (5 mL) was prepared in a Schlenk flask. The resulting solution was stirred for about 1 h before adding ^{17}O enriched H_2O (25 µL, 1.3647 mmols). After stirring for further 1 h, the solution was pumped dry under vacuum to remove the volatiles. Solids crystals were washed with Et_2O (4 mL x 2) and pumped dry for 30 min before recording

^{17}O NMR spectrum of the white solid material "$(TBA)_2W_2O_5(OMe)_4$" (**0.669 g, 90 % yield**). **^{17}O NMR** (41 MHz) δ (ppm) 701, 674, 665, 647, 636, 602, 574, 537, 522, 504, 492, 474, 441, 431, 425, 404, 323, 300, 248, 229, 201 and -15.

2.6.4.2. Hydrolysis reaction of 1:2 mixture of $(TBA)_2[WO_4]$ and $WO(OCH_3)_4$ in MeCN

A solution of "$(TBA)_2W_2O_5(OMe)_4$" (0.669 g, 0.6145 mmols) in MeCN (3 mL) in a Schlenk flask was added $WO(OMe)_4$ (0.200 g, 0.6145 mmols). The resulting solution was stirred for about 1 h before adding ^{17}O enriched H_2O (22.2 µL, 1.229 mmols). After stirring for further 1 h, the solution was pumped dry under vacuum to remove the volatiles. The solid crystalline material was washed with Et_2O (4 mL x 2) and pumped dry for 1 h before recording the ^{17}O NMR spectrum of the white solid material "$[W_3O_{10}]^{2-}$" (**0.706 g, 87 % yield**). **^{17}O NMR** (41 MHz,) δ (ppm) 777, 722, 709, 705, 668, 417, 391 356 ppm.

2.6.4.3. Hydrolysis reaction of 1:3 mixture of $(TBA)_2[WO_4]$ and $WO(OCH_3)_4$, in MeCN

A solution of "$(TBA)_2W_3O_{10}(OMe)_4$" (0.706 g, 0.5346 mmols) and $WO(OMe)_4$ (0.1732 g, 0.5346 mmols) in MeCN (3 mL) prepared in a Schlenk flask was stirred for 1 h before adding ^{17}O enriched H_2O (19 µL, 1.0692 mmols). The resulting clear solution was stirred for further 1 h and pumped to dryness under vacuum to remove the volatiles. The solid crystalline material was washed with Et_2O (4 mL x 2) and pumped dry for 1 h before recording the ^{17}O NMR spectrum of the white solid material "$[W_4O_{13}]^{2-}$" obtained (**0.664 g, 80 % yield**). **^{17}O NMR** (41 MHz,) δ (ppm) 777, 708, 678 527 and 416 ppm

2. 6.4.4. Hydrolysis reaction of 1:4 mixture of $(TBA)_2[WO_4]$ and $WO(OCH_3)_4$, in MeCN

A solution of "$(TBA)_2W_4O_{13}(OMe)_4$" (0.664 g, 0.4277 mmols) and $WO(OMe)_4$ (0.1386 g, 0.4277 mmols) in MeCN (3 mL) prepared in a Schlenk was stirred for 1 h before adding ^{17}O enriched H_2O (15.4 µL, 0.8554 mmols). The resulting clear solution was stirred for further 1 h and pumped dried under vacuum to remove the volatiles. The solid crystalline material washed with Et_2O (4 mL x 2) and pumped dry for 1 h before recording the ^{17}O NMR spectrum of the white solid material "$[W_5O_{16}]^{2-}$" obtained (**0.595 g, 78 % yield**). **^{17}O NMR** (41 MHz,) δ (ppm) 777, 708, 678 527 and 416 ppm.

2.6.4.5. Hydrolysis reaction of 1:5 mixture of $(TBA)_2[WO_4]$ and $WO(OCH_3)_4$ in MeCN

A solution of "$(TBA)_2W_5O_{16}(OMe)_4$" (0.595 g, 0.3336 mmols) and $WO(OMe)_4$ (0.1081 g, 0.3336 mmols) in MeCN (3 mL) prepared in a Schlenk was stirred for 1 h and add ^{17}O enriched H_2O (12 µL, 0.6672 mmols). The resulting clear solution was stirred for further 1 h before it was pumped dry under vacuum to remove the volatiles. The solid crystalline material washed with Et_2O (4 mL x 2) and pumped dried for 1 h. The ^{17}O NMR spectrum of the white solid material $(TBA)_2[W_6O_{19}]$ obtained (**0.511 g, 76 % yield**). **^{17}O NMR** (41 MHz,) δ (ppm) 777 and 416. **IR (4000 – 400 cm^{-1}):** 2959 (m), 2872 (m), 1481 (m), 1380 (m), 1345(w), 1151(w), 1107(vw), 1041 (w), 976882 (m), 809(s), 760(s), 675 (s), 608(m), 548(m), 528 (m), 451 (m).

2.6.4.6. Formation of $(TBA)_2[W_6O_{19}]$ and isolation of intermediate by hydrolysis of a 1:5 mixture of $(TBA)_2[WO_4]$ and $WO(OCH_3)_4$ in MeCN

A solution of $(TBA)_2WO_4$ (0.5 g, 0.6823 mmols) and $WO(OMe)_4$ (1.1053 g, 3.4117 mmols) in MeCN (~5 mL) was prepared in a Schlenk flask. The resulting clear solution was stirred for about 1 h and added ^{17}O enriched H_2O (123 µL, 6.8234 mmols). The solution was heated overnight at 60 ^oC and cool down to –20 ^oC. White crystalline solid was formed and separated *via* cannula filtration and pumped to dryness under vacuum. Crystals were washed with Et_2O (4 mL x 2) and pumped dried for 1 h. (**0.236 g)**. **^{17}O NMR** (41 MHz,) δ (ppm) 721, 709, 705, 415 354 ppm. **IR (4000 – 400 cm^{-1}):** 2959 (s), 2934 (m), 2873 (m), 2810 (vw) 2112 (w) 1605(m), 1483 (m), 1461 (m), 1428 (m), 1383 (m), 1154(w), 1105(vw), 1077 (w), 1017 (m), 948 (s), 904 (m), 725(vs), 548(m) and 508 (m). **^{1}H NMR** (300 MHz, acetonitrile-d_3) 4.41, 4.27, 4.19 and 3.96 **^{183}W NMR** (21 MHz, acetonitrile-d_3) δ (ppm) -66 and -72.

2.6.5 Novel and efficient route to $(TBA)_3[(RO)M'M_5O_{18}]$ (R = CH_3; M′ = Ti, Sn; M = W, Mo and $(TBA)_3[NbW_5O_{19}]$

2.6.5.1 Preparation of $[(MeO)TiW_5O_{18}]^{3-}$ from degradation of $(TBA)_2[W_6O_{19}]$ using $Ti(OMe)_4$ precursor in MeCN

A 1.0 M methanolic TBAOH (0.43 mL, 0.43 mmol) was placed in a Schlenk flask and dissolved in MeCN (2 mL) and vacuum dried. This process was repeated twice to remove all volatiles before adding MeCN (5 mL). In a separate Schlenk flask, $(TBA)_2W_6O_{19}$ (0.5 g, 0.2643 mmol) was dissolved in MeCN (10 mL) and stirred for 1 h until all solids dissolved. The clear solution was transferred into the flask containing the dried TBAOH solution *via* cannula transfer. The resulting solution was stirred for 1

h at room temperature before adding ^{17}O enriched H_2O (~5 µL, 0.2643 mmols). The solution was stirred for further 30 mins and added $Ti(OMe)_4$ (0.055 g, 0.3172 mmols). A milky suspension formed immediately which was stirred for further 18 h at room temperature leaving a clear solution which was pumped to dryness under vacuum. The crude product was re-dissolved in a minimum of MeCN (~3 mL) and placed in a freezer at - 20 °C. The white crystalline solid were separated by cannula filtration and pumped dry under vacuum. Et_2O was added to the mother liquor and placed into freezer at – 20 °C. This process was repeated twice more to give a total of 0.43 g of $(TBA)_3[(MeO)TiW_5O_{18}]$ (**0.434 g, 68% yield**). **FT-IR ATR (4000 – 400 cm^{-1})** 2958 (m), 2871(m), 2801(w), 1481(m), 1380 (m), 1151 (m), 1106 (m), 1025 (w), 943 (s), 882 (m), 793 (m), 616, 618, 593, 519, 485, 421 cm^{-1}. **^{1}H NMR** (300 MHz, acetonitrile-d_3) δ (ppm) 4.11 in addition to $^nBu^+$. **^{17}O NMR** (41 MHz, acetonitrile-d_3) δ (ppm) 722, 715, 526, 392, 382, -55.

2.6.5.2 Preparation of $[(MeO)TiW_5O_{18}]^{3-}$ from degradation of $(TBA)_2[W_6O_{19}]$ using $Ti(^iOPr)_4$ precursor in MeCN

A solution of 1.5 M methanolic TBAOH (0.85 mL, 0.846 mmol) was placed in a Schlenk flask and dissolved in MeCN (3 mL) the solution was then pumped to dryness under vacuum. This process was repeated twice to remove the volatiles before adding MeCN (5 mL). In a separate Schlenk flask, $(TBA)_2W_6O_{19}$ (1.0 g, 0.527 mmol) was dissolved in MeCN (10 mL) and the content stirred for 1 h to dissolve all solids. The clear solution was transferred into the flask containing the dried TBAOH solution *via* cannula transfer. The resulting solution was stirred for 1 h at room temperature before adding ^{17}O-enriched H_2O (~10 µL, 0.5286 mmols). After the addition of ^{17}O-enriched H_2O, the resulting solution was stirred for further 30 mins before adding $Ti(^iOPr)_4$ (192 µL, 0.6342 mmols). The solution immediately became pale yellow and was stirred for 18 h. The clear yellowish-brown solution was pumped to dryness under vacuum. The crude product was washed with hot toluene (5 mL) pumped dry and washed with Et_2O (5 mL x 3).

The solid crystalline material was re-dissolved in a minimum of MeCN (3 mL) precipitated with Et_2O and placed in a freezer at -20 °C. The white crystalline solid formed separated by cannula filtration and pumped dry under vacuum. A minimum amount of Et_2O was added to the mother liquor to form white suspension, which was warmed up gently to re-dissolved the solute and placed into freezer at –20 °C This process was repeated twice more to give a total of 0.37 g of $(TBA)_3[(MeO)TiW_5O_{18}]$ (**0.37 g, 58%**). **FT-IR ATR (4000 – 400 cm^{-1})** 2958 (m), 2871(m), 2801(w), 1481(m),

1380 (m), 1151 (m), 1106 (m), 1025 (w), 943 (s), 882 (m), 793 (m), 616, 618, 593, 519, 485, 421 cm^{-1}. **^{1}H NMR** (300 MHz, acetonitrile-d_3) δ(ppm) a single peak at 4.11 and some minor impurity peaks at 4.17, 4.31 and 4.4 ppm. **^{17}O NMR** (41 MHz, acetonitrile-d_3) δ 722, 715, 526, 392, 382, -55.

2.6.5.3 Preparation of $(TBA)_3[(MeO)_3Ti_2W_4O_{16}]$ from degradation of $(TBA)_2[W_6O_{19}]$ using $Ti(^{i}OPr)_4$ precursor in MeCN

In a Schlenk flask A, was charged with $(TBA)_2WO_4$ (2.42 g, 3.303 mmols), $Ti(OMe)_4$ (0.568 g, 3.303 mmols) and dissolved in MeCN (20 mL) the solution was heated to 70 ^{o}C in an oil bath which turns pale yellow as the reaction proceeded. In a separate Schlenk flask B, $WO(OMe)_4$ (1.07 g, 3.303 mmols) was dissolved in hot MeCN (5 mL) at 70 ^{o}C in an oil bath. The two solutions were combined *via* cannula transfer and the resulting solution was heated to 70 ^{o}C for 1 h. ^{17}O enriched H_2O (505.85 µL, 56.43 mmols) was added and the mixture was further heated with stirring at 90 ^{o}C for 20 h. The solution was cooled down to room temperature before pumping to dryness under vacuum. The solid product was dissolved in excess MeOH (~1.0 mL, 20 mmols.) and heated at 90 ^{o}C for ~2 h. The solution was cooled down to room temperature and pumped to dryness under vacuum. The crude product was dissolved in a minimum amount of MeCN (5 mL) and Et_2O was added. The solution was gently warmed and allowed to cool to room temperature before placing in a freezer at -20 ^{o}C. The crystalline material formed were separated by cannula filtration and pumped dry under vacuum. Diethyl ether was added to the mother liquor and placed in a freezer at -20 ^{o}C. The white crystalline solid formed were separated by cannula filtration and pumped dry under vacuum. This process was repeated several times more to give a total of 0.9 g of (**$(TBA)_3[(MeO)_3Ti_2W_4O_{16}]$**) (**0.91 g, 45%**).

FT-IR ATR (4000 – 400 cm^{-1}) 2958 (m), 2873 (m), 2808 (w), 1481(m), 1381 (m), 1152 (m), 1105 (m), 1028 (w), 949 (s), 883 (m), 785 (m), 591, 540, 426 cm^{-1}. **^{1}H NMR** (300 MHz, acetonitrile-d_3) δ (ppm) 4.11 and 3.81 ppm in 2:1 respectively. **^{17}O NMR** (41 MHz, acetonitrile-d_3) δ (ppm) 723, 715, 704, 697, 546, 541, 527, 513, 392, 382, -56. **^{183}W NMR** (21 MHz, acetonitrile-d_3) δ (ppm) 8 and 7 ppm.

2.6.5.4 Preparation of $[(MeO)SnW_5O_{18}]^{3-}$ from degradation of $(TBA)_2[W_6O_{19}]$ using $Sn(^{t}OBu)_4$ precursor in MeCN

A solution of 1.0 M methanolic TBAOH (0.85 mL, 0.846 mmol) was placed in a Schlenk flask and dissolved in MeCN (2 mL). The solution was pumped dry under vacuum. This process was repeated twice to remove all volatiles before adding MeCN (5 mL). In a separate Schlenk flask $(TBA)_2W_6O_{19}$ (1.0 g, 0.527 mmol) was dissolved in MeCN (20

mL) with stirring. The clear solution was transferred into the flask containing the dried TBAOH solution *via* cannula transfer. The resulting solution was stirred for 1 h at room temperature before adding ^{17}O-enriched H_2O (~10 µL, 0.5286 mmols). After stirring for ~30 mins, $Sn(^tOBu)_4$ (0.261 g, 0.6342 mmols) was added. The solution was subsequently stirred for further 18 h resulting to a clear brown solution which was pumped to dryness under vacuum. The crude product was dissolved in MeCN and heated in excess MeOH (1 mL) for 1 h. The solution was pumped dry and washed with Et_2O (5 mL x 2). The solid crystalline material was re-dissolved in a minimum of MeCN (5 mL) and placed in a freezer at -20 ^oC. The white crystal solid formed was separated by cannula filtration and pumped dry under vacuum. Et_2O was added to the mother liquor and placed in freezer at –20 ^oC. This process was repeated to give a total of 0.278 g of $(TBA)_3[(MeO)SnW_5O_{18}]$ (**0.278 g, 42 %**). **FT-IR ATR (4000 – 400 cm^{-1})** 2959 (m), 2873 (m), 2809 (m), 1674 (m), 1482 (s), 1381(m), 1045 (w), 973 (w), 951(s), 882 (w), 827 (m), 799 (s), 756 (s), 623, 569, 537, 445, 423 cm^{-1} **^1H NMR** (300 MHz, acetonitrile-d_3) δ(ppm) 3.65 ppm. **^{17}O NMR** (41 MHz, acetonitrile-d_3) δ (ppm) 721, 686, 397, 384, 369 and 18.

2.6.5.5 Preparation of $(TBA)_3[(MeO)TiMo_5O_{18}]$ by degradation of $(TBA)_2Mo_6O_{19}$ using $Ti(^iOPr)_4$ precursor in MeCN

A 1.0 M methanolic TBAOH (0.6 mL, 0.5862 mmol) was placed in a Schlenk flask and dissolved in MeCN (2 mL) and then pumped to dryness under vacuum. This process was repeated twice more to remove volatiles before adding MeCN (5 mL). In a separate Schlenk flask $(TBA)_2Mo_6O_{19}$ (0.5 g, 0.3664 mmol) was dissolved in MeCN (20 mL) with stirring to dissolve all solid. The clear yellow solution was transferred into the flask containing the dry TBAOH solution *via* cannula transfer. The resulting solution was stirred for 1 h at room temperature before adding ^{17}O-enriched H_2O (~7 µL, 0.3664 mmols). The solution was stirred for a further 30 min before adding $Ti(^iOPr)_4$ (133 µL, 0.4397 mmols). The yellow solution was further stirred for 1 h and added MeOH (1.5 mL). The clear yellow solution was pumped dry under vacuum. The crude product (greenish yellow) was washed with hot toluene several times and then with Et_2O (2 x 5 mL). The product was dissolved in a minimum of MeCN and precipitated with Et_2O which was gently warmed to re-dissolve suspension and placed into a freezer ~20 ^oC. The greenish yellow crystals formed were separated by cannula filtration and pumped dry under vacuum. This process was repeated to give a total of 0.3876 g of $(TBA)_3[(MeO)TiMo_5O_{18}]$ (**0.3876 g, 56 %**). **FT-IR ATR (4000 – 400 cm^{-1})** 2959 (m), 2872 (m), 2804 (m), 1480 (s), 1380 (m), 1152 (w), 1105 (w), 1027 (w), 956(s), 927 (w),

852 (w), 780 (s), 648, 563 cm^{-1} **^{1}H NMR** (300 MHz, Acetonitrile-d_3) δ 4.02 ppm. **^{17}O NMR** (41 MHz, acetonitrile-d_3) δ (ppm) 878, 858, 620, 539, 521, 13.

2.6.5.6 Attempted preparation of $(TBA)_3[(MeO)SnMo_5O_{18}]$ by degradation of $(TBA)_2Mo_6O_{19}$ using $Sn(^tOBu)_4$ precursor.

A solution of 1.0 M methanolic TBAOH (1.2 mL, 1.1725 mmol) was placed in a Schlenk flask, dissolved in MeCN (2 mL) then pumped dry under vacuum. This process was repeated twice to evacuate volatiles before adding MeCN (5 mL). In a separate Schlenk flask $(TBA)_2Mo_6O_{19}$ (1.0 g, 0.7328 mmol) was dissolved in MeCN (20 mL) with stirring until all solids dissolved. The bright yellow solution was transferred into the flask containing the dry TBAOH solution *via* cannula transfer. The resulting solution was stirred for 1 h at room temperature before adding ^{17}O enriched H_2O (~13 µL, 0.7328 mmols). To the bright-yellow solution was added $Sn(^tOBu)_4$ (0.36 g, 0.8797 mmols) and a further 18 h stirring. The clear yellow solution was pumped dry under vacuum to obtain the crude yellow crystalline solids. The crude product was dissolved in MeCN (5 mL) and heated in excess MeOH (1 mL) for 1 h, pumped dry and washed with Et_2O (5 mL x 2). The solid was re-dissolved in a minimum of MeCN (5 mL) and placed in a freezer at -20 ^oC. The yellow crystalline solid formed was separated by cannula filtration and pumped dry under vacuum. Diethyl ether (2 mL) was added to the solution forming a white milky solution which was gently warmed to dissolve the suspension and placed into a freezer at -20 ^oC. The greenish yellow crystals formed were separated by cannula filtration and pumped dry under vacuum. This process was repeated few times to give a total of 0.278 g of $(TBA)_3[(MeO)SnMo_5O_{18}]$ (**0.251 g, 52 %**). **FT-IR ATR (4000 – 400 cm^{-1})** 2959 (m), 2873 (m), 2809 (m), 1674 (m), 1482 (s), 1381(m), 1045 (w), 973 (w), 951(s), 882 (w), 827 (m), 799 (s), 756 (s), 623, 569, 537, 445, 423 cm^{-1} **^{1}H NMR** (300 MHz, acetonitrile-d_3) δ (ppm) 3.73 ppm with $^3J(^{119}Sn\{^1H\})$ = 46 Hz and $^3J(^{117}Sn\{^1H\})$ = 44 Hz. **^{17}O NMR** (41 MHz, acetonitrile-d_3) δ (ppm) 867, 842, 717, 499 and 400.

2.6.5.7 Preparation of $(TBA)_2[(O)NbW_5O_{18}]$ by degradation of $(TBA)_2W_6O_{19}$ using $Nb(OMe)_5$ precursor.

A solution of 1.0 M methanolic TBAOH (0.63 mL, 0.6343 mmol) was placed in a Schlenk flask, dissolved in MeCN (2 mL) then pumped dry under vacuum. The process was repeated twice to remove volatiles before adding 5 mL MeCN. In a separate Schlenk flask $(TBA)_2W_6O_{19}$ (0.75 g, 0.3964 mmol) was dissolved in MeCN (20 mL) and stirred to dissolve all solid. The clear solution was transferred into the flask containing the dried TBAOH solution *via* cannula transfer. The resulting brownish solution was

stirred for 1 h at room temperature before adding ^{17}O-enriched H_2O (~16 µL, 0.8721 mmols). $Nb(OMe)_5$ (0.118 g, 0.4757 mmols) was added and subsequent further 18 h stirring. A clear solution resulted which was pumped dry under vacuum. The crude product was dissolved in MeCN (3 mL) and placed in a freezer at -20 °C. The crystalline solid formed was separated by cannula filtration and pumped dry under vacuum (**0.297 g, 52 %**). **FT-IR ATR (4000 – 400 cm^{-1})** 2958 (m), 2872 (m), 1481 (s), 1380 (m), 1151 (w), 1107 (w), 1055 (w), 1025 (w), 951(s), 908 (w), 774 (s), 569, 424 cm^{-1} **^{17}O NMR** (41 MHz, acetonitrile-d_3) δ (ppm) 733 (W=O), 456 (NbOW) 394 (WOW) -64 (μ_6-O).

2.6.5.8 Attempted preparation of $(TBA)_3[(O)NbW_5O_{18}]$ by degradation of $(TBA)_2W_6O_{19}$ plus $Nb(OMe)_5$ precursor.

A solution of 1.0 M methanolic TBAOH (0.41 mL, 0.41 mmol) was placed in a Schlenk flask, dissolved in MeCN (2 mL) and then pumped to dryness under vacuum. The process was repeated twice to remove volatiles before adding MeCN (5 mL). In a separate Schlenk flask $(TBA)_2W_6O_{19}$ (1.93 g, 1.02 mmol) was dissolved in MeCN (20 mL) with stirring until all the solids dissolved. The clear solution was transferred into the Schlenk flask containing the dried TBAOH solution *via* cannula transfer. The resulting brown solution was stirred for 1 h at room temperature before adding ^{17}O-enriched H_2O (~41 µL, 2.24 mmols). $Nb(OMe)_5$ (0.30 g, 1.22 mmols) was added and subsequently stirred for further 18 h. The solution was pumped to dryness under vacuum. The crude product was dissolved in MeCN (5 mL) and placed in a freezer at -20 °C. The crystalline solid material formed was separated by cannula filtration and pumped dry under vacuum. Diethyl ether (3 mL) was added to the mother liquor forming a milky solution which was gently warm to re-dissolve and place in freezer at -20 °C. Crystalline solids formed, separated to give a total of 0.278 g of $(TBA)_3[(MeO)NbW_5O_{18}]$ (**0.220 g, 38 %**). **FT-IR ATR (4000 – 400 cm^{-1})** 2959 (m), 2933 (m), 2873 (m), 2814 (m), 1671 (m), 1592 (w), 1481 (s), 1380 (m), 1151 (w), 1104 (w), 1028 (w), 950 (s), 908 (w), 790 (s), 587, 569, 517, 427 cm^{-1} **^1H NMR** (300 MHz, acetonitrile-d_3) δ (ppm) peak at 4.11 was observed due to OCH_3. **^{17}O NMR** (41 MHz, acetonitrile-d_3) δ (ppm) 734, 453, 394, -65.

2.6.5.9 Attempted preparation of $(TBA)_3[(HO)PtW_5O_{18}]$ by degradation of $(TBA)_2W_6O_{19}$ using $H_2Pt(OH)_6$ precursor

A solution of 1.0 M methanolic TBAOH (0.42 mL, 0.42 mmol) was placed in a Schlenk flask A, dissolved in MeCN (2 mL) and then pumped to dryness under vacuum. The

process was repeated twice more to remove volatiles before adding MeCN 5 mL. To the solution was added $(TBA)_2W_6O_{19}$ (0.5 g, 0.26 mmol) with subsequent 1 h stirring before adding ^{17}O-enriched H_2O (~ 5 µL, 0.26 mmols). In a separate Schlenk flask B a 40 % aqueous TBAOH (0.42 mL, 0.64 mmols) and $H_2Pt(OH)_6$ (0.095 g, 0.32 mmol) was placed and stir for 1 h until all the solids dissolved.

The bright yellow solution was pumped dry leaving a yellow sticky material which was combined with the content of flask A and stir for ~1 h before pumping dried. The crude product was re-dissolved in a minimum amount of MeCN (~2 mL). To the solution $HBF_4.Et_2O$ (0.5 M, 23 µL, 12 mmols) was added step wise over 30 mins period. The resulting solution was stirred for ~30 mins at room temperature before pumping to dryness under vacuum and washed with (5 mL x 3) EtOAc and Et_2O (5 mL x 3) and finally pumped to dryness under vacuum to obtained dark brown solids. **^{17}O NMR** (41 MHz, acetonitrile-d_3) δ (ppm) 724, 694, 530, 501, 442, 432, 383 ppm. **^{195}Pt NMR** (108 MHz, acetonitrile-d_3) δ 3487, 3392, 3228, 2888, 2868, 2727 ppm.

References

1. L. Vilà-Nadal, A. Rodríguez-Fortea, L.-K. Yan, E. Wilson, L. Cronin and J. Poblet, *Nucleation Mechanisms of Molecular Oxides: A Study of the Assembly-Dissassembly of [W6O19](2-) by Theory and Mass Spectrometry*, 2009.
2 L. Vilà-Nadal, A. Rodríguez-Fortea and J. M. Poblet, *Eur. J. Inorg. Chem.*, 2009, **2009**, 5125-5133.
3 Z.-L. Lang, W. Guan, L.-K. Yan, S. Wen, Z.-M. Su and L.-Z. Hao, *The self-assembly mechanism of the Lindqvist anion [W6O 19]2- in aqueous solution: A density functional theory study*, 2012.
4 J. J. Hastings and O. W. Howarth, *J. Chem. Soc., Dalton Trans.*, 1992, 209-215.
5 R. I. Maksimovskaya and K. G. Burtseva, *Polyhedron*, 1985, **4**, 1559-1562.
6 W. Clegg, R. J. Errington, K. A. Fraser and D. G. Richards, *J.Chem.Soc. Chem. Commun.*, 1993, 1105-1107.
7. *Inorg. Syn.*, pp. 71-85.
8. Y. Du, A. L. Rheingold and E. A. Maatta, *J. Am. Chem. Soc.*, 1992, **114**, 345-346.
9. A. Proust, R. Thouvenot, M. Chaussade, F. Robert and P. Gouzerh, *Inorg.Chem. Acta*, 1994, **224**, 81-95.
10. H. Kwen, J. V. G. Young and E. A. Maatta, *Angew. Chemie Int.Ed.*, 1999, **38**, 1145-1146.
11. J. B. Strong, R. Ostrander, A. L. Rheingold and E. A. Maatta, *J.Am.Chem. Soc.*, 1994, **116**, 3601-3602.
12. M. Pope and A. M]ller, *Polyoxometalates: From Platonic Solids to Anti-Retroviral Activity:*, Springer Netherlands, 1994.
13. D. N. Zarubin and N. A. Ustynyuk, *Russian Chem. Rev.*, 2006, **75**, 671-707.
14. Y. Wei, B. Xu, C. L. Barnes and Z. Peng, *J. Am. Chem. Soc.*, 2001, **123**, 4083-4084.
15. Z. Peng, *Angew. Chem. Int. Ed.*, 2004, **43**, 930-935.
16. S. Xue, A. Chai, Z. Cai, Y. Wei, C. Xiang, W. Bian and J. Shen, *Dalton Trans.*, 2008, 4770-4775.
17. S. Gatard, S. Blanchard, B. Schollhorn, P. Gouzerh, A. Proust and K. Boubekeur, *Eur. J.*, 2010, **16**, 8390-8399.
18. A. Proust, R. Thouvenot and P. Gouzerh, *Chem. Commun.*, 2008, 1837-1852.

19. R. J. Errington, M. D. Kerlogue and D. G. Richards, *J. Chem. Soci., Chem. Commun.*, 1993, 649-651.
20. R. J. Errington, S. S. Petkar, P. S. Middleton, W. McFarlane, W. Clegg, R. A. Coxall and R. W. Harrington, *Dalton Trans.*, 2007, 5211-5222.
21. R. J. Errington, L. Coyle, P. Middleton, C. Murphy, W. Clegg and R. Harrington, *J Clust Sci*, 2010, **21**, 503-514.
22. R. J. Errington, in *Polyoxometalate Molecular Science*, eds. J. Borrás-Almenar, E. Coronado, A. Müller and M. Pope, Springer Netherlands, 2003, vol. 98, ch. 3, pp. 55-78.
23. V. W. Day and W. G. Klemperer, *Science*, 1985, **228**, 533-541.
24. W. G. Klemperer, *Science*, 1985, **228**, 533-541
25. W. Clegg, M. R. J. Elsegood, R. J. Errington and J. Havelock, *J.Chem.Soc., Dalton Trans.* 1996, 681-690.
26. B. Kandasamy, C. Wills, W. McFarlane, W. Clegg, R. W. Harrington, A. Rodríguez-Fortea, J. M. Poblet, P. G. Bruce and R. J. Errington, *Eur. J.* 2012, **18***A*, 59-62.
27. D. Bradley, R. C. Mehrotra, I. Rothwell and A. Singh, *Alkoxo and Aryloxo Derivatives of Metals*, Elsevier Science, 2001.
28. R. J. Errington, G. Harle, W. Clegg and R. W. Harrington, *Eur. J. Inorg. Chem.*, 2009, **2009**, 5240-5246.
29. L. Coyle, P. S. Middleton, C. J. Murphy, W. Clegg, R. W. Harrington and R. J. Errington, *Dalton Trans.*, 2012, **41**, 971-981.
30. G. A. Seisenbaeva, S. Gohil and V. G. Kessler, *J. Mater. Chem.*, 2004, **14**, 3177-3190.
31. W. G. Klemperer, *Angew. Chemie Int. Ed. Eng.*, 1978, **17**, 246-254.
32. M. Filowitz, R. K. C. Ho, W. G. Klemperer and W. Shum, *Inorg. Chem.*, 1979, **18**, 93-103.
33. N. Belai and M. T. Pope, *Polyhedron*, 2006, **25**, 2015-2020.
34. R. J. Errington, L. Coyle, P. S. Middleton, C. J. Murphy, W. Clegg and R. W. Harrington, *J Clust Sci*, 2010, **21**, 503-514.
35. L. Coyle, P. S. Middleton, C. J. Murphy, W. Clegg, R. W. Harrington and R. J. Errington, *Dalton Trans.*, 2012, **41**, 971-981.
36. C. J. Besecker, W. G. Klemperer, D. J. Maltbie and D. A. Wright, *Inorg. Chem.*, 1985, **24**, 1027-1032.
37. M. Misono, *Chem. Commun.*, 2001, 1141-1152.

38. C. L. Hill, *J. Am. Chem. Soc.*, 2002, **124**, 10935-10936.

39. U. Lee, A. Kobayashi and Y. Sasaki, *Acta Cryst. (*1983). **39***C*, 817-819.

40. A. Kobayashi, H. Hara, S.-i. Noro and M. Kato, *Dalton Trans.*, 2010, **39**, 3400-3406.

41. P. Klonowski, J. C. Goloboy, F. J. Uribe-Romo, F. Sun, L. Zhu, F. Gándara, C. Wills, R. J. Errington, O. M. Yaghi and W. G. Klemperer, *Inorg. Chem.*, 2014, **53**, 13239-13246.

42. T. Liu, K. Asakura, u. Lee, Y. Matsui and Y. Iwasawa, *Structures and catalytic activity of PtMo bimetallic ensembles derived from a new planar [PtMo6O24]8− heteropolyanion supported on Al2O3 and SiO2: I. Characterization of the supported [PtMo6] catalysts*, 1992.

43. D. A. Tocher, *Applied Organo. Chem.*, 1998, **12**, 301-301.

44. T. M. Che, V. W. Day, L. C. Francesconi, C. M. F. Fredrich, W. G. Klemperer and W. Shum, *Inorg. Chem.* , 1985, **24**, 4055-4062.

45. William Clegg, R. John Errington, P. Kraxner and C. Redshaw, *J. Chem. Soc., Dalton Trans.*, 1992, 1431-1438.

46 CrysAlisPro, *Rigaku Oxford Diffraction*.

47 R. C. Clark and J. S. Reid, *Acta Cryst. (*1995). **51***A*,, 887-897.

48 G. Sheldrick, *Acta Cryst. (*2015). **71***A*, 3-8.

49 G. Sheldrick, *Acta Cryst. (*2008). **64***A*, 112-122.

50 O. V. Dolomanov, L. J. Bourhis, R. J. Gildea, J. A. K. Howard and H. Puschmann, *J. Appl. Cryst..*, 2009, **42**, 339-341.

Chapter 3

Hydrolysis and Condensation studies on $(TBA)_3[(MeO)M'W_5O_{18}]$ (M′ = Ti, Sn)

In this chapter, the hydrolysis and condensation of tetrabutylammonium (TBA) salts of Lindquist-type polyoxometalates, $(TBA)_3[(MeO)TiW_5O_{18}]$ and $(TBA)_3[(MeO)SnW_5O_{18}]$ are discussed using a combination of ^1H, ^{17}O and 2D ^1H EXSY NMR spectroscopy and DFT calculations. Two main aspects underpinned the study firstly, the hydrolysis of $(TBA)_3[(MeO)TiW_5O_{18}]$ and $(TBA)_3[(MeO)SnW_5O_{18}]$ were compared to assess subtle differences in the hydrolysis of the two anions. Secondly, the condensation of intermediate hydroxido species to form the oxo-bridge dimer, $(TBA)_6[(\mu\text{-}O)(MW_5O_{18})_2]$ were investigated. This, has provided some understanding on the fundamental factors influencing the rate of hydrolysis of $(TBA)_3[(MeO)TiW_5O_{18}]$ and $(TBA)_3[(MeO)SnW_5O_{18}]$ from both experimental and theoretical points of view and for the first time, has resulted in the isolation and characterization of $(TBA)_3[(HO)TiW_5O_{18}]$, a new member of the $[M'M_5]^{3-}$ family.

The studies showed that under similar conditions, the tin hydroxido $(TBA)_3[(HO)SnW_5O_{18}]$ was more readily accessible than the titanium analogue $(TBA)_3[(HO)TiW_5O_{18}]$ whereas the tin oxo-bridge dimer $(TBA)_6[(\mu\text{-}O)(SnW_5O_{18})_2]$ was less stable and more difficult to isolate than the titanium oxo-bridged species $(TBA)_6[(\mu\text{-}O)(TiW_5O_{18})_2]$. These observations were linked to the difference in their free energies and the experimental results were supported by DFT calculations.

3.1 Introduction

There has been a growing interest in the chemistry of metal alkoxide compounds in recent years particularly with respect to their use as soluble precursors for the formation of metal oxides and the basis for the "sol–gel" method for metal oxide synthesis.[1,2] The hydrolysis of metal alkoxides compounds generally involves two fundamental steps firstly, the hydrolysis of the metal alkoxide to form an intermediate metal hydroxide (Equation 3.1) and the subsequent condensation of the intermediate with further metal alkoxide (or hydroxide) to form M-O-M bridges (Equazction 3.2 and 3.3)

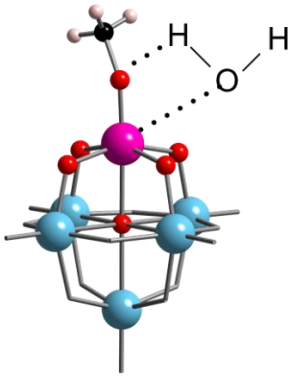

Figure 3.1: *Hydrolysis of M-OR bond in $[(MeO)M'M_5O_{18}]^{3-}$ anions*

$$(TBA)_3[(MeO)MW_5O_{18}] + H_2O \rightleftharpoons (TBA)_3[(HO)MW_5O_{18}] + MeOH \quad 3.1$$

$$(TBA)_3[(HO)MW_5O_{18}] + (TBA)_3[(MeO)MW_5O_{18}] \rightleftharpoons (TBA)_6[O(MW_5O_{18})_2] + MeOH \quad 3.2$$

$$2(TBA)_3[(HO)MW_5O_{18}] \rightleftharpoons (TBA)_6[O(MW_5O_{18})_2] + H_2O \quad 3.3$$

The formation and interconversion of these intermediates in the hydrolysis and condensation process are still poorly understood mainly because of their moisture sensitivity.[3-6] The intermediate species formed during the hydrolysis of metal alkoxides are often less stable probably due to thermodynamics of the reaction. Investigations have suggested that a way of circumventing this problem is to conduct the hydrolysis of the metal alkoxide compounds in the presence of less labile groups such as multidentate ligands[3,7] or by introducing sterically demanding alkoxide ligands to limit the steric accessibility of reagents to the metal center.[8] Although both strategies have proven to be complicated if the hydrolysis reactions are carried out in the presence of alcohol which is often the case. Indeed, reactions between alcohols and metal alkoxides is a well-established method of metal alkoxide preparation.[8]

The solubility of these compounds is an important factor for their used as molecular models in the design of selective, single–site heterogeneous catalyst[9,10] and this formed the basis for heterometallic POMs as potential models for heterogeneous catalysts wherein an active metal site is incorporated or supported on another metal oxide matrix.

This project aimed to investigate these hydrolysis and condensation reactions and the process involved in the formation of the intermediates for both titanium and tin substituted alkoxides compounds $(TBA)_3[(RO)MW_5O_{18}]$ (R = CH_3O; M = Ti, Sn).

Hydrolysis of Ti(IV)-monosubstituted Keggin-type POMs $[Bu_4N]_4[(OH)\ PTiW_{11}O_{39}]$ with aqueous H_2O_2 have been investigated and their relevance in titanium-catalysed H_2O_2 based oxidations has been reported.[11,12] In another reports it was demonstrated that Ti-substituted Keggin type POMs play an important role in H_2O_2-oxidation catalysis[13-15] and as models for heterogeneous metal oxide catalyst[16,17] including single sight variants[18-20].

An in-depth knowledge in the fundamental chemistry involved in these protonolysis reactions with the Lindqvist-type POMs can establish a platform for similar chemistry on the titanium substituted Lindqvist-type POMs as models for heterogeneous metal oxide catalyst. In addition, the reactivity of Sn-OC bond in the Lindqvist-type POM can be assessed which has not yet been fully explored.

In previous investigations into the hydrolysis reactions of $(TBA)_3[(RO)MW_5O_{18}]$ (R = CH_3O; M = Ti, Sn), attempts to isolate the titanium hydroxido intermediate $(TBA)_3[(HO)TiW_5O_{18}]$ were unsuccessful. When the hydrolysis reaction of $(TBA)_3[(MeO)TiW_5O_{18}]$ in MeCN was monitored by ^1H NMR it was observed that the hydrolysis at room temperature with a stoichiometric amount of water was apparently slow but when the reaction was heated in order to complete the hydrolysis, the product obtained was the oxo-bridged $(TBA)_6[(\mu\text{-}O)(TiW_5O_{18})_2]$ dimer as a result of condensation of the intermediate hydroxido derivative.[21] Subsequently, the first member of $[SnW_5]$ Lindqvist family, $(TBA)_3[(MeO)SnW_5O_{18}]$, was shown to hydrolyse readily and $(TBA)_3[(HO)SnW_5O_{18}]$ was isolated and characterized by ^{119}Sn NMR spectroscopy.[22] These observations were interesting but were not fully explored.

It was therefore important to investigate the reactions in detailed in order to obtain more information on these subtle differences. The results in this chapter described the

investigations and revealed some detailed knowledge on some of the factors influencing the hydrolysis and condensation of $(TBA)_3[(RO)MW_5O_{18}]$ (R = CH_3O; M = Ti, Sn). And this led to the isolation and characterisation for the first time of $(TBA)_3[(HO)TiW_5O_{18}]$.

The results also show by ^{119}Sn that the oxo-bridged $(TBA)_6[(\mu\text{-}O)(SnW_5O_{18})_2]$ is accessible although the species is less thermodynamically stable. This is important because Lindqvist-type POMs containing terminal Ti-OH group have, to our knowledge not yet been reported. The importance of terminal Ti-OH POMs in modelling catalysis has already been highlighted by Kholdeeva in the Keggin system and we wished to develop similar chemistry with Lindqvist-type POMs.

3.2 Results and Discussion

3.2.1 Hydrolysis of $(TBA)_3[(MeO)TiW_5O_{18}]$

3.2.2. Solvent Effects: MeCN vs. DMSO

(a) Reaction in MeCN

The Ti-substituted Lindqvist-type POM $(TBA)_3[(MeO)TiW_5O_{18}]$[23] prepared by the non-aqueous degradation of $[W_6O_{19}]^{2-}$ described in (**Section 2.5.2**) was hydrolysed with stochiometric amount of H_2O according to Equation 3.4 and the reaction was monitored by ^1H NMR spectroscopy over a 4 h period.

$$(TBA)_3[(MeO)TiW_5O_{18}] + H_2O \rightleftharpoons (TBA)_3[(HO)TiW_5O_{18}] + MeOH \qquad 3.4$$

The hydrolysis of $(TBA)_3[(MeO)TiW_5O_{18}]$ was carried out by dissolving $(TBA)_3[(MeO)TiW_5O_{18}]$ (50 mg, 0.025 mmols) in 0.5 mL dried MeCN in 5 mm screw top NMR tube (**see experimental section 3.10.1**) and recording the initial ^1H NMR spectrum which showed a $TiOCH_3$ peak at δ 4.11 ppm Figure 3.2 (a). Stoichiometric amount of distilled H_2O was added immediately after the initial ^1H NMR spectrum which led to the release of MeOH and the appearance of MeOH peak at δ 3.30 ppm indicating hydrolysis of $TiOCH_3$ group Figure 3.2(b). Subsequent ^1H NMR spectra were recorded in a 5 minute intervals for over 4 h period.

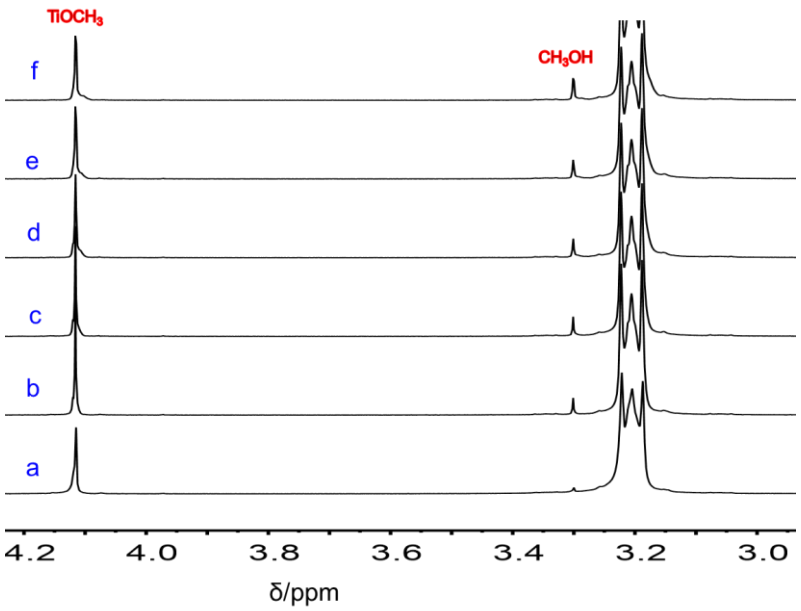

Figure 3.2: *^{1}H-NMR spectra of $(TBA)_3[(MeO)TiW_5O_{18}]$ in CD_3CN (a) without hydrolysis (b) immediately after the addition of 1 mole equivalent H_2O (c) 30 min after H_2O added (d) 1 h after H_2O added (e) 2 h after H_2O added and (f) 4 h after H_2O added.*

The peak integration of $TiOCH_3$ relative to MeOH shows a steady decrease in peak intensity of $TiOCH_3$ until equilibrium was attained in about 2 h. Within this time period only 17 % of $TiOCH_3$ was hydrolysed This was consistent with previous results reported by the Errington group.[23]

In order to push the equilibrium further, the volume of H_2O in the hydrolysis reaction was increased from 1 mole equivalent to 20 mole equivalents and monitored reactions by ^{1}H NMR spectroscopy over similar time period. This amounted to a steady decrease in peak intensity of the $TiOCH_3$ group according to peak integrations of $TiOCH_3$ and MeOH. It is important to note that within 2 h period equilibrium was established and 40 % of the $TiOCH_3$ group disappeared as shown in Figure 3.3.

The results suggest that although the hydrolysis of $(TBA)_3[(MeO)TiW_5O_{18}]$ is relatively slow at room temperature in MeCN, the reaction can go further with excess H_2O. The $TiOCH_3$ peak integrations and the amount of H_2O added were used to determine the equilibrium constant as 0.03 and 0.01 for 1 and 20 mole equivalent H_2O respectively in MeCN. Note that the values for K are within experimental error.

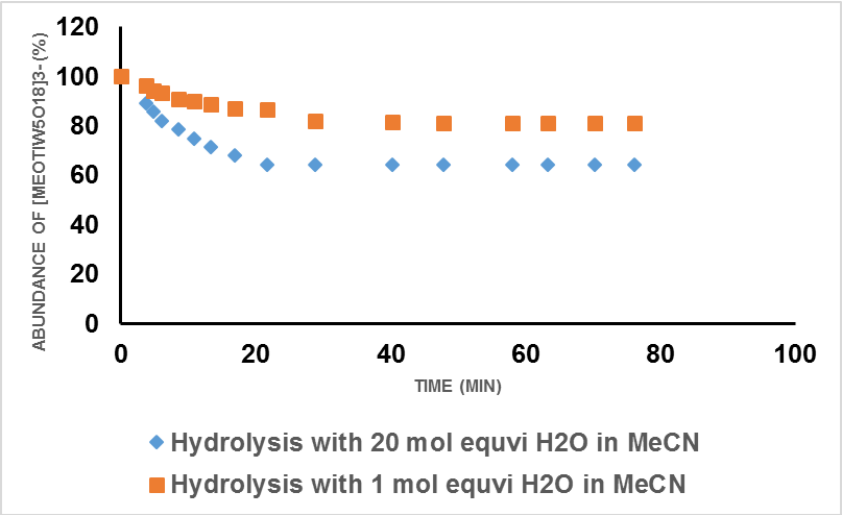

Figure 3.3: *Hydrolysis of 0.05 M solution of $(TBA)_3[(CH_3O)TiW_5O_{18}]$ with 1 and 20 mole equivalents H_2O in CD_3CN.*

The equilibrium constant (*K*) from equation 3.4 for 1 mole equivalent was calculated as;

$$K = \frac{[0.14][0.14]}{[0.86][0.86]} = 0.03$$

And for 20 mole equivalent the equilibrium constant (*K*) was calculated as;

$$K = \frac{[0.36][(0.36]}{[0.64][19.64]} = 0.01$$

(b) Reaction in DMSO

When the reaction was repeated in dmso under similar conditions over the same time period, the reaction was remarkably different. ^{1}H NMR spectra shows the hydrolysis reaction of $(TBA)_3[(MeO)TiW_5O_{18}]$ is significantly faster in dmso than in MeCN. The ^{1}H NMR peak integration for 1 and 20 mole equivalent H_2O is shown in Figure 3.4

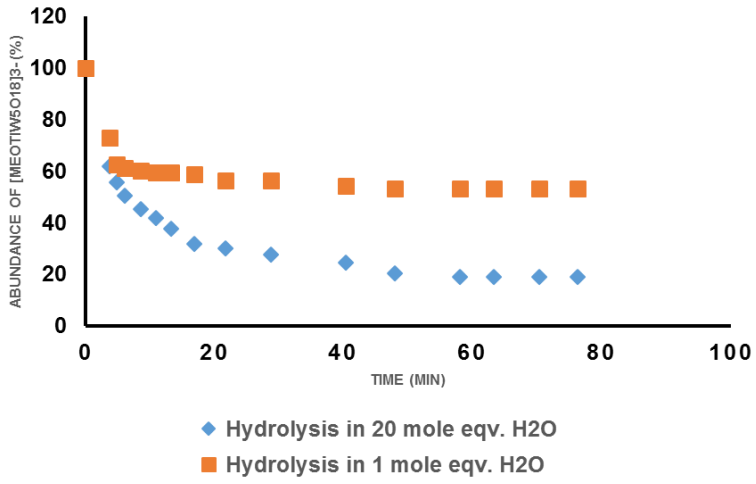

Figure 3.4: *Hydrolysis of 0.05 M solution of $(TBA)_3[(CH_3O)TiW_5O_{18}]$ with 1 and 20 mole equivalents H_2O in dmso.*

The faster rate of hydrolysis in dmso may be ascribed to the lower effective pK_a for water in dmso than in MeCN. The reaction more readily proceeded to completion with an excess of H_2O in dmso than in MeCN. It is worth noting that the first few hydrolysis data points were difficult to obtain from ^1H NMR spectroscopy in the dmso reaction.

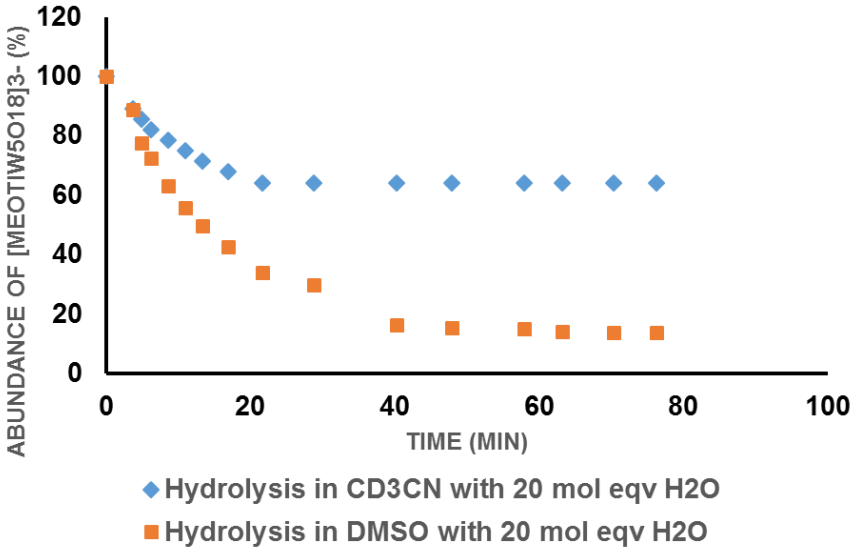

Figure 3.5: *Hydrolysis of 0.05 M solution of $(TBA)_3[(CH_3O)TiW_5O_{18}]$ with 20 mole equivalents H_2O in CD_3CN and DMSO.*

The equilibrium constant (*K*) for the hydrolysis reaction with 20 mole equivalent H_2O in dmso was calculated as;

$$K = \frac{[0.86][0.86]}{[0.14][19.14]} = 0.27$$

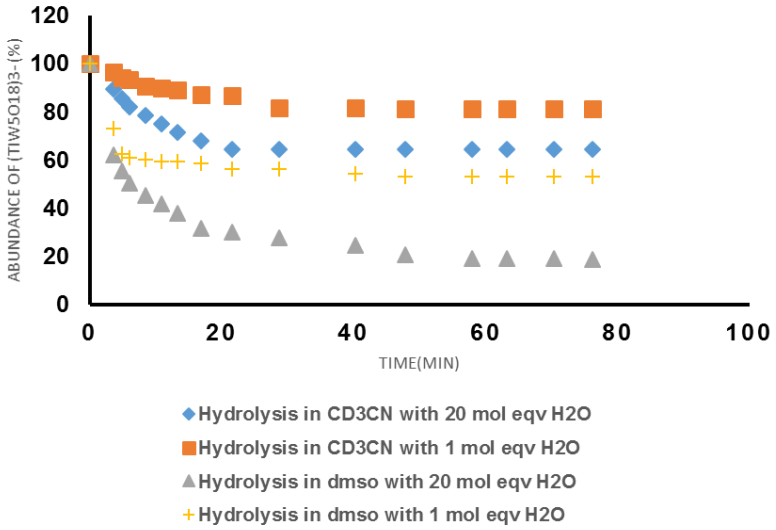

Figure 3.6: *Comparative plot for the hydrolysis of a 0.05 M solution of $(TBA)_3[(CH_3O)TiW_5O_{18}]$ with 1 and 20 mole equivalents H_2O in CD_3CN and dmso.*

The peak integrations for 1 and 20 mole equivalents in both solvents is shown in Figure 3.6 and the data suggest that the hydrolysis proceeds further in dmso than in MeCN in both 1 and 20 mole equivalents. These effects together enabled us to isolate and characterised for the first time, $(TBA)_3[(HO)TiW_5O_{18}]$ as a new member of the $[MW_5]$ POM family, details of which are discussed below.

3.3. Preparation and characterization of $(TBA)_3[(OH)TiW_5O_{18}]$

The results obtained from the hydrolysis reactions of $(TBA)_3[(MeO)TiW_5O_{18}]$ with a stoichiometric amount of H_2O in MeCN shows the reaction to be relatively slow and that excess H_2O results in only partial hydrolysis. In order to isolate the intermediate hydroxido titanium $(TBA)_3[(HO)TiW_5O_{18}]$ species, initial attempts of repeated hydrolysis in MeCN at 20 °C with removal of the volatiles under reduced pressure after each hydrolysis step gave a product which showed a band at 3676 cm^{-1} in the ATR FTIR spectrum. This vibrational frequency was assigned to ν(OH) and the observation is consistent with the formation of $(TBA)_3[(HO)TiW_5O_{18}]$. However, an additional IR band at 673 cm^{-1} was observed in the spectrum. This band was assigned to ν(TiOTi) of $(TBA)_6[(\mu\text{-}O)(TiW_5O_{18})_2]$ and it indicated that some condensation had occurred, even under these mild conditions.

When the reaction was conducted in dmso with an excess of H_2O, condensation was inhibited, presumably because dmso is a stronger ligand than MeCN as stated above. In addition, the hydrolysis proceeded to completion more readily in dmso. This strategy enabled us to isolate $(TBA)_3[(HO)TiW_5O_{18}]$ before condensation occurred *via* repeated cycles of mild hydrolysis in dmso followed by precipitation with diethyl ether after each cycle as confirmed by the absence of ν(TiOTi) in the ATR FTIR spectrum.

(a) FTIR spectroscopy

The FTIR spectrum of $(TBA)_3[(HO)TiW_5O_{18}]$ indicated that substitution of $[Ti\text{-}OH]^{3+}$ for $[Ti\text{-}OCH_3]^{3+}$ in the Lindqvist anion does not have much effect on the bonding in the anion as the vibrational frequencies are similar with the exception of the TiOH stretching frequency. The ATR FTIR spectrum (Figure3.7) contains bands 2900 - 2800 (broad), 1481 (s), 1380 (m), 1152 (w), 1107 (w), 1025 (sh), 946 (s), 884 (m), 790 (s), 616 (s), 568 (m), 542 (m). In addition to the bands due to M-O stretching frequencies, the spectrum contain a characteristic OH absorption band ν(OH) at 3676 cm^{-1}, as noted earlier which is close to 3684 cm^{-1} observed for the aminetris(aryloxido)-titanium(IV) 'atrane' complex LTiOH, where L is the bulky trianionic ligand derived from

tris(2-hydroxy-3,5-di-*tert*-butylbenzyl)amine.[25] The IR spectrun confirms the formation of $(TBA)_3[(HO)TiW_5O_{18}]$ with no band at 673 cm^{-1} due to ν(TiO) of Ti-O-Ti of $(TBA)_6[(\mu\text{-}O)(TiW_5O_{18})_2]$.

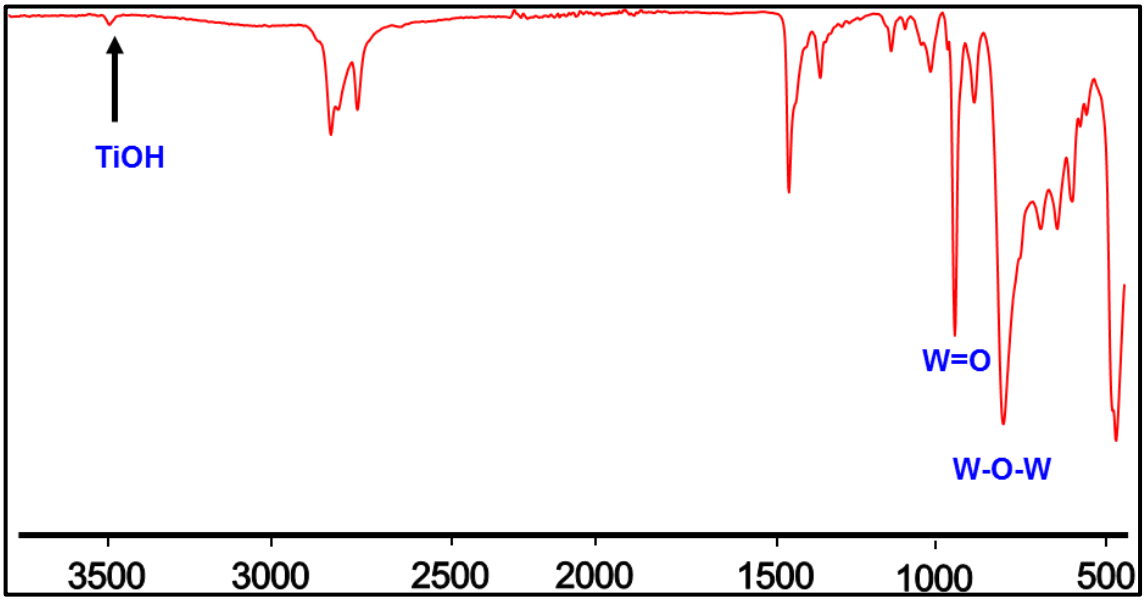

Figure 3.7: *FTIR spectrum of $(TBA)_3[(HO)TiW_5O_{18}]$*

The deuterated species was obtained by adding D_2O to $(TBA)_3[(HO)TiW_5O_{18}]$ to form $(TBA)_3[(DO)TiW_5O_{18}]$. The FTIR spectrum of the product obtained showed an extra weak peak for ν(OD) at 2707 cm^{-1} as shown in Figure 3.8, an additional band was observed at 3673 cm^{-1} due to ν(TiOH) of non-exchanged material.

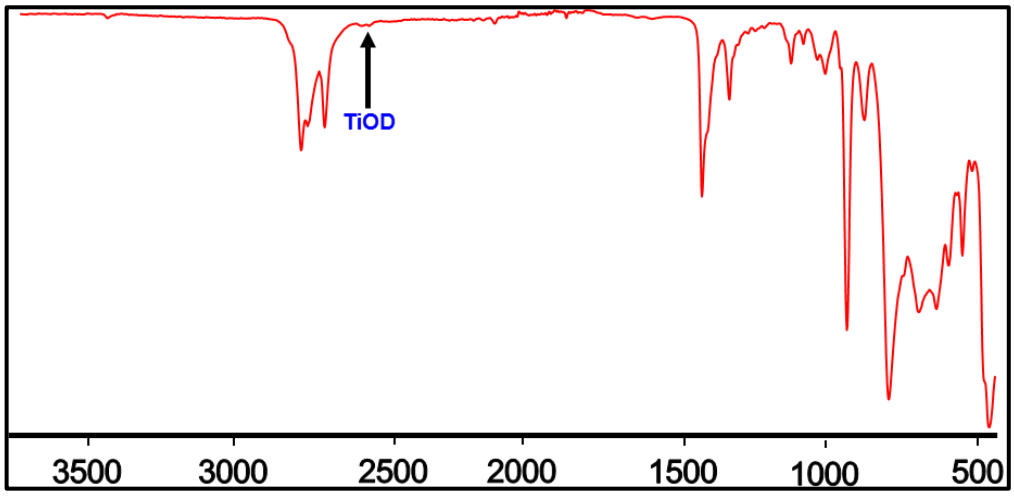

Figure 3.8: *FTIR spectrum of $(TBA)_3[(DO)TiW_5O_{18}]$.*

(b) Multinuclear NMR spectroscopy

The ^1H NMR spectrum (Figure 3.9) of the hydrolysis product, $(TBA)_3[(HO)TiW_5O_{18}]$ in $(CD_3)_2SO$ contained a singlet at δ 9.58 ppm for TiOH, and in CD_3CN a singlet at δ 7.8 ppm, which is consistent with the OH peak observed in the ^1H NMR spectrum of

[Cp*Ti(OH)OSi(*t*Bu)$_2$O]$_2$.[26] The protons of the OH group exchange with D_2O, as the OH peak disappeared upon treatment with D_2O, concomitant with the appearance of a peak at δ 3.33 ppm due to HOD.

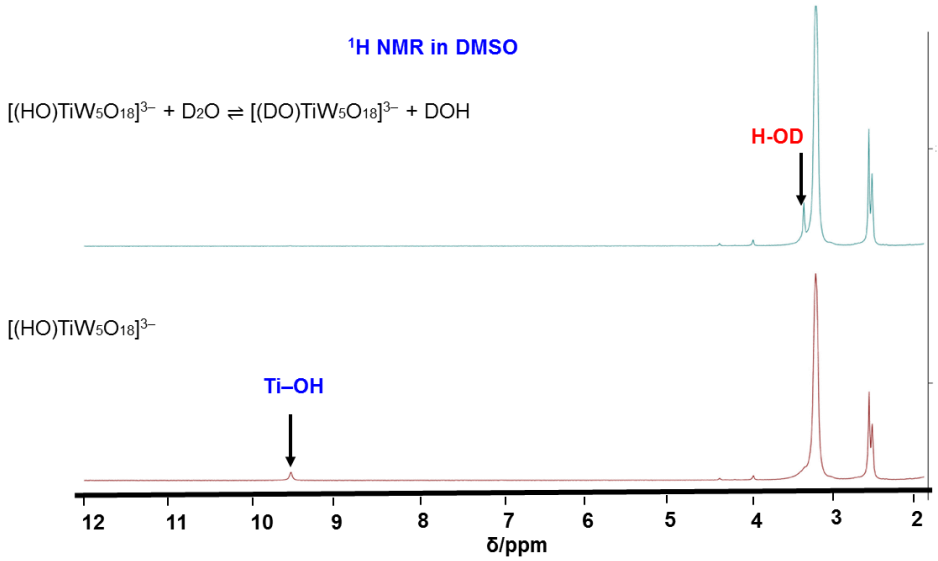

Figure 3.9: *^{1}H NMR spectrum of reaction between $(TBA)_3[(HO)TiW_5O_{18}]$ and D_2O in dmso*

In an effort to identify the ^{17}O chemical shift of the TiOH peak, we prepared non-enriched $(TBA)_3(HO)TiW_5O_{18}]$ and reacted it with 10 % ^{17}O-enriched H_2*O (Equation 3.5). We expected exchange between enriched oxygen from the ^{17}O-enriched H_2*O and the non-enriched Ti-OH oxygen.

$$[(HO)TiW_5O_{18}]^{3-} + H_2{}^{*}O \rightleftharpoons [(H{}^{*}O)TiW_5O_{18}]^{3-} + H_2O \qquad 3.5$$

The ^{17}O NMR spectrum (Figure 3.10) of non-enriched $(TBA)_3[(HO)TiW_5O_{18}]$ after stirring with a ten-fold excess of ^{17}O-enriched H_2O in CD_3CN overnight at 80^{o}C, with subsequent precipitation with diethyl ether and drying under vacuum contains peaks at δ 681, 555, 535 and 473 ppm. Apparently, some ^{17}O exchange into the polyoxometalate framework had occurred and we were able to observe the bridging M-O-M and M-O-W peaks in the spectrum. Peaks at δ 681 and 535 ppm were due to bridging Ti-O-Ti and Ti-O-W of oxo-bridged $(TBA)_6[(\mu\text{-}O)(TiW_5O_{18})_2]$ respectively reported in previous work.[23] The peak at δ 473 is tentatively assigned to the Ti-OH although we have been unable to unambiguously confirm this. The peak observed at δ 555 was assigned to Ti-O-W of the enriched bridging oxygen of $(TBA)_3[(HO)TiW_5O_{18}]$.

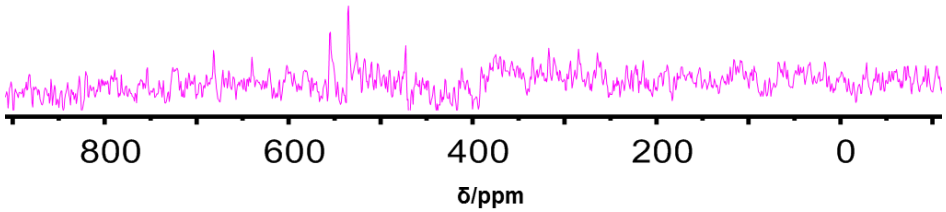

Figure 3.10: *^{17}O NMR spectrum of non-enriched $(TBA)_3[(HO)TiW_5O_{18}]$ after addition of ^{17}O enriched H_2O and heating in MeCN at 80 ^oC.*

(c) ^{183}W NMR

Although condensation of $(TBA)_3[(HO)TiW_5O_{18}]$ is slowed sufficiently in dmso to enable its isolation, significant amounts of $(TBA)_6[(\mu\text{-}O)(TiW_5O_{18})_2]$ are formed in dmso over extended periods, as was evident in the ^{183}W NMR spectrum acquired over 3 days (Figure 3.11), which contained peaks for W_{eq} at δ 39 ppm and W_{ax} at δ 76 ppm for $(TBA)_3[(HO)TiW_5O_{18}]$ in addition to corresponding peaks for $(TBA)_6[(\mu\text{-}O)(TiW_5O_{18})_2]$ at δ 42 ppm and 80 ppm respectively, *ca* 7 ppm downfield of the shifts observed in MeCN. In comparison, the chemical shift for both $(TBA)_3[(HO)TiW_5O_{18}]$ and $(TBA)_6[(\mu\text{-}O)(TiW_5O_{18})_2]$ are higher than the peaks observed for $(TBA)_3[(MeO)TiW_5O_{18}]$ at 32 and 65 ppm for the W(eq) and W(ax) respectively.

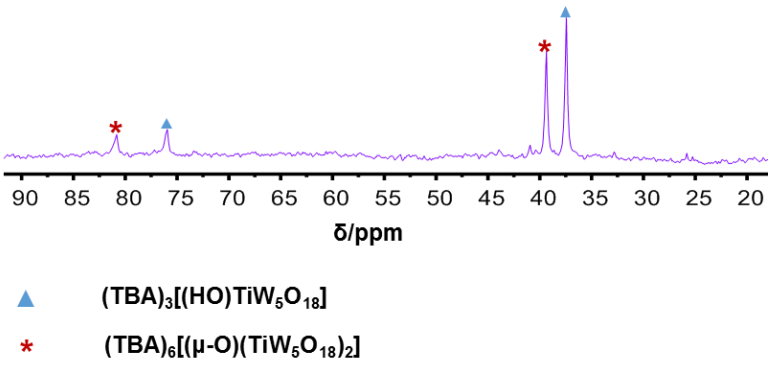

Figure 3.11: *^{183}W NMR spectrum of a mixture of $(TBA)_3[(HO)TiW_5O_{18}]$ and $(TBA)_6[(\mu\text{-}O)(TiW_5O_{18})_2$ in dmso.*

(d) X-ray crystallography

Crystals of $(TBA)_3[(HO)TiW_5O_{18}]$ were grown by vapor diffusion of Et_2O into a mixture of MeCN and dmso and used for a single-crystal X-ray structure determination (Figure 3.12).

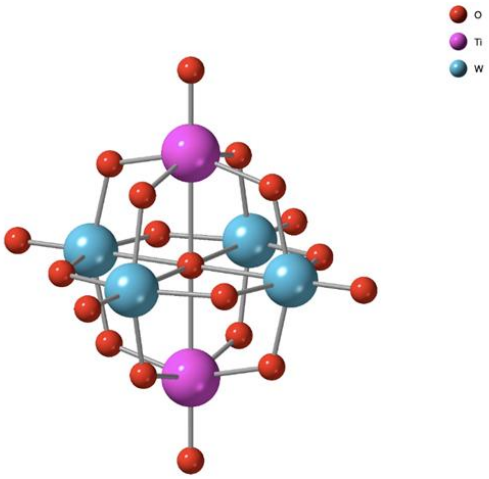

Figure 3.12: *Structure of one of the two independent disorder $[(HO)TiW_5O_{18}]$ anions with trans-disordered Ti/W sites.*

The crystal structure disordered prevented proper analysis of meaningful bond lengths and angles.

Although it is evident from ^{183}W NMR spectroscopy that condensation does occur even under this mild conditions over longer periods of time, we presume that any $(TBA)_6[(\mu\text{-}O)(TiW_5O_{18})_2]$, formed was more soluble and remained in solution during crystallization of $(TBA)_3[(HO)TiW_5O_{18}]$. Data refinement showed two independent anions, within which the [TiOH] group was equally disordered over two *trans* positions in one case and over all six positions in the other. The disordered positions in the trans-disordered anion are at the two Ti1/W1 sites (**See Supplementary data S3**) which are each 0.5 Ti and 0.5 W and there are two of these in the trans-positions. The other sites in the anion are W2 and W3 – there are two each of these and they are each fully occupied W sites.

3.4. Equilibrium studies of $(TBA)_3[(MeO)TiW_5O_{18}]$ and $(TBA)_3[(\mu\text{-}O)(TiW_5O_{18})_2]$

In an effort to understand the reaction between MeOH and $(TBA)_6[(\mu\text{-}O)(TiW_5O_{18})_2]$ in order to convert $(TBA)_6[(\mu\text{-}O)(TiW_5O_{18})_2]$ to $(TBA)_3[(MeO)TiW_5O_{18}]$, ^{17}O-enriched $(TBA)_6[(\mu\text{-}O)(TiW_5O_{18})_2]$ was prepared by dissolving $(TBA)_3[(MeO)TiW_5O_{18}]$ in MeCN and add excess amount of distilled H_2O the resultant solution was heated at 80 - 90 ^oC for 18 h (**see experimental section 3.10.10**)

Alcoholysis of $(TBA)_6[(\mu\text{-}O)(TiW_5O_{18})_2]$ at elevated temperature is expected to convert some of the oxo-bridged dimer back into the mono-substituted $(TBA)_3[(MeO)TiW_5O_{18}]$ anions. After complete reaction it is expected to establish equilibrium within the two anions. This reaction was attempted by adding 2 mole equivalents of MeOH to ^{17}O-enriched $(TBA)_6[(\mu\text{-}O)(TiW_5O_{18})_2]$ (Equation. 3.6) and heated to 80 ^oC for ~ 2 h. The solution was allowed to cool to room temperature before recording the ^{17}O NMR spectrum.

$$(TBA)_6[(\mu\text{-}O)(TiW_5O_{18})_2] + 2MeOH \rightleftharpoons 2(TBA)_3[(MeO)TiW_5O_{18}] + H_2O \quad 3.6$$

As expected, the ^{17}O NMR spectrum (Figure. 3.13) shows two peaks at the centre μ_6-O region indicating two types of species with chemical shift at δ –55 and –60 ppm for the monomeric $(TBA)_3[(MeO)TiW_5O_{18}]$ and the oxo-bridged dimer $(TBA)_6[(\mu\text{-}O)(TiW_5O_{18})_2]$ respectively based on other reactions. Peak integrations give a 1:1.4 ratio. The terminal peaks were not well resolved and therefore broad peaks are observed at δ 715 and 723 ppm for terminal W=O peaks for $(TBA)_3[(MeO)TiW_5O_{18}]$ and $(TBA)_6[(\mu\text{-}O)(TiW_5O_{18})_2]$ respectively.

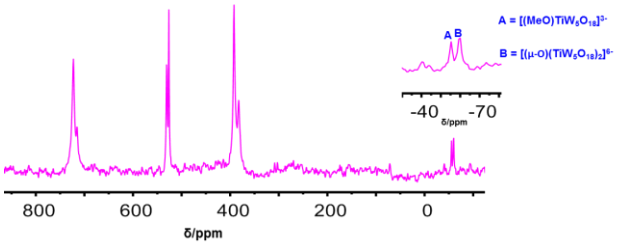

Figure 3.13: *^{17}O NMR spectra of reaction between $(TBA)_6[(\mu\text{-}O)(TiW_5O_{18})_2]$ and 2 mole equivalents of MeOH*

The ^1H NMR NMR spectrum (Figure. 3.14) of the above solution contained a single peak at δ 4.11 ppm due to $Ti\text{-}OCH_3$ confirming the formation of $(TBA)_3[(MeO)TiW_5O_{18}]$ anion. The equilibrium constant was determined to be 0.35 from the relative integrals of the $Ti\text{-}OCH_3$ and CH_3OH peaks in the ^1H NMR spectrum.

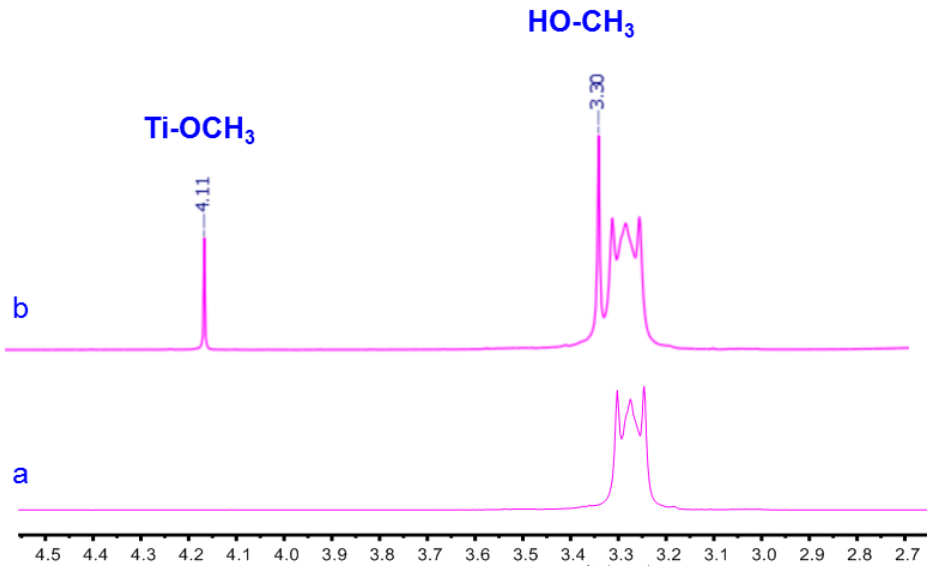

Figure 3.14: *^{1}H NMR spectra of reaction between $(TBA)_6[(\mu\text{-}O)(TiW_5O_{18})_2]$ and 2 mole of MeOH (a) $(TBA)_6[(\mu\text{-}O)(TiW_5O_{18})_2]$ without MeOH and (b) heated at 80 ^oC with 2 mole equivalents MeOH in MeCN and then cooled to room temperature.*

The equilibrium constant (*K*) for peak intensities in the ^{1}H NMR data was calculated from Equation 3.7 as;

$$K = \frac{[0.74][0.37]}{[0.63][1.26]} = 0.35 \qquad 3.7$$

3.5 Hydrolysis of $(TBA)_3[(MeO)SnW_5O_{18}]$

3.5.1 Hydrolysis of $(TBA)_3[(MeO)SnW_5O_{18}]$ in MeCN

In order to investigate the hydrolysis of $(TBA)_3[(MeO)SnW_5O_{18}]$ for comparison with the $(TBA)_3[(MeO)TiW_5O_{18}]$ analogue, $(TBA)_3[(MeO)SnW_5O_{18}]$ was prepared by the non-aqueous degradation method described above (**see section 2.4.3)**. In the hydrolysis reaction, $(TBA)_3[(MeO)SnW_5O_{18}]$ (50 mg, 0.025 mmols) was dissolved in 0.5 mL dried MeCN in a 5 mm screw top NMR tube and record initial ^{1}H NMR spectrum. The reaction was monitored in a similar way as described for the titanium analogue, the ^{1}H NMR spectrum of $(TBA)_3[(MeO)SnW_5O_{18}]$ consist of a peak at δ 3.65 ppm for $SnOCH_3$.

The peak integration of Sn-OCH_3 group shown in Figure 3.15 from the ^{1}H NMR spectra shows that 60 % of the Sn-OCH_3 group disappeared immediately after the addition of 1 mole equivalent of H_2O, suggesting that hydrolysis of $(TBA)_3[(MeO)SnW_5O_{18}]$ occurred significantly more rapidly than the Ti analogue in MeCN consistent with previous report.[21] The rapid hydrolysis did not allow accurate measurement of data within the first few minutes. Note that data is from ^{1}H NMR spectra. This rapid

hydrolysis and the kinetic stability of $(TBA)_3[(HO)SnW_5O_{18}]$ makes it much easier to access the $(TBA)_3[(HO)SnW_5O_{18}]$ intermediate.

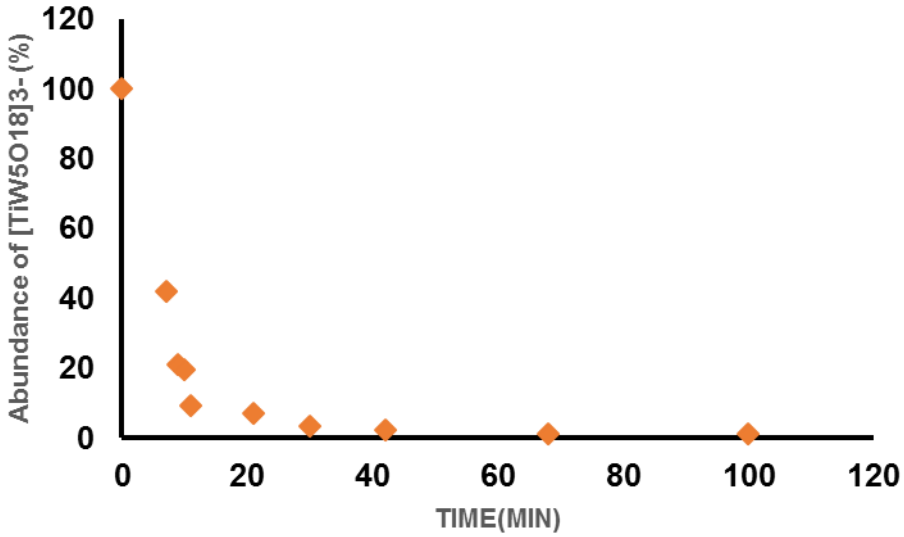

Figure.3.15: *Data from ^1H NMR spectra for the hydrolysis of a 0.05 M solution of $(TBA)_3[(CH_3O)SnW_5O_{18}]$ with 1 mole equivalents H_2O in CD_3CN.*

3.5.2 Formation of $(TBA)_3[(HO)SnW_5O_{18}]$ in MeCN

The hydroxido-tin analogue $(TBA)_3[(HO)SnW_5O_{18}]$ was obtained readily from the hydrolysis of $(TBA)_3[(MeO)SnW_5O_{18}]$ with an excess of water at room temperature and precipitation with diethyl ether. Condensation of $(TBA)_3[(HO)SnW_5O_{18}]$ was notably much slower than that of the titanium analogue, $(TBA)_3[(HO)TiW_5O_{18}]$ and the formation of the oxo-bridged dimer $(TBA)_6[(\mu\text{-}O)(SnW_5O_{18})_2]$ was achieved by carrying out the reaction at higher temperature, in benzonitrile because of it high boiling point (**see experimental section 3.10.11**). The product of this reaction was characterized by ^{119}Sn NMR spectrocopy

(a) ATR FTIR spectrum

The FTIR spectrum (Figure 3.16) of $(TBA)_3[(HO)SnW_5O_{18}]$ contains a weak band at 3648 cm^{-1} for ν(OH) in addition to the characteristic peaks for ν(W=O) at 951, ν(W–O) at 784 and ν(Sn–O) of bridging SnOW at 748 cm^{-1}. Note that the ν(OH) band for SnOH compound is shifted to lower wavenumber (3648 cm^{-1}) compared to the ν(OH) band in TiOH (3676 cm^{-1}) again, emphasizing the electronic effect of SnW_5 substitution in Lindqvist-type POMs. When the product was reacted with D_2O, ν(OD) was observed at 2688 cm^{-1}.

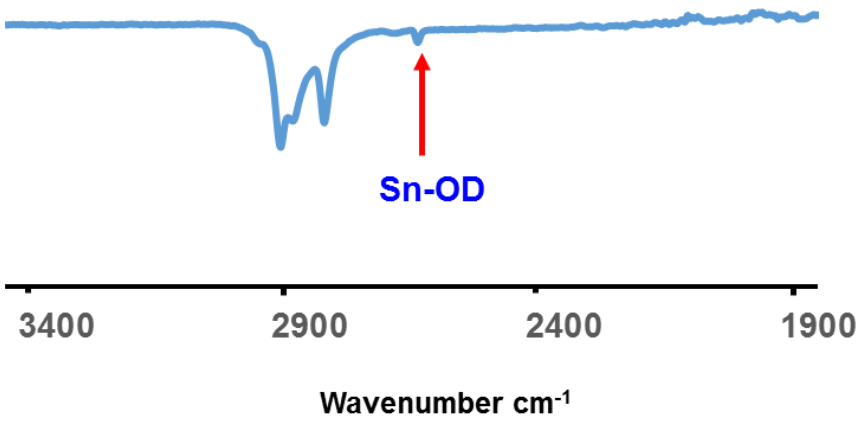

Figure 3.16: *FTIR spectrum of $(TBA)_3[(HO)SnW_5O_{18}]$ after treatment with D_2O*

(b) Multinuclear NMR spectroscopy

The ^{1}H NMR spectrum (Figure 3.17) of $(TBA)_3[(HO)SnW_5O_{18}]$ in $(CD_3)_2SO$ showed a single broad peak for Sn-OH at δ 3.42 ppm with $^2J(^{183}W^{119/117}Sn)$ of *ca* 44 Hz. This resonance disappeared after addition of D_2O consistent with previous result.[27]

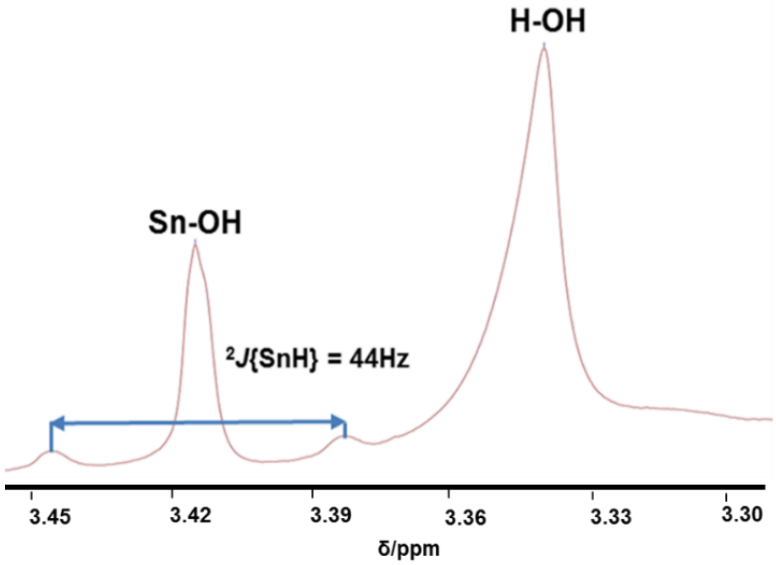

Figure 3.17: *^{1}H NMR spectrum of $(TBA)_3[(HO)SnW_5O_{18}]$ in dmso*

A doublet in the ^{1}H-coupled ^{119}Sn NMR spectrum at –633 ppm with $^2J(^{119}Sn^1H)$ = 47.7 Hz and tungsten satellites with $^2J(^{183}W^{119}Sn)$ = 37 Hz confirmed the presence of SnOH in $(TBA)_3[(HO)SnW_5O_{18}]$,[21] and the terminal nature of the OH group is consistent with the C_{4v} symmetry implied by the 4:1 intensity ratio of peaks at δ 72 and –122 ppm for W_{eq} and W_{ax} respectively in the ^{183}W NMR spectrum (Figure 3.18) of $(TBA)_3[(HO)SnW_5O_{18}]$. In addition, a significant amount of $(TBA)_6[(\mu\text{-}O)(SnW_5O_{18})_2]$

was formed in MeCN over 3 days at 20 °C due to condensation, as is evident from the peaks for W_{eq} at δ -130.16 ppm and W_{ax} at 70.51 ppm in addition to W_{eq} = 121.42 ppm and W_{ax} at 72.68 ppm for $(TBA)_3[(HO)SnW_5O_{18}]$.

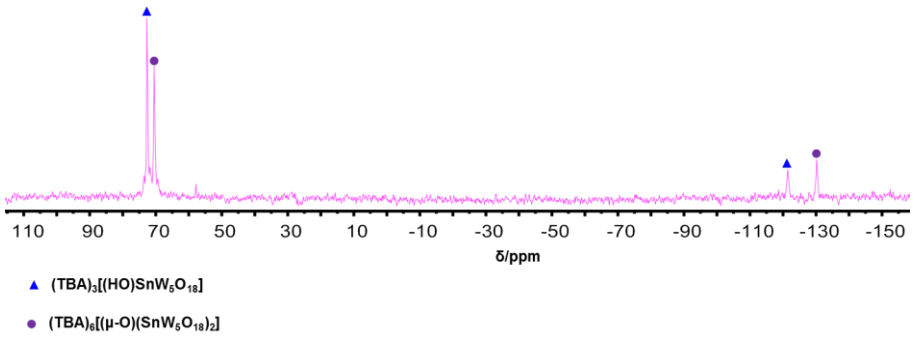

Figure 3.18: *^{183}W NMR spectrum of $(TBA)_3[(HO)SnW_5O_{18}]$ in MeCN.*

The ^{17}O NMR spectrum obtained by the hydrolysis of ^{17}O-enriched $(TBA)_3[(MeO)SnW_5O_{18}]$ with non-enriched H_2O contains the expected peaks for W_{eq}=O at δ 720, W_{ax}=O at δ 683, Sn-O-W at δ 396, W-O-W at 382 and 367, and μ_6-O at 17 ppm. The ^{17}O NMR spectrum of the dried product obtained after treatment of $(TBA)_3[(HO)SnW_5O_{18}]$ with ^{17}O-enriched H_2O contained a broadened peak at δ –5 ppm which was assigned to SnOH, although this may be due to residual water or to exchanging SnOH / H_2O.

3.5.3 Condensation studies on $((TBA)_3[(HO)SnW_5O_{18}]$

The detailed studies on the hydrolysis of {MeOMW$_5$} (M = Ti, Sn) in this project, have established that hydrolysis of $(TBA)_3[(MeO)TiW_5O_{18}]$ in MeCN is much slower than the tin analogue, $(TBA)_3[(MeO)SnW_5O_{18}]$ and that it is much easier to isolate the tin hydroxido compound $(TBA)_3[(HO)SnW_5O_{18}]$. The conversion of $(TBA)_3[(HO)SnW_5O_{18}]$ to the oxo-bridged dimer was found to be more difficult to achieve compared to the titanium homologue $(TBA)_6[(\mu\text{-}O)(TiW_5O_{18})_2]$ which can be easily isolated by hydrolysis of $(TBA)_3[(MeO)TiW_5O_{18}]$ at elevated temperature.

In an effort to broaden the Lindqvist-type POMs family through systematic manipulation in a well-defined synthetic routes, it was important to explore possible route to access the oxo-bridged tin analogue $(TBA)_6[(\mu\text{-}O)(SnW_5O_{18})_2]$ for structural analysis and possible reactivity studies. This was achieved by dissolving 250 mg of $(TBA)_3[(HO)SnW_5O_{18}]$ in dried benzonitrile and heating the solution at elevated temperature.

The high boiling point solvent PhCN was heated at 110 °C allowing the volatiles to evaporate in a sealed system and partial removal of the volatiles under reduced pressure. The repeated cycle of this process resulted to the transformation of $(TBA)_3[(HO)SnW_5O_{18}]$ to the oxo-bridged dimer $(TBA)_6[(\mu\text{-}O)(SnW_5O_{18})_2]$. The ^{119}Sn NMR spectra of the product obtained in solution showed a chemical shift at δ 667 ppm in its ^{119}Sn NMR spectrum after repeated cycles (Figure.3.19).

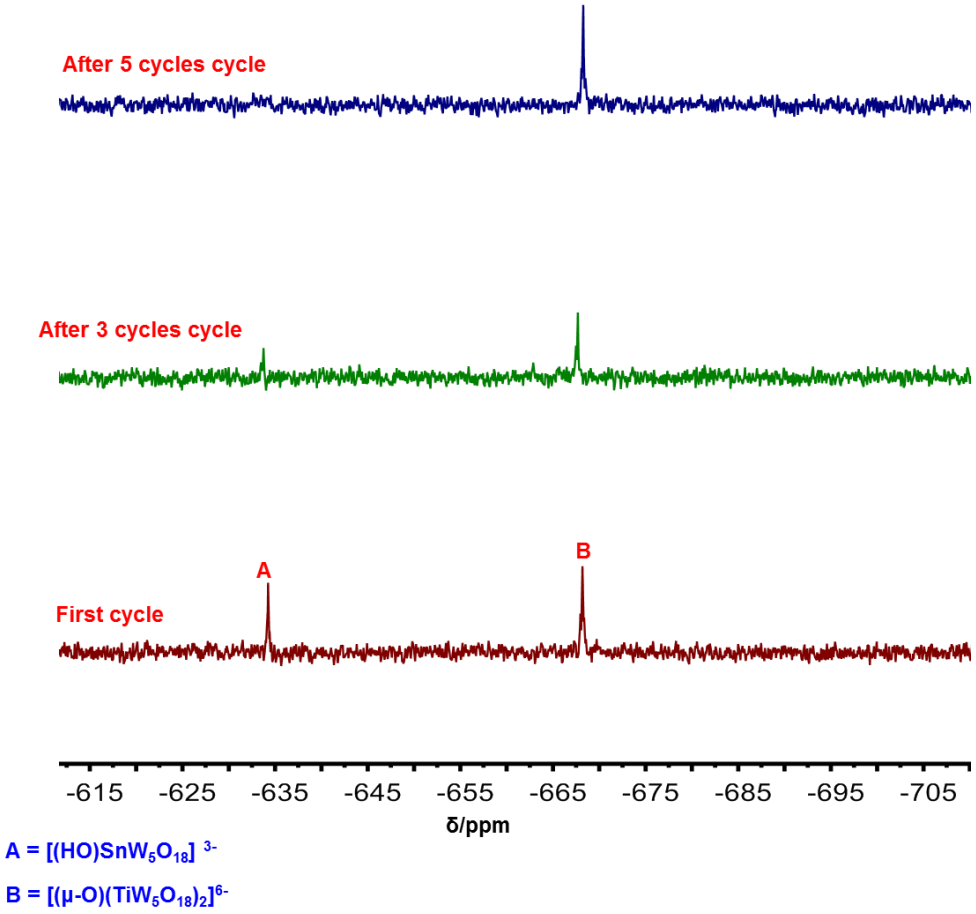

Figure 3.19: *^{119}Sn NMR for the conversion of $(TBA)_3[(HO)SnW_5O_{18}]$ to $(TBA)_6[(\mu\text{-}O)(SnW_5O_{18})_2]$ in* PhCN.

(a) FTIR spectroscopy

In the FTIR spectrum after recrystallisation and the removal of volatiles, consist of a characteristic peak for ν(W=O) at 951 in addition ν(W–O) peak is observed at 784 while ν(Sn–O) of bridging SnOW is at 748 cm^{-1}, a band was observed at 573 cm^{-1} which is assigned to ν(SnOSn) in $(TBA)_6[(\mu\text{-}O)(SnW_5O_{18})_2]$ and this band occurred at a lower wavenumber than ν(TiOTi) in $(TBA)_6[(\mu\text{-}O)(TiW_5O_{18})_2]$ at 673 cm^{-1} due to the heavier tin compared to titanium. Unfortunately, we have been unsuccessful after several attempts to obtain single crystals of the product for X-ray diffraction analysis.

3.6 Alcoholysis of $(TBA)_3[(MeO)MW_5O_{18}]$ in MeCN (M = Ti, Sn)

3.6.1 Alcohol exchange in M-OR (M = Ti, Sn)

Alcohol-alkoxide exchange has been previously investigated and the kinetic parameters reported.[8] It is expected that addition of alcohol R′OH to $[(RO)M'M_5O_{18}]^{3-}$ (Equation 3.8) should result in alkoxido exchange but, surprisingly, after several attempts with the mixture of MeOH/$[(MeO)TiW_5O_{18}]^{3-}$ a 2D ^{1}H NMR EXSY experiment did not show any TiOMe/MeOH exchange peaks even after addition of water at 60 °C.

$$(TBA)_3[(CH_3O)MW_5O_{18}] + {}^*CH_3OH \rightleftharpoons (TBA)_3[({}^*CH_3O)MW_5O_{18}] + CH_3OH \quad 3.8$$

However, off-diagonal $SnOCH_3/CH_3OD$ cross-peaks were observed in a 2D ^{1}H NMR EXSY experiment for MeOH/$[(MeO)SnW_5O_{18}]^{3-}$ mixtures as shown in Figure 3.20. The slow MeOH/$[(MeO)TiW_5O_{18}]^{3-}$ exchange observations in the 2D ^{1}H NMR EXSY experiment are consistent with the general suggestion that alkoxido-tin(IV)-substituted POMs are much more moisture-sensitive than their titanium analogues.[21] The off diagonal $SnOCH_3/{}^*CH_3OH$ exchange led us to determine the exchange rate of methanol / methoxido for $(TBA)_3[(MeO)SnW_5O_{18}]$ calculated as 0.234 s^{-1} which is significantly higher in comparison with the values obtained for the zirconium analogue at 0.03 s^{-1}.[28] In addition, we have also measured the ^{1}H NMR T_1 relaxation time for M-OCH_3 of both anions (shown in Table 3.1)

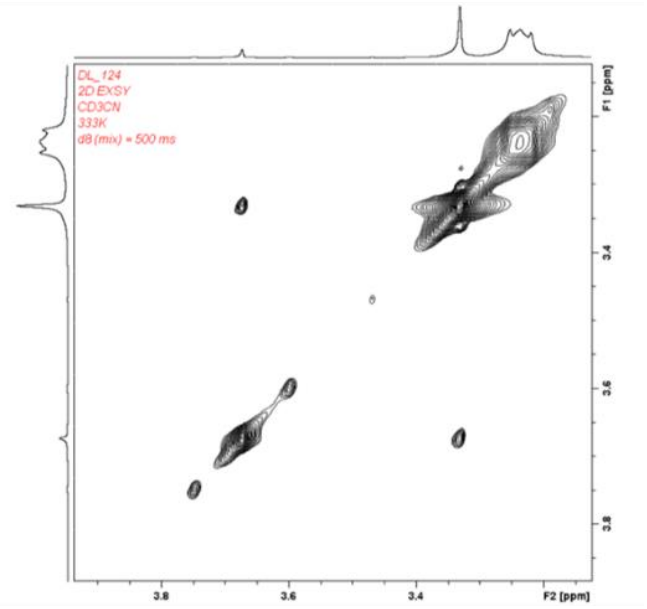

Figure 3.20: *2D ^{1}H EXSY spectra for alcohol-alkoxide exchange in CD_3CN between CH_3OH and $(TBA)_3[(MeO)SnW_5O_{18}]$.*

Table 3.1: *^{1}H NMR T_1 relaxation times for $MOCH_3$ in the anions $[(MeO)MW_5]^{3-}$.*

Anion	T_1/sec	Solvent
$(TBA)_3[(MeO)TiW_5O_{18}]$	4.7	CD_3CN
$(TBA)_3[(MeO)SnW_5O_{18}]$	2.79	$(CD_3)_2SO$
$(TBA)_3[(MeO)SnW_5O_{18}]$	4.47	CD_3CN

In order to study the rate of alcohol exchange with $[(MeO)TiW_5O_{18}]^{3-}$, the M-OCH_3 peaks in the ^1H NMR spectra were monitored after addition of CD_3OD. The ^1H NMR data for the reaction between one mole equivalent of CD_3OD and $(TBA)_3[(MeO)TiW_5O_{18}]$ is shown in Figure 3.21. The plot shows that the rate of exchange with CD_3OD much faster than the reaction with H_2O". Note that we expect equal amounts of OCH_3 and OCD_3 species i.e. 50 % conversion. Any deviation could be due to different pK_a of CH_3OH vs CD_3OD.

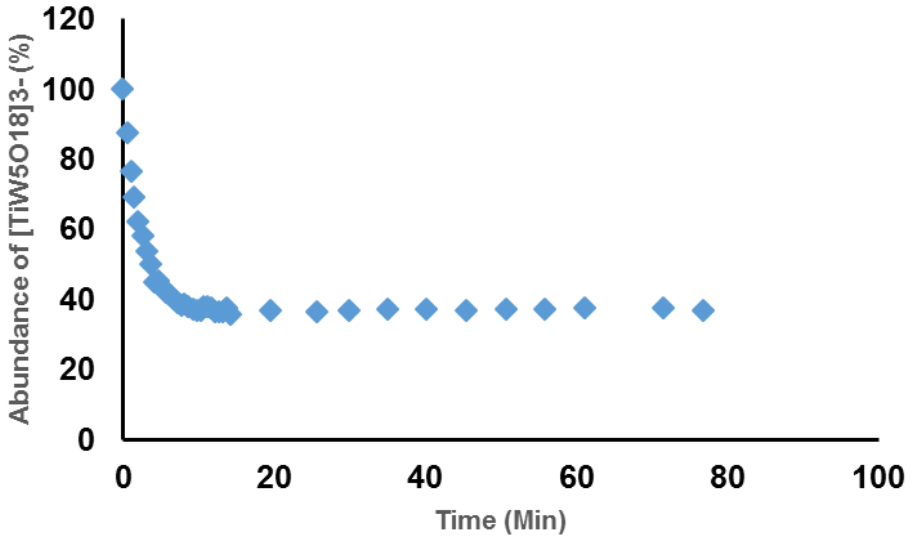

Figure 3.21: *^1H NMR data for reaction of a 0.05 M solution of $(TBA)_3[(CH_3O)TiW_5O_{18}]$ with CH_3OH in CD_3CN.*

3.7 Reaction with H_2O_2.

The role of hydrogen peroxide in olefin epoxidation has been extensively studied in recent years but the mechanisms of these reactions are still not fully understood.[29-31] Hydrogen peroxide is known to be oxygen-rich and forms H_2O as the only by product.[32,33] POMs have become increasingly interesting in catalytic activity and selectivity particularly the Keggin-type substituted POMs for example the silicodecatungstates, $[\gamma\text{-}SiW_{10}O_{36}]^{8-}$ and $[\gamma\text{-}SiW_{10}O_{34}(H_2O)_2]^{4-}$ have been investigated.[33,34]

Previous investigations on epoxidation by POMs with H_2O_2 suggested that the catalytic reaction of H_2O_2 involve two-step mechanisms, i.e. the activation of H_2O_2 and a subsequent transfer of oxygen. Kuznetsov and co-workers reported divanadium-substituted POM $[\gamma\text{-}1,2\text{-}H_2SiV_2W_{10}O_{40}]^{4-}$ which contain $[OV\text{-}(\eta\text{-}OH)_2\text{-}VO]$[35] core and

the proposed peroxo-type mechanism was reported. The group suggest that the oxygen transfer is performed favorably through "*water-assisted"* pathway as shown in Scheme 3.1.

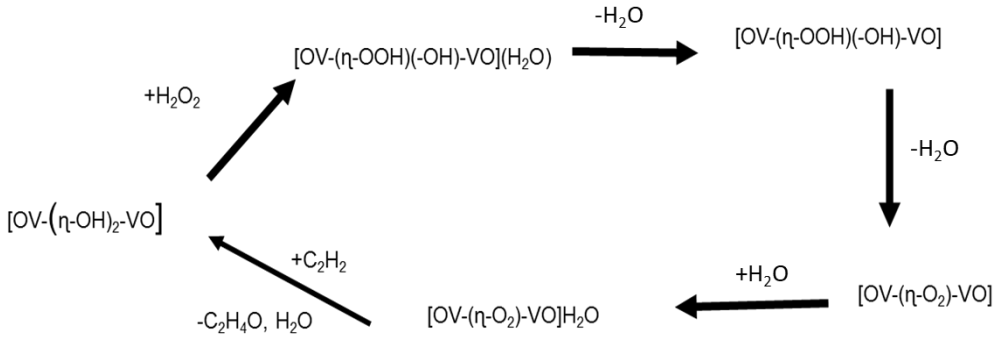

Scheme 3.1: *Proposed mechanism for the divanadium-substituted POM [γ-1,2-$H_2SiV_2W_{10}O_{40}$]$^{4-}$* [35]

A two-step reaction mechanism has also been proposed for mono- and dititanium-substituted POMs $[PTi(OH)W_{11}O_{39}]^{4-}$ and $[Ti_2(OH)_2As_2W_{19}O_{67}(H_2O)]^{8-}$.[12,36-38] Quite recently Kholdeeva's group have been interested in the Lindqvist-type POMs and they reported the monomeric niobium substituted Lindqvist POM, $(TBA)_2[(HO)NbW_5O_{18}]$ and proposed that the niobium substituted POM interacts with H_2O_2 to produce the protonated η^2-peroxo complex $(TBA)_2[(O_2)NbW_5O_{18}H]$.[39] In collaboration with the Kholdeeva group we investigated reactions between Lindqvist type Nb and Ti-substituted POM with aqueous H_2O_2 for detailed studies on the mechanistic reaction pathway selectivity for Nb(V) and Ti(IV) in alkene epoxidation with H_2O_2.

The hydrolysis reaction of $(TBA)_3[(CH_3O)TiW_5O_{18}]$ with H_2O_2 that was dried by dissolving it in dried MeCN followed by removal of the volatiles under vacuum (**see experimental section 3.10.13**) produced a yellow solution immediately upon addition of 1 mole equivalent of dried H_2O_2 (Equation 3.9 and Scheme 3.2).

$$(TBA)_3[(MeO)TiW_5O_{18}] + H_2O_{2(aq)} \rightleftharpoons (TBA)_3[(HOO)TiW_5O_{18}] + MeOH \qquad 3.9$$

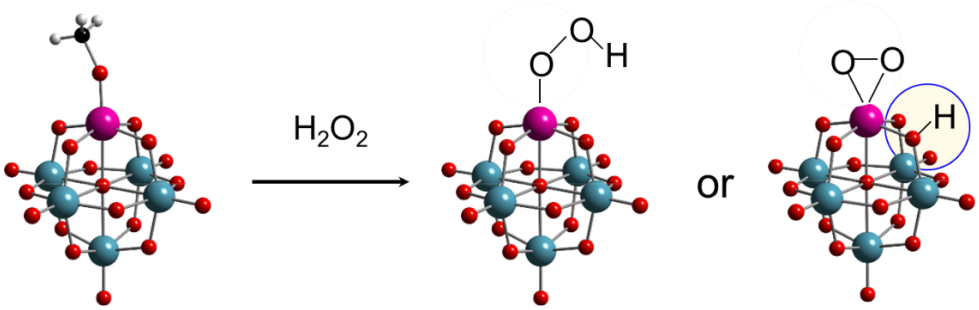

Scheme 3.2: *Reactivity of $(TBA)_3[(CH_3O)TiW_5O_{18}]$ towards H_2O_2 in dry MeCN*

(a) Multinuclear NMR spectroscopy

The reaction between H_2O_2 and $[(CH_3O)TiW_5O_{18}]^{3-}$ was studied by adding 1 mole equivalent of dried H_2O_2 to a solution of $(TBA)_3[(CH_3O)TiW_5O_{18}]$ with stirring for 1h before removing volatiles under reduced pressure. This cycle was repeated 3 times before recording the ^1H NMR spectrum. The ^1H NMR spectrum (Figure 3.21) shows that only 20 % of Ti-OCH_3 had reacted. When an extra 10 mole equivalents of H_2O_2 was added, the reaction proceeded further but a significant amount of the methoxy peak was still present. In order to push the reaction to completion, an excess of H_2O_2 was added and this resulted in complete removal of Ti-OCH_3.

The results show that after addition of an excess of H_2O_2 (111 mole equivalent), the $TiOCH_3$ peak at δ 4.11 ppm disappeared indicating the reaction had gone to completion. The slow rate of interaction of H_2O_2 with Ti-OCH_3 is consistent with the hydrolysis and alcoholysis reactions discussed in previous sections. This emphasises that Ti in the rigid 6 coordinate is very reluctant to expand its coordination to 7 in the reaction. ^1H NMR spectra of products from the reaction of TiW_5 with 1, 11 and 111 mole equivalents of H_2O_2 are shown in Figure 3.22 and the the peaks integration is shown in Figure 3.23.

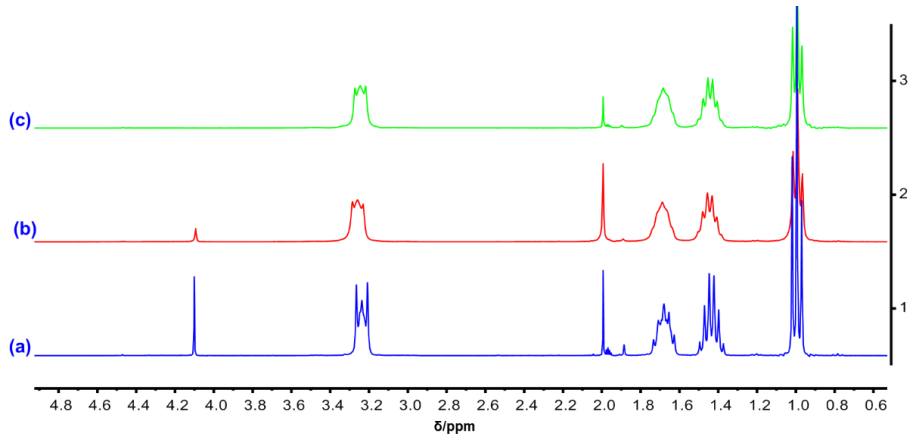

Figure 3.22: *^1H NMR spectra of the reactivity of $(TBA)_3[(MeO)TiW_5O_{18}]$ towards H_2O_2; (a) with 1 mole H_2O_2 after 24 h, (b) with 11 mole H_2O_2 after 14 h (c) with 111 mole H_2O_2 after 2 h; Condition [POM] = 0.15 mmol, solvent MeCN.*

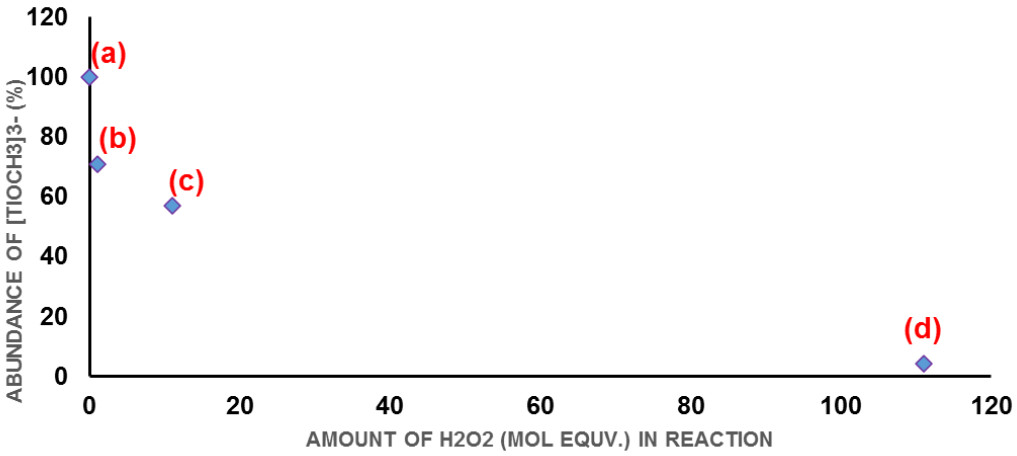

Figure 3.23: *Data from ^{1}H NMR spectrum of the reactivity of $(TBA)_3[(MeO)TiW_5O_{18}]$ towards H_2O_2; (a) without H_2O_2 (b) with 1 mole equivalent H_2O_2, (c) with 11 mole equivalent H_2O_2 and (d) with 111 mole equivalent H_2O_2 in MeCN. Condition [POM] = 0.15 M.*

(b) ^{17}O NMR spectroscopy

The ^{17}O NMR spectrum after addition of 111 mole equivalents of H_2O_2 showed an upfield shift of bridging TiOW peaks indicating protonation of the TiOW bridging oxygen.[39-41] Notably, the ^{17}O NMR spectra (Figure. 3.24c) showed a characteristic peak at δ 408 ppm due to $HTi(O_2)W_5$ as expected (Equation 3.10). This peak appeared only after all the Ti-OCH_3 peak at δ 4.11 ppm disappeared in the corresponding ^{1}H NMR spectrum. Apparently, a new peak at δ –51 ppm assigned to the μ_6-O was observed which we think to be associated with the protonated bridging TiOW peak at δ 408 ppm.

$$[HOOTiW_5O_{18}]^{3-} \rightleftharpoons [(O_2)TiW_5O_{18}H]^{3-} \qquad 3.10$$

Subsequently within two days, the peaks for $HTi(O_2)W_5$ diminished and the ^{17}O NMR spectrum consisted of peaks that correspond to the oxo-bridged dimer. At the initial stages of the reaction, ^{17}O NMR showed peaks for TiOW and μ_6-O at δ 534 and −61 ppm, respectively, suggesting the generation of an intermediate before complete reaction of TiW_5 and formation of $HTi(O_2)W_5$ although it is not clear whether this intermediate species is the hydroperoxo species $(HOO)TiW_5$. However, the intermediate species was subsequently converted to either $HTi(O_2)W_5$ or $[(\mu\text{-}O)(TiW_5O_{18})_2]^{6-}$ as a result of decomposition reactions. Note that TiW_5 hydroperoxido and peroxido species apparently decompose to give the oxo-bridged species.

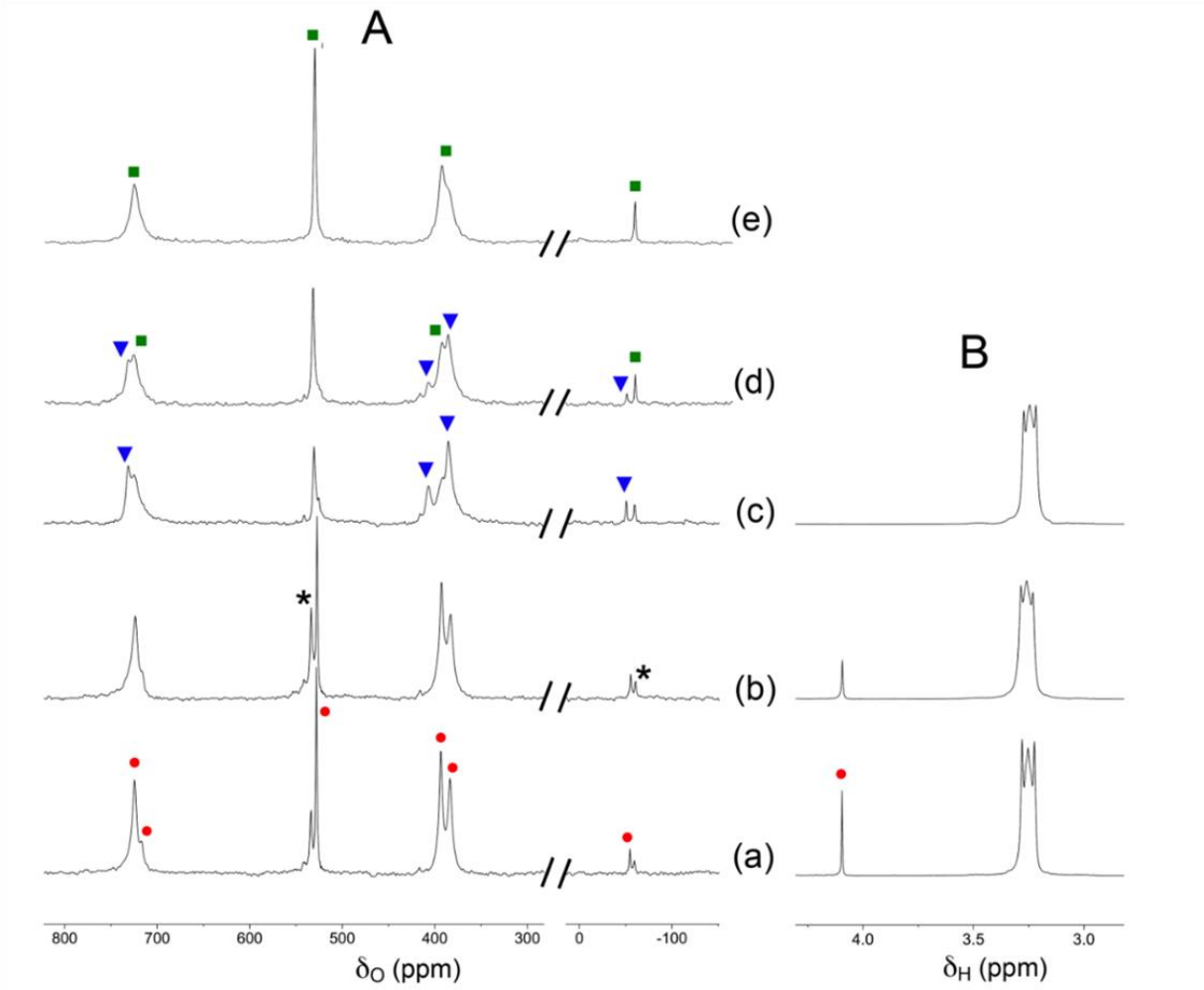

Figure 3.24: *^{17}O (A) and ^{1}H (B) NMR spectra of the products after treatment of TiW_5 with (a) 1, (b) 11 and (c) 111 mole equivalents of dried H_2O_2. Spectra (d) and (e) were recorded 22 and 44 h respectively after spectrum (c). Peaks assigned to TiW_5, $HTi(O_2)W_5$ and $(TiW_5)_2O$ are indicated by ●, ▼and ■ respectively. Peaks due to an apparent intermediate prior to formation of HTi(O2)W5 are marked with an asterisk. POM 0.03 M, CH3CN, RT.*

These results together with the results obtained from Kholdeeva's group for the niobium analogue showed that both Ti and Nb peroxo species "HMO_2" are more stable than the hydroperoxo species "MOOH", but the latter show more catalytic reactivity analogous to that of heterogeneous Ti- and Nb containing catalysts in alkene oxidation with aqueous hydrogen peroxide (Figure 3.25).[42]

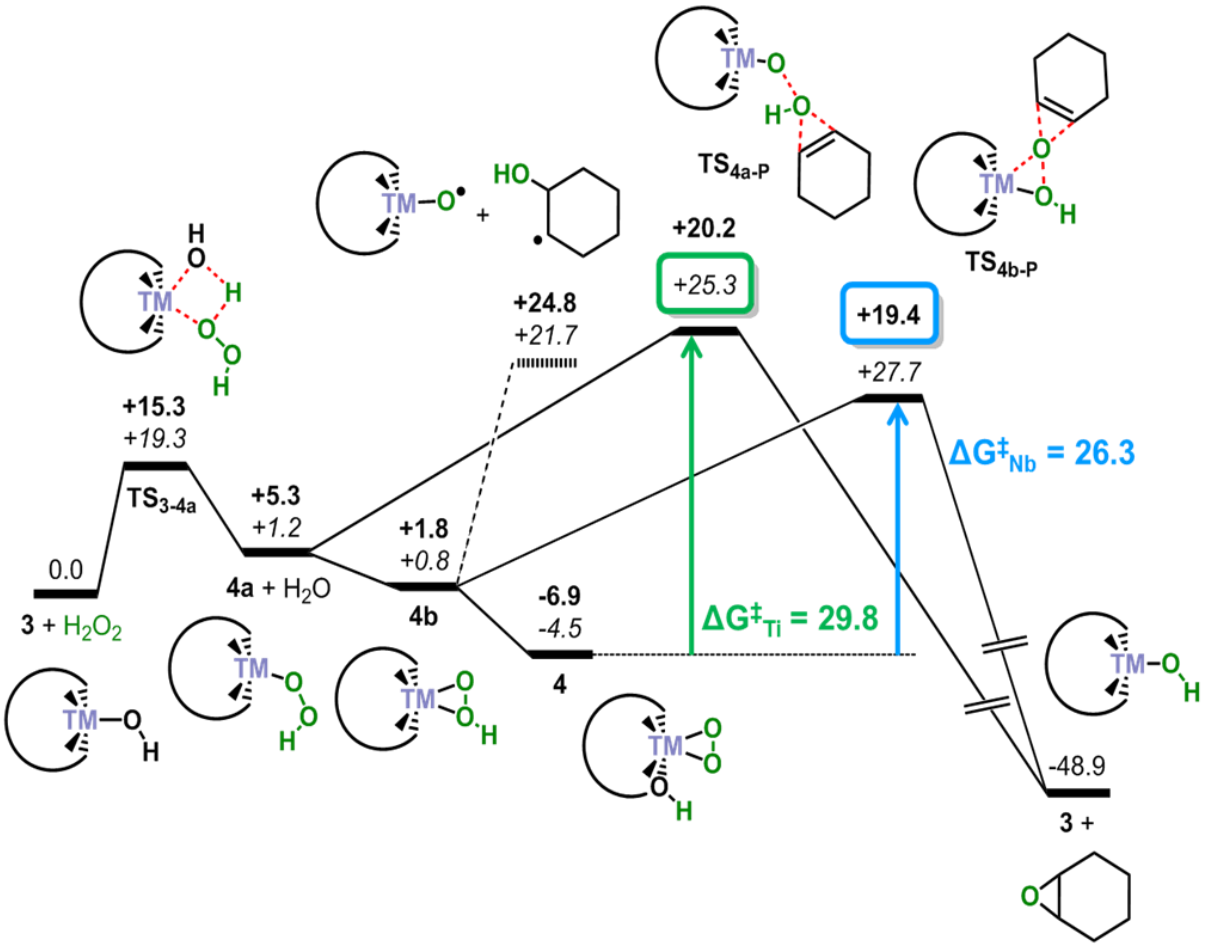

Figure. 3.25: *Free energy profiles for cyclohexene epoxidation by* ***NbW₅ vs TiW₅*** *(Values in* ***bold*** *are associated to* ***NbW₅*** *while those in italics describe the energy profile for* TiW_5*).*[42]

3.8 Computational studies on hydrolysis and condensation of $(TBA)_3[(MeO)MW_5O_{18}]$ (M = Ti, Sn)

3.8.1 Hydrolysis

Density Function Theory (DFT) has been used extensively for the theoretical analysis of POMs,[37,41] including the prediction of spectroscopic properties.[43-45] DFT analysis,[47] conducted in an attempt to rationalize our experimental data for hydrolysis of $(TBA)_3[(MeO)TiW_5O_{18}]$ and $(TBA)_3[(MeO)SnW_5O_{18}]$ predicts similar proton transfer process for hydrolysis of $(TBA)_3[(MeO)TiW_5O_{18}]$ and $(TBA)_3[(MeO)SnW_5O_{18}]$ and the preferred condensation reaction pathways for both hydroxido anions were determined (Figure 3.26). The prediction shows that the initial hydrolysis step involved nucleophilic attack by the OH group of one $(TBA)_3[(HO)MW_5O_{18}]$ anion at the heterometal **M** of an adjacent anion with subsequent hydrogen transfer and elimination of H_2O molecule (Scheme 3.3). It is worth noting that the pathways for Ti and Sn differ slightly because an extra transition state was identified for the initial Sn–O bond formation in the $\{SnW_5\}$ case wherein hydrogen transfer and loss of water molecule occur in a second step.

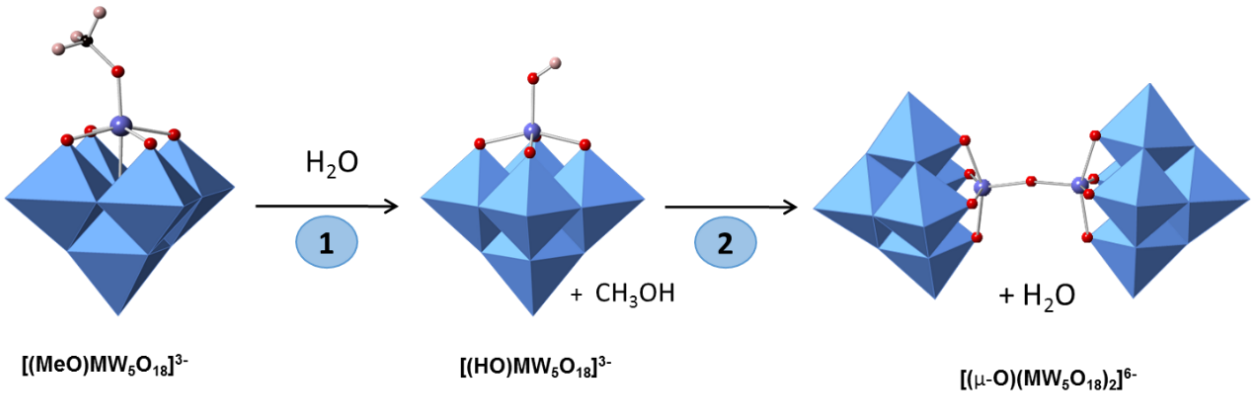

Scheme 3.3: *Polyhedral and ball-and-stick representation of hydrolysis reaction for $[(MeO)MW_5O_{18}]^{3-}$ code: Blue polyhedral W, Red –O, purple –M, Black-C and Pink-H.*

Activation energies were similar for each of these condensation reactions, but the titanium oxo-bridged product $(TBA)_6[(\mu\text{-}O)(TiW_5O_{18})_2]$ was predicted to be significantly more thermodynamically stable. Again, this is consistent with the experimental observations, as it was more difficult to prepare pure samples of $(TBA)_6[(\mu\text{-}O)(SnW_5O_{18})_2]$ than the oxo-bridged dimer of the titanium compound $(TBA)_6[(\mu\text{-}O)(TiW_5O_{18})_2]$.

Table 3.2: *Relative energies with respect to reactants for transitions state and products for step 1 of the hydrolysis of $[(MeO)MW_5O_{18}]^{3-}$, where M = Ti and Sn.*

Reactant	$E_{rel\text{-}step1}$ TS1[a]	$E_{rel\text{-}step1}$ Product[a]
$[(MeO)TiW_5O_{18}]^{3-}$	15.80 (20.23)	1.13 (3.37)
$[(MeO)SnW_5O_{18}]^{3-}$	9.80 (13.84)	-3.11 (-0.30)

[a] *Relative energies with respect to reactants (in kcal-mol^{-1}); in parenthesis, relative Gibbs free energies (in kcal mol^{-1}) for step1 of the hydrolysis.*[47]

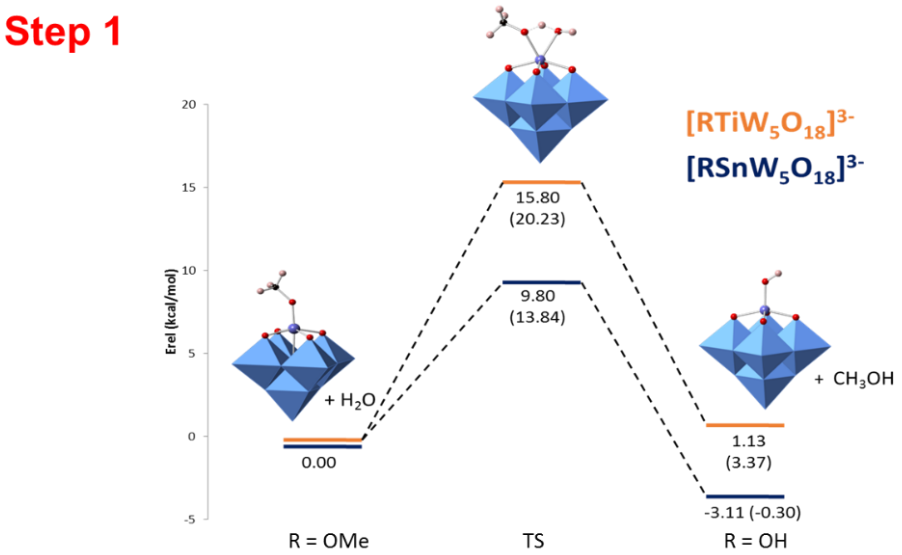

Figure 3.26: *Energy profile for hydrolysis of $[(MeO)MW_5O_{18}]^{3-}$ (M = Ti and Sn).*[47]

The effect of the heterometal on the system is evident in the experimental data obtained from ^{17}O NMR peaks for terminal W_{ax}=O *trans* to Sn. This appeared upfield to those for W_{ax}=O *trans* to Ti. While those for W_{eq}=O situated *cis* to Ti or Sn are shifted to almost similar position. This effect is also observed in the ^{183}W NMR spectra for {SnW_5} anions where the chemical shifts for W_{ax} *trans* to Sn in {SnW_5} anions are shifted significantly lower values compared to those for W_{ax} *trans* to Ti in {TiW_5} anions. Figure 3.27 also reflects these differences in the calculated transition state bond lengths for Sn-OCH_3 (2.16 Å) which is longer compared to 2.08 Å for Ti-OCH_3. The longer bond length in Sn-OCH_3 is indicative of higher polarity and hence more ionic character compared to the covalent character in Ti-OCH_3.

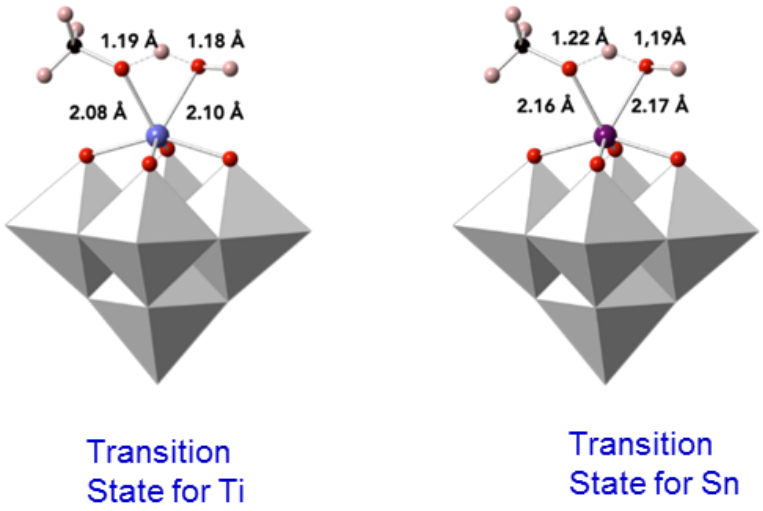

Figure 3.27: *Optimized transition state structure of step 1 in the hydrolysis of $[(MeO)SnW_5O_{18}]^{-}$ and $[(MeO)SnW_5O_{18}]^{3-}$*

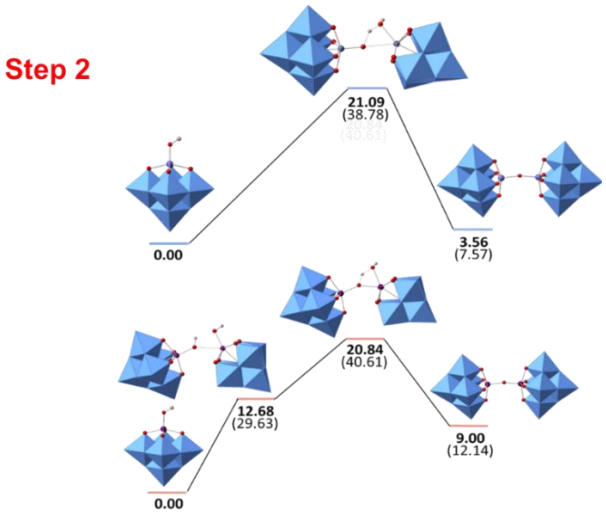

Figure 3.28: *Energy profile for condensation of $[(HO)MW_5O_{18}]^3$ (M = Ti and Sn).*

In Figure 3.28, the results showed that $(TBA)_6[(\mu\text{-}O)(SnW_5O_{18})_2]$ is less thermodynamically stable than $(TBA)_6[(\mu\text{-}O)(TiW_5O_{18})_2]$ which is consistent with the

experimental results. In contrast, the energy of Ti oxo-bridged dimer $(TBA)_6[(\mu\text{-}O)(TiW_5O_{18})_2]$ compared to TiOH which is readily accessible under experimental conditions.

Table 3.3: *Relative energies with respect to reactants for different transitions states and products for step2 of the hydrolysis of $[(MeO)MW_5O_{18}]^{3-}$, where M = Sn and Ti.*

Reactant	E_{rel}-TS2$_1$[a]	E_{rel}-TS2$_2$[a]	$E_{rel\text{-}step2}$ Product[a]
$[(HO)TiW_5O_{18}]^{3-}$	-	21.1 (38.8)	3.6 (7.5)
$[(HO)SnW_5O_{18}]^{3-}$	12.7 (13.84)	20.8 (40.6)	9.0 (12.1)

[a] *Relative energy with respect to reactants (in kcal-mol^{-1}); in parenthesis, relative Gibbs free energies (in kcal mol^{-1}) for step2 of the hydrolysis.*[47]

3.8.2 Alcoholysis

The reactions between methanol and the methoxido anions $[(MeO)TiW_5O_{18}]^{3-}$ and $[(MeO)SnW_5O_{18}]^{3-}$ were studied by DFT calculations in order to explain better why the mixture of MeOH/$[(MeO)TiW_5O_{18}]^{3-}$ did not show any TiOMe/MeOH exchange peaks, whereas off-diagonal $SnOCH_3/CH_3OH$cross-peaks were observed in 2D ^{1}H NMR EXSY experiments for MeOH/$[(MeO)SnW_5O_{18}]^{3-}$. The results from DFT calculations, indicate that the slow exchange rate for the Ti-POM is related to the activation energy associated with the proton transfer process involving a seven-coordinate titanium. This is likely to be elevated due to the reluctance of titanium in $(TBA)_3[(MeO)TiW_5O_{18}]$ to increase its coordination number from 6 to 7.

3.9 Conclusion

The hydrolysis and condensation reactions of monosubstituted $\{TiW_5\}$ and $\{SnW_5\}$ Lindqvist tungstate anions were monitored by ^{17}O and ^{1}H NMR spectroscopy which enabled detailed investigation of the reactivity of $[(MeO)TiW_5O_{18}]^{3-}$ and $[(MeO)SnW_5O_{18}]^{3-}$ at the M-OR bonds. It was shown that condensation of $[(HO)TiW_5O_{18}]^{3-}$ can be inhibited in the presence of strong donor ligand solvent. These studies show that the nature of the M-OC bond plays a crucial role in the hydrolysis of these Lindqvist POMs. Controlled hydrolysis of $[(MeO)TiW_5O_{18}]^{3-}$ led to the isolation and characterization of titanium hydroxido $[(HO)TiW_5O_{18}]^{3-}$ intermediate for the first time. While DFT calculations confirm that the energy pathway for the formation of $[(HO)TiW_5O_{18}]^{3-}$ was more energetically demanding. In the 2D ^{1}H EXSY NMR study, an off-diagonal peak was observed in the alcohol exchange and the exchange rate calculated. The reaction between $[(MeO)TiW_5O_{18}]^{3-}$ and an excess of anhydrous H_2O_2 showed the formation of $HTi(O_2)W_5$ or $(HOO)TiW_5$ intermediates. The formation of

these intermediates has been shown to be crucial for heterolytic oxygen transfer to alkenes over both Ti(IV) and Nb(V). DFT calculations showed that hydroperoxo species “MOOH” (M = Ti or Nb) was more reactive than “HMO_2” toward epoxidation of alkenes.

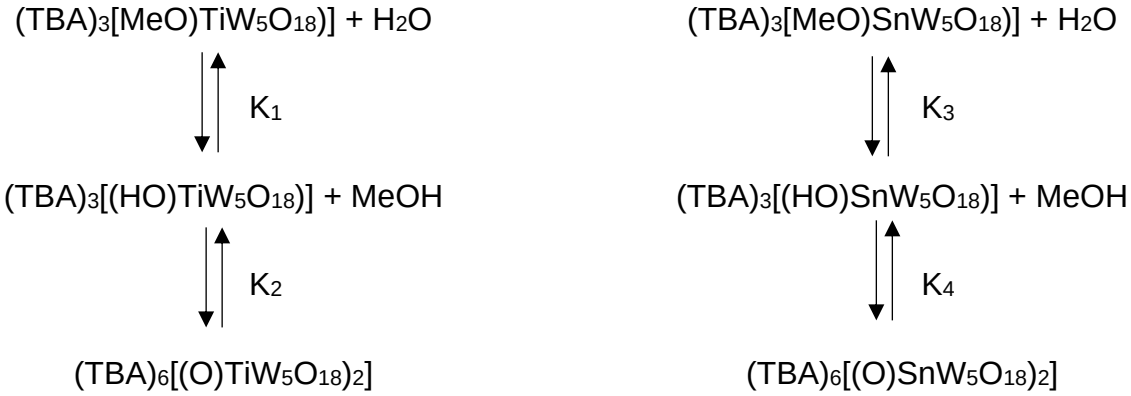

$K_3 >> K_1$ and $K_2 > K_4$

Scheme 3.4: *Equilibrium reactions of hydrolysis and condensation of tin and titanium substituted lindqvist POMs.*

3.10 Experimental

3.10.1 Hydrolysis of $(TBA)_3[(MeO)TiW_5O_{18}]$ with 1.0 mole equivalent of H_2O in MeCN

$(TBA)_3[(MeO)TiW_5O_{18}]$ (50 mg, 0.025 mmols) was dissolved in CD_3CN (0.5 mL) in a sealed screw top NMR tube and an initial ^1H NMR spectrum was recorded. After the first spectrum, deionized H_2O (1.0 µL, 0.024 mmols) was added and vigorously shake and monitored the reaction by ^1H NMR spectroscopy over a 2 h period until equilibrium was established. **^1H NMR** (300 MHz, Acetonitrile-d_3) δ (ppm) 4.11 due to unreacted $TiOCH_3$ and 3.30 for methanol CH_3.

3.10.2 Hydrolysis of $(TBA)_3[(MeO)TiW_5O_{18}]$ with 20 mole equivalents of H_2O in MeCN

In a sealed screw top NMR tube was placed $(TBA)_3[(MeO)TiW_5O_{18}]$ (50 mg, 0.025 mmols) and dissolved in MeCN (0.5 mL) and the initial ^1H NMR spectrum recorded. After the initial ^1H NMR spectrum, deionized H_2O (22.0 µL, 1.25 mmols) was added

and subsequent ^{1}H NMR spectra were recorded over a 2 h period until equilibrium established.

3.10.3 Hydrolysis of $(TBA)_3[(MeO)TiW_5O_{18}]$ with 1.0 mole equivalent of H_2O in DMSO-d_6

In a sealed screw top NMR tube was placed $(TBA)_3[(MeO)TiW_5O_{18}]$ (50 mg, 0.025 mmols) was dissolved in DMSO-d_6 (0.5 mL) in a sealed screw top NMR tube and an initial ^{1}H NMR spectrum was recorded. After the first spectrum, deionized H_2O (1.0 µL, 0.024 mmols) was added and the reaction was monitored by ^{1}H NMR spectroscopy over a 2 h period until equilibrium was established.

3.10.4 Hydrolysis of $(TBA)_3[(MeO)TiW_5O_{18}]$ with 20 mole equivalents of H_2O in DMSO-d_6

In a sealed screw top NMR tube was placed $(TBA)_3[(MeO)TiW_5O_{18}]$ (50 mg, 0.025 mmols) and dissolved in DMSO-d_6 (0.5 mL) and the initial ^{1}H NMR spectrum recorded. After the initial ^{1}H NMR spectrum, deionized H_2O (22.0 µL, 1.25 mmols) was added and subsequent ^{1}H NMR spectra were recorded over a 2 h period until equilibrium established.

3.10.5 Alcoholysis of $(TBA)_3[(MeO)TiW_5O_{18}]$ with 1.0 mole equivalents of CH_3OH in MeCN

In a sealed screw top NMR tube was added $(TBA)_3[(MeO)SnW_5O_{18}]$ (50 mg, 0.025 mmols) and dissolved in MeCN (0.5 mL) and an initial ^{1}H NMR spectrum was recorded. After the first spectrum, deuterated MeOH (1.0 µL, 0.024 mmols) was added and the reaction was monitored by ^{1}H NMR spectroscopy until equilibrium was established.

3.10.6 Preparation of $(TBA)_3[(HO)TiW_5O_{18}]$ in MeCN

In a Schlenk flask was added ^{17}O-enriched $(TBA)_3[(CH_3O)TiW_5O_{18}]$ (0.5 g, 0.248 mmol) and dissolved in MeCN (2 mL).To the solution was added deionized H_2O (0.45 mL, 24.83 mmol, 100 eq.) with stirring for 1 h and vacuum dried to give a white solid. The hydrolysis step was repeated 5 more times to obtain a white solid which was a mixture of $(TBA)_3[(HO)TiW_5O_{18}]$ and $(TBA)_6[(\mu\text{-}O)(TiW_5O_{18})_2]$ (**0.2975 g, 60 %**). **IR (4000 – 400 cm^{-1}):** 3671 (w) (OH), 2959 (m), 2934 (m), 2872 (m), 1482 (m), 1381 (w), 1152 (vw), 1070 (s), 946 (vs), 884 (s), 790 (vs, br), 673 (m) 616 (w) 568 (w), 542 (w), 522 (w); **^{17}O NMR** (41 MHz, acetonitrile-d_3): δ (ppm), 722 – 717 (W=O), 536, 526 (TiOW), 392 – 382 (WOW), -59 and -61.

3.10.7 Preparation of $(TBA)_3[(HO)TiW_5O_{18}]$ in DMSO:

A 0.5 g, 0.248 mmol of ^{17}O enriched $(TBA)_3[(CH_3O)TiW_5O_{18}]$ was placed in a Schlenk flask and dissolved in ~ 3 mL DMSO. To the solution was added deionized H_2O (0.45 mL, 24.83 mmol, 100 eq.) with stirring for ~4 h and vacuum dried for 2 h to remove volatiles (MeOH and H_2O). The resulting colorless solution was triturated with diethyl ether (30 mL x 6) to obtain a white solid $(TBA)_3[(CH_3O)TiW_5O_{18}]$ **(0.258 g, 52 %**).

FT-IR (4000 – 400 cm^{-1}): 3673 (w) (OH), 2958 (m), 2872 (m), 1481 (m), 1380 (w), 1152 (vw), 1106 (vw), 1024 (w), 946 (vs), 884 (m), 790 (vs, br), 670 (m) 616 (m), 568 (m) 542 (m), 521 (m), 426 (m); **^{1}H NMR** (400 MHz, DMSO-d_6): 3.19−3.15, 1.61−1.54, 1.37−1.28, and 0.96−0.92, δ (ppm), 9.59 (OH). **^{183}W NMR** (21 MHz, acetonitrile-d_3): obtained over 3 days δ (ppm), 80, 76, 42, and 38.

3.10.8 Reaction of $(TBA)_3[(HO)TiW_5O_{18}]$ with D_2O in MeCN

In a sealed screw top NMR tube was added ^{17}O enriched $(TBA)_3[(HO)TiW_5O_{18}]$ (80 mg, 0.04 mmols) was dissolved in MeCN (~2 mL) in Schlenk flask. D_2O (~ 8 µL, 10 mmols) was added with stirring. The resulting solution was stirred for 1 h and pumped dry under vacuum. **IR (4000 – 400 cm^{-1}):** In addition to peaks observed for $(TBA)_3[(HO)TiW_5O_{18}]$ at 2707 cm^{-1} was assigned to TiOD. 3673 (w) is assigned to OH, 2958 (m), 2872 (m), 1481 (m), 1380 (w), 1152 (vw), 1106 (vw), 1024 (w), 946 (vs), 884 (m), 790 (vs, br), 670 (m) 616 (m), 568 (m) 542 (m), 521 (m), 426 (m);

3.10.9 Reaction of non-enriched $(TBA)_3[(HO)TiW_5O_{18}]$ with ten-fold excess of ^{17}O enriched H_2O in MeCN

A non-enriched $(TBA)_3[(HO)TiW_5O_{18}]$ (80 mg, 0.04 mmols) was dissolved in MeCN (~2 mL) in Schlenk flask and was added ten-fold excess of ^{17}O-enriched H_2O in CD_3CN. The resulting solution was stirred overnight at 80 ^oC, with subsequent precipitation with diethyl ether and drying under vacuum. **^{17}O NMR** (41 MHz,) δ (ppm) 681, 555, 535, 473.

3.10.10 Reaction to established equilibrium between $(TBA)_3[(MeO)TiW_5O_{18}]$ and $(TBA)_6[(\mu\text{-}O)(TiW_5O_{18})_2]$ in MeCN

In a sealed screw top NMR tube was added ^{17}O-enriched $(TBA)_6[(\mu\text{-}O)(TiW_5O_{18})_2]$ (50 mg, 0.0125 mmols) and dissolved in MeCN (0.5 mL). To the solution was added MeOH (0.45 µL, 0.025 mmols 2 eqv.) and heated to 80 – 90 ^oC for 1 h. The solution was cooled to room temperature before recording ^1H NMR spectrum. **^{1}H NMR** (300 MHz, Acetonitrile-d_3) δ (ppm) 4.11 with CH_3:^{n}Bu 0.5:8 **^{17}O NMR** (41 MHz, Acetonitrile-d_3) δ

(ppm) 723 and 715 (W_{eq}=O and W_{ax}=O) respectively, 531 and 526 (TiOW), 392 and 383 (WOW), -55 and -60.

3.10.11 Preparation of $(TBA)_3[(HO)SnW_5O_{18}]$ in CD_3CN

In a sealed screw top NMR tube was added ^{17}O-enriched $(TBA)_3[(MeO)SnW_5O_{18}]$ (0.1 g, 0.048 mmols) and dissolved in CD_3CN (~0.5 mL) and it was added ten-fold excess of deionized H_2O. The initial ^{1}H NMR spectrum was recorded, and the solution was then transferred into a Schlenk flask and stirred for 2 h at room temperature, with subsequent precipitation with diethyl ether and drying under vacuum. **^{1}H NMR** (300 MHz, dmso-d_6) δ (ppm) 3.42 due to SnOH with **$^{119/117}$Sn** satellites and $^2J(^{183}W^{119/117}Sn)$ of *ca* 44 Hz. A doublet in the ^{1}H-coupled ^{119}Sn NMR spectrum at –633 ppm with $^2J(^{119}Sn^1H)$ = 47.7 Hz and tungsten satellites with $^2J(^{183}W^{119}Sn)$ = 37 Hz and 3.33 (HOH). **FT-IR ATR (4000 – 400 cm^{-1})** 3646 (w) assigned to OH, 2958 (m), 2872 (m), 1482 (s), 1380 (m), 1151 (w), 1106 (w), 1025 (w), 973 (w), 949 (s), 884 (m), 795 (s), 754 (s), 597, 566, 470, 444, 420 cm^{-1}. **^{183}W NMR** (21 MHz, acetonitrile-d_3): δ (ppm) 72 and –122 ppm for W_{eq} and W_{ax} respectively. Impurity peaks observed at -130 and 71 ppm assign to W_{eq} and W_{ax} respectively for $(TBA)_6[(\mu\text{-}O)(SnW_5O_{18})_2]$**.**

3.10.12 Condensation of $(TBA)_3[(HO)SnW_5O_{18}]$ in PhCN

In a sealed screw top Schlenk flask was added $(TBA)_3[(HO)SnW_5O_{18}]$ (100 mg, 0.0483 mmols) and dissolved in PhCN (~2 mL). Repeated hydrolysis in PhCN at elevated temperature (110 °C) with removal of the volatiles under reduced pressure after each hydrolysis step gave $(TBA)_6[(\mu\text{-}O)(SnW_5O_{18})_2]$**. FT-IR ATR (4000 – 400 cm^{-1})** 2959 (m), 2873 (m), 2809 (m), 1674 (m), 1482 (s), 1381(m), 1045 (w), 951(s), 882 (w), 827 (m), 799 (s), 756 (s), 569, 518, 445, 423 cm^{-1}. ^{119}Sn **NMR** (112 MHz, acetonitrile-d_3) δ -667 ppm.

3.10.13 Reaction of $(TBA)_3[(MeO)TiW_5O_{18}]$ with H_2O_2 in MeCN

A solution of 40 % aqueous H_2O_2 (3.50 uL, 0.1490 mmol) was placed in a Schlenk flask and dissolved in MeCN (5 mL) and was pumped to dryness. This process was repeated twice to remove the volatiles and re-dissolved in MeCN (5 mL). $(TBA)_3[(MeO)TiW_5O_{18}]$ (0.3 g,0.1490 mmol) was added and a yellow solution was immediately formed. The yellow solution was stirred for 1 h and pumped to dryness. The yellow solid material was dissolved in CD_3CN (0.5 mL) and the first ^{1}H NMR spectrum was recorded. The NMR solution was placed back into the Schlenk flask and re-dissolved in MeCN (5 mL)

and stirred for further 3 h before pumping the solution to dryness under vacuum. The reaction procedure was repeated several times over 65 h.

The ^{1}H NMR spectrum after 3 days showed 75 % of methoxy peak present. The NMR sample was replaced back into the flask with stirring for 4 weeks. ^{1}H NMR spectrum suggest 71 % methoxide present. H_2O_2 (10 mol eqv.) was added and stirred for 2 h, the solution was pump dry and ^{1}H NMR spectrum was recorded. H_2O_2 (100 mol eqv.) was added and stirred for 2 h before pumping the solution to dryness under vacuum. The ^{1}H NMR spectrum suggest 95 % of OCH_3 peak has been reacted.

IR (4000 – 400 cm^{-1}): 3633 (w) assigned to free OH, 2959 (m), 2934 (m), 2872 (m), 1482 (m), 1381 (w), 1152 (vw), 1070 (s), 960 (vs), 884 (s), 791 (vs, br), 689 (m) 594 (m), 515 (s) 501 (s), 472 (m), 432 (w), 410 (m); **^{17}O NMR** (41 MHz, Acetonitrile-*d*$_3$) δ (ppm) W_{eq}=O at 724, W_{ax}=O at 716, TiOW at 534 and 529, WOW at 394 and 383, and μ_6-O at -55 and -59.

3.10.14 Computational studies

Density Functional Theory (DFT) calculations and Classical Molecular Dynamics (CMD) simulations were performed by the Quantum Chemistry Group at the Universitat Rovira i Virgili, Tarragona (Spain). The Calculations were performed with the GGA-type OPBE functional, including spin–orbit and scaling corrections, provide a mean absolute error < 30 ppm a small value considering the range of δ(^{17}O) values in these systems is ~1200 ppm.

References

1. L. L. Hench and J. K. West, *Chem. Rev.*, 1990, **90**, 33-72.
2. M. I. Youssif, R. M. El-Maghraby, S. M. Saleh and A. A. Elgibaly, *Energy & Fuels*, 2018, **32**, 12373-12382.
3. C. Sanchez, F. Ribot and B. Lebeau, *J. Mater. Chem.*, 1999, **9**, 35-44.
4. C. D. Chandler, C. Roger and M. J. Hampden-Smith, *Chem. Rev.*, 1993, **93**, 1205-1241.
5. V. W. Day, T. A. Eberspacher, W. G. Klemperer and C. W. Park, *J. Am.Chem. Soc.*, 1993, **115**, 8469-8470.
6. K. G. Caulton and L. G. Hubert-Pfalzgraf, *Chem. Rev.*, 1990, **90**, 969-995.
7. R. Papiernik, L. G. Hubert-Pfalzgraf, J. Vaissermann and M. C. Henriques Baptista Goncalves, *J. Chem. Soc., Dalton Trans.*, 1998, 2285-2288.
8. J. Caruso, T. M. Alam, M. J. Hampden-Smith, A. L. Rheingold and G. A. P. Yap, *J. Chem.Soc., Dalton Trans.*, 1996, 2659-2664.
9. J. M. Thomas, R. Raja and D. W. Lewis, *Angew. Chemie Int. Ed.*, 2005, **44**, 6456-6482.
10. L. Hua, Y. Qiao, Y. Yu, W. Zhu, T. Cao, Y. Shi, H. Li, B. Feng and Z. Hou, *New J. Chem.*, 2011, **35**, 1836-1841.
11. O. A. Kholdeeva, T. A. Trubitsina, G. M. Maksimov, A. V. Golovin and R. I. Maksimovskaya, *Inorg. Chem.*, 2005, **44**, 1635-1642.
12. P. Jiménez-Lozano, I. D. Ivanchikova, O. A. Kholdeeva, J. M. Poblet and J. J. Carbó, *Chem. Commun.*, 2012, **48**, 9266-9268.
13. N. S. Antonova, J. J. Carbó, U. Kortz, O. A. Kholdeeva and J. M. Poblet, *J. Am. Chem. Soc.*, 2010, **132**, 7488-7497.
14. O. A. Kholdeeva, B. G. Donoeva, T. A. Trubitsina, G. Al-Kadamany and U. Kortz, *Eur. J. Inorg. Chem.*, 2009, **2009**, 5134-5141.
15. H. Lv, Y. V. Geletii, C. Zhao, J. W. Vickers, G. Zhu, Z. Luo, J. Song, T. Lian, D. G. Musaev and C. L. Hill, *Chem. Soc. Rev.*, 2012, **41**, 7572-7589.
16. M. Fournier, C. Louis, M. Che, P. Chaquin and D. Masure, *J. Catalysis*, 1989, **119**, 400-414.
17. Q. Chen and J. Zubieta, *Coord.Chem. Rev.*, 1992, **114**, 107-167.
18. O. A. Kholdeeva and O. V. Zalomaeva, *Coord. Chem. Rev.*, 2016, **306**, 302-330.

19. O. A. Kholdeeva and R. I. Maksimovskaya, *J. Mole. Catalysis:* 2007, **262***A*, 7-24.
20. O. A. Kholdeeva, *Eur. J. Inorg. Chem.*, 2013, **2013**, 1595-1605.
21. B. Kandasamy, C. Wills, W. McFarlane, W. Clegg, R. W. Harrington, A. Rodríguez-Fortea, J. M. Poblet, P. G. Bruce and R. J. Errington, *Eur. J.*, 2012, **18***A*, 59-62.
22. W. Clegg, M. R. J. Elsegood, R. J. Errington and J. Havelock, *J. Chem.Soc., Dalton Trans.*, 1996, 681-690.
23. R. J. Errington, S. S. Petkar, P. S. Middleton, W. McFarlane, W. Clegg, R. A. Coxall and R. W. Harrington, *Dalton Trans.*, 2007, 5211-5222.
24. L. Coyle, P. S. Middleton, C. J. Murphy, W. Clegg, R. W. Harrington and R. J. Errington, *Dalton Trans.*, 2012, **41**, 971-981.
25. V. Ugrinova, G. A. Ellis and S. N. Brown, *Chem. Commun.*, 2004, 468-469.
26. F. Q. Liu, H. W. Roesky, H. G. Schmidt and M. Noltemeyer, *Organometallics*, 1992, **11**, 2965-2967.
27 D. Lebbie, MPhil thesis, Newcastle University, 2015
28. R. J. Errington, S. S. Petkar, P. S. Middleton, W. McFarlane, W. Clegg, R. A. Coxall and R. W. Harrington, *J. Am. Chem. Soc.*, 2007, **129**, 12181-12196.
29. G. De Faveri, G. Ilyashenko and M. Watkinson, *Chem. Soc. Rev.*, 2011, **40**, 1722-1760.
30. O. A. Kholdeeva, *Catalysis Science & Technology*, 2014, **4**, 1869-1889.
31. S.-S. Wang and G.-Y. Yang, *Chem. Rev.*, 2015, **115**, 4893-4962.
32. R. Noyori, M. Aoki and K. Sato, *Chem. Commun.*, 2003, 1977-1986.
33. N. Mizuno, K. Yamaguchi and K. Kamata, *Coord. Chem. Rev.*, 2005, **249**, 1944-1956.
34. A. Sartorel, M. Carraro, A. Bagno, G. Scorrano and M. Bonchio, *Angew. Chemie*, 2007, **119**, 3319-3322.
35. K. Kamata, K. Yonehara, Y. Sumida, K. Yamaguchi, S. Hikichi and N. Mizuno, *Science*, 2003, **300**, 964-966.
36. A. E. Kuznetsov, Y. V. Geletii, C. L. Hill, K. Morokuma and D. G. Musaev, *Inorg. Chem.*, 2009, **48**, 1871-1878.
37. N. S. Antonova, J. J. Carbó, U. Kortz, O. A. Kholdeeva and J. M. Poblet, *J. Am. Chem. Soc.*, 2010, **132**, 7488-7497.
38. I. Y. Skobelev, O. V. Zalomaeva, O. A. Kholdeeva, J. M. Poblet and J. J. Carbó, *Eur. J.*, 2015, **21A**, 14496-14506.

39. P. Jiménez-Lozano, I. Y. Skobelev, O. A. Kholdeeva, J. M. Poblet and J. J. Carbó, *Inorg. Chem.*, 2016, **55**, 6080-6084.
40. N. V. Maksimchuk, G. M. Maksimov, V. Y. Evtushok, I. D. Ivanchikova, Y. A. Chesalov, R. I. Maksimovskaya, O. A. Kholdeeva, A. Solé-Daura, J. M. Poblet and J. J. Carbó, *ACS Catalysis*, 2018, **8**, 9722-9737.
41. R. J. Errington, in *Advances in Inorg. Chem.*, eds. R. van Eldik and L. Cronin, Academic Press, 2017, vol. 69, pp. 287-336.
42. M. Pascual-Borras, X. Lopez, A. Rodriguez-Fortea, R. J. Errington and J. M. Poblet, *Chemical Science*, 2014, **5**, 2031-2042.
43. N. V. Maksimchuk, I. D. Ivanchikova, G. M. Maksimov, I. V. Eltsov, V. Y. Evtushok, O. A. Kholdeeva, D. Lebbie, R. J. Errington, A. Solé-Daura, J. M. Poblet and J. J. Carbó, *ACS Catalysis*, 2019, **9**, 6262-6275.
44. A. Bagno and M. Bonchio, *Angew. Chemie*, 2005, **117**, 2059-2062.
45. A. Bagno, M. Bonchio and J. Autschbach, *Eur. J.*, 2006, **12A**, 8460-8471.
46. J. Gracia, J. M. Poblet, J. Autschbach and L. P. Kazansky, *Eur. J. Inorg.Chem.*, 2006, **2006**, 1139-1148
47 M. Pascual-Borras, PhD thesis, UVR Taragona 2015.

Chapter 4

Understanding the Protonation and Electrophilic Behaviour of $(TBA)_3[(MeO)TiW_5O_{18}]$ and $(TBA)_6[(\mu\text{-}O)(TiW_5O_{18})_2]$

Catalysis by metal-oxide clusters, like POMs are generally associated with proton transfer processes. Thus, a sound knowledge of protonation sites and mechanism in such systems is fundamental to their application as catalysts. This chapter describes our detailed investigation of surface oxygen basicity of two Lindqvist-type polyoxometalates, $(TBA)_3[(MeO)TiW_5O_{18}]$ and $(TBA)_6[(\mu\text{-}O)(TiW_5O_{18})_2]$ using ^{17}O NMR technique. The results of the protonation studies triggered our interest on exploring the electrophilic behaviour of the POMs towards a range of electrophiles. This was aimed at designing and possibly isolating series of POM-pincer complexes. Pincer complexes have been implicated in green catalysis.

4.1 Introduction

Studies of proton transfer mechanisms in Ti-substituted POMs have been attracting much attention in recent years due to the crucial role of protonated peroxo species in titanium based catalytic oxidation process.[1-5] We embarked on detailed investigations on protonolysis of the Lindqvist-type polyoxoanions in order to understand these protonation process and the proton transfer mechanisms within these oxoanions. A thorough understanding of proton transfer mechanisms involving POMs is still poorly addressed although studies have shown the relevance of protonated intermediates in catalytic alkene epoxidation,[1, 6-9]

Both the Lindqvist $(TBA)_2[W_6O_{19}]$ and Keggin-type $(TBA)_3[PW_{12}O_{40}]$ types POMs have only two types of outer oxygens i.e. the bridging W-O-W and the terminal W=O oxygens. In each case, the bridging W-O-W sites are considered to be the most basic sites and in terms of protonation, these bridging W-O-W sites are more likely to be protonated rather than the terminal W=O oxygens.[10-12] The addition of heterometal or metal ligand (metal alkoxides) into the POM structure can result in different electronic properties of the POMs which influence the nature of the basicity of these outer oxygens in the anions. For example in substituted $[(R)M'M_5O_{18}]^{n-}$, the replacement of $[WO]^{4+}$ with $[ML]^{n+}$ (were L = CH_3O, OH; M = Ti, Sn) generates R-O-M (R = Me, H), M′-O-M or M-O-M oxygen sites and the bonding nature in these species has a significant influence on the protonation sites in the anion.

In the Keggin-type $(TBA)_8[[(\mu\text{-}O)(TiPW_{11}O_{39})_2]$,[13] it was recently proposed that the oxygen at the bridging Ti-O-Ti is the most basic site in the anion and therefore more likely to be protonated. Although in more recent studies the results suggested otherwise.[14] In Chapter 3 the studies explored the interaction of MeOH with $(TBA)_3[(MeO)TiW_5O_{18}]$ and $(TBA)_3[(MeO)SnW_5O_{18}]$ for the exchange of $MOCH_3/CH_3OH$ for detailed reactivity of M-OC bond by ^{1}H NMR and 2D EXSY ^{1}H NMR spectroscopy. In this section the interest is to investigate the protonation of $[(RO)M'W_5O_{18}]^{3-}$ (M′ =Ti, Sn) with $HBF_4.Et_2O$ by ^{17}O NMR spectroscopy. This might lead to generate new reactive $[M'W_5O_{18}]^{2-}$ species in solution and in addition might reveal the site(s) of protonation for $[(RO)M'W_5O_{18}]^{3-}$ and subsequently for $[(\mu\text{-}O)(TiW_5O_{18})_2]^{6-}$.

Previous investigations on the Lindqvist-type POM proposed mechanism for ligand exchange (Scheme 4.1)[15] reaction of $[(RO)M'M_5O_{18}]^{3-}$ (M = W, Mo; M′ = Ti) with protic reagents HL. The proposed mechanisms suggested that the reaction proceeds via

protonation at the Ti-OMe position after initial interaction of the proton in HL with the TiOM oxygen. It is important to note that the mechanisms in Scheme 4.1 were proposed prior to detailed DFT calculations and that the DFT analysis suggested initial approach of H in HL to MOW oxygen and then low energy migration to MOC oxygen without cleavage of H–L bond.[16]

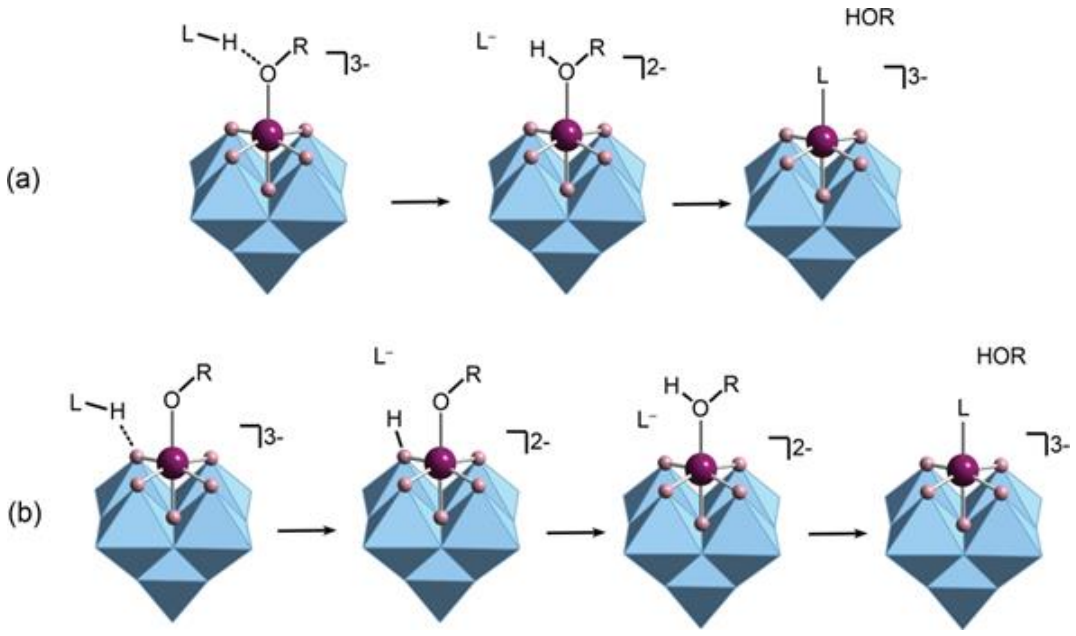

Scheme 4.1: *Reported ligand exchange mechanism between $[(RO)TiW_5O_{18}]^{3-}$ and HL.*[15]

In this investigation reacting $Et_2OH^+BF_4^-$ with $[(RO)M'M_5O_{18}]^{3-}$ (M = W; M′ = Ti; Sn) It is expected that the initial interaction of proton from $Et_2OH^+BF_4^-$ might occur with either OMe or the bridging TiOW. If the reaction proceeds through the latter mechanism, the pathway requires subsequent migration of a proton from TiOW to the alkoxide prior to loss of methanol, by analogy with monoprotonated $[(\eta^5\text{-}C_5R_5)TiW_5O_{18}H]^{2-}$ (R = H, Me) previously characterised by Klemperer.[17] If interaction proceeds through OMe group, i.e. path (b) in Scheme 4.2, this will result in the dissociation of $Et_2OH\text{-}BF_4$ and the formation of the protonated intermediate $[(MeOH)TiW_5O_{18}]^{2-}$. In both cases there is a possibility of creating new active intermediate POMs in solution.

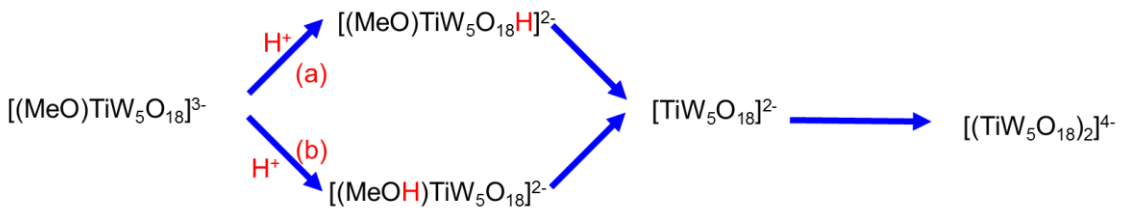

Scheme 4.2: *Possible mechanisms for protonation of $(TBA)_3[(MeO)TiW_5O_{18}]$ with $HBF_4.Et_2O$ in MeCN.*

4.2 Results and Discussion

4.2.1 Protonation of $(TBA)_3[(MeO)TiW_5O_{18}]$ with $HBF_4.Et_2O$ in MeCN

Protonation of $(TBA)_3[(MeO)TiW_5O_{18}]$ was investigated by gradual addition of $HBF_4{\cdot}OEt_2$ to ^{17}O-enriched $(TBA)_3[(MeO)TiW_5O_{18}]$ while the reaction was monitored by ^{17}O NMR spectroscopy. ^{17}O NMR spectra showed that the addition of up to 1 mole equivalent of H^+ resulted in downfield shifts for W=O peaks from δ 721 to δ 733 ppm, the bridging Ti-O-W peaks moved from δ 526 to δ 534 ppm and the two bridging W-O-W peaks shifted from δ 390 and 380 to δ 395 and 386 ppm.

These downfield shifts for all the peaks are consistent with an overall decrease in the anion charge. Most importantly, there is no apparent shift of any of the peaks to higher field, suggesting that the ultimate site of protonation is the (non-enriched) Ti-OMe.

Interestingly when DFT analysis were conducted on the same system the results indicated that protonation occurred at the bridging Ti-O-W sites considered the most basic oxygens, but these NMR results suggest that subsequent migration of protons to Ti-OMe is facile and rapid.

Upon addition of about 1.5 mole equivalent of $HBF_4.Et_2O$, the Ti-OW sites appear to be protonated to give more complex species derived from $[TiW_5O_{18}H_x]^{(2-x)-}$ units indicating the formation of $[(MeOH)TiW_5O_{18}]^{2-}$ or $[TiW_5O_{18}]^{2-}$ intermediate species in solution.

The chemical shift for TiOW moved from δ 526 to δ 462 ppm and a downfield shift for terminal W=O peaks at δ 753 ppm. The changes in the ^{17}O NMR spectrum reflect initial protonation at Ti-OMe indicating the formation of $(TBA)_2[(MeOH)TiW_5O_{18}]$ intermediate species in solution. This does not rule out initial protonation at TiOW or even WOW with subsequent proton migration as shown in Scheme 4.3.

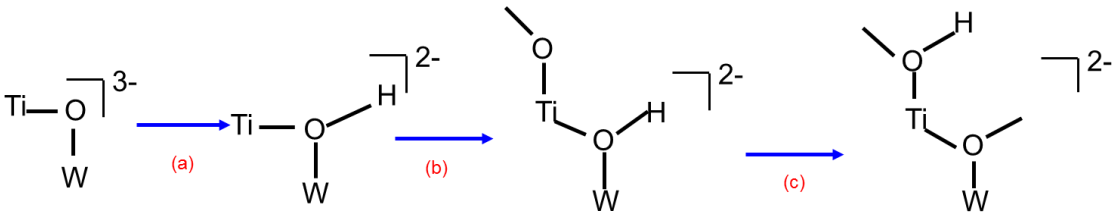

Scheme 4.3: *Possible proton migration in solution.*

These chemical shift changes are consistent with protonated oxygen in ^{17}O NMR spectrum and indicate the weakening of metal-oxygen bonds causing the ^{17}O NMR

resonance to shift upfield.[18] Note that for > 2 mole equivalents of acid added, a peak was observed for bridging W-O-W marked with asterisk this might be due to an intermediate species with a bridging W-O-W peak at δ 448 ppm and also a peak at δ –5 ppm this might be due to H_2O or the central peak of anion with lower charge as showed in the in the ^{17}O NMR spectrum (Figure 4.1).

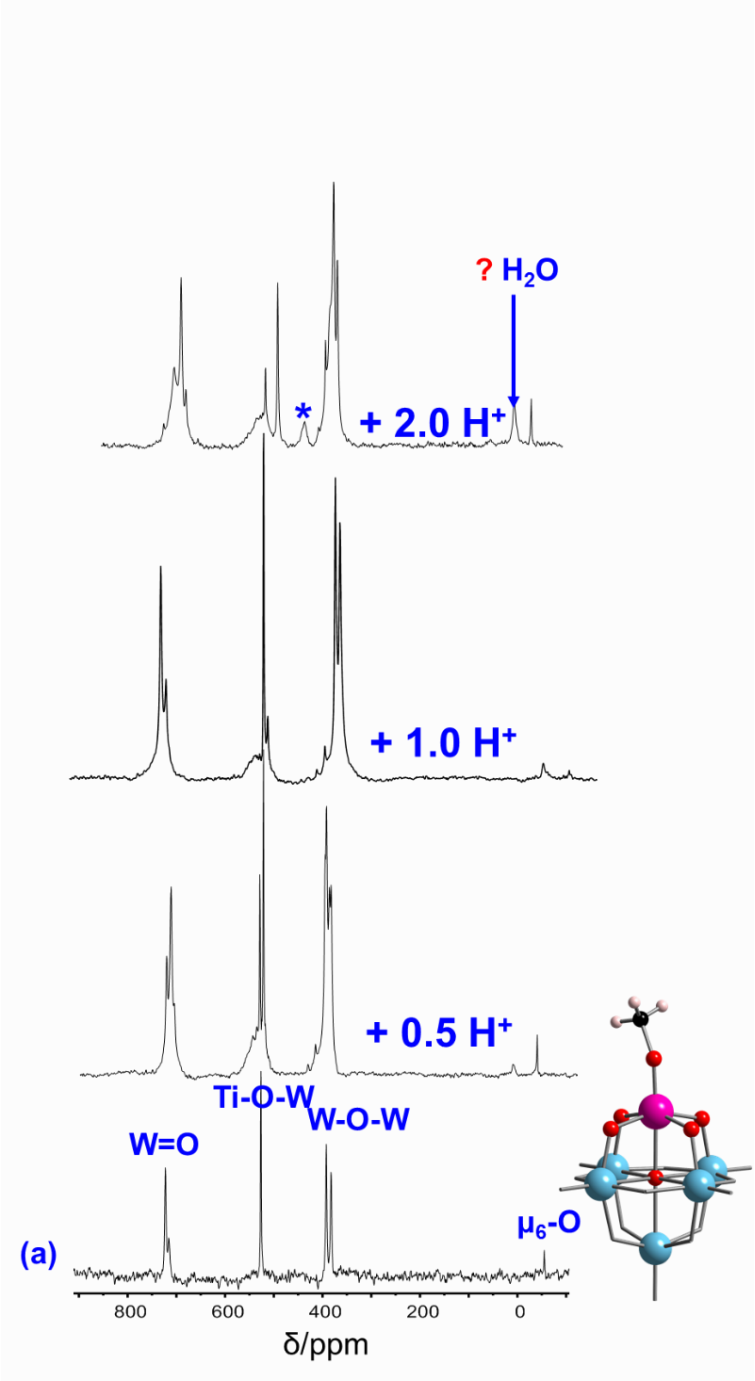

Figure 4.1: *^{17}O NMR spectra of the protonation of $(TBA)_3[(MeO)TiW_5O_{18}]$ (a) without $HBF_4.Et_2O$; POM = 0.05 mmols, $HBF_4.Et_2O$ = 0.45 M, solvent MeCN.*

4.2.2 Protonation of $(TBA)_3[(HO)SnW_5O_{18}]$ with $HBF_4.Et_2O$ in MeCN

Similar protonation reactions were conducted on the hydroxide tin $(TBA)_3[(HO)SnW_5O_{18}]$ anion. In the protonation of $(TBA)_3[(HO)SnW_5O_{18}]$ with $HBF_4{\cdot}OEt_2$ to the same sequential addition of the $HBF_4{\cdot}OEt_2$ to was adopted i.e. aliquot addition of $HBF_4{\cdot}OEt_2$ to to the solution of $(TBA)_3[(HO)SnW_5O_{18}]$ in a 5 mm screwed top NMR tube and monitor the reaction with ^{17}O NMR spectroscopy. As the protons gradually added it is expected that protonation can occur in either of the two reaction pathways shown in Scheme 4. 4.

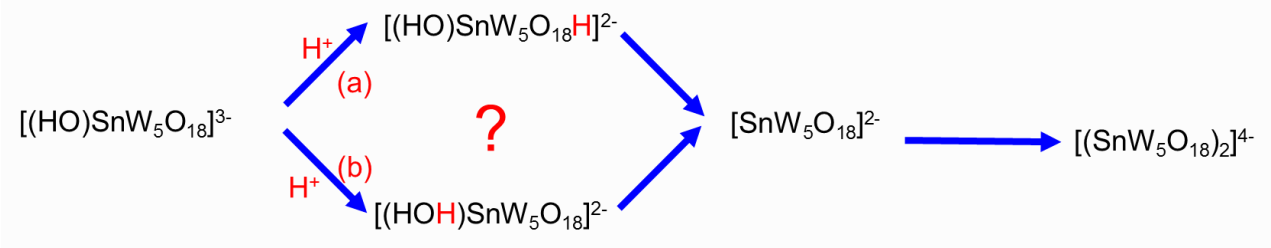

Scheme 4.4: *Possible mechanisms for the reaction between $[(HO)SnW_5O_{18}]^{3-}$ and $HBF_4.Et_2O$*

The ^{17}O NMR spectrum (Figure 4.2) after addition of 1 mole equivalent of $HBF_4{\cdot}OEt_2$ to $(TBA)_3[(HO)SnW_5O_{18}]$ showed no significant upfield shift of the SnOW peak, indicating that the reaction proceeded *via* protonation at SnOH rather than SnOW. There are several peaks in the ^{17}O NMR spectrum suggesting a mixture of different species as indicated by the μ_6-O peaks.

^{119}Sn NMR spectroscopy provided extra insight into possible products and suggested the formation of a Sn–F bond which might be as a result of degradation of BF_4^- shown in Figure 4.2. It is important to know that, after removal of the hydroxido ligand, surprisingly, the Sn(IV) centre is sufficiently Lewis acidic to abstract fluoride from BF_4^- which emphases that protonation can enhance reactivity at the heterometal site.

The ^{119}Sn NMR spectrum showed $^1J(^{119}Sn^{19}F)$ = 2613 Hz which is close to $^1J(^{119}Sn^{19}F)$ = 2797 Hz observed for mixed-valence adducts $Sn^{II}Sn^{IV}F_2(OR)_4$ (R = *tert*-butyl, *tert*-amyl)[19] and $^2J(^{119}Sn^{183}W)$ = 56 Hz. The formation of this Sn-F bond prompted the design of a rational synthesis route to $(TBA)_3[FSnW_5O_{18}]$ by reacting $(TBA)_3[(MeO)SnW_5O_{18}]$ and NH_4F, whereby $(TBA)_3[FSnW_5O_{18}]$ species was prepared and characterised by ^{119}Sn NMR spectroscopy. The ^{119}Sn NMR spectrum of $(TBA)_3[FSnW_5O_{18}]$ has a coupling of $^1J(^{119}Sn^{19}F)$ = 2616 Hz and $^2J(^{119}Sn^{183}W)$ = 55 Hz which is consistent with the results of the protonation reactions.

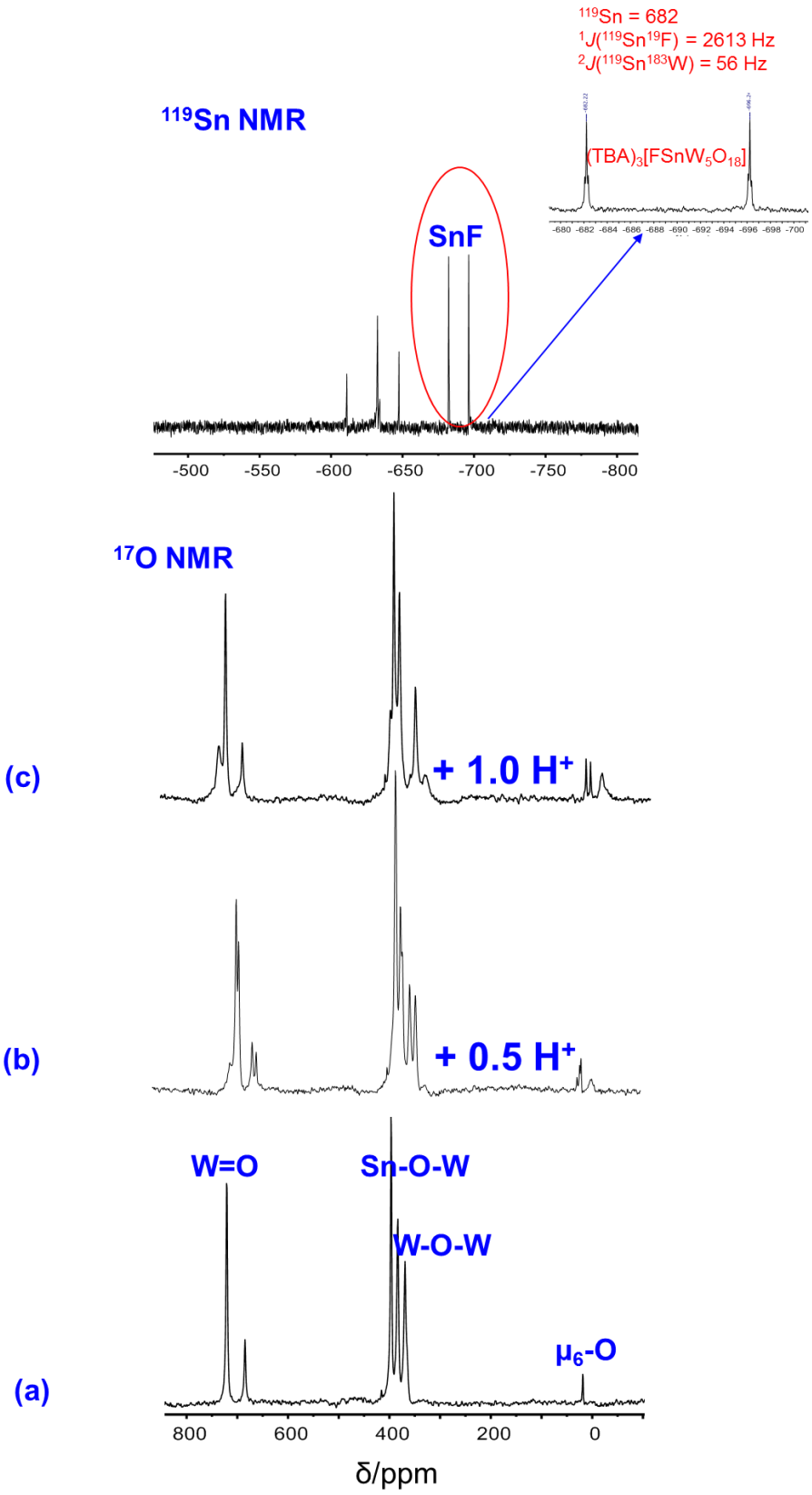

Figure 4.2: *^{17}O NMR spectra of protonation of $(TBA)_3[(HO)SnW_5O_{18}]$ with $HBF_4.Et_2O$ (a) without $HBF_4.Et_2O$; (b) with the addition of 25 µL of acid; (c) with the addition of 50 µL of acid; (d) with the addition of 100 µL of acid and. Conditions; POM = 0.048 mmols, $HBF_4.Et_2O$ = 0.45 M, solvent MeCN*

4.2.3 Protonation of $(TBA)_6[(\mu\text{-}O)(TiW_5O_{18})_2]$ with $HBF_4.Et_2O$

Protonation of $(TBA)_6[(\mu\text{-}O)(TiW_5O_{18})_2]$ was an important part of the project because of the interest in understanding the Lewis basicity of this anion. As mentioned above when protonation studies on the Keggin type POM the report suggested that the bridging TiOTi is the most basic site. The reaction between $(TBA)_6[(\mu\text{-}O)(TiW_5O_{18})_2]$ and $HBF_4.Et_2O$ shown in Equation 4.1 was monitored by ^{17}O NMR spectroscopy.

$$(TBA)_6[(\mu\text{-}O)(TiW_5O_{18})_2] + 2HBF_4.Et_2O \rightarrow (TBA)_4[(\mu\text{-}O)(TiW_5O_{18}H)_2] + 2TBABF_4 \quad 4.1$$

The ^{17}O NMR spectrum showed that addition of up to 1 equivalent of H^+ had no effect on the peaks as they were all virtually in the same position. This might suggest a possible hydrogen bond at the outer Ti-O-W site between two TiW_5O_{18} fragments having less significant change in the chemical shifts within the cage. Addition of 2 mole equivalents of $HBF_4.Et_2O$ to the POM resulted in significant changes in chemical shifts in all the peaks.

The ^{17}O NMR spectrum contained peaks for terminal W=O oxygens at δ 723, 735 and 744 ppm. These peaks are broad compared to the terminal W=O peaks observed in the mono-substituted $[(MeO)TiW_5O_{18}]^{3-}$ anion. The overall downfield shifts suggest a decrease in overall anion charge. The peak at δ 723 ppm might be a presence of small amount of unreacted $(TBA)_6[(\mu\text{-}O)(TiW_5O_{18})_2]$ although the central peak is not sufficiently enriched to be observed. The bridging TiOW peak was shifted upfield from δ 535 to δ 488 ppm due to protonation at the Ti-O-W oxygen that resulted in the weakening of the metal-oxygen bond.[18]

The unique central μ_6-O peak is shifted downfield to δ –47 ppm compared to the central peak for $(TBA)_6[(\mu\text{-}O)(TiW_5O_{18})_2]$ observed at δ –61 ppm. This suggests that the dominant species in solution is the protonated $(TBA)_4[(\mu\text{-}O)(TiW_5O_{18}H)_2]$ and this was confirmed by X-ray crystal structure analysis.

These changes in chemical shifts especially the new peak at δ 488 ppm, indicated protonation at TiOW, which is therefore considered to be the most basic site in the anion as shown in the labelled ^{17}O NMR spectrum in Figure 4.3.

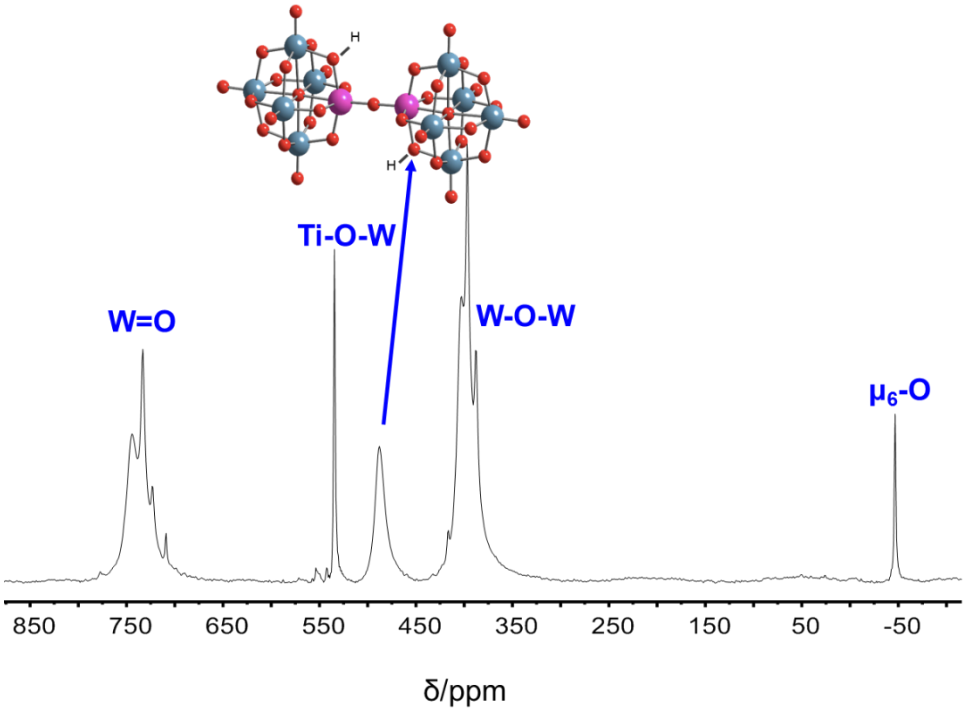

Figure 4.3: *^{17}O NMR spectrum of addition of 2 mole equivalent of $HBF_4.Et_2O$ to $(TBA)_6[(\mu\text{-}O)(TiW_5O_{18})_2]$ conditions; POM = 0.025 mmols, $HBF_4.Et_2O$ = 0.45 M, solvent MeCN*

(a) ^{183}W NMR spectroscopy

The ^{183}W NMR spectrum (Figure 4.4) of $(TBA)_4[(\mu\text{-}O)(TiW_5O_{18}H)_2]$ contained a relatively small peak at δ 64 ppm and 3 major peaks at δ 30, 18 and 5 ppm with peak integrations 1:3:1.6:1 respectively. Although four peaks are observed the peak intensities given do not add up to 5 although if re-ratio can obtain 0.8 : 2.3 : 1.2 : 0.8 which is closer to 1 : 2 : 1 : 1 consistent with previous ^{183}W NMR spectrum in hexatungstate Lindqvist-type POMs and the impurity peak in the spectrum is $[W_6O_{19}]^{2-}$.

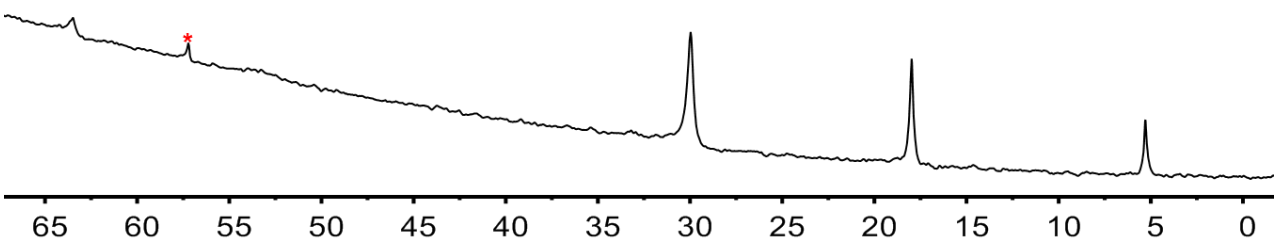

Figure 4.4: *^{183}W NMR spectrum of $(TBA)_6[(\mu\text{-}O)(TiW_5O_{18}H)_2]$ in MeCN*

(b) FTIR spectroscopy

The FTIR spectrum of the protonated oxo-bridged dimer $(TBA)_4[(\mu\text{-}O)(TiW_5O_{18}H)_2]$ shown in Figure 4.5, contains a band assigned to ν(WO) for terminal W=O at 963 cm^{-1}. This band is shifted to higher wavenumber compared to the corresponding band for $(TBA)_6[(\mu\text{-}O)(TiW_5O_{18})_2]$ at 946 cm^{-1}, due to lower charge on the anion.[20] The bands observed at 883 and 783 cm^{-1} are due to ν(WO) associated with the WOW bridges. The peak at 576 cm^{-1} is assigned to ν(TiO) of the TiOTi vibration. This band is slightly shifted lower compare to the oxo-bridged $(TBA)_4[(\mu\text{-}O)(TiW_5O_{18})_2]$ at 616 cm^{-1}

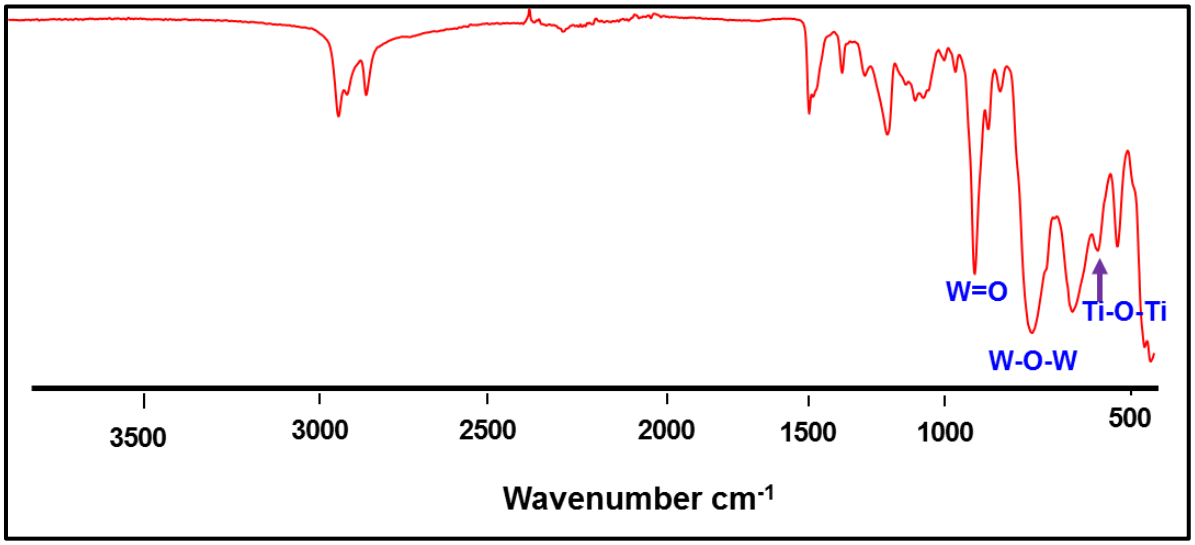

Figure 4.5: *FTIR spectrum of $(TBA)_4[(\mu\text{-}O)(TiW_5O_{18}H)_2]$.*

(c) X-Ray Analysis

The X-Ray crystal structure (Figure 4.6) and the structural analyses (**Appendixes: Table S2**) confirmed the protonation of the oxo-bridged dimer $(TBA)_4[(\mu\text{-}O)(TiW_5O_{18}H)_2]$ and the presence of TiOTi (bond angle of 180.00°) bridge between two TiW_5O_{18} fragments in the structure. The Ti-O-W bond lengths are slightly longer than average distance (1.950(4) Å) indication of protonation of TiOW sites.[21]

It is worth to note that the H atoms were not detected directly but their positions were inferred from Ti–OW bond lengths.

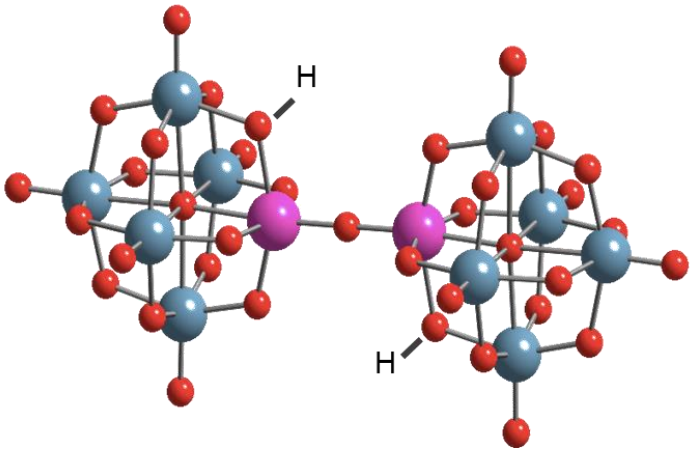

Figure 4.6: X-ray crystal structure of $(TBA)_4[(\mu\text{-}O)(TiW_5O_{18}H)_2$ Red = oxygen, pale blue = tungsten, purple = titanium.

4.2.4 Protonation of $(TBA)_6[(\mu\text{-}O)(TiW_5O_{18})_2]$ with $HBF_4.Et_2O$ in the presence of dmso

The protonation of $(TBA)_6[(\mu\text{-}O)(TiW_5O_{18})_2]$ and prolonged recrystallisation in the presence of adventitious dmso resulted in isolation of the protonated dmso adduct $(TBA)_4[(\mu\text{-}O)(TiW_5O_{18}H)_2(dmso)]$. As expected, the ^{17}O NMR spectrum is similar to the protonated dimer due to the same overall charge on the anion. The ^{17}O NMR peaks are consistent with the Lindqvist TiW_5O_{18} core after protonation and a peak at δ 488 ppm in the ^{17}O NMR spectrum (Figure 4.7) was assigned to Ti-O(H)W. The μ_6-O peak was observed at δ –47 ppm similar to the oxo-bridged species. In addition to the line broadening, more peaks were observed at the terminal W=O position due to lower symmetry of the protonated anion.

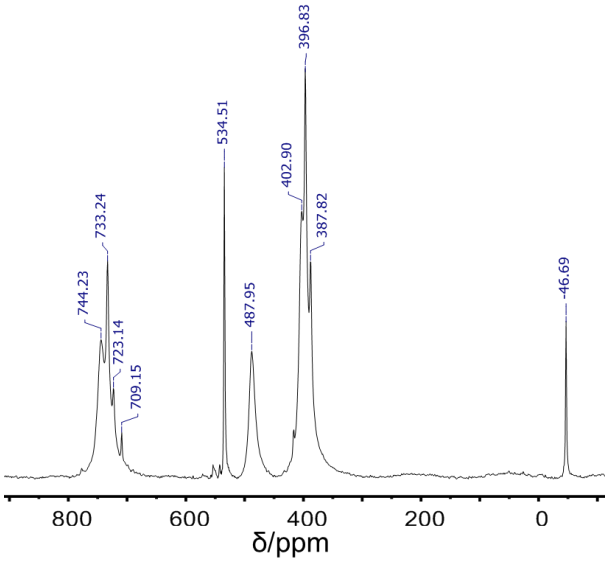

Figure 4.7: *^{17}O NMR spectrum of $(TBA)_4[(\mu\text{-}O)(TiW_5O_{18}H)_2(dmso)]$ by addition of 2 mole equivalent of $HBF_4.Et_2O$ to $(TBA)_6[(\mu\text{-}O)(TiW_5O_{18})_2]$ conditions; POM = 0.025 mmols, $HBF_4.Et_2O$ = 0.45 M, solvent MeCN*

(a) ATR FT-IR spectroscopy

The FTIR spectrum of $(TBA)_4[(\mu\text{-}O)(TiW_5O_{18}H)_2(dmso)]$ (Figure 4.8) contained a band at 961 cm^{-1} assigned to ν(WO) for terminal W=O. This band is slightly lower than the non-solvated protonated species (963 cm^{-1}) although shifted more to higher wavenumber compared to the corresponding band for $(TBA)_6[(\mu\text{-}O)(TiW_5O_{18})_2]$ at 946 cm^{-1}, due to the lower charge on the anion.[20] The bands observed at 883 and 783 cm^{-1} are assigned to ν(WO) associated with the WOW bridges. By comparing the spectrum in Figure 4.6 and with literature,[22, 23] the band observed at 1059 cm^{-1} can be assigned to ν(SO) of the dmso ligand which is consistent with the band for dmso-d_6 stretching frequency.

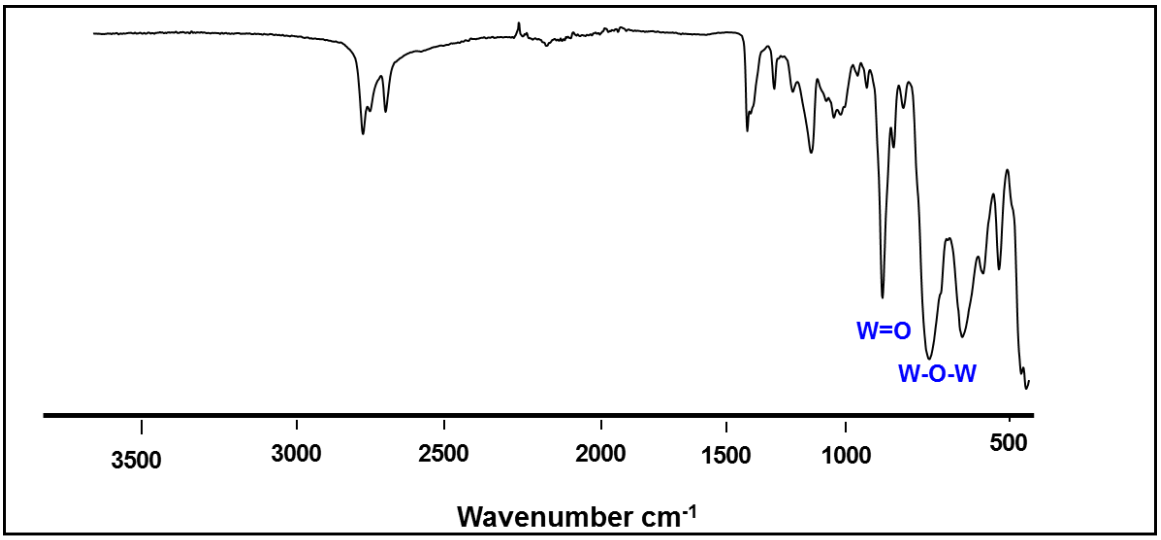

Figure 4.8: *FT-IR spectrum of $(TBA)_4[(\mu\text{-}O)(TiW_5O_{18}H)_2(dmso)]$*

(b) X-ray crystal structure analysis

The X-ray crystal structure analysis (**Supplementry Data Table S3**), confirmed the formation of the protonated dmso adduct $(TBA)_4[(\mu\text{-}O)(TiW_5O_{18}H)_2(dmso)]$. The crystal structure (Figure 4.9) differs from that of $(TBA)_6[(\mu\text{-}O)(TiW_5O_{18}H)_2]$ in that the TiOTi bond angle is significantly smaller $(162.8(3))^o$ for $(TBA)_4[(\mu\text{-}O)(TiW_5O_{18}H)_2(dmso)]$ due to dmso interaction with neighbouring atoms *via* hydrogen bonding. Selected bond lengths are given in **Supplementry Data Table S4**. The Ti-μ_2O bond length of 1.786(4) Å is close to those in titanium-substituted Keggin and Dawson-type polyoxometalates,[15,24-26] and also similar to those reported in the titanatrane complex LTiOTiL (L = trianion of tris (2-hydroxy-3,5-di-tert-butylbenzyl)amine.[27] Ti-O bond lengths are on average 1.982(4) Å whilst W-O bond lengths are on average 1.851(4) Å. Selected bond angles (**Supplementry Data Table S5**), at W are typical to those in

related polytungstates,[28] WOW angles lie in the range 116.9 to 178.5°, larger than the TiOW angles which lie between 117.0(2) – 116.3(2)° due to the influence of dmso.

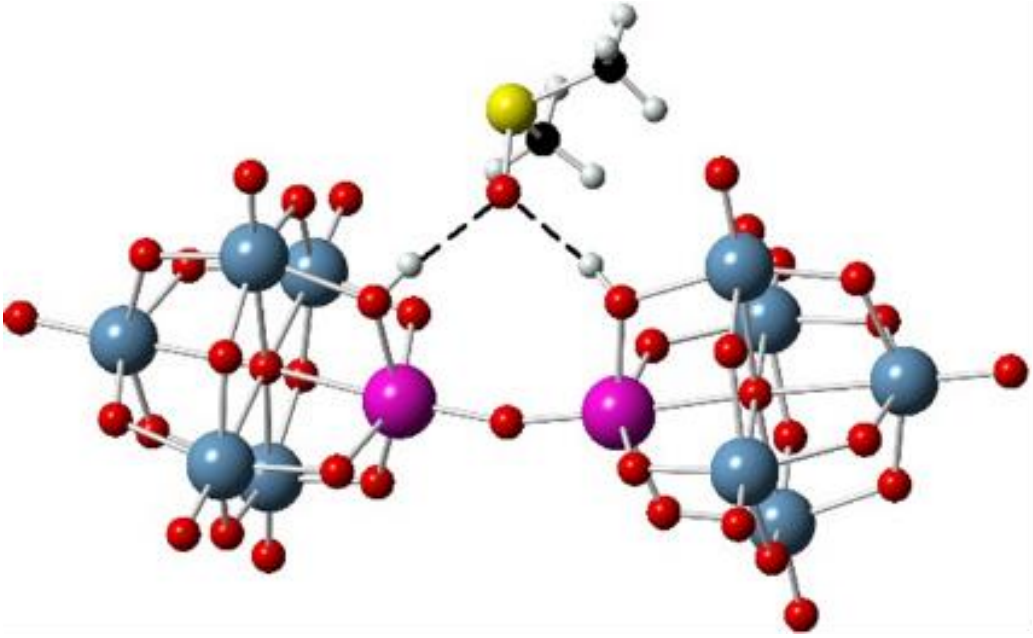

Figure 4.9: *X-ray crystal structure of $(TBA)_4[(\mu\text{-}O)(TiW_5O_{18}H)_2)(dmso)]$ Red = oxygen, pale blue = tungsten, purple = titanium, black = carbon, grey = hydrogen and yellow = sulphur*

4.3 Electrophilic Addition to $(TBA)_6[(\mu\text{-}O)(TiW_5O_{18})_2]$ in MeCN

Our interest in adding electrophile onto the bridging TiOW site is essentially similar to the protonation studies. As we have established the Lewis basic sites in the oxo-bridged $(TBA)_6[(\mu\text{-}O)(TiW_5O_{18})_2]$ we expect the electrophile to behave in a similar way like the H^+. The added metal centre in this case can provide additional active site on the POM for important reactivity studies for example a model for catalysts or as chelating or “pincer” ligand.

Organotin groups have been identified as good candidates in the derivatization of POMs because Sn-C bond is relatively stable and the size of Sn(IV) is appropriate to substitute into the addenda metal centers in POM framework. The groups of Knoth,[29, 30] Pope [31, 32] and Liu [33] have investigated the substitution of mono-organotin moieties (RSn^{3+}) into the vacant sites of lacunary Keggin type POMs. In this work we were interested in investigating the addition of Sn(IV) onto the Lewis basic Ti-O-W sites to isolate and characterise Sn(IV) bonded to TiOW in oxo-bridged dimer. The Sn(IV) centre could potentially open up new area of research in POM chemistry.[34,35]

4.3.1 Reaction between $(TBA)_6[(\mu\text{-}O)(TiW_5O_{18})_2]$ and Me_2SnCl_2 in MeCN

The reaction between $(TBA)_6[(\mu\text{-}O)(TiW_5O_{18})_2]$ and Me_2SnCl_2 was conducted by dissolving $(TBA)_6[(\mu\text{-}O)(TiW_5O_{18})_2]$ (100 mg 0.025 mmols) in 0.5 mL dried MeCN and added 5 mg of Me_2SnCl_2 (Eqn.4.2). The resulting solution was allowed to stir for 4 h which resulted to a clear solution.

$$(TBA)_6[(\mu\text{-}O)(TiW_5O_{18})_2] + Me_2SnCl_2 \rightarrow (TBA)_4[(\mu\text{-}O)(TiW_5O_{18})_2(SnMe_2)] + 2TBACl \quad 4.2$$

(a) ^{17}O NMR spectroscopy

The ^{17}O NMR spectrum (Figure 4.10) contained 5 characteristic peaks each assigned to a unique oxygen in the POM framework. The terminal W=O peak was observed at δ 751 ppm. The peak was broad and did not allow for resolution of the axial (W_{ax}=O) and equatorial (W_{eq}=O) terminal oxygens. The bridging TiOW peak was observed at δ 467 ppm. This is remarkably different in comparison with bridging TiOW peak of $(TBA)_6[(\mu\text{-}O)(TiW_5O_{18})_2]$ (535 ppm). The peak for the bridging WOW oxygens were observed at δ 403 and 413 ppm. The central μ_6-O peak was observed at δ –38 ppm and was also shifted further upfield in comparison with $(TBA)_6[(\mu\text{-}O)(TiW_5O_{18})_2]$ at δ –48 ppm. The data for $(TBA)_4[(\mu\text{-}O)(TiW_5O_{18})_2(SnMe_2)]$ further demonstrate that the bridging TiOW are the most basic sites in $(TBA)_6[(\mu\text{-}O)(TiW_5O_{18})_2]$.

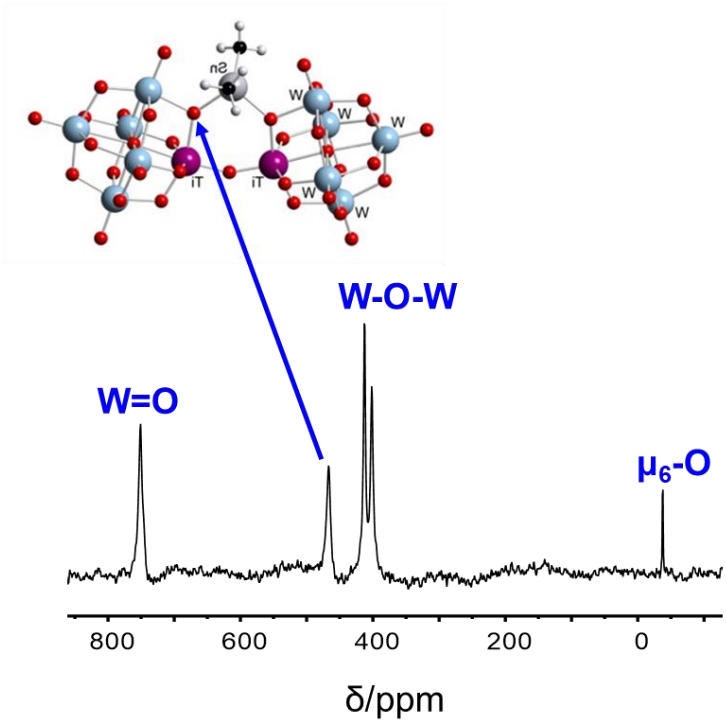

Figure 4.10: *^{17}O NMR spectrum of $(TBA)_6[(\mu\text{-}O)(TiW_5O_{18})_2(SnMe_2)]$. conditions; POM = 0.025 mmols, Me_2SnCl_2 = 0.025 mmols, solvent MeCN*

(b) ATR FT-IR Spectroscopy

In the FTIR spectrum shown in Figure 4.11, the bands below 1000 cm^{-1} are attributed to the metal-oxo polyanion bonds. In comparison with the IR spectra of $(TBA)_4[(\mu\text{-}O)(TiW_5O_{18}H)_2(dmso)]$ and $(TBA)_6[(\mu\text{-}O)(TiW_5O_{18})_2]$, there are some similarities in the overall shape of the spectra although there are some differences in several band positions and intensities. This suggest that the Lindqvist core structure was not altered by the addition of electrophiles to $(TBA)_6[(\mu\text{-}O)(TiW_5O_{18})_2]$. The peak observed at 961 cm^{-1} was assigned to terminal W=O stretching vibrations and is close to the terminal W=O stretching frequencies of $(TBA)_4[(\mu\text{-}O)(TiW_5O_{18}H)_2(dmso)]$ and $(TBA)_6[(\mu\text{-}O)(TiW_5O_{18}H)_2]$ (963 cm^{-1}) but shifted to higher wavenumber compared to the oxobridged dimer, $(TBA)_6[(\mu\text{-}O)(TiW_5O_{18})_2$. The peak at 775 cm^{-1} was assigned to the bridging W-O-W stretching vibrations. The peak observed at 665 cm^{-1} was associated to ν(TiO) vibration which is similar to the peaks observed in $(TBA)_4[(\mu\text{-}O)(TiW_5O_{18}H)_2(dmso)]$ and $(TBA)_6[(\mu\text{-}O)(TiW_5O_{18})_2]$ (667 cm^{-1}). It is worth mentioning that the lower number of peaks than expected from the structure may be the result of a dynamic (i.e. non-static) structure in solution.

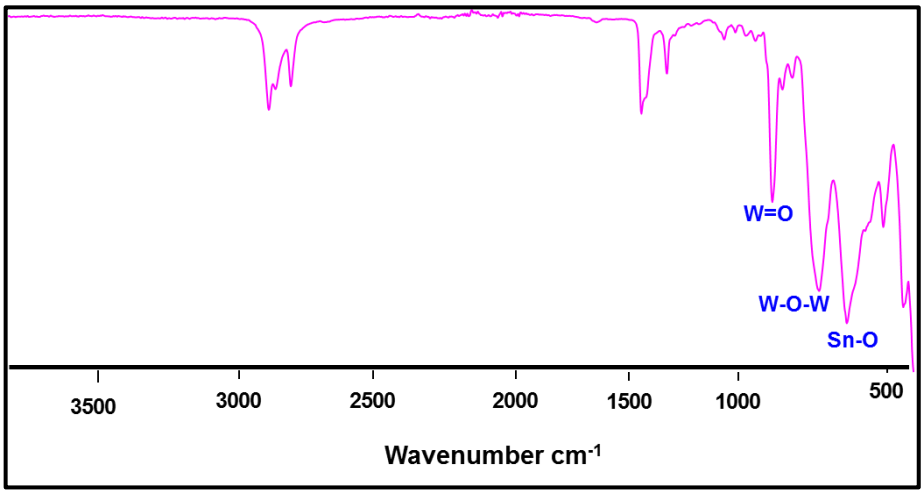

Figure 4.11: *FT-IR spectrum of $(TBA)_4[(\mu\text{-}O)(TiW_5O_{18})_2(SnMe_2)]$.*

(c) X-ray crystallography

Single crystals were obtained by vapour diffusion of Et_2O into MeCN solution and the X-ray crystal structure analysis (**Suplementry Data Table S6**) was determined. The structure obtained confirmed the Lindqvist type $(TBA)_4[(\mu\text{-}O)(TiW_5O_{18})_2(SnMe_2)]$ (Figure 4.12). Selected bond lengths are given in (**Suplementry Data Table S7)**, while selected bond angles are given in (**Suplementry Data Table S8)**, the Ti-O bond length

1.800(15) Å is close to those in titanium-substituted POMs, the TiOTi bond angle is smaller (Ti2OTi1 152.4º (9)) than that for TiOTi in $(TBA)_4[(\mu\text{-}O)(TiW_5O_{18}H)_2(dmso)]$, 162.8(3) and for $(TBA)_6[(\mu\text{-}O)(TiW_5O_{18}H)_2]$, 180.00º (11) emphasising the electronic effect of Me_2Sn. This was expected as we and others have shown that substitution of a metal atom or ligands into POM framework can have profound electronic effect on the POM.[35,36] Ti-O bond lengths of 2.033(15) Å is longer than the average W-O bond (1.814(16)) Å. Bond length for SnO is 2.025(14) Å which is similar to those observed in SnW_5 Linqvist POM. SnC bond is from 2.10(3) to 2.14(3) Å similar to those reported.[31] Angles at W are typical in related polytungstates[15] while WOW angles are significantly larger, 116.5(8) to 118.4(9)º than the TiOW angles which lie between 87.4(5) and 95.4(4)º indicating the profound electronic effect of the SnO bond on the anion.

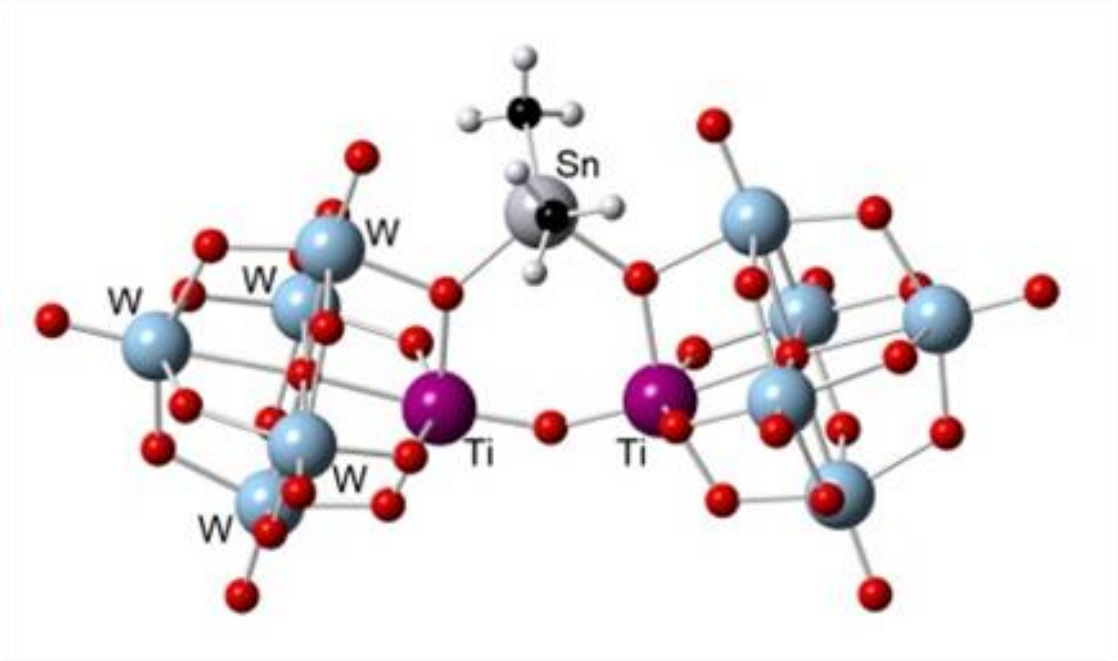

Figure 4.12: *X-ray crystal structure of $(TBA)_4[(\mu\text{-}O)(TiW_5O_{18}H)_2)(SnMe_2)]$ Red = oxygen, pale blue = tungsten, purple = titanium, black = carbon and grey = hydrogen*

(d) ^{119}Sn NMR spectroscopy

The ^{119}Sn NMR spectrum (Figure 4.13) for $(TBA)_4[(\mu\text{-}O)(TiW_5O_{18})_2(SnMe_2)]$ showed a single broad peak at δ –22.16 ppm which is shifted significantly downfield compare to other R_2SnX_2 compounds. For example, the mono-substituted SnW_5 has a peak at δ –648 ppm while the oxo-bridge POMs, $(TBA)_6[(\mu\text{-}O)(SnW_5O_{18})_2]$ has a peak at δ – 667 ppm. Satellite peaks associate with $^2J(^{119}Sn^{183}W)$ coupling were not determined due to peak broadening. The line broadening might be due to spin-spin coupling in the

^{119}Sn environment or slow tumbling of the anion in solution or migration of the Sn atom to different TiOW oxygen sites in the POM.

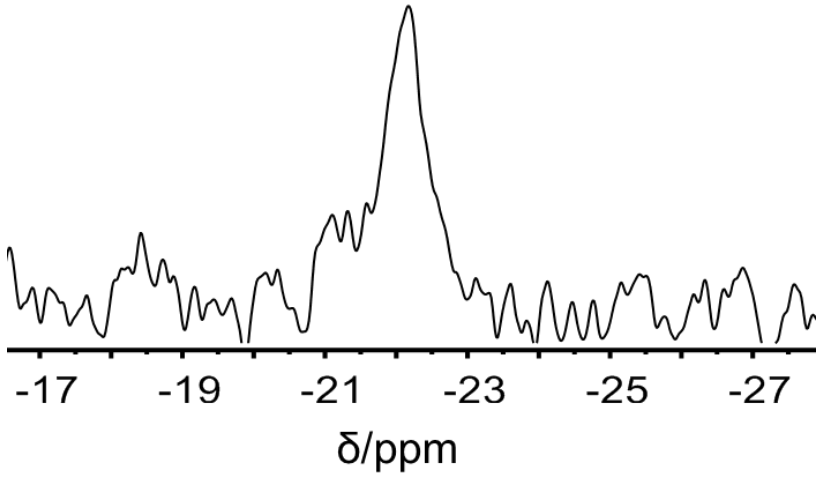

Figure 4.13: *^{119}Sn NMR spectrum of $(TBA)_4[(\mu\text{-}O)(TiW_5O_{18}H)_2(SnMe_2)]$*

Table 4.1: *^{17}O NMR chemical shifts for $[TiW_5]$ anions (ppm).*

Anion	W=O	TiOTi	TiOW	WOW	μ_6-O
$(TBA)_6[(\mu\text{-}O)(TiW_5O_{18})_2]$	723	680	536	391,384	-61
$(TBA)_4[(\mu\text{-}O)(TiW_5O_{18}H)_2]$	743	680	532,487	400,396	-48
$(TBA)_4[(\mu\text{-}O)(TiW_5O_{18}H)_2(dmso)]$	742	-	535	403,396	-43
$(TBA)_4[(\mu\text{-}O)(TiW_5O_{18})_2(SnMe_2)]$	751		467	412,401	-38

Table 4.2: *ATR FT-IR stretching frequencies of TiW_5 anions (cm^{-1}).*

Anion	W=O	WOW	TiO
$(TBA)_6[(\mu\text{-}O)(TiW_5O_{18})_2]$	944	881,793	674,618,574,518
$(TBA)_4[(\mu\text{-}O)(TiW_5O_{18}H)_2]$	963	920,883,783	656,576,515
$(TBA)_4[(\mu\text{-}O)(TiW_5O_{18}H)_2(dmso)]$	963	914,882,781	656,576,515
$(TBA)_4[(\mu\text{-}O)(TiW_5O_{18})_2(SnMe_2)]$	950	914,882,781	665,576,515

4.3.2 Reactions between $(TBA)_6[(\mu\text{-}O)(TiW_5O_{18})_2]$ and $SnCl_4$ or $SnCl_2$

Tin-substituted POMs and oxides have also been implicated as good candidates for catalysts and catalyst supports for CO_2 reduction,[37] sensors,[38,39] and p-type semiconductors.[40] Consequently we further explored $SnCl_4$ and $SnCl_2$ as a way of adding these electrophiles to $(TBA)_6[(\mu\text{-}O)(TiW_5O_{18})_2]$. The reaction between $SnCl_4$ (0.25 M, 0.025 mmols) and the POM (0.25 M) (Equation 4.3) while reaction between $(TBA)_6[(\mu\text{-}O)(TiW_5O_{18})_2]$ and $SnCl_2$ was carried out by reacting 0.16 M solution of the POM and 0.3 M solution $SnCl_4$ (Equation 4.4). The ^{17}O NMR spectrum for both reactions suggested the reaction went cleanly to the desired product within 4 h

although there was an extra peak present in the ^{17}O NMR spectrum for $SnCl_2$ reaction due to some amount of unreacted starting material.

$$(TBA)_6[(\mu\text{-}O)(TiW_5O_{18})_2] + SnCl_4 \rightarrow (TBA)_4[(\mu\text{-}O)(TiW_5O_{18})_2(SnCl_2)] + 2TBACl \quad 4.3$$

$$(TBA)_6[(\mu\text{-}O)(TiW_5O_{18})_2] + SnCl_2 \rightarrow (TBA)_4[(\mu\text{-}O)(TiW_5O_{18})_2(Sn)] + 2TBACl \quad 4.4$$

The ^{17}O NMR spectrum of "$(TBA)_4[(\mu\text{-}O)(TiW_5O_{18})_2SnCl_2]$" (Figure 4.14) contained peaks consistence with peaks observed in previous ^{17}O NMR spectra in the reactions discussed above. Terminal W=O peaks were observed at δ 749 ppm due to decrease in overall charge. As expected, the chemical shift of the bridging Sn-O-W peak was shifted downfield (415, 404 ppm) because of the electronic environment of the neighbouring atoms compared to SnOW peak observed in ^{17}O NMR spectrum for Sn-substituted POMs. For example, in the mono-substituted $\{SnW_5\}$ and the dimeric $(TBA)_6[(\mu\text{-}O)(SnW_5O_{18})_2]$ the peaks occur at δ 395 and 398 ppm respectively. The central μ_6-O peak was observed at δ –36 ppm.

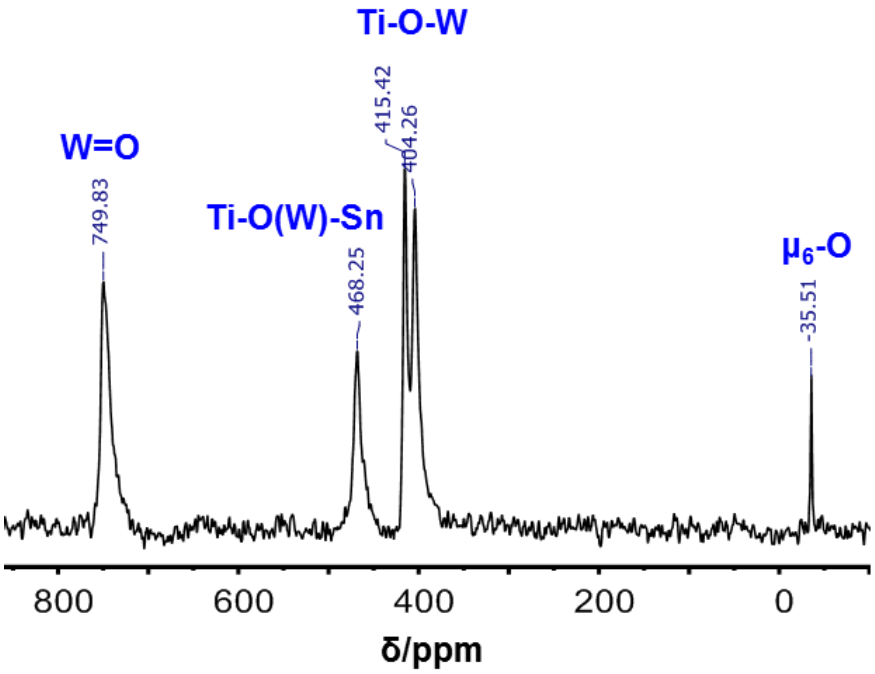

Figure 4.14: *^{17}O NMR spectrum of the reaction between $(TBA)_6[(\mu\text{-}O)(TiW_5O_{18})_2]$ with $SnCl_4$. conditions; POM = 0.025 mmols, $SnCl_4$ = 0.025 mmols, solvent MeCN*

In the ^{17}O NMR spectrum of "$(TBA)_4[(\mu\text{-}O)(TiW_5O_{18})_2Sn]$" (Figure 4.15), the chemical shifts were similar although an additional peak marked with asterisks was observed in the spectrum. This might be due to some unreacted starting material. The characteristic peak observed at δ 468 ppm in both spectra further supported our proposition that Sn(IV) bonded at TiOW bridging Lewis basic site.

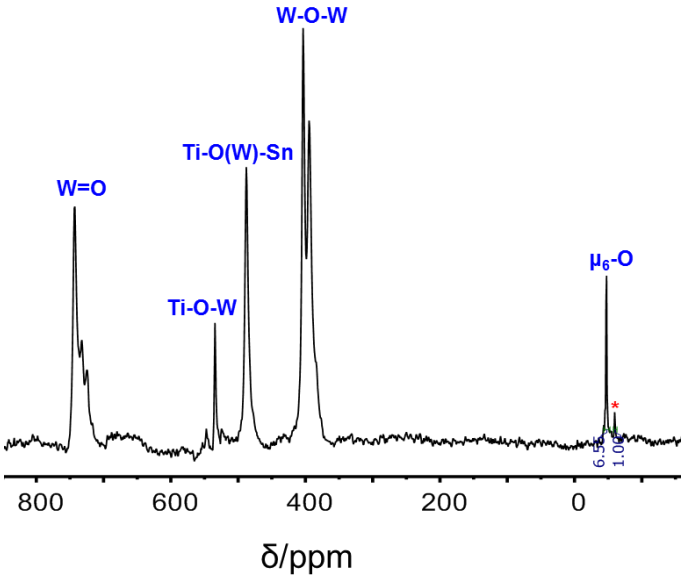

Figure 4.15: *^{17}O NMR spectrum of the reaction between $(TBA)_6[(\mu\text{-}O)(TiW_5O_{18})_2]$ with $SnCl_2$. conditions; POM = 0.025 mmols, $SnCl_2$ = 0.03 M, solvent MeCN.*

4.3.3 Reaction between $(TBA)_6[(\mu\text{-}O)(TiW_5O_{18})_2]$ and $CsAuCl_4$

We extended the electrophilic addition reactions to other metals including Au(III), Ag(I), Pd(II) and Pt(IV). Incorporation of Au(III) metal into the metal oxides framework is interesting because of the array of potential reactivities they show in for example catalysis,[41] photothermal therapy,[42] and imaging.[43] Several recent reviews reported by Nadjo,[44] Mitchell [45] and Weinstock [46] have described that POMs or POM-based materials can act both as reducing agents and as stabilisers for the preparation of metallic nanostructures containing Au(III), Ag(I), Pd(II), and Pt(IV) heterometals.

Our interest in investigating the addition of Au(III) onto the surface of the Lindqvist POM is to explore some reactivity studies at the Au(III) metal centre. We expect the d^8 metal to prefer a square planar geometry because of the low energy of the orbitals of Au(III) ($d_{x^2-y^2}$ and d_{z^2}). When the stability of the complex was investigated by DFT calculations it indicated that the hypothetical structure with one Au-Cl bond in the square planar environment could be stable.

The reaction between $CsAuCl_4$ and $(TBA)_6[(\mu\text{-}O)(TiW_5O_{18})_2]$ was conducted by reacting 100 mg 0.025 mmols of $(TBA)_6[(\mu\text{-}O)(TiW_5O_{18})_2]$ with $CsAuCl_4$ (12 mg, 0.025 mmoles according to (Equation 4.5) and the ^{17}O NMR spectrum of the resulting pale yellow solution was recorded.

$$(TBA)_6[(\mu\text{-}O)(TiW_5O_{18})_2] + CsAuCl_4 \rightarrow (TBA)_4[(\mu\text{-}O)(TiW_5O_{18})_2(AuCl)] + 2TBACl + CsCl \qquad 4.5$$

The ^{17}O NMR spectrum (Figure 4.16) showed a significant shift in all the peaks of $(TBA)_6[(\mu\text{-}O)(TiW_5O_{18})_2]$ anion although there were more peaks than expected. This suggested a mixture of 2 species because of the two central (μ_6-O) peaks at δ –48 and –58 ppm. The terminal W=O peaks observed at δ 742 ppm an indication of decrease in total over all charge. The peak at δ 722 might be related to the starting material possibly due to incomplete solubility of $CsAuCl_4$ in MeCN. As expected, the bridging M-O-W peak was observed at δ 488 which is consistent with an interaction between TiOW and an electrophile. The bridging WOW shifts were observed at δ 402 and 394 ppm.

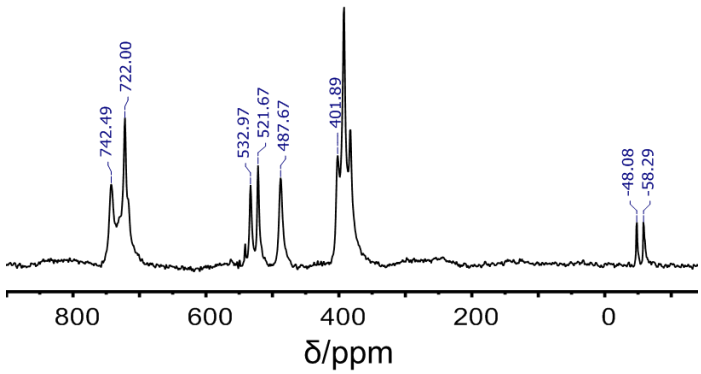

Figure 4.16: *^{17}O NMR spectrum of $(TBA)_6[(\mu\text{-}O)(TiW_5O_{18})_2(AuCl)]$ in reaction with $CsAuCl_4$. conditions; POM = 0.025 mmols, $CsAuCl_4$ = 0.025 mmols, solvent MeCN in MeCN*

4.3.4 Reaction between $(TBA)_6[(\mu\text{-}O)(TiW_5O_{18})_2]$ and $AuCl_3$

When the reaction was repeated with $AuCl_3$ under similar conditions (Equation 4.6), the result was slightly different and gave a more simplified ^{17}O NMR spectrum.

$$(TBA)_6[(\mu\text{-}O)(TiW_5O_{18})_2] + AuCl_3 \rightarrow (TBA)_4[(\mu\text{-}O)(TiW_5O_{18})_2(AuCl)] + 2TBACl \qquad 4.6$$

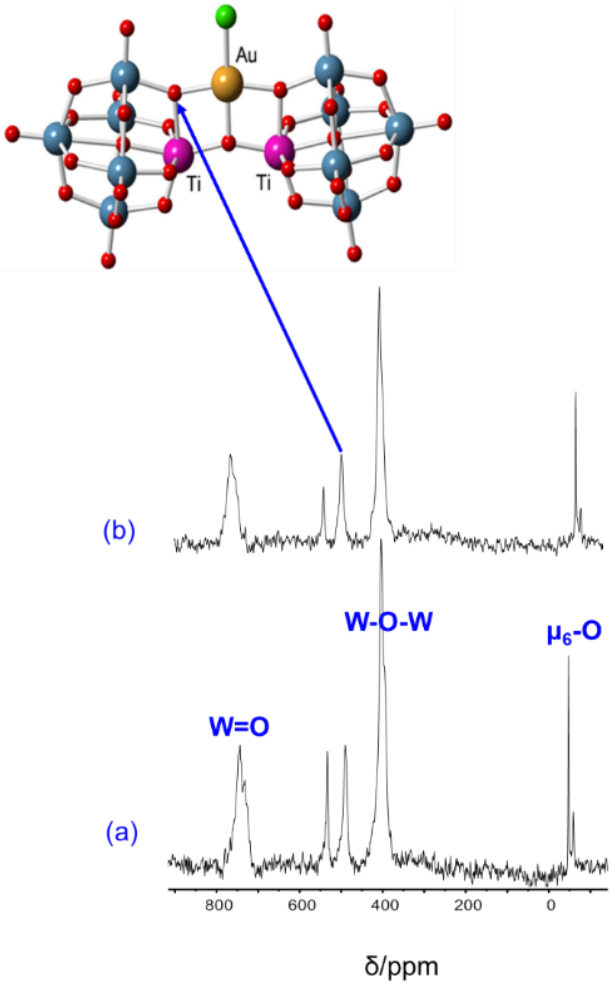

Figure 4.17: *^{17}O NMR spectrum of the reaction between $(TBA)_6[(\mu\text{-}O)(TiW_5O_{18})_2(AuCl)]$ and $AuCl_3$. (a) at room temperature (b) heated at 60 ^{o}C for 4 h. conditions; POM = 0.025 mmols, $AuCl_3$ = 0.075 mmols, solvent MeCN.*

The ^{17}O NMR spectrum of the reaction at room temperature suggest that 73 % of Au(III) has reacted as showed in Figure 4.17a, however, when the reaction was heated at 60^{o}C for 4 h the ^{17}O NMR spectrum (Figure 4.17b) showed that 93 % had reacted. The terminal W=O peak is observed at δ 742 ppm, the bridged Ti-O(W)-Au peak was observed at δ 490 ppm while the peak at δ 403 ppm was assigned to the bridging WOW peak. The centre μ_6-O peak is observed at δ –47 ppm significant difference with the oxo-bridged $[(\mu\text{-}O)(TiW_5O_{18})_2]^{6-}$ which is observed at δ –61 ppm. Comparing the ^{17}O NMR results with the previous reactions suggest that the Au(III) metal was bonded to the TiOW bridging site further supporting our general proposition that TiOW sites are the most basic sites in the Lindqvist POM.

(a) DFT calculation

The hypothetical structure was analysed by DFT calculations[16] [M. Pascual-Borras] to predict the stability of this compound (Figure 4.18) and it shows that the structure can

be stable. Several unsuccessful attempts were made to grow single crystals for X-ray analysis.

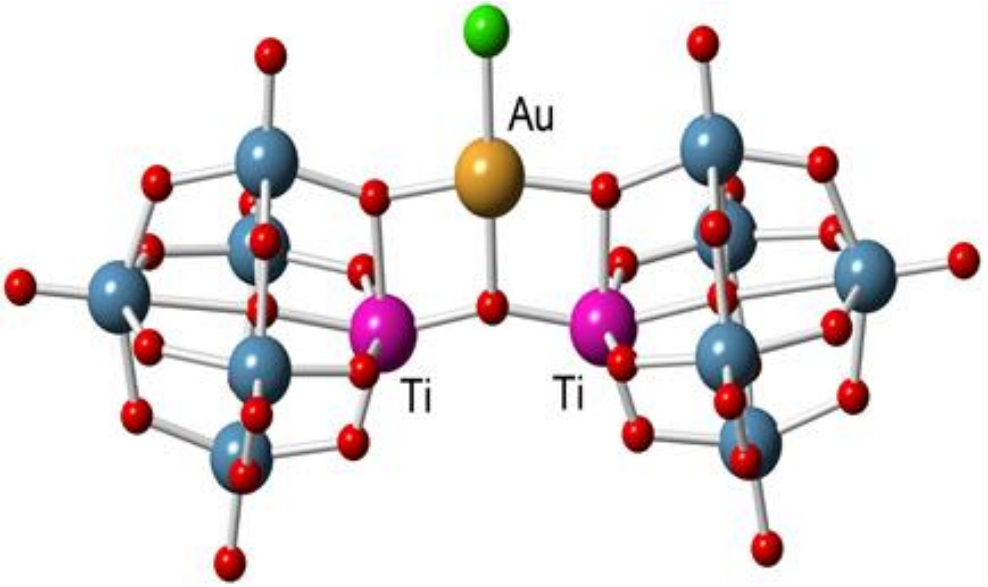

Figure 4.18: *Minimum energy theoretical structure of $(TBA)_4[(\mu\text{-}O)(TiW_5O_{18})_2(AuCl)]$ Red = oxygen, pale blue = tungsten, purple = titanium, yellow = gold and green = chloride.*

4.3.5 Reaction between $(TBA)_6[(\mu\text{-}O)(TiW_5O_{18})_2]$ and $PdCl_2$.

The addition of Pd(II) onto metal oxides was attempted according Equation 4.7 and the reaction was monitored by ^{17}O NMR spectroscopy. Pd(II) substituted POMs are rare although there are few structurally characterized Pd-based POMs most of which are the Keggin type for example $K_{10}Na_3[Pd^{IV}O(OH)WO(OH_2)(PW_9O_{34})_2]$.[47] Pd substituted POM have shown to be significant important in oxidation catalysis.[48] Our interest is to prepare the Lindqvist type Pd(II) POM as models for similar chemistry.

The attempted preparation of the Pd(II) substituted type POMs was conducted by reacting 100 mg 0.25 mmols of $(TBA)_6[(\mu\text{-}O)(TiW_5O_{18})_2]$ with $PdCl_2$ (1.5 mg 0.025 mmoles according to (Equation 4.7) and the ^{17}O NMR spectrum of the resulting dark brown solution was recorded.

$$(TBA)_6[(\mu\text{-}O)(TiW_5O_{18})_2] + PdCl_2 \rightarrow (TBA)_4[(\mu\text{-}O)(TiW_5O_{18})_2(Pd)] + 2TBACl \qquad 4.7$$

The ^{17}O NMR spectrum of "$(TBA)_6[(\mu\text{-}O)(TiW_5O_{18})_2Pd]$" (Figure 4.19) contain peaks which are characteristic of core TiW_5 species consisting of terminal W=O peaks observed at δ 744 and 737 ppm. The peaks are broad and therefore not well resolved. The bridged Ti-O(W)-Pd peak is observed at δ 488 ppm this is shifted slightly upfield suggested that Pd(II) therefore appeared to react with the oxo-bridged $(TBA)_6[(\mu\text{-}$

O)(TiW_5O_{18})$_2$. The WOW peaks are observed at δ 404, 400, 395 ppm while the the unique centre μ_6-O peak is observed at δ -47 ppm.

The changes in these chemical shifts suggested that reaction with Pd(II) therefore appeared to reacted with the oxo-bridged dimer given the ^{17}O NMR spectrum similar to the shifts observed for the protonated and the Me_2Sn^{2+} reactions.

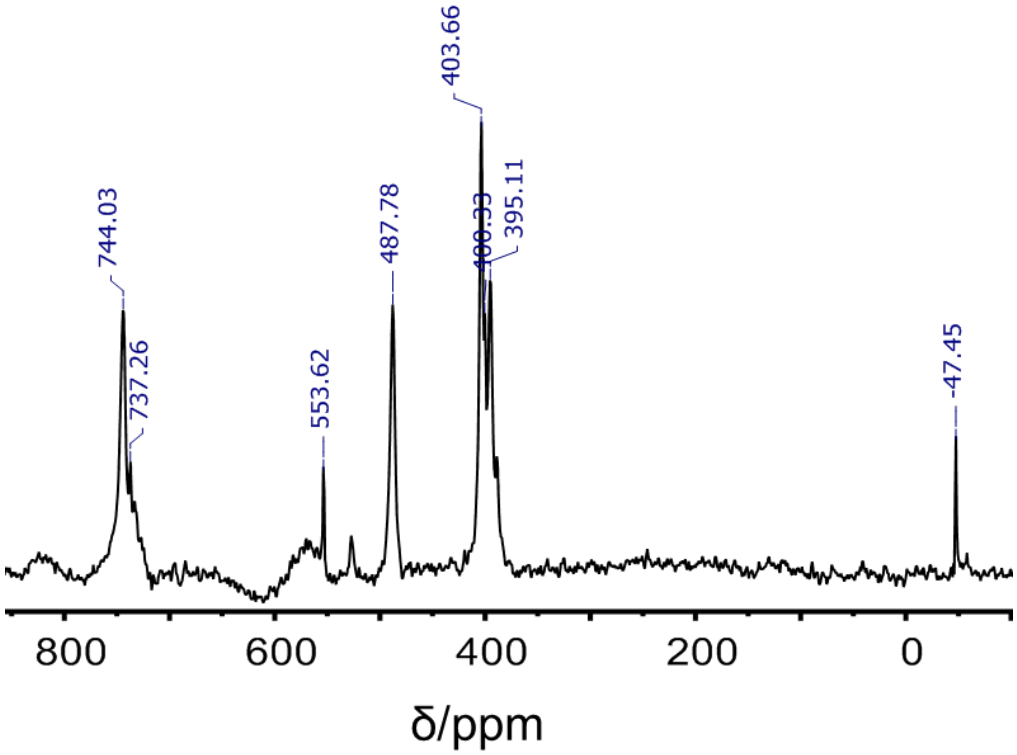

Figure 4.19: *^{17}O NMR spectrum of (TBA)$_4$[(μ-O)(TiW_5O_{18})$_2$(Pd)] in reaction with $PdCl_2$. Conditions; POM = 0.025 mmols, $PdCl_2$ = 0.085 mmols, solvent MeCN.*

in MeCN

4.3.6 Reaction between (TBA)$_6$[(μ-O)(TiW_5O_{18})$_2$] and $AgBF_4$

The reaction between $AgBF_4$ was attempted because we wanted to see if Ag^+ would behave in a similar way as H^+. A reaction of 1:1 mixture of $AgBF_4$ and (TBA)$_6$[(μ-O)(TiW_5O_{18})$_2$] was attempted according to Equation 4.8 and the reaction was monitored by ^{17}O NMR spectroscopy.

(TBA)$_6$[(μ-O)(TiW_5O_{18})$_2$] + $AgBF_4$ → (TBA)$_5$[(μ-O)(TiW_5O_{18})$_2$(Ag)] + $TBABF_4$ 4.8

The ^{17}O NMR spectrum of "[(μ-O)(TiW_5O_{18})$_2$Ag]$^{5-}$" after removal of $TBABF_4$ (Figure 4.20) consisted of peaks at δ 732 and 724 ppm assigned to the terminal W=O oxygens. The peak at δ 513 ppm was assigned to the bridging Ti-O(W)-Ag which is different

from TiOW bridging peak for $(TBA)_6[(\mu\text{-}O)(TiW_5O_{18})_2]$ (at δ 535 ppm) suggesting that Ag(I) bonded to the bridging TiOW site. Again, this is consistent to the previous results discussed above. The central μ_6-O peak was observed at δ –55 ppm.

Although the results obtained from ^{17}O NMR spectroscopy gave an indication that there is indeed a binding of the metal atom at the bridging sites, growing single crystals for X-ray analysis has been a major challenge for the determination of bond lengths and bond angles.

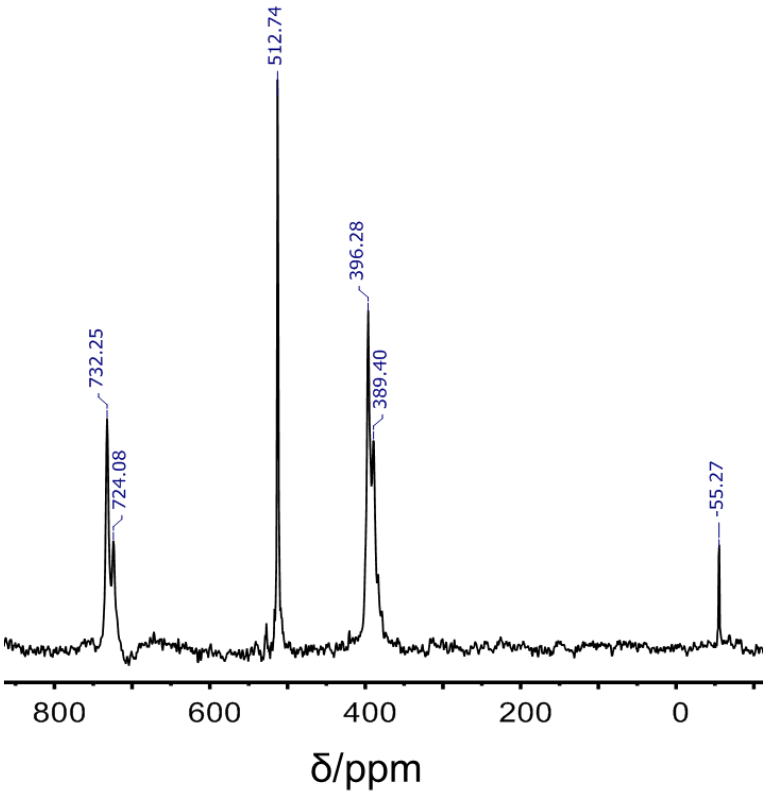

Figure 4.20: *^{17}O NMR spectrum of 1:1 mixture of $(TBA)_6[(\mu\text{-}O)(TiW_5O_{18})_2]$ and $AgBF_4$. Conditions; POM = 0.025 mmols, $AgBF_4$ = 0.025 M, solvent MeCN.*

4.4 Spectroscopic comparison

^{17}O NMR chemical shifts for the terminal W=O oxygen sites for the products of all the reactions were higher than the corresponding peaks in $(TBA)_6[(\mu\text{-}O)(TiW_5O_{18})_2]$ (see Table 4.3). This is consistent with the trend in decrease in overall charge on the heterometalates and the consequent W–O bond weakening and net negative charge build-up on oxygen atoms, as described previously.[49] The ^{17}O NMR chemical shifts for the protonated POM and products of the reactions of $[(\mu\text{-}O)(TiW_5O_{18})_2]^{6-}$ anion and electrophiles have chemical shifts between 732 ppm to 752 ppm. This is consistent with weakening of W-O bonds in the electrophiles investigated. Similarly, an upfield

shift is observed for all of the bridging TiOW oxygen sites compare to the corresponding peaks for $(TBA)_6[(\mu\text{-}O)(TiW_5O_{18})_2]$ due to metal oxygen bonding in the sites. The unique central μ_6-O as expected also shifted downfield with higher chemical shift ranging from –55 ppm to –38 ppm. These results strongly supports the TiOW oxygen sites as the most basic in $(TBA)_6[(\mu\text{-}O)(TiW_5O_{18})_2]$.

Table 4.3: *Trend in ^{17}O NMR chemical shifts for electrophiles in substituted $(TBA)_6[(\mu\text{-}O)(TiW_5O_{18})_2]$ in MeCN.*

Anion	W=O	TiOW	WOW	μ_6-O
$[(\mu\text{-}O)(TiW_5O_{18})_2]^{6-}$	723	536	391	–61
$[(\mu\text{-}O)\{TiW_5O_{18}H\}_2]^{4-}$	748	448	416	–39
			405	
$[(\mu\text{-}O)\{TiW_5O_{18}\}_2(Me_2Sn)]^{4-}$	751	467	412	–38
			402	
$[(\mu\text{-}O)\{TiW_5O_{18}\}_2(SnCl_2)]^{4-}$	757	489	412	–48
	743		403	
$[(\mu\text{-}O)\{TiW_5O_{18}\}_2(Sn)]^{4-}$	743	494	405	–42
	733	489	397	
$[(\mu\text{-}O)\{TiW_5O_{18}\}_2(AuCl)]^{4-}$	744	488	403	–48
			395	
$[(\mu\text{-}O)\{TiW_5O_{18}\}_2(PdCl)]^{4-}$	745	488	407	–47
			395	
$[(\mu\text{-}O)\{TiW_5O_{18}\}_2(Co)]^{4-}$	751	469	416	–36
			405	
$[(\mu\text{-}O)\{TiW_5O_{18}\}_2(Mo)]^{4-}$	743	486	402	-
	732		395	
$[(\mu\text{-}O)\{TiW_5O_{18}\}_2(Ag)]^{5-}$	732	513	396	–55
	724		390	

4.5 Structural comparison

A comparison of the bond lengths and bond angles (Table 4.4) in the titanium environments of $(TBA)_6[(\mu\text{-}O)(TiW_5O_{18})_2]$ $(TBA)_6$ **1**, $(TBA)_4[(\mu\text{-}O)(TiW_5O_{18}H)_2]$ $(TBA)_4$ **2**, $(TBA)_4[(\mu\text{-}O)(TiW_5O_{18}H)_2(dmso)]$ $(TBA)_4$ **3**, $(TBA)_4[(\mu\text{-}O)(TiW_5O_{18})_2(SnMe_2)]$ $(TBA)_4$ **4**, shows that Ti–O bonds in $(TBA)_6$ **1** and $(TBA)_4$ **2** are longer than the corresponding Ti–O bonds in $(TBA)_4$ **3** and $(TBA)_4$ **4** indicating the influence of electrophiles added onto the POM surface at the TiOW bridging positions.

The data suggest that the bonds in the non-substituted $(TBA)_6$ **1** are slightly longer than the bonds observed in $(TBA)_4[(\mu\text{-}O)(TiW_5O_{18})_2(SnMe_2)]$ $(TBA)_4$ **4.** The longer bond length indicates weaker bonds and therefore increase the susceptibility to protonation and or electrophilic metal atom. This further provides some support for our

proposal that protonation in the Lindqvist-type anions proceeds *via* TiOW bridging position which has identified as the most basic site.

Table 4.4: *Average bond lengths [Å] and angles [°]*

Anion	TiO	$W_{eq}O/W_{ax}O$	TiOTi
$(TBA)_6[(\mu\text{-}O)(TiW_5O_{18})_2]$	2.093	1.697 1.705	173.1
$(TBA)_6[(\mu\text{-}O)(TiW_5O_{18}H)_2]$	2.065	1.861 1.946	180
$(TBA)_6[(\mu\text{-}O)(TiW_5O_{18}H)_2$ (dmso)]	1.987	1.703 1.707	162.85
$(TBA)_6[(\mu\text{-}O)(TiW_5O_{18})_2(SnMe_2)]$	1.907	1.875 1.855	152.4

4.6 Conclusion

The investigations described in this chapter are summarized in Figure 4.21 and the data obtained from the ^{17}O NMR spectroscopy shown that initial interaction of H^+ to $[(MeO)(TiW_5O_{18})]^{3-}$ occurred at TiOW site but there is a rapid migration of H^+ to Ti-OMe sites. This rapid proton migration effect is evidence by the chemical shifts at the terminal W=O peaks. As the amount of H^+ increase in the reaction, there is an overall change in all the chemical shifts indicating protonation of $(TBA)_3[(MeO)(TiW_5O_{18})]$ occurred at the TiOW. Results from DFT calculations suggested that initial protonation of $(TBA)_3[(MeO)(TiW_5O_{18})]$ occurred at the TiOW but results from the ^{17}O NMR spectrum suggest that the proton exchange is facile and rapid with the M-OR bond thereby releasing MeOH.

^{17}O NMR spectra coupled with X-Ray crystal structural analysis have shown generally that TiOW is the most basic site in $(TBA)_6[(\mu\text{-}O)(TiW_5O_{18})_2]$. The studies enabled to isolate and structurally characterize the dmso adduct $(TBA)_6[(\mu\text{-}O)(TiW_5O_{18})_2(dmso)]$ and $(TBA)_4[(\mu\text{-}O)(TiW_5O_{18})_2(SnMe_2)]$ wherein Sn(IV) is bonded to the Ti-O-W oxygens emphasising their Lewis basicity.

The hypothetical $(TBA)_4[(\mu\text{-}O)(TiW_5O_{18})_2(AuCl)]$ structure containing Au(III) indicated that the POM might possess “pincer” behaviour and provide interesting Lindqvist-type models for metal oxide catalysts.

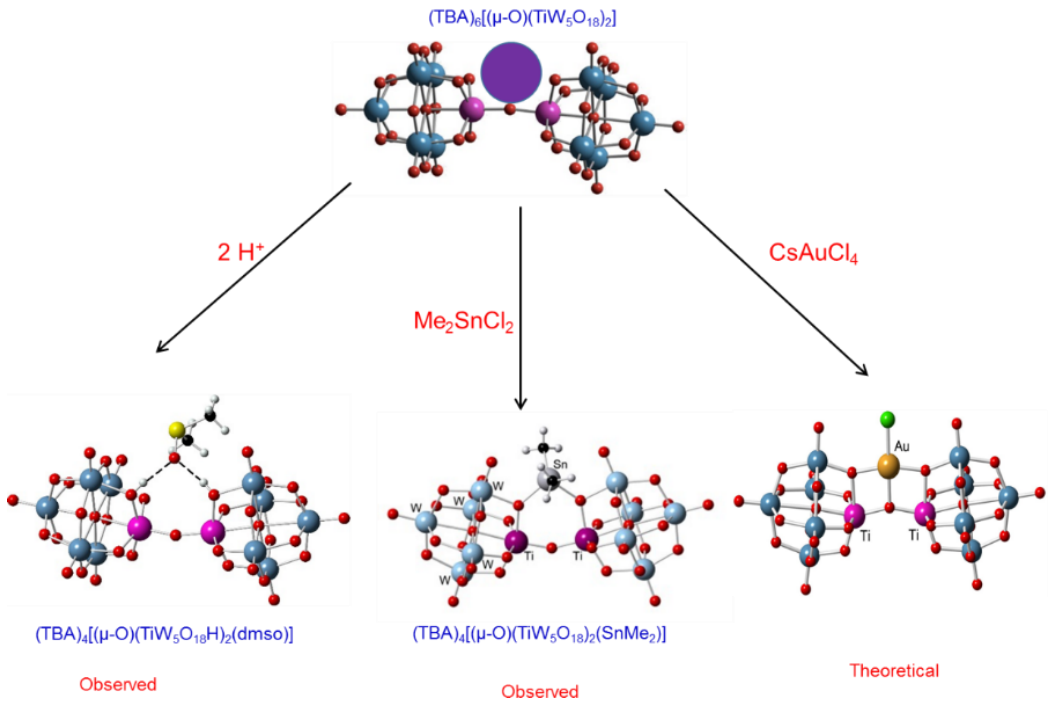

Figure 4.21: *Products from protonation and addition of electrophiles to $(TBA)_6[(\mu\text{-}O)(TiW_5O_{18})_2]$.*

4.7 Experimental

4.7.1 Protonation studies

Protonation studies were carried out with freshly prepared 0.5 M solution of $HBF_4.Et_2O$ in MeCN.

4.7.2 Preparation of reagents

a. $HBF_4.Et_2O$ (61 µL, 0.45 mmol) was dissolve in CH_3CN (0.50 mL) in a 1.0 mL volumetric flask and made up to the 1.00 mL mark with dry CH_3CN to give a 0.45 M solution.
b. $AgBF_4$ (5 mg, 0.025 mmols) was dissolved in dry CH_3CN (1.00 mL) volumetric flask and made up to the 1.0 mL mark with dry CH_3CN to give a 0.025 M solution.
c. $SnCl_4$ (2.9 µL, 0.025 mmols) was dissolved in dry CH_3CN (0.50 mL) in a 1.0 mL volumetric flask in glove box and made up to 1.00 mL mark with dry CH_3CN to give a 0.025 M solution.
d. $SnCl_2$ (6 mg, 0.03 mmols) was dissolved in dry CH_3CN (0.50 mL) in a 1.0 mL volumetric flask in a glove box and made up to the 1.00 mL mark with dry CH_3CN to give a 0.03 M solution.

4.7.3 Protonation of $(TBA)_3[(MeO)TiW_5O_{18}]$ with $HBF_4.Et_2O$

In a sealed screw-capped NMR tube was added $(TBA)_3[(MeO)TiW_5O_{18}]$ (100 mg, 0.05 mmols) and dissolved in dried CH_3CN (0.5 mL). To the solution was added $HBF_4.Et_2O$ (0.45 M, 25 µL, 0.011 mmols). The resultant clear solution was vigorously shake for 5 min before recording the ^{17}O NMR spectrum. Subsequent aliquots were added up to 2 mole equivalents of $HBF_4.Et_2O$. **^{17}O NMR** (41 MHz, acetonitrile-*d*$_3$) δ (ppm) 776, 753, 738, 727, 549, 522, 462, 416, 397, 389, -5, -43.

4.7.4 Protonation of $(TBA)_3[(HO)SnW_5O_{18}]$ with $HBF_4.Et_2O$

In a sealed screw-capped NMR tube was added $(TBA)_3[(HO)SnW_5O_{18}]$ (100 mg, 0.048 mmols) and dissolved in dried CH_3CN (0.5 mL). To the solution was added $HBF_4.Et_2O$ (0.45 M, 25 µL, 0.011 mmols). The resultant clear solution was vigorously shaken for 5 min before recording the ^{17}O NMR spectrum. Subsequent aliquots were added up to 1 mole equivalent of $HBF_4.Et_2O$**. ^{17}O NMR** (41 MHz, acetonitrile-*d*$_3$) δ 739, 726, 694, 399, 388, 356, 335, 24, 16, -8. **^{119}Sn NMR** (186 MHz, acetonitrile-*d*$_3$) δ -611, -633, -648, -682, -696. **^{183}W NMR** (21 MHz, acetonitrile-*d*$_3$) δ 72.20, 71.31, -122.49, -131.27.

4.7.5 Protonation of $(TBA)_6[(\mu\text{-}O)(TiW_5O_{18})_2]$ with $HBF_4.Et_2O$

In a sealed screw-capped NMR tube was added ^{17}O-enriched $(TBA)_6[(\mu\text{-}O)(TiW_5O_{18})_2]$ (100 mg, 0.025 mmols) and dissolved in dried CH_3CN (0.5 mL). To the solution was added $HBF_4.Et_2O$ (0.45 M, 25 µL, 0.011 mmols). The resultant solution was vigorously shaken for 5 min before recording the initial ^{17}O NMR spectrum. Subsequent aliquots of 0.45 M $HBF_4.Et_2O$ were added up to 2 mole equivalents. **^{17}O NMR** (54 MHz) δ (ppm) 744, 733, 709, 535, 488, 403, 397, 388, -47. The solution was vacuum-dried, washed with ethyl acetate $C_4H_8O_2$ (5 mL x 3), dried under reduced pressure and the IR spectrum of the solid was recorded. **IR (4000 – 400 cm^{-1}):** 2961 (m), 2874 (m), 2256 (m), 1483 (m), 1379 (w), 1308 (w), 1237 (m), 1150 (vw), 1059 (s), 1024 (w), 963 (vs), 921 (m), 883 (s), 783 (vs, br), 656 (m) 576 (m), 515 (s) 430 (w). **^{183}W NMR** (21 MHz, acetonitrile-d_3) δ 63.55, 29.99, 17.99, 5.30, -98.90.

4.7.6 Isolation of $(TBA)_4[(\mu\text{-}O)(TiW_5O_{18}H)_2(dmso)]$

In a sealed screw-capped NMR tube was added ^{17}O-enriched $(TBA)_6[(\mu\text{-}O)(TiW_5O_{18})_2]$ (100 mg, 0.025 mmols) and dissolved in dried CH_3CN (0.5 mL). To the solution was added $HBF_4.Et_2O$ (0.45 M, 25 µL, 0.011 mmols). The resultant solution was vigorously shaken for 5 min before recording initial ^{17}O NMR spectrum. Subsequent aliquots of 0.45 M $HBF_4.Et_2O$ were added up to 2 mole equivalents. The solution was vacuum-dried, washed with ethyl acetate (5 mL x 3), vacuum-dried and crystals were grown by slow vapour diffusion of diethyl ether into a MeCN solution in the presence of dmso. **^{17}O NMR** (54 MHz) δ (ppm) 744, 733, 709, 535, 488, 403, 397, 388, -37. **IR (4000 – 400 cm^{-1}):** 2961 (m), 2874 (m), 2256 (m), 1483 (m), 1379 (w), 1308 (w), 1237 (m), 1150 (vw), 1059 (s), 1024 (w), 963 (vs), 921 (m), 883 (s), 783 (vs, br), 656 (m) 576 (m), 515 (s) 430 (w); **^{17}O NMR** (54 MHz,) δ (ppm) 744, 733, 709, 535, 488, 403, 397, 388, -47.

4.7.7 Reaction between $(TBA)_6[(\mu\text{-}O)(TiW_5O_{18})_2]$ and Me_2SnCl_2 in MeCN

In a Schlenk flask was added $(TBA)_6[(\mu\text{-}O)(TiW_5O_{18})_2]$ (100 mg, 0.025 mmols) and Me_2SnCl_2 (5 g, 0.025 mmols) and dissolved in dried CH_3CN (5 mL). The mixture was stirred overnight (~18 h) at room temperature. The solution was pumped dry and washed with ethyl acetate (5 ml x 3), vacuum-dried and washed with diethyl ether (5 ml x 2) and dried under vacuum for 1 h to give a white crystalline solid of $(TBA)_6[(\mu\text{-}O)(TiW_5O_{18})_2(SnMe_2)]$ (**0.693 g, 76.1 %**). Crystals were grown by slow vapour diffusion of diethyl ether into MeCN solution. **^{17}O NMR** (54 MHz,) δ (ppm) 751, 695, 467, 413,

402, -5, -38. **IR (4000 – 400 cm^{-1}):** 2961 (m), 2934 (m), 2873 (m), 1480 (m), 1379 (w), 1245 (vw), 1153 9 (vw), 1107 (w), 953 (vs), 884 (s, br), 777 (vs, br), 667 (m) 522 (m) 432 (w).

4.7.8 Reaction between $(TBA)_6[(\mu\text{-}O)(TiW_5O_{18})_2]$ and $SnCl_2$ in MeCN

In a Schlenk flask was added $(TBA)_6[(\mu\text{-}O)(TiW_5O_{18})_2]$ (63 mg, 0.016 mmols) and dissolved in dried CH_3CN (0.5 mL). To the solution was added $SnCl_2$ (6.0 mg, 0.032 mmols) in MeCN. The resultant solution was vigorously shaken for 5 min before recording the ^{17}O NMR spectrum which showed a mixture of two species. The NMR sample was transferred back into a Schlenk flask and stirred for a further 18 h at room temperature. The volume of the solution was reduced by half and the ^{17}O NMR spectrum was recorded again, showing a single species. The solution was pumped dry, washed with diethyl ether (5 ml x 3), and vacuum dried. **^{17}O NMR** (54 MHz,) δ (ppm) 744, 733, 487, 404, 395, -48.

4.7.9 Reaction between $(TBA)_6[(\mu\text{-}O)(TiW_5O_{18})_2]$ and $SnCl_4$ in MeCN

$(TBA)_6[(\mu\text{-}O)(TiW_5O_{18})_2]$ (100 mg, 0.025 mmols) was added to a Schlenk flask and dissolved in dried CH_3CN (0.5 mL). A solution of $SnCl_4$ in dry MeCN (0.025 M, 1.0 mL, 0.025 mmols) was added and the resultant solution was stirred for 30 min before recording the ^{17}O NMR spectrum. The NMR sample was transferred back into the Schlenk flask and stirred overnight at room temperature (~18 h). The solution was vacuum-dried, washed with ethyl acetate (5 ml x 3), and vacuum dried for 1 h and recording the ^{17}O NMR spectrum. **^{17}O NMR** (54 MHz,) δ (ppm) 761 (W=O), 758 W=O), 592, 570 Ti-O(W)-Sn, 412, 403 (WOW) and -39 ppm.

4.7.10 Reaction between $(TBA)_6[(\mu\text{-}O)(TiW_5O_{18})_2]$ and $CsAuCl_4$ in MeCN

A mixture of $(TBA)_6[(\mu\text{-}O)(TiW_5O_{18})_2]$ (100 mg, 0.025 mmols) and $CsAuCl_4$ (12 mg, 0.025 mmols) was dissolved in dried CH_3CN (5 mL) in a Schlenk flask and stirred for 2 h at room temperature. The volume of the solution was reduced by half and the ^{17}O NMR spectrum was recorded. The NMR sample was transferred back into Schlenk flask and stirred for a further 18 h at room temperature. The solution was pumped dry, washed with diethyl ether (5 ml x 3) and vacuum-dried. **^{17}O NMR** (54 MHz,) δ (ppm) 742, 538, 487, 402, 394, -48.

4.7.11 Reaction between $(TBA)_6[(\mu\text{-}O)(TiW_5O_{18})_2]$ and $AuCl_3$ in MeCN

In a Schlenk flask was added $(TBA)_6[(\mu\text{-}O)(TiW_5O_{18})_2]$ (300 mg, 0.0754 mmols) and dissolved in dried CH_3CN (2 mL). In a separate Schlenk flask, $AuCl_3$ (34 mg, 0.112 mmols) was dissolved in dried CH_3CN (1 mL). The two solutions were combined *via* cannula transfer with stirring. The bright yellow solution was stirred for 1 h at room temperature and the ^{17}O NMR spectrum was recorded. The sample was transferred back in to the Schlenk flask and stirred for a further 4 h then reduced the volume by one half before recording another ^{17}O NMR spectrum. The solution was pumped to dryness, washed with ethyl acetate (5 ml x 3) and diethyl ether (5 ml x 2) vacuum dried. **^{17}O NMR** (54 MHz,) δ (ppm) 743 (W=O), 490 (Ti-O(W)-Au), 403 (WOW) -47.

4.7.12 Reaction between $(TBA)_6[(\mu\text{-}O)(TiW_5O_{18})_2]$ and $PdCl_2$ in MeCN

In a Schlenk flask was added $(TBA)_6[(\mu\text{-}O)(TiW_5O_{18})_2]$ (100 mg, 0.025 mmols) in dried CH_3CN (1 mL). To the solution was added an excess of $PdCl_2$ (15 mg, 0.085 mmols). The dark brown solution was stirred for 18 h at room temperature and became bright yellow as the reaction progressed. The ^{17}O NMR spectrum of the solution was recorded and the sample was transferred back in to the Schlenk flask, pumped to dryness, washed with ethyl acetate (5 ml x 3) and diethyl ether (5 ml x 2) vacuum dried. **^{17}O NMR** (54 MHz,) δ (ppm) 743, 737, 488 404, 400, 395 and -48.

4.7.13 Reaction between $(TBA)_6[(\mu\text{-}O)(TiW_5O_{18})_2]$ and $PdCl_2$ with $AgBF_4$ in MeCN

$(TBA)_6[(\mu\text{-}O)(TiW_5O_{18})_2]$ (100 mg, 0.025 mmols) was added to a Schlenk flask and added and dissolved in dried CH_3CN (1 mL). To the solution was added an exces of $PdCl_2$ (15 mg, 0.085 mmols) was added and dissolved in dried CH_3CN (1.0 mL) resulting to a brown solution containing $[PdCl_2(MeCN)_2]$. The two solutions were combined *via* cannula transfer with stirring. After stirring for 30 min. $AgBF_4$ (5 mg, 0.025 mmols) was added and the mixture was stirred overnight. The solution was allowed to settle and then it was filtered using a cannula filter stick to separate any AgCl from the solution. The solution was pumped to dryness and washed with ethyl acetate (5 ml x 3) and diethyl ether (5 ml x 2). **^{17}O NMR** (54 MHz,) δ (ppm) 742,726 540,527, 487 402, 394 387 and -48.

4.7.14 Reaction between $(TBA)_6[(\mu\text{-}O)(TiW_5O_{18})_2]$ and $AgBF_4$ 2:1 ratio

$(TBA)_6[(\mu\text{-}O)(TiW_5O_{18})_2]$ (50 mg, 0.0125 mmols) and dissolved in dried CH_3CN (1 mL). In a separate Schlenk flask, $AgBF_4$ (5 mg, 0.025 mmols) was added and dissolved in dried CH_3CN (1.0 mL). The two solutions were combined *via* cannula transfer with stirring. The resulting solution was stirred for 4 h at room temperature before it pumped to dryness, washed with ethyl acetate (5 ml x 3) and diethyl ether (5 ml x 2) before vacuum dried. **^{17}O NMR** (54 MHz,) δ (ppm) 736, 727, 503, 397, 392 and -54.

4.7.15 Reaction between $(TBA)_6[(\mu\text{-}O)(TiW_5O_{18})_2]$ and $AgBF_4$ 1:1 ratio

$(TBA)_6[(\mu\text{-}O)(TiW_5O_{18})_2]$ (50 mg, 0.0126 mmols) was dissolved in dried CH_3CN (1 mL). In a separate Schlenk flask $AgBF_4$ (2.5 mg, 0.0126 mmols) was dissolved in dried CH_3CN (1.0 mL) and the two solutions were combined *via* cannula transfer with stirring. The resulting solution was stirred for 1 h at room temperature, pumped to dryness, washed with ethyl acetate (5 ml x 3) and diethyl ether (5 ml x 2) then pumped dry again. **^{17}O NMR** (54 MHz,) δ (ppm) 732, 724, 513, 396, 389 and -55.

4.7.16 Computational studies

Density Functional Theory (DFT) calculations and Classical Molecular Dynamics (CMD) simulations were performed by the Quantum Chemistry Group at the Universitat Rovira i Virgili, Tarragona (Spain). The Calculations were performed with the GGA-type OPBE functional, including spin–orbit.

References

1. N. S. Antonova, J. J. Carbó, U. Kortz, O. A. Kholdeeva and J. M. Poblet, *J. Am.Chem. Soc.*, 2010, **132**, 7488-7497.
2. N. V. Maksimchuk, G. M. Maksimov, V. Y. Evtushok, I. D. Ivanchikova, Y. A. Chesalov, R. I. Maksimovskaya, O. A. Kholdeeva, A. Solé-Daura, J. M. Poblet and J. J. Carbó, *ACS Catalysis*, 2018, **8**, 9722-9737.
3. I. Y. Skobelev, O. V. Zalomaeva, O. A. Kholdeeva, J. M. Poblet and J. J. Carbó, *Eur. J.*, 2015, **21**A, 14496-14506.
4. S. Bordiga, F. Bonino, A. Damin and C. Lamberti, *Phy. Chem. Chem. Phy.*, 2007, **9**, 4854-4878.
5. G. M. Zhidomirov, A. L. Yakovlev, M. A. Milov, N. A. Kachurovskaya and I. V. Yudanov, *Catalysis Today*, 1999, **51**, 397-410.
6. O. A. Kholdeeva, T. A. Trubitsina, R. I. Maksimovskaya, A. V. Golovin, W. A. Neiwert, B. A. Kolesov, X. López and J. M. Poblet, *Inorg. Chem.*, 2004, **43**, 2284-2292.
7. N. S. Antonova, J. J. Carbó, U. Kortz, O. A. Kholdeeva and J. M. Poblet, *J. Am. Chem. Soc.*, 2010, **132**, 7488-7497.
8. B. G. Donoeva, T. A. Trubitsina, N. S. Antonova, J. J. Carbó, J. M. Poblet, G. Al-Kadamany, U. Kortz and O. A. Kholdeeva, *Eur. J. Inorg. Chem.*, 2010, **2010**, 5312-5317.
9. P. Jiménez-Lozano, I. D. Ivanchikova, O. A. Kholdeeva, J. M. Poblet and J. J. Carbó, *Chem. Commun.*, 2012, **48**, 9266-9268.
10. J. M. Maestre, J. P. Sarasa, C. Bo and J. M. Poblet, *Inorg. Chem.*, 1998, **37**, 3071-3077.
11. B. B. Bardin, S. V. Bordawekar, M. Neurock and R. J. Davis, *J. Phy. Chem.*, 1998, **102**B, 10817-10825.
12. V. W. Day, W. G. Klemperer and C. Schwartz, *J. Am. Chem. Soc.*, 1987, **109**, 6030-6044.
13. O. A. Kholdeeva, G. M. Maksimov, R. I. Maksimovskaya, L. A. Kovaleva, M. A. Fedotov, V. A. Grigoriev and C. L. Hill, *Inorg. Chem.*, 2000, **39**, 3828-3837.
14 T.Izuagie, PhD thesis 2017, Newcastle University
15. R. J. Errington, S. S. Petkar, P. S. Middleton, W. McFarlane, W. Clegg, R. A. Coxall and R. W. Harrington, *Dalton Trans.*, 2007, 5211-5222.
16 M. Pascual-Borras, PhD thesis, UVR Taragona 2015.

17. T. M. Che, V. W. Day, L. C. Francesconi, W. G. Klemperer, D. J. Main, A. Yagasaki and O. M. Yaghi, *Inorg. Chem.*, 1992, **31**, 2920-2928.
18. W. G. Klemperer and W. Shum, *J. Am. Chem. Soc.*, 1978, **100**, 4891-4893.
19. D. Boegeat, B. Jousseaume, T. Toupance, G. Campet and L. Fournès, *Inorg. Chem.*, 2000, **39**, 3924-3927.
20. J. A. Fernández, X. López and J. M. Poblet, *J. Molecular Catalysis* 2007, **262** A, 236-242.
21 D. Lebbie; MPhil thesis, Newcastle University, 2015
22. W. R. Fawcett and A. A. Kloss, *J. Phy. Chem.*, 1996, **100**, 2019-2024.
23 X. López, C. Bo and J. M. Poblet, *J. Am. Chem. Soc.*, 2002, **124**, 12574-12582.
24. R. K. C. Ho and W. G. Klemperer, *J. Am. Chem. Soc.*, 1978, **100**, 6772-6774.
25. K. Nomiya, M. Takahashi, K. Ohsawa and J. A. Widegren, *J.Chem. Soc., Dalton Trans.*, 2001, 2872-2878.
26. Y. Lin, T. J. R. Weakley, B. Rapko and R. G. Finke, *Inorg. Chem.*, 1993, **32**, 5095-5101.
27. V. Ugrinova, G. A. Ellis and S. N. Brown, *Chem. Commun.*, 2004, 468-469.
28. W. Clegg, M. R. J. Elsegood, R. J. Errington and J. Havelock, *J.Chem.Soc., Dalton Trans.*, 1996, 681-690.
29. W. H. Knoth, *J. Am. Chem. Soc.*, 1979, **101**, 759-760.
30. P. J. Domaille and W. H. Knoth, *Inorg. Chem.*, 1983, **22**, 818-822.
31. F. Xin, M. T. Pope, G. J. Long and U. Russo, *Inorg. Chem.*, 1996, **35**, 1207-1213.
32. G. Sazani, M. H. Dickman and M. T. Pope, *Inorg. Chem.*, 2000, **39**, 939-943.
33. A. R. Tomşa, A. Koutsodimou, P. Falaras, M. C. Bernard and M. Rusu, *Synthesis and Reactivity in Inorganic, Metal-Organic, and Nano-Metal Chemistry*, 2005, **35**, 651-659.
34. D. Morales-Morales, *Revista de la Sociedad Química de México*, 2004, **48**, 338-346.
35. M. Albrecht and G. van Koten, *Angew. Chemie Int. Ed.*, 2001, **40**, 3750-3781.
36. R. J. Errington, S. S. Petkar, P. S. Middleton, W. McFarlane, W. Clegg, R. A. Coxall and R. W. Harrington, *Dalton Trans.*, 2007, 5211-5222.
37. Y. Chen and M. W. Kanan, *J. Am. Chem. Soc.*, 2012, **134**, 1986-1989.
38. A. Kolmakov, Y. Zhang, G. Cheng and M. Moskovits, *Advanced Materials*, 2003, **15**, 997-1000.
39. X. Xu, J. Zhuang and X. Wang, *J. Am. Chem. Soc.*, 2008, **130**, 12527-12535.

40. O. Yoichi, H. Hidenori, N. Kenji, Y. Hiroshi, K. Toshio, H. Masahiro and H. Hideo, *App. Phy. Lett.*, 2008, **93**, 032113.
41. A. Corma and H. Garcia, *Chem. Soc. Rev.*, 2008, **37**, 2096-2126.
42. M. Pérez-Hernández, P. del Pino, S. G. Mitchell, M. Moros, G. Stepien, B. Pelaz, W. J. Parak, E. M. Gálvez, J. Pardo and J. M. de la Fuente, *ACS Nano*, 2015, **9**, 52-61.
43. C. Bao, N. Beziere, P. del Pino, B. Pelaz, G. Estrada, F. Tian, V. Ntziachristos, J. M. de la Fuente and D. Cui, *Small*, 2013, **9**, 68-74.
44. B. Keita, T. Liu and L. Nadjo, *J. Mater. Chem.*, 2009, **19**, 19-33.
45. S. G. Mitchell and J. M. de la Fuente, *J. Mater. Chem.*, 2012, **22**, 18091-18100.
46. Y. Wang and I. A. Weinstock, *Chem. Soc. Rev.*, 2012, **41**, 7479-7496.
47. T. M. Anderson, R. Cao, E. Slonkina, B. Hedman, K. O. Hodgson, K. I. Hardcastle, W. A. Neiwert, S. Wu, M. L. Kirk, S. Knottenbelt, E. C. Depperman, B. Keita, L. Nadjo, D. G. Musaev, K. Morokuma and C. L. Hill, *J. Am. Chemical Soc.*, 2005, **127**, 11948-11949.
48. A. Singh and P. R. Sharp, *Dalton Trans.*, 2005, 2080-2081.
49. M. Pascual-Borras, X. Lopez, A. Rodriguez-Fortea, R. J. Errington and J. M. Poblet, *Chem. Sci.*, 2014, **5**, 2031-2042.

Chapter 5

Synthesis, Characterization and Reactivity of $(TBA)_4[O{=}TiW_5O_{18}]$ - the First Member of the Lindqvist-type oxo-titanium Family

This chapter discusses an efficient synthetic approach to $[O{=}TiW_5O_{18}]^{4-}$, which is possibly the first member of the oxo-titanium Lindqvist family. Terminal Ti=O Lindqvist POMs are rare probably due to lack of synthetic methodology. The method involves treating the mono-substituted POM, $[(CH_3O)TiW_5O_{18}]^{3-}$ with an organic base and the reaction resulted in an excellent yield of the product, $[O{=}TiW_5O_{18}]^{4-}$. The chapter also discussed reactions of the new POM with alkyl and aryl isocyanate providing insights into the titanyl bond reactivity.

5.1 Introduction

The Lindqvist-type polyoxometalates, $[W_6O_{19}]^{2-}$ has traditionally proven difficult to derivatize. However, substitution of WO^{4+} in $[W_6O_{19}]^{2-}$ by $\{TiOMe\}^{3+}$,[1] and $\{SnOMe\}^{3+}$ [2] can introduce a reactive metal site. Chapters 3 and 4 have extensively discussed reactivities of a range of Sn- and Ti-substituted Lindqvist-type polytungstates. An important member of the Ti-family yet to be reported or studied is Ti(IV)-substituted Lindqvist POM containing terminal Ti=O. This class of POMs is rare, probably due to lack of synthetic methodology. Ti(IV)-substituted POMs are of particular interest due to the role of Ti=O in catalytic transformations and as models for the active sites in heterogeneous processes.[3-6] To the best of our knowledge, the few reported oxo Ti-substituted POMs are mainly of the Keggin type. Kortz and co-workers studied Ti(IV)-substituted oxo-[7] and hydroxo-substituted[8] and these Ti(IV) POMs have served as molecular models to investigate mechanisms of selective oxidation.[9] Herein, rational methods are described in Equation 5.1 to generate a terminal titanyl bond within a Lindqvist-type polyoxometalate. The reactivity of the titanyl bond was further investigated through attempted protonation, metathesis and oxygen abstraction reactions by ^{17}O NMR spectroscopy.

5.2 Results and Discussion

5.2.1 Attempted preparation of $(TBA)_4[O=TiW_5O_{18}]$ by deprotonation of $(TBA)_3[(HO)TiW_5O_{18}]$

An initial attempt to synthesise $(TBA)_4[O=TiW_5O_{18}]$ involved deprotonation of $(TBA)_3[(HO)TiW_5O_{18}]$ with TBAOH. In this reaction, a 1:1 mixture of ^{17}O-enriched $(TBA)_3[(HO)TiW_5O_{18}]$ and TBAOH were reacted (Equation 5.1) and the reaction was monitored by ^{17}O NMR spectroscopy.

$$[(HO)TiW_5O_{18}]^{3-} + OH^- \rightarrow [O=TiW_5O_{18}]^{4-} + H_2O \qquad 5.1$$

After stirring for 4 h, the ^{17}O NMR spectrum contained some additional peaks associated with a protonated species (Figure 5.1). The two terminal W=O peaks with high δ_o i.e. the peak with chemical shift at δ_o 960 ppm is assigned to Ti=O in an anion with a high overall negative charge $[O=TiW_5O_{18}]^{4-}$ while the signal observed at δ 1015 ppm is assigned to a protonated species with lower overall negative charge $[O=TiW_5O_{18}H]^{3-}$. The characteristic peak at δ 443 ppm is tentatively assigned to exchanged,^{17}O-enriched oxygen in the TiOH site. The peak at δ 16 ppm might be due

to the presence of some small amount of dmso because the hydroxido $(TBA)_3[(HO)TiW_5O_{18}]$ was prepared in dmso (as discussed in Chapter 3).

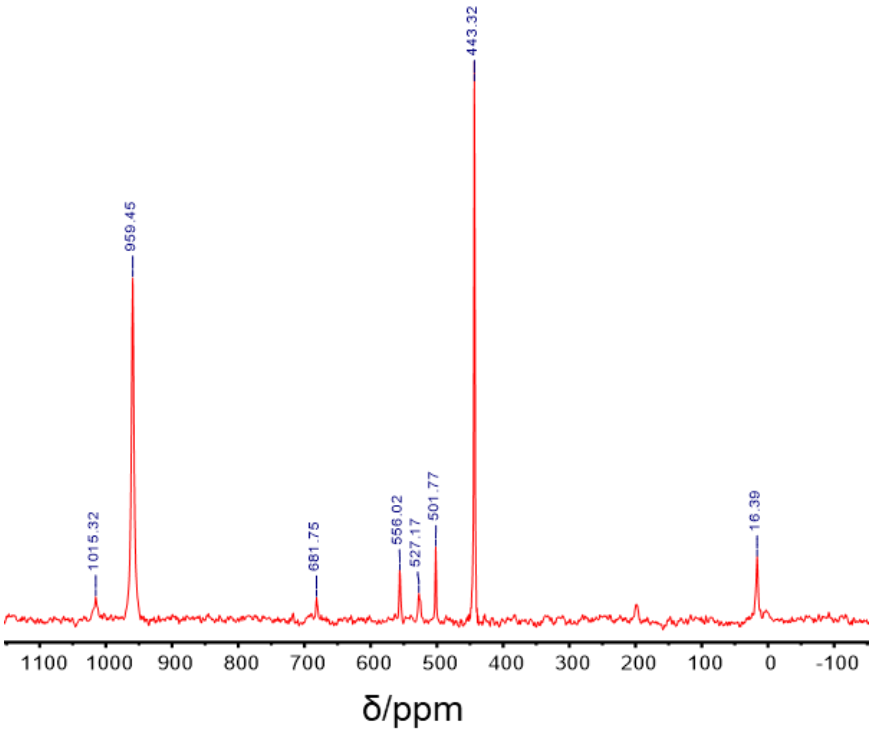

Figure 5.1: *^{17}O NMR spectrum for reaction between $(TBA)_3[(HO)TiW_5O_{18}]$ and TBAOH in MeCN at room temperature.*

5.2.2 Synthesis and characterization of $(TBA)_4[O=TiW_5O_{18}]$

The above reaction and the ^{17}O NMR spectrum (Figure 5.1) did not show a clear formation of a single species but rather a mixture of different species. In order to get the desired product, the methoxy compound $(TBA)_3[(MeO)TiW_5O_{18}]$ was reacted with TBAOH in a 1:1 ratio (Equation 5.2) at room temperature and monitored the reaction by ^{17}O NMR spectroscopy.

$$(TBA)_3[(MeO)TiW_5O_{18}] + OH^- \rightarrow [O=TiW_5O_{18}]^{4-} + MeOH \qquad 5.2$$

The ^{17}O NMR spectrum (Figure 5.2) of the greenish brown compound after removal of all the volatiles contained a peak for terminal Ti=O at δ 960 ppm. In comparison, it is consistent with that reported for the Keggin anion $[O=TiPW_{11}O_{39}]^{5-}$ at δ 963 ppm by Kholdeeva and co-workers.[9] The peak observed at δ 695 ppm was assigned to the terminal W=O peak. In comparison $\{TiW_5\}^{3-}$ anions with W=O bond in other compounds, the low δ_o shift for the terminal W=O for $[O=TiW_5O_{18}]^{4-}$ was due to higher anionic charge. Note that the equatorial and axial terminal W_{eq}=O and W_{ax}=O peaks were not resolved due to line broadening. Bridging TiOW was observed at δ 501 ppm

while the peaks at δ 381 and 368 ppm were assigned to the bridging W-O-W. The unique central u_6-O was observed at δ –64 ppm. The peaks marked with asterisks are due to small amount of unidentified impurities.

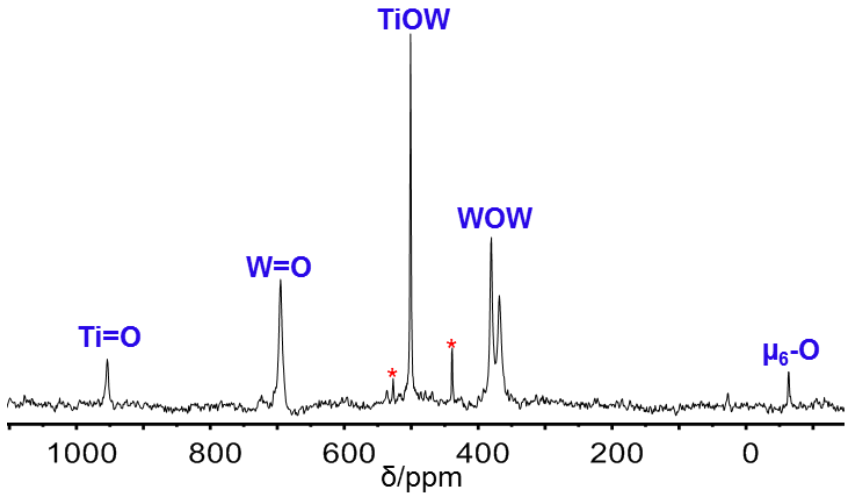

Figure 5.2: *^{17}O NMR of $(TBA)_4[O=TiW_5O_{18}]$ in MeCN.*

(a) FT-IR Spectroscopy

The FTIR spectrum of ^{17}O enriched $(TBA)_4[O=TiW_5O_{18}]$ shown in Figure 5.3 contains ν(W=O) bands at 931 cm^{-1} which is at a lower wavenumber than ν(W=O) bands for $[(Ti^{IV}O)_2(\alpha\text{-}As^{III}W_9O_{33})_2]^{14-}$,[10] (945 cm^{-1}) $(TBA)_3[(MeO)TiW_5O_{18}]$,[1] (945 cm^{-1}) $(TBA)_3[(MeO)SnW_5O_{18}]$ [2] (952 cm^{-1}) and $(TBA)_3[(Ph_2PO_2)ZrW_5O_{18}]$ [11] (945 cm^{-1}) and is consistent with higher anion charge. The strong characteristic band for ν(W-O-W) is observed at 781 cm^{-1} while the weak band at 889 cm^{-1} may be due to ν(Ti-O) in TiOW.

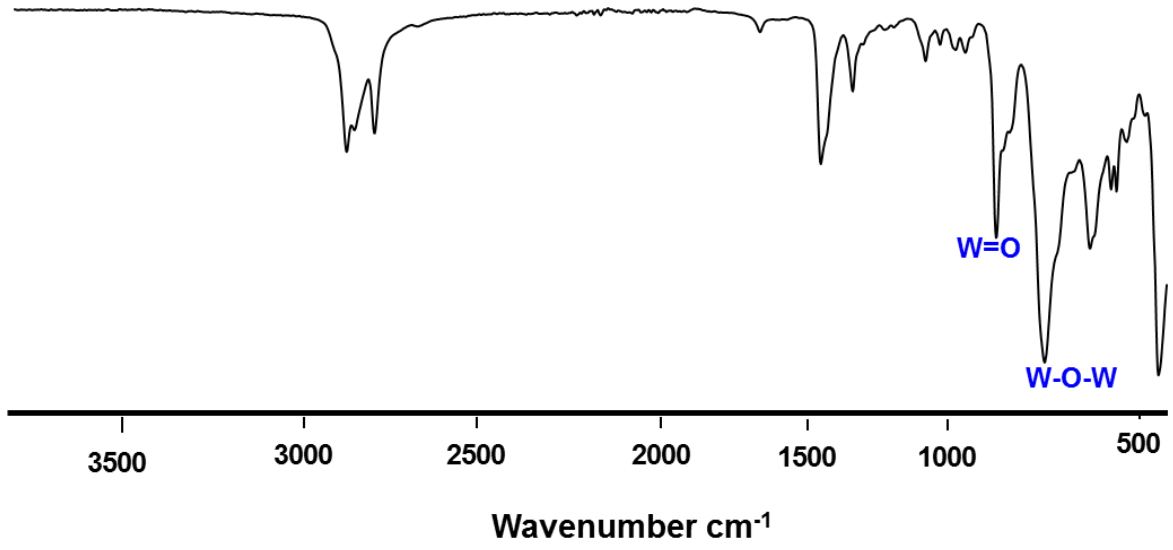

Figure 5.3: *FT-IR spectrum of $(TBA)_4[O=TiW_5O_{18}]$*

(b) ^{183}W NMR spectroscopy

The ^{183}W NMR spectrum of $(TBA)_4[O=TiW_5O_{18}]$ acquired over 3 days in MeCN (Figure 5.4) contained two peaks at δ 82 and 47 ppm for W_{eq} and W_{ax} respectively in a 4:1 ratio. It is interesting to compare the relative shifts for W_{ax} and W_{eq} with those for other Lindqvist type POMs such as $(TBA)_3[(MeO)TiW_5O_{18}]$,[1] $(TBA)_3[(MeO)SnW_5O_{18}]$[2], $[(HO)TiW_5O_{18}]^{3-}$ and $[(u_6\text{-}O)(TiW_5O_{18}H)_2]^{4-}$. It is important to note that the electronic influence at the tungsten metal trans to the substituted metal-ligand site as a result of substituting $\{WO\}^{4+}$ by $\{TiOMe\}^{3+}$, $\{SnOMe\}^{3+}$ or $\{Ti=O\}^{2+}$ is remarkably different as shown in Table 5.1

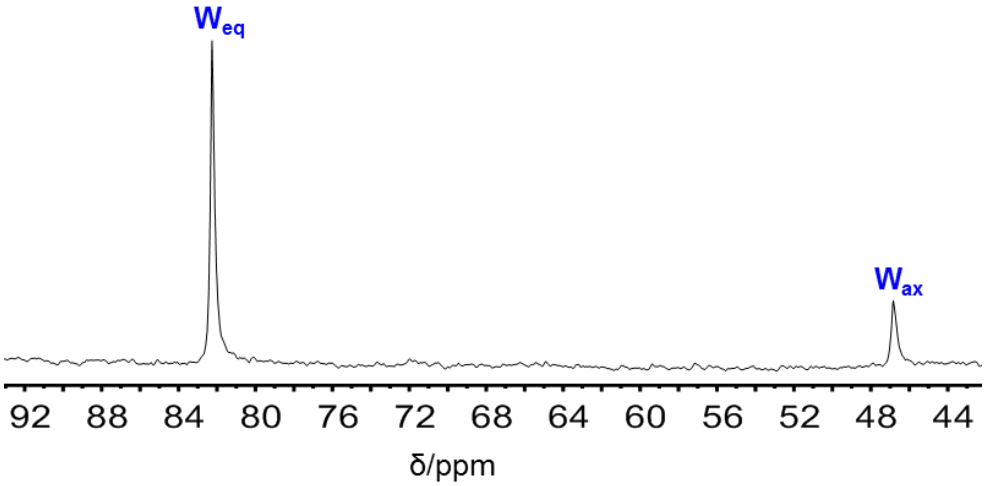

Figure 5.4: *^{183}W NMR for $(TBA)_4[O=TiW_5O_{18}]$ in MeCN.*

Table 5.1: *Electronic influence at **W** as a result of substituting $\{WO\}^{4+}$*

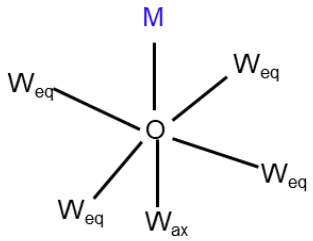

Anion[b]	δ[a] (ppm)		Reference
$[W_6O_{19}]^{2-}$	47.8		1
$[(MeO)TiOW_5O_{18}]^{3-}$	32.3	64.5	1
$[(MeO)SnOW_5O_{18}]^{3-}$	76	–156	2
$[O=TiW5O18]^{4-}$	82	47	This work
$[(HO)TiW_5O_{18}]^{3-}$	80	38	This work
$[(u\text{-}O)(TiW_5O_{18}H)_2]^{4-}$	64	30	This work

[a] Positive values are downfield of reference (2 mol dm^{-3} aqueous Na_2MO_4 for ^{183}W; [b] all as $NBu^n{}_4^+$ salt.

(c) X-ray Diffraction analysis

Crystals were grown by slow vapour diffusion of Et_2O into MeCN for several days and the X-ray crystal structure was obtained, which contained a disordered anion, four associated TBA cations and solvent of crystallisation as shown in Figure 5.5. Crystallographic details are given in **Supplementary Data Table S13**, with selected bond lengths and angles in **Supplementary Data Tables S14 and S15**. The Ti=O is disordered over all metal sites with ~0.1 occupancy at each of the two axial sites and ~0.2 occupancy at each of the sites in the equatorial plane indicated in Figure 5.5. Ti-O bonds in the structure range between 1.714(3) - 1.941(3) Å. The tungsten at the axial position has bond length 1.720(3) Å, which is shorter than the average W_{ax}-O bond in W_{ax}-O bond in $[(MeO)TiW_5O_{18}]^{3-}$ anions at 1.740 Å.[1]

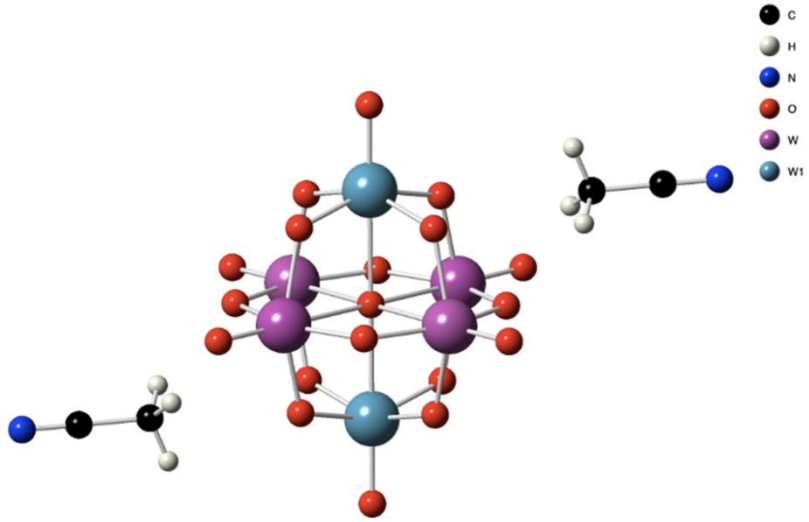

Figure 5.5: *X-ray crystal structure of $[O=TiW_5O_{18}]^{4-}$ including solvent of crystallisation.*

Another attempt to grow single crystals of $(TBA)_4[(O=TiW_5O_{18}]$ gave an unexpected crystal structure containing the anion $[O=TiW_5O_{17}(OMe)]^{3-}$ (Figure 5.6) that must have been formed during crystallisation as solution NMR prior to recrystallization is not consistent with this asymmetric structure. However, the lack of disorder in the anion enabled the Ti=O bonding parameters to be characterised.
The structure is an isomer of $(TBA)_3[(MeO)TiW_5O_{18}]$ apparently resulting from methylation of the highly charged $[O=TiW_5O_{18}]^{4-}$ anion to give a chiral centre. Interestingly the methyl group is located on a WOW bridging site rather than TiOW. The Ti=O bond length in the structure is 1.692(6) Å. The tungsten at the axial position (W_{ax}-O) has a bond length of 1.698(6) Å, shorter than the average W_{ax}-O bond in $[(MeO)TiW_5O_{18}]^{3-}$ anions at 1.740 Å.[1] The WOW angle at the chiral centre is

109.9(2)Å significantly smaller than WOW angles of 115.95(19) to 117.59(19)º in $[(HO)TiW_5O_{18}]^{3-}$. The bond angles at the TiOW bridging position range between 114.9(3) - 118.2(3)º , which is also smaller than those observed for $[(HO)TiW_5O_{18}]^{3-}$ at 121.96(12) to 135.80(15)º. Crystallographic details are given in **Supplementry Data Supplementry Data Table S9**.

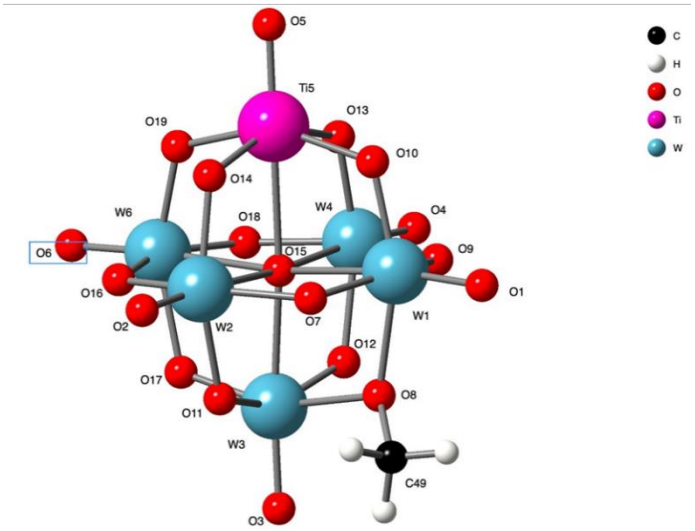

Figure 5.6: *X-ray crystal structure of $[O=TiW_5O_{17}(OMe)]^{3-}$ in MeCN. Red = oxygen, pale blue = tungsten, purple = titanium, black = carbon and grey = hydrogen*

5. 3 Reactivity studies of $(TBA)_4[O=TiW_5O_{18}]$

5.3.1 Reaction between $(TBA)_4[O=TiW_5O_{18}]$ and $4\text{-}MeC_6H_4NCO$

The reactivity of $[O=TiW_5O_{18}]^{4-}$ towards organic isocyanates was investigated in order to compare with the behaviour of Mo=O in $[Mo_6O_{19}]^{2-}$. It was expected that substitution of $\{TiOCH_3\}^{+}$ by $\{Ti=O\}^{2+}$ provided a higher anionic charge on the POM and therefore, it is expected to increase the reactivity of the system towards electrophiles. Metathesis reactions with Lindqvist type isopolymolybdate has been previously investigated and a wide range of organoimido derivatives $[Mo_6(NR)_xO_{19-x}]^{2-}$ have been characterised and reported.[12] Although the analogous isopolytungstate was rather inert with similar reactions.[13]

Our aim was to convert $(TBA)_4[O=TiW_5O_{18}]$ to organoimido $[RN=TiW_5O_{18}]^{4-}$ with the release of CO_2 which could be monitored by ^{17}O NMR spectroscopy when the Ti=O group is ^{17}O-enriched. The initial reaction between $(TBA)_4[O=TiW_5O_{18}]$ and p-toly isocyanate according to Equation 5.3 was monitored by ^{17}O NMR spectroscopy (see experimental for details).

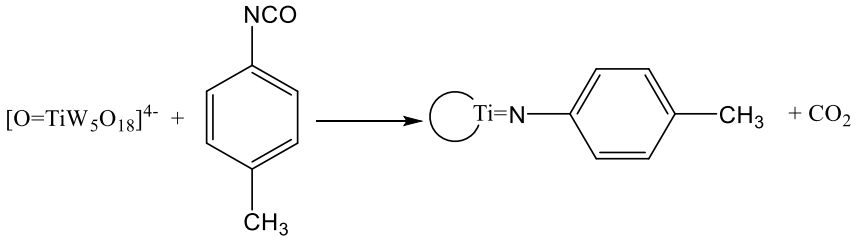

5.3

(a) ^{17}O NMR spectroscopy

The ^{17}O NMR spectrum of the product after recrystallization (Figure 5.7) contained four characteristic peaks with chemical shifts at δ 500, 437, 380 and 330 ppm. The spectrum has no Ti=O peak at 960 ppm suggesting that Ti=O is reactive to the isocyanate. The peak at δ 500 ppm is assigned to bridging TiOW and is similar to the bridging TiOW bond in $(TBA)_4[O=TiW_5O_{18}]$ which is consistent with a 4– charge anion. The peaks at δ 380 ppm is associated with the bridging WOW bond. We think that the peak at δ 330 ppm could be associated with a product due to insertion rather than substitution. If insertion occurred without elimination of CO_2 then peaks in the C=O region would be expected.

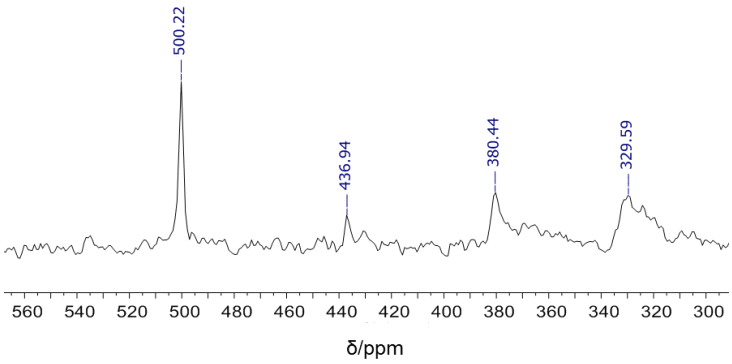

Figure 5.7: ^{17}O NMR spectrum of a reaction between $(TBA)_4[O=TiW_5O_{18}]$ and 4-MeC_6H_4NCO in MeCN

(b) ^{1}H NMR Spectroscopy

The ^{1}H NMR spectrum of the solution suggested that there were up to five types of species in a form of AB patterns with chemical shifts in the aromatic region observed between δ 6.5 – 7.8 ppm. In order to understand the correlation between these peaks, the reaction was investigated by conducting ^{1}H-^{1}H COSY (Correlated Spectroscopy) to determine which signal arise from spin-spin coupling from neighbouring protons. The ^{1}H-^{1}H COSY NMR spectrum (Figure 5.8) enabled the determination by off diagonal peak correlation and the labelled ^{1}H NMR spectrum in Figure 5.9 shows the different AB patterns suggesting multiple insertions in the reaction.

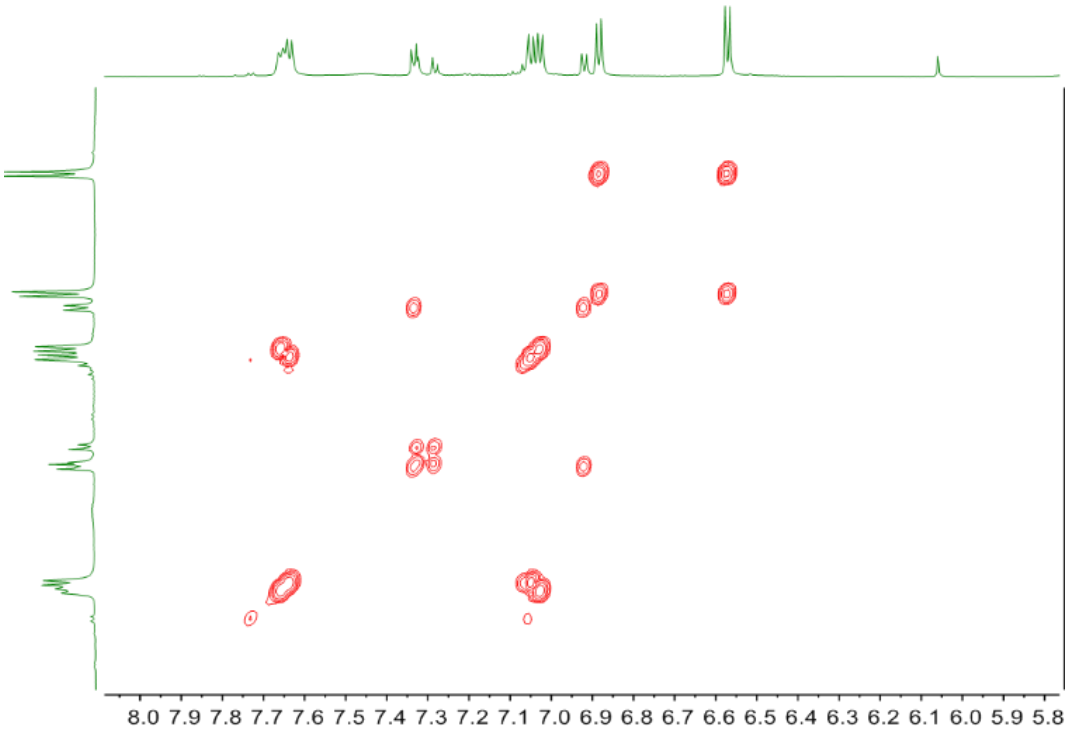

Figure 5.8: *^1H COSY NMR spectrum of a reaction between $(TBA)_4[O=TiW_5O_{18}]$ and 4-MeC_6H_4NCO in MeCN*

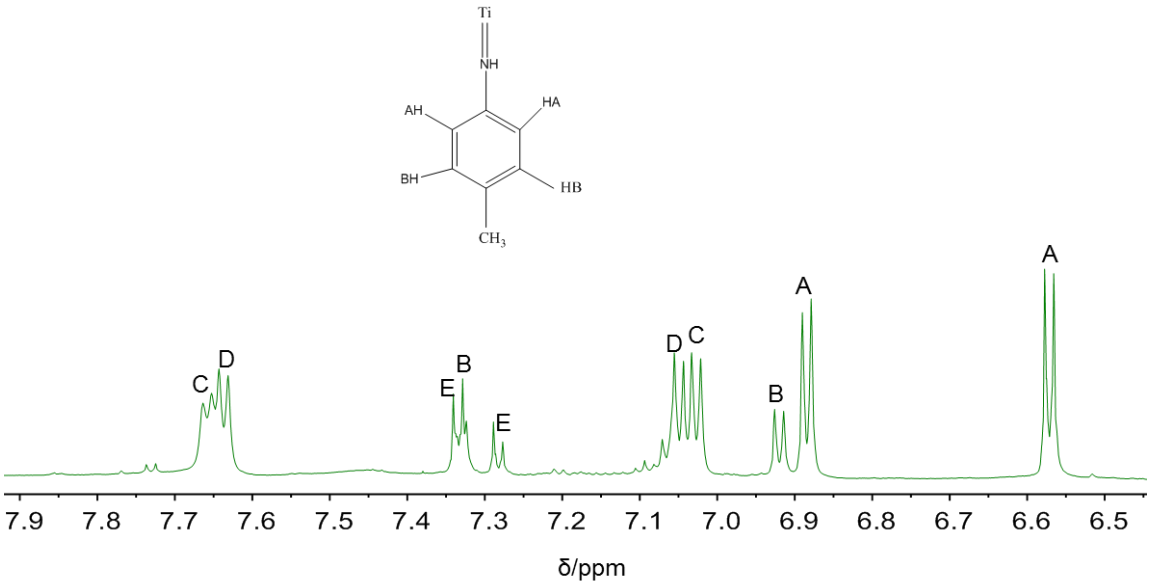

Figure 5.9: *^1H NMR spectrum of a reaction between $(TBA)_4[O=TiW_5O_{18}]$ and 4-MeC_6H_4NCO in MeCN*

These results provided the basis for an undergraduate project in which $(TBA)_4[O=TiW_5O_{18}]$ was reacted with ^{t}BuNCO (Equation 5.4).

$$(TBA)_4[O=TiW_5O_{18}] + {}^t\text{BuNCO} \rightarrow (TBA)_4[({}^t\text{BuN})TiW_5O_{18}] + CO_2 \qquad 5.4$$

The X-ray diffraction and structural analysis shows an unexpected compound (Figure 5.10) with two distinct polyoxometalate (POM) species in the structure. The titanium

atom on the POM surface has been modelled as disordered over two positions one of which has a hydroxyl group bound to it and another which was a carbamate ligand coordinated to it. The presence of the protons on each of these is inferred from the overall 3+ charge of the POM as indicated by the presence of three tetrabutylammonium cations per POM in the structure. i.e. 0.82 carbamate anion and 0.18 hydroxido anion disordered on the same site with the Ti-X on opposite axial sites. This was also proposed as being an insertion product as predicted in Scheme 5.1 (path d). The X-ray crystal structure analysis in **Supplementry Data Table S9** confirmed the two distinct polyoxometalate (POM) species. The tungsten at the axial position W_{ax}-O has a bond length of 1.700(7) Å close to the WO bond observed in $[O=TiW_5O_{18}(MeO)]^{3-}$ although shoter than the average W_{ax}-O bond in other $[XMW_5]^{3-}$ anion of 1.916 Å. The TiOC bond angle is 130.8(7) significantly smaller than WOW angles of 116.5(8) to 118.4(9)^o in $[(MeO)TiW_5O_{18}]^{3-}$ or $[(MeO)TiW_5O_{18}]^{3-}$. X-ray crystal structure analysis is given in **Supplementry Data Table S9**.

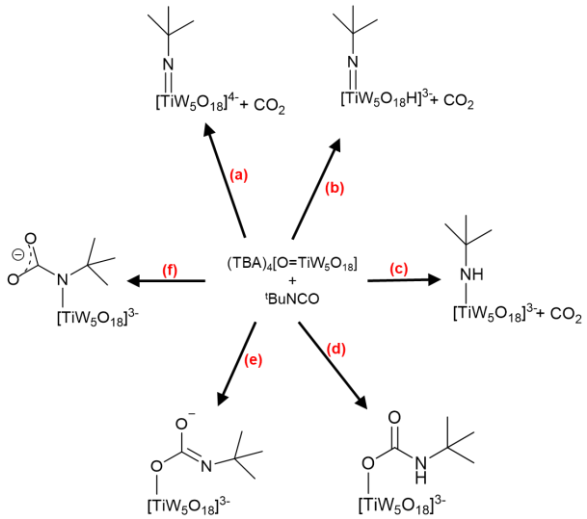

Scheme 5.1: *Expected products from reaction between $TBA_4[O=TiW_5O_{18}]$ and tBuNCO. Path a produces the expected product, paths b and c are a result of protonation of the expected product and paths d, e and f represent possible insertion/addition reaction.*

The product from the reaction was an interesting observation as it gives an insight into the reactivity of the titanyl bond as rather than being attacked by the nitrogen analogous to a carbonyl, the oxygen acted as the nucleophile attacking the carbonyl carbon within the isocyanate. This was significantly different from similar reactions

carried out by Errington *et al* in which $TBA_2[Mo_6O_{19}]$ acted as a carbonyl accepting the electron density of the nucleophilic nitrogen atom.[14] This could have arisen as the M=O π bonding is weaker in titanium than molybdenum due to it lower oxidation state i.e. less back-bonding from the oxygen into the metal leaving more electron density on oxygen atom.

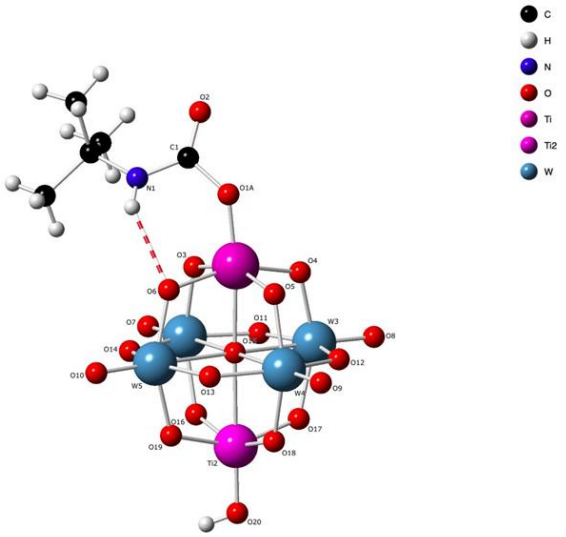

Figure 5.10: *Structure obtained from the reaction between $(TBA)_4[O=TiW_5O_{18}]$ and ^tBuNCO[15]*

5.3.2 Reaction between $(TBA)_4[O=TiW_5O_{18}]$ and $Ph_3P=N^tBu$

We also attempted the metathesis reaction between ^{17}O enriched $(TBA)_4[O=TiW_5O_{18}]$ and $Ph_3P=NBu^t$ (Equation 5.4) and monitored the reaction by ^{31}P and ^{17}O NMR spectroscopy. $(TBA)_4[O=TiW_5O_{18}]$ and $Ph_3P=NBu^t$ were reacted in a 1:1 ratio for 1 h before recording the ^{31}P NMR spectrum. The Ti=O is expected to react with $Ph_3P=NBu^t$ with the release of phosphine oxide which could be observed in the ^{17}O NMR spectrum as a P=O peak. However, after 4 h reaction, the ^{31}P NMR spectrum of the solution showed that the reaction was slow as shown in (Figure 5.11). When the reaction was heated overnight to about 80 ^oC the ^{31}P NMR spectrum suggested the reaction had gone to 97 % completion according to peak integration. The ^{31}P NMR spectrum consists of a characteristic peak at δ 26 ppm assigned to $O=PPh_3$ and a minor peak at -14 ppm which is as a result of small amount of unreacted $Ph_3P=NBu^t$ as shown in Figure 5.12

$$(TBA)_4[O=TiW_5O_{18}] + Ph_3P=NBu^t \rightarrow (TBA)_4[^tBuN=TiW_5O_{18}] + O=PPh_3 \qquad 5.4$$

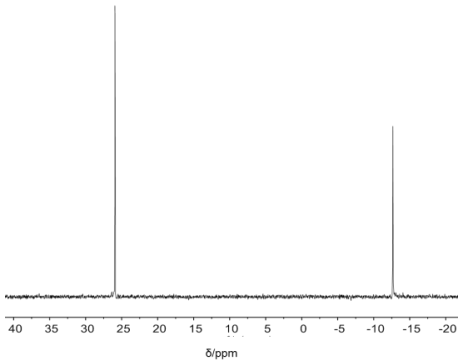

Figure 5.11: *^{31}P NMR for reaction of (TBA)$_4$[O=TiW$_5$O$_{18}$] with Ph$_3$P=NBu^t at room temperature after 2 h in MeCN*

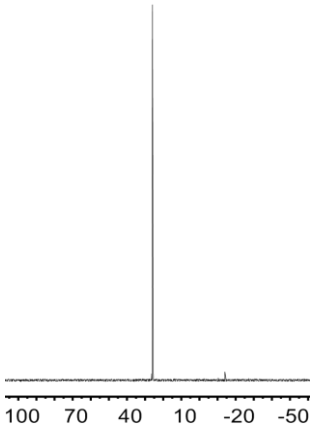

Figure 5.12: *^{31}P NMR for reaction of (TBA)$_4$[O=TiW$_5$O$_{18}$] with Ph$_3$P=NBu^t at room temperature in MeCN*

(a) ^{17}O NMR Spectroscopy

The ^{17}O NMR spectrum (Figure 5.13) of the solution after recrystallization consists of terminal W=O peaks at δ 727 and 695 ppm in a 4:1 expected for W$_{eq}$=O and W$_{ax}$=O respectively. Note that the chemical shifts in the spectrum are similar compared to (TBA)$_4$[O=TiW$_5$O$_{18}$] which is expected for an anion with 4– charge anion. The bridging TiOW is observed at δ 501 ppm and the bridging WOW are observed at δ 381 and 368 ppm. In addition a doublet peak is also observed in the spectrum at δ 48 ppm which is assigned to phosphine oxide ^{17}O=P and is consistent with reported chemical shift for phosphine oxide ^{17}O=P.[16] The peaks at δ -64 ppm is assigned to the central u$_6$-O. The changes in the chemical shifts and the observed ^{17}O=P doublet in the ^{17}O NMR spectrum suggest that the (TBA)$_4$[O=TiW$_5$O$_{18}$] is reactive towards Ph$_3$P=NBu^t.

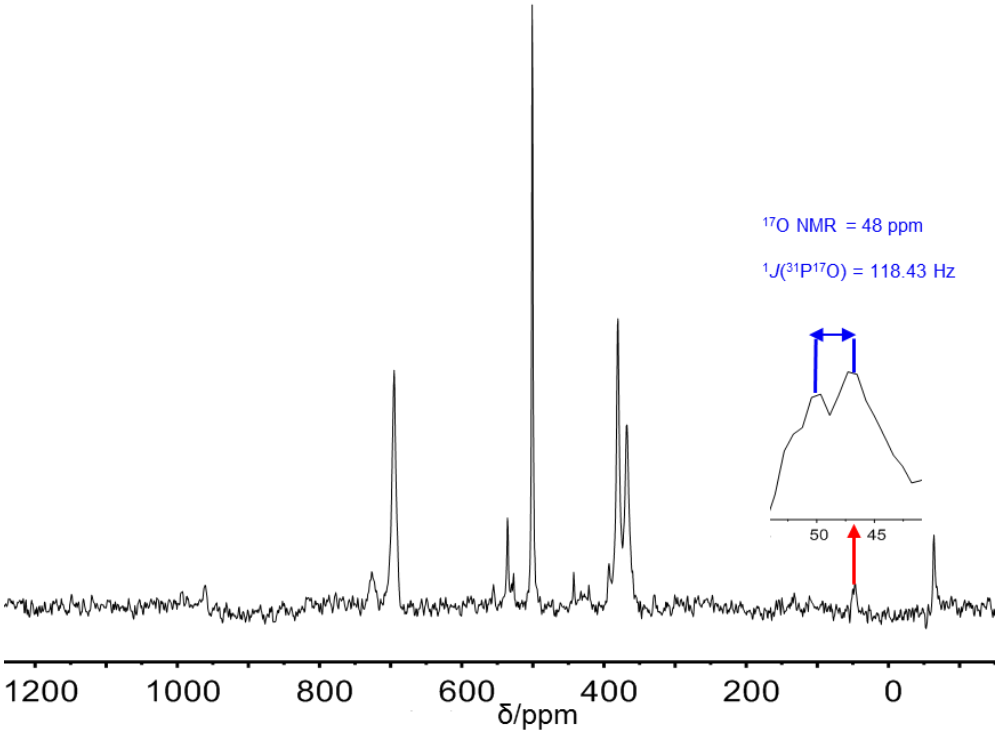

Figure 5.13: *^{17}O NMR for reaction of $(TBA)_4[O=TiW_5O_{18}]$ with $Ph_3P=N^tBu$ at 80 ^oC in MeCN*

5.4 Conclusion

The work in this chapter discussed an efficient approach to prepare Lindqvist-type POM containing for the first-time terminal titanium oxo $(TBA)_3[(MeO)TiW_5O_{18}]$ characterized by ^{17}O NMR spectroscopy. The structure is an isomer of the methoxido $(TBA)_3[(MeO)TiW_5O_{18}]$ species as a result of protonation and subsequent methylation of the highly charged $[O=TiW_5O_{18}]^{4-}$ anion. Reactions of the POM with alkyl or aryl isocyanate gave an insight into the titanyl bond reactivity. It is assumed that in both cases an addition reaction mechanism was preferred over a metathesis reaction in which case the lone pair on the titanyl oxygen seem to attacked the C=O bond on the isocyanate, which remain bound to the titanium rather than forming a Ti=NR bond. Although more investigation is needed to fully understand the reactivity and possibly isolate novel structures.

5.5 Experimental

5.5.1 Attempted preparation of $(TBA)_4[O=TiW_5O_{18}]$ by deprotonation of $(TBA)_3[(HO)TiW_5O_{18}]$ with TBAOH

In a Schlenk flask was added 1.0 M methanolic TBAOH (0.8 mL, 0.8 mmol) and dissolved in MeCN (2 mL) and the solution was pumped dried under reduced pressure to removed volatiles. This process was repeated twice more to remove all volatiles before dissolving in dried MeCN (5 mL). In a separate Schlenk flask, ^{17}O enriched $(TBA)_3[(HO)TiW_5O_{18}]$ (150 mg, 0.07 mmol) was dissolved in MeCN (5 mL) with stirring. The two solutions were combined by cannula transfer and stirred for 2 h before pumped to dryness under vacuum. The resulting solid was washed with diethyl ether (5 ml x 3) and vacuum dried to obtain crystalline solid, **^{17}O NMR** (41 MHz, acetonitrile-d_3) δ (ppm) 1015, 960 556, 527, 502, 443 and 16

5.5.2 Preparation of $(TBA)_4[O=TiW_5O_{18}]$ from $(TBA)_3[(MeO)TiW_5O_{18}]$ with TBAOH

A solution of 1.0 M methanolic TBAOH (0.8 mL, 0.8 mmol) was placed in a Schlenk flask and dissolved in MeCN (2 mL). The solution was evaporated, then this process was repeated twice more to remove all volatiles before redissolving in MeCN (5 mL). In a separate Schlenk flask $(TBA)_3[(MeO)TiW_5O_{18}]$ (0.80 g, 0.3973 mmol) was dissolved in MeCN (5 mL) with stirring to dissolve all solids. The two solutions were combined by cannula transfer and the dark brown solution was stirred for 2 h before evaporation to dryness under vacuum. The resulting solid was washed with diethyl ether (5 ml x 3) and vacuum-dried to obtain dark brown crystalline solid of $(TBA)_4[O=TiW_5O_{18}]$ (0.712 g, 80 **%**).**^{17}O NMR** (41 MHz, acetonitrile-d_3) δ (ppm) 954 , 695, 501, 439, 381, 368, and -64; **FT-IR ATR (4000 – 400 cm^{-1})** cm^{-1} 2959 (m), 2873 (m), 1668 (m), 1482 (s), 1379 (m), 1152 (w), 1107 (w), 1058 (w), 1028 (vw), 932 (vs), 884 (w), 781 (m), 639, 574, 556, 523, 426 cm^{-1}. **^{183}W NMR** (21 MHz, acetonitrile-d_3): δ (ppm) 82 and 47.

5.5.3. Reaction of $(TBA)_4[O=TiW_5O_{18}]$ with 4-MeC_6H_4NCO in MeCN

In a 5 mm screw top NMR tube was added $(TBA)_4[O=TiW_5O_{18}]$ (100 mg, 0.045 mmols) and dissolved in MeCN (1 mL). A solution of 4-MeC_6H_4NCO (5,6 uL, 0.045 mmols) was added producing a reddish solution immediately. The resulting solution was vigorously shaken for 5 minutes before recording the ^{17}O NMR spectrum. The sample

was transferred back into a Schlenk flask, pumped dry, then washed with diethyl ether (5 mL x 2). **^{17}O NMR** (41 MHz, acetonitrile-d_3) δ (ppm) 500, 437, 380 and 330. **^{1}H NMR** (300 MHz, acetonitrile-d_3) δ (ppm) 7.67, 7.64, 7.62, 7.35, 7.32, 7.30, 7.06, 7.04, 7.01, 6.93, 6.90, 6.59, 6.56

5.5.4. Reaction of $(TBA)_4[O=TiW_5O_{18}]$ with $^{t}BuN=PPh_3$

In a Schleck flask was added $(TBA)_4[O=TiW_5O_{18}]$ (100 mg, 0.045 mmols) and ^{t}BuN=PPh3 (15 mg, 0.045 mmoles) and dissolved in MeCN (3 mL). The resulting dark brown solution was heated with stirring at 80 – 90 ^{o}C for 4 h in an oil bath. After heating, the solution was pumped to dryness under vacuum. Initial ^{31}P NMR spectrum was recorded which suggested reaction has gone to 50 % completion. The sample was transferred back into the Schlenk flask and heated overnight at 80 – 90 ^{o}C before the solution pumped to dryness under vacuum and washing in diethyl ether (5 ml x 3) to obtained dark brown crystalline solids. **^{17}O NMR** (41 MHz, acetonitrile-d_3) δ (ppm) 727, 695,536, 501, 381, 368 and -64. **^{31}P NMR** (121 MHz, acetonitrile-d_3) δ (ppm) 26 and 14

References

1. W. Clegg, M. R. J. Elsegood, R. J. Errington and J. Havelock, *J.Chem.Soc., Dalton Trans.*, 1996, 681-690.
2. B. Kandasamy, C. Wills, W. McFarlane, W. Clegg, R. W. Harrington, A. Rodríguez-Fortea, J. M. Poblet, P. G. Bruce and R. J. Errington, Chem. *Eur. J*, 2012, **18**A, 59-62.
3. J. M. Thomas, R. Raja and D. W. Lewis, *Angew. Chem. Int. Ed.*, 2005, **44**, 6456-6482.
4. F. J. Feher, D. A. Newman and J. F. Walzer, *J. Am. Chem.Soc.*, 1989, **111**, 1741-1748.
5. R. Murugavel, A. Voigt, M. G. Walawalkar and H. W. Roesky, *Chem. Rev.*, 1996, **96**, 2205-2236.
6. T. M. Che, V. W. Day, L. C. Francesconi, M. F. Fredrich, W. G. Klemperer and W. Shum, *Inorg. Chem.*, 1985, **24**, 4055-4062.
7. G. S. Kim, K. S. Hagen and C. L. Hill, *Inorg.Chem.*, 1992, **31**, 5316-5324.
8. O. A. Kholdeeva, B. G. Donoeva, T. A. Trubitsina, G. Al-Kadamany and U. Kortz, *Eur. J. Inorg. Chem.*, 2009, **2009**, 5134-5141.
9. O. A. Kholdeeva, *Eur. J. Inorg.Chem.*, 2013, **2013**, 1595-1605
10 K.-Y. Wang, Z. Lin, B. S. Bassil, X. Xing, A. Haider, B. Keita, G. Zhang, C. Silvestru and U. Kortz, *Inorg. Chem.*, 2015, **54**, 10530-10532.
11. R. J. Errington, S. S. Petkar, P. S. Middleton, W. McFarlane, W. Clegg, R. A. Coxall and R. W. Harrington, *J. Am. Chem. Soc.*, 2007, **129**, 12181-12196.
12. M. T. Pope and A. Müller, *Polyoxometalates: From Platonic Solids to Anti-Retroviral Activity*, Springer Netherlands, 2012.
13. Z. Peng, *Angew. Chemie Int. Ed.*, 2004, **43**, 930-935.
14. L. D. Quin, *A Guide to Organophosphorus Chemistry*, Wiley, 2000
15 G. Smith MSc Project report, Newcastle University, 2019.
16 J. Zhang, F. Xiao, J. Hao and Y. Wei, *Dalton Trans,* 2012, **41**, 3599-3615

Appendix: Suplementry Data for Crystallographic analysis

Table S1*:* *X-ray c*rystal data and structure refinement for $(TBA)_3[(HO)TiW_5O_{18}]$

Empirical formula	**$C_{50}H_{109}N_4O_{19}TiW_5$**
Formula weight	2037.56
Temperature/K	150.0(2)
Crystal system	monoclinic
Space group	I2/a
a/Å	31.1936(9)
b/Å	18.4834(2)
c/Å	27.5332(10)
α/°	90.0
β/°	120.793(4)
γ/°	90.0
Volume/$Å^3$	13636.7(6)
Z	8
ρcalcg/cm^3	1.985
μ/mm^{-1}	8.577
F(000)	7848.0
Crystal size/mm^3	0.24 × 0.1 × 0.06
Radiation	MoKα (λ = 0.71073)
2Θ range for data collection/°	6.544 to 56.584
Index ranges	-39 ≤ h ≤ 37, -24 ≤ k ≤ 22, -35 ≤ l ≤ 31
Reflections collected	54968
Independent reflections	15035 [R_{int} = 0.0379, R_{sigma} = 0.0422]
Data/restraints/parameters	15035/792/760
Goodness-of-fit on F^2	1.042
Final R indexes [I>=2σ (I)]	R_1 = 0.0344, wR2 = 0.0682
Final R indexes [all data]	R = 0.0598, wR2 = 0.0786
Largest diff. peak/hole / e $Å^{-3}$	2.60/-2.78

Table S2: *Bond lengths for $(TBA)_3[(HO)TiW_5O_{18}]$*

AtomAtom	Length/Å	AtomAtom	Length/Å
W2 O2	1.710(4)	O7 W1	1.919(4)
W2 O4	1.911(4)	O7 Ti1	1.919(4)
W2 O8	1.944(4)	O10 Ti1	2.3245(3)
W2 O9	1.932(4)	O11 Ti4	1.719(5)
O21 Ti5	1.926(3)	O11 W4	1.719(5)
W2 O10	2.3160(3)	O14 Ti5	1.904(4)
W2 Ti1	3.2820(4)	O14 W4	1.922(5)
W3 O3	1.715(4)	O15 W6	1.926(5)
W3 O5	1.911(4)	O15 W4	1.898(5)
W3 O8	1.925(4)	O16 W4	1.932(3)
W3 O10	2.3247(2)	O17 W4	1.902(5)
W3 Ti1	3.2958(4)	O18 W5	1.911(5)
O1 W1	1.720(4)	O18 Ti5	1.911(5)
O1 Ti1	1.720(4)	O18 W6	1.882(5)
O4 W1	1.935(4)	O19 W5	1.903(4)
O4 Ti1	1.935(4)	O19 Ti5	1.903(4)
O5 W1	1.946(4)	O20 W5	2.316(4)
O5 Ti1	1.946(4)	O20 Ti5	2.316(4)
O6 W1	1.944(4)	O20 W6	2.3122(4)
O6 Ti1	1.944(4)	O20 Ti6	2.3122(4)

Table S3: *Atom occupancy for disordered position in the trans-disordered $(TBA)_3[(HO)TiW_5O_{18}]$ anion*

Atom	Occupancy
W1	0.5
Ti1	0.5

Table S4*:* Crystal data and structure refinement for $(TBA)_4[(\mu\text{-}O)(TiW_5O_{18}H)_2]$

Chemical formula (total)	$C_{64}H_{142}N_4O_{37}Ti_2W_{10}$	
Formula weight	3494.12	
Temperature	150(2) K	
Radiation, wavelength	MoKα, 0.71073 Å	
Crystal system, space group	triclinic, P $\bar{1}$	
Unit cell parameters	a = 11.6924(4) Å	α = 94.280(3)°
	b = 12.8110(4) Å	β = 101.989(3)°
	c = 17.3366(6) Å	γ = 108.432(3)°
Cell volume	2382.21(14) Å^3	
Z	1	
Calculated density	2.436 g/cm3	
Absorption coefficient μ	12.250 mm−1	
F(000)	1634	
Reflections for cell refinement	9316 (θ range 2.9 to 29.5°)	
θ range for data collection	2.9 to 26.0°	
Index ranges	h −14 to 14, k −15 to 15, l −21 to 21	
Completeness to θ = 26.0°	99.9 %	
Reflections collected	21365	
Independent reflections	9361 (Rint = 0.0365)	
Reflections with $F^2>2\sigma$	6350	
Min. and max. transmission	0.0842 and 0.0842	
Refinement method	Full-matrix least-squares on F2	
Weighting parameters a, b	0.0510, 0.0000	
Data / restraints / parameters	9361 / 0 / 538	
Final R indices [$F^2>2\sigma$]	R_1 = 0.0390, wR_2 = 0.0903	
R indices (all data)	R_1 = 0.0647, wR_2 = 0.0960	
Goodness-of-fit on F^2	0.944	
Largest and mean shift/su	0.035 and 0.001	
Largest diff. peak and hole	3.29 and −1.43 e Å$^-$	

Table S5: *Bond lengths for $(TBA)_4[(\mu\text{-}O)(TiW_5O_{18}H)_2]$*

Bond	lengths [Å]	Bond	lengths [Å]
W(1)–Ti(1)	3.1864(17)	W(1)–O(1)	1.711(6)
W(1)–O(7)	1.955(7)	W(1)–O(8)	1.921(5)
W(1)–O(19)	1.874(6)	W(1)–O(10)	1.919(6)
W(1)–O(19)	2.353(5)	W(2)–Ti(1)	3.1933(17)
W(2)–O(17)	1.704(6)	W(2)–O(10)	1.924(6)
W(3)–O(2)	1.959(6)	W(2)–O(14)	1.854(7)
W(3)–O(11)	1.952(6)	W(2)–O(19)	2.301(5)
W(3)–O(18)	1.694(7)	W(3)–O(7)	1.892(6)
W(4)–Ti(1)	1.909(6)	W(3)–O(12)	1.901(5)
W(4)–O(8)	1.972(6)	W(3)–O(19)	2.379(6)
W(4)–O(13)	3.1880(16)	W(4)–O(3)	1.705(6)
W(4)–O(19)	1.930(6)	W(4)–O(12)	1.951(6)
W(5)–O(15)	1.847(6)	W(4)–O(15)	1.935(6)
W(5)–O(17)	2.292(5)	W(5)–O(6)	1.710(6)
W(5)–O(19)	1.897(6)	W(5)–O(16)	2.023(7)
Ti(1)–O(9)	1.897(6)	W(5)–O(18)	1.877(7)
Ti(1)–O(14)	2.334(5)	Ti(1)–O(5)	1.7990(17)

Table S6: *Bond Angle for $(TBA)_4[(\mu\text{-}O)(TiW_5O_{18}H)_2]$*

Bond	Angle [°]	Bond	Angle [°]
Ti(1)–W(1)–O(1)	136.9(3)	Ti(1)–W(1)–O(7)	121.28(17)
Ti(1)–W(1)–O(8)	81.81(18)	Ti(1)–W(1)–O(9)	32.62(19)
Ti(1)–W(1)O(10)	81.16(19)	Ti(1)–W(1)–O(19)	44.39(14)
O(1)–W(1)–O(7)	101.9(3)	O(1)–W(1)–O(8)	103.8(3)
O(1)–W(1)–O(9)	104.2(3)	O(1)–W(1)–O(10)	104.0(3)
O(1)–W(1)O(19)	178.7(3)	O(7)–W(1)–O(8)	84.4(2)
O(7)–W(1)–O(9)	153.9(3)	O(7)–W(1)–O(10)	85.4(3)
O(7)–W(1)O(19)	76.9(2)	O(8)–W(1)–O(9)	89.2(3)
O(8)–W(1)O(10)	151.7(2)	O(8)–W(1)–O(19)	76.2(2)
O(9)–W(1)O(10)	88.5(3)	O(9)–W(1)–O(19)	77.0(2)
O(10)–W(1O(19)	75.9(2)	Ti(1)–W(2)–O(4)	137.9(3)
Ti(1)–W(2)O(10)	80.90(19)	Ti(1)–W(2)–O(11)	120.30(16)
Ti(1)–W(2)O(14)	33.22(17)	Ti(1)–W(2)–O(17)	82.50(19)
Ti(1)–W(2)O(19)	44.30(14)	O(4)–W(2)–O(10)	104.1(3)
O(4)–W(2)O(11)	101.7(3)	O(4)–W(2)–O(14)	104.7(3)
O(4)–W(2)O(17)	102.7(3)	O(4)–W(2)–O(19)	177.4(3)
O(10)–W(2O(11)	85.7(3)	O(10)–W(2)O(14)	89.3(3)

Table S7: *Crystallographic data for $(TBA)_4[(\mu\text{-}O)(TiW_5O_{18}H)_2(dmso)]$*

Empirical formula	**$C_{66}H_{152}N_4O_{38}STi_2W_{10}$**
Formula weight	3576.27
Temperature/K	150.0(2)
Crystal system	monoclinic
Space group	P21/c
a/Å	16.7396(3)
b/Å	18.3861(3)
c/Å	33.3462(6)
α/°	90
β/°	95.9811(15)
γ/°	90
Volume/Å^3	10207.3(3)
Z	4
ρcalcg/cm^3	2.327
μ/mm-1	11.459
F(000)	6720.0
Crystal size/mm^3	0.26 × 0.16 × 0.11
Radiation	MoKα (λ = 0.71073)
2Θ range for data collection/°	5.712 to 56.598
Index ranges	-20 ≤ h ≤ 21, -24 ≤ k ≤ 18, -43 ≤ l ≤ 39
Reflections collected	83111
Independent reflections	22350 [R_{int} = 0.0415, R_{sigma} = 0.0421]
Data/restraints/parameters	22350/622/1178
Goodness-of-fit on F^2	1.081
Final R indexes [I>=2σ (I)]	R_1 = 0.0334, wR2 = 0.0611
Final R indexes [all data]	R_1 = 0.0483, wR2 = 0.0656
Largest diff. peak/hole / e Å^{-3}	1.81/-1.11

Table S8: *Bond lengths for $(TBA)_4[(\mu\text{-}O)(TiW_5O_{18}H)_2(dmso)]$*

Bond	Distance [A]
$Ti_1\ O_{06}$	1.940(4)
$Ti_1\ O_{010}$	1.913(4)
$Ti_1\ O_{011}$	2.028(4)
$Ti_1\ O_{014}$	1.939(4)
$Ti_1\ O_{015}$	1.786(4)
$Ti_1\ O_{018}$	2.220(4)
$Ti_2\ O_{015}$	1.795(4)
$Ti_2\ O_{24}$	1.922(4)
$Ti_2\ O_{25}$	2.051(4)
$Ti_2\ O_{26}$	1.941(4)
$Ti_2\ O_{27}$	1.909(4)
$Ti_2\ O_{36}$	2.228(4)
$W_{ax}O_5$	1.703(4)
$W_{ax}O_{23}$	1.712(4)
$W_{eq}O_2$	1.710(4)
$W_{eq}O_4$	1.707(4)
$W_{eq}O_{21}$	1.719(4)
$W_{eq}O_{19}$	1.700(4)
$O_{25}H_{25}$	0.806(4)
$O_{11}H_{11}$	0.813(4)

Table S9: *Selected bond angles for $(TBA)_4[(\mu\text{-}O)(TiW_5O_{18}H)_2(dmso)]$*

Bond (W-O-W)	**Angle**	**Bond (Ti-O-W)**	**Angle**
W4 O12W5	116.3(2)	W1 O6 Ti1	115.7(2)
W5 O13 W2	118.3(2)	W2 O10 Ti1	115.6(2)
W2 O15 W3	117.9(2)	W4 O11 Ti1	112.46(18)
W4 O16 W3	116.9(2)	W3 O14 Ti1	114.8(2)
W5 O17 W3	118.4(2)	Ti1 O18 W1	89.81(14)
W1 O18 W2	88.82(13)	Ti1 O18 W2	88.06(13)
W1 O18 W5	90.13(13)	Ti1 O18 W3	89.92(14)
W2 O18 W5	88.17(12)	Ti1 O18 W4	95.47(13)
W3 O18 W1	178.47(19)	Ti1 O18 W5	176.23(18)
W3 O18 W2	89.67(13	W6 O24 Ti2	114.8(2)
W3 O18 W4	91.08(13)	W7 O25 Ti2	112.5(2)
W3 O18 W5	90.03(13)	W8 O26 Ti2	114.6(2)
W4 O18 W1	90.44(13)	W9 O27 Ti2	115.33(19)
W4 O18 W2	176.40(18)	Ti2 O36 W6	89.10(14)
W4 O18 W5	88.30(13)	Ti2 O36 W7	95.85(15)

Table S10: *Crystal data and structure refinement of $(TBA)_4[(\mu\text{-}O)(TiW_5O_{18})_2(SnMe_2)]$.*

Empirical formula	$C_{66}H_{150}N_4O_{37}SnTi_2W_{10}$
Formula weight	3644.88
Temperature/K	150.0(2)
Crystal system	orthorhombic
Space group	$P2_12_12_1$
a/Å	16.0697(3)
b/Å	17.2587(3)
c/Å	39.7248(9)
α/°	90
β/°	90
γ/°	90
Volume/Å^3	11017.4(4)
Z	4
ρ_{calc}g/cm^3	2.197
μ/mm^{-1}	10.818
F(000)	6816.0
Crystal size/mm^3	0.53 × 0.21 × 0.07
Radiation	MoKα (λ = 0.71073)
2Θ range for data collection/°	5.93 to 56.032
Index ranges	-21 ≤ h ≤ 20, -22 ≤ k ≤ 22, -52 ≤ l ≤ 52
Reflections collected	86985
Independent reflections	23660 [R_{int} = 0.0602, R_{sigma} = 0.0669]
Data/restraints/parameters	23660/2191/1255
Goodness-of-fit on F^2	1.046
Final R indexes [I>=2σ (I)]	R_1 = 0.0648, wR_2 = 0.1285
Final R indexes [all data]	R_1 = 0.0857, wR_2 = 0.1376
Largest diff. peak/hole / e Å^{-3}	2.42/-2.17
Flack parameter	0.024(5)

Table S11: *Selected bond Lengths of $(TBA)_4[(\mu\text{-}O)(TiW_5O_{18})_2(SnMe_2)]$.*

Atom Atom	Length/Å	Atom Atom	Length/Å
W1 O6	1.716(16)	W1 O2	2.043(14)
W1 O7	1.897(17)	Ti2 O32	2.211(14)
W1 O13	1.951(16)	W2 O9	1.879(18)
W1 O14	2.257(15)	W2 O14	2.315(15)
W1 O15	1.899(15)	W2 O16	1.997(18)
W2 Ti1	3.199(4)	W3 Ti1	3.196(4)
W2 O3	1.814(16)	W3 O4	1.855(16)
W2 O7	1.937(16)	W3 O9	1.964(17)
W2 O8	1.688(19)	Ti2 O32	2.211(14
Ti1 O1	1.800(15)	Ti2 O22)	1.902(14)
Ti1 O2	2.033(15)	W10 O3	1.919(18)
Ti1 O3	1.952(17)	W10 O3	1.831(16)
Ti1 O4	1.895(16)	W10 O3	1.875(19)
Ti1 O5	1.961(16)	W10 O3	1.696(18)
Ti1 O14	2.228(17)	Sn1 O2	2.007(14)
Ti2 O1	1.785(14)	Sn1 O20	2.025(14)
Ti2 O20	2.030(13)	Sn1 C65	2.14(3)
Ti2 O21	1.933(16)	Sn1 C66	2.10(3)

Table S12: *Selected bond angles of $(TBA)_4[(\mu\text{-}O)(TiW_5O_{18})_2(SnMe_2)]$.*

AtomAtomAtom	Angle/°	AtomAtomAtom	Angle/°
W2 O3 Ti1	116.2(8)	W2 O9 W3	117.7(9)
O12 W4 O14	177.2(8)	O13 W4 O14	75.6(6)
W3 O4 Ti1	116.9(8)	W3 O11 W4	118.4(9)
O12 W4 O18	102.5(9)	O13 W4 O18	84.2(7)
W4 O5 Ti1	115.1(8)	W4 O13 W1	116.5(8)
O13 W4 Ti1	83.1(5)	O14 W4 Ti1	44.1(4)
W1 O7 W2	116.9(8)	W1 O14 W2	91.2(5)
O13 W4 O11	152.1(7)	O18 W4 Ti1	119.4(5)
W2 O9 W3	117.7(9)	W1 O14 W3	177.0(8)
O13 W4 O14	75.6(6)	O18 W4 O14	75.4(7)
W2 O3 Ti1	116.2(8)	W1 O14 W4	91.6(5)
O12 W4 O14	177.2(8)	O15 W5 O14	75.9(6)
W3 O4 Ti1	116.9(8)	W1 O14 W5	89.3(5)
O12 W4 O18	102.5(9)	O16 W5 O14	75.3(6)
W4 O5 Ti1	115.1(8)	W2 O14 W3	88.5(5)
O13 W4 Ti1	83.1(5)	O2 W1 O14	77.1(6)
W1 O7 W2	116.9(8)	O3 Ti1 W4	123.1(5)
O13 W4 O11	152.1(7)	O6 W1 O2	96.1(7)

Table S13: *X-ray analysis data for $(TBA)_4[O{=}TiW_5O_{18}]$.*

Empirical formula	$C_{68}H_{150}N_6O_{19}TiW_5$
Formula weight	2323.08
Temperature/K	150.0(2)
Crystal system	orthorhombic
Space group	Pbca
a/Å	17.8710(3)
b/Å	16.95440(18)
c/Å	28.4030(4)
α/°	90
β/°	90
γ/°	90
Volume/Å3	8605.88(19)
Z	4
ρcalcg/cm3	1.793
μ/mm-1	13.267
F(000)	4576.0
Crystal size/mm3	0.42 × 0.12 × 0.06
Radiation	CuKα (λ = 1.54184)
2Θ range for data collection/°	7.832 to 133.722
Index ranges	-21 ≤ h ≤ 21, -20 ≤ k ≤ 14, -33 ≤ l ≤ 32
Reflections collected	35775
Independent reflections	7619 [Rint = 0.0431, Rsigma = 0.0331]
Data/restraints/parameters	7619/0/457
Goodness-of-fit on F2	1.053
Final R indexes	[I>=2σ (I)] R1 = 0.0252, wR2 = 0.0499
Final R indexes [all data]	R1 = 0.0375, wR2 = 0.0545
Largest diff. peak/hole / e $Å^{-3}$	0.70/-0.60

Table S14: *Bond lengths for $(TBA)_4[(O=TiW_5O_{18})$*

Atom Atom	Length/Å	Atom Atom	Length/Å
Ti1 O2	1.923(3)	W1 O10	1.931(3)
Ti1 O3	1.921(3)	W2 O2	1.932(3)
Ti1 O4	1.932(3)	W2 O5	1.954(3)
Ti1 O9	2.31943(18)	W2 O6	1.714(3)
Ti1 O1	1.720(3)	W2 O7	1.923(3)
W1 O1	1.720(3)	W2 O9	2.32556(19)
W1 O2	1.923(3)	W3 O3	1.927(3)
W1 O3	1.921(3)	Ti2 O2	1.932(3)
W1 O4	1.932(3)	W3 O7	1.929(3)
W1 O9	2.31943(18)	W3 O8	1.714(3)

Table S15: *Selected bond angles for $(TBA)_4[(O=TiW_5O_{18})$*

Atom Atom Atom	Angle/°	Atom Atom Atom	Angle/°
O1 W1 O2	102.37(12)	O6 Ti2 O41	102.98(13)
O1 W1 O3	102.61(13)	O6 Ti2 O5	101.62(12)
O1 W1 O4	103.47(13)	O6 Ti2 O7	104.28(12)
O1 W1 O9	178.99(10)	O6 Ti2 O9	178.34(10)
O7 Ti2 O2	87.29(11)	O6 Ti2 O9	178.34(10)
O2 W1 O4	154.15(12)	O7 Ti2 O2	87.29(11)
O2 W1 O4	154.15(12)	O7 Ti2 O5	154.10(11)
O2 W1 O9	77.07(8)	O7 Ti2 O9	77.33(8)
O2 W1 O101	87.65(11)	O3 Ti3 O51	86.46(11)
O3 W1 O2	87.25(11)	O3 Ti3 O7	87.82(11)
O3 W1 O4	86.72(11)	O3 Ti3 O9	76.29(8)
O3 W1 O9	76.55(8)	O3 Ti3 O10	153.04(11)
O4 W1 O9	77.08(8)	O51 Ti3 O9	76.79(8)
O101 W1 O4	86.71(11)	O7 Ti3 O51	154.01(11)
O101 W1 O9	77.11(8)	O7 Ti3 O9	77.22(8)
O2 W2 O41	153.37(11)	O7 Ti3 O10	87.32(12)
O2 W2 O5	86.79(11)	O8 Ti3 O3	102.98(13)
O2 W2 O9	76.74(7)	O8 Ti3 O51	102.21(13)

Table S16: *X-ray analysis data for $(TBA)_3[O{=}TiW_5O_{17}(OMe)]$.*

Empirical formula	**$C_{49}H_{111}N_3O_{19}TiW_5$**
Formula weight	2013.55
Temperature/K	150.0(2)
Crystal system	orthorhombic
Space group	Pbca
a/Å	17.6224(4)
b/Å	23.8384(7)
c/Å	31.5626(8)
α/°	90
β/°	90
γ/°	90
Volume/Å^3	13259.1(6)
Z	8
ρcalcg/cm^3	2.017
μ/mm^{-1}	8.819
F(000)	7760.0
Crystal size/mm^3	0.21 × 0.13 × 0.04
Radiation	MoKα (λ = 0.71073)
2Θ range for data collection/°	6.61 to 52.744
Index ranges	-21 ≤ h ≤ 21, -29 ≤ k ≤ 29, -38 ≤ l ≤ 26
Reflections collected	55604
Independent reflections	13307 [Rint = 0.0683, Rsigma = 0.0690]
Data/restraints/parameters	13307/1019/712
Goodness-of-fit on F^2	1.089
Final R indexes [I>=2σ (I)]	R_1 = 0.0407, wR2 = 0.0753
Final R indexes [all data]	R_1 = 0.0823, wR2 = 0.0909
Largest diff. peak/hole / e Å^{-3}	1.35/-2.01

Table S17: *Bond lengths for $(TBA)_3[(O=TiW_5O_{18})(MeO)]$*

Bond	Length/Å	Bond	Length/Å
W4 O4	1.728(5)	O7 W1	1.934(5)
W4 O9	1.928(5)	O7 W2	1.925(5)
W4 O12	1.987(6)	O7 Ti1	1.934(5)
W4 O13	1.851(5)	O8 C49	1.445(10)
W4 O15	2.299(5)	O8 W1	2.139(6)
W4 O18	1.938(5)	O8 W3	2.106(6)
W4 Ti5	3.2602(8)	O8 Ti1	2.139(6)
W4 Ti1	3.2460(5)	O8 Ti3	2.106(6)
W4 Ti3	3.2975(5)	O9 W1	1.916(5)
W4 Ti6	3.3007(5)	O9 Ti1	1.916(5)
O2 W2	1.710(6)	O10 W1	1.836(5)
O3 W3	1.698(6)	O19 Ti5	1.972(5)
O3 Ti3	1.698(6)	O19 W5	1.972(5)
O5 Ti5	1.692(6)	O19 Ti6	1.848(6)
O5 W5	1.692(6)	O15 Ti1	2.292(5)
O6 W6	1.712(5)	O15 Ti3	2.285(5)
O6 Ti6	1.712(5)	O15 Ti6	2.385(5)

Table S18: *Selected bond angles for TBA)$_3$[(O=TiW$_5$O$_{18}$)(MeO)]*

Bond	Angle [°]	Bond	Angle [°]
W3 O8 W1	**109.9(2)**	O19 W6 Ti5	32.01(17)
Ti3 O8 Ti1	109.9(2)	W4 Ti5 W2	89.669(19)
W1 O9 W4	115.2(3)	W4 Ti5 W6	60.631(15)
Ti1 O9 W4	115.2(3)	O5 Ti5 W4	134.3(2)
W1 O10 Ti5	114.9(3)	O5 Ti5 O10	104.2(2)
Ti1 O10 W5	114.9(3)	O5 Ti5 O13	103.9(3)
O10 Ti5 W2	80.93(16)	O5 Ti5 O14	105.3(3)
O10 Ti5 W6	123.06(16	O5 Ti5 O15	178.9(2)
O13 Ti5 W4	30.39(16)	O5 Ti5 O19	102.9(3)
O13 Ti5 O10	86.5(2)	O5 Ti5 W1	135.38(19)
O13 Ti5 O14	150.8(2)	O5 Ti5 W2	136.0(2)
O13 Ti5 O15	75.2(2)	O5 Ti5 W6	132.72(19)
Ti1 O9 W4	115.2(3)	O10 Ti5 W4	80.57(16)
O19 Ti5 O13	86.1(2)	O10 Ti5 O15	76.5(2)
W1 O15 Ti5	86.47(17)	O10 Ti5 W1	31.17(15)
O19 Ti5 O14	86.6(2)	O10 Ti5 W2	80.93(16)
W2 O15 W6	89.35(17)	O10 Ti5 W6	123.06(16